Excess Freshwater Outflow from the Black Sea-Lake during Glacial and Deglacial Periods and Delayed Entry of Marine Water in the Early Holocene Require Evolving Sills

Anastasia Gennadyevna Yanchilina

Submitted in partial fulfillment of the

requirements for the degree of Doctor of Philosophy

in the Graduate School of Arts and Sciences

COLUMBIA UNIVERSITY

2016

ABSTRACT

Excess freshwater outflow from the Black Sea-Lake during glacial and deglacial periods and delayed entry of marine water in the early Holocene require evolving sills

Anastasia Gennadyevna Yanchilina

The Black Sea becomes periodically isolated from the global ocean during each glacial period. This occurs when the elevation of the global ocean is lower than the Bosporus sill, putting a stop to inflow of salt water to the Black Sea. This phenomenon allows the Black Sea to evolve from a marine environment to a freshwater one. It is also evident that the depth of the Bosporus sill does not remain at the same elevation, and instead is dynamic. The sill becomes filled with sediments during periods of its sub-aerial exposure but is subsequently eroded to its bedrock during periods of outflow from the Black Sea-Lake to the global ocean.

This interpretation comes from the observations that during the last glacial period, the Black Sea-Lake was in a positive hydrological balance, fresh, and predominantly outflowing to the global ocean over a deep Bosporus sill, at approximately 80 meters below sea level (mbsl). It is highly likely that there were brief periods when the lake froze and the outflow suspended, such as during the extreme stadial conditions associated with the North Atlantic iceberg-discharge Heinrich Event 2 (HE 2) at ~24 kyr before present, when there is also no evident carbonate accumulation in stalagmites that receive water from evaporated Black Sea surface water.

Upon the onset of deglaciation, large floods originating from the Fennoscandinavian Ice Sheet and the Alps, delivered meltwater so as to fully ventilate the Black Sea-Lake and even potentially replace all of the water in the basin. These floods occurred near the time of the

deglacial iceberg-discharge Heinrich Event 1 (HE 1 at~17 kyr before present), and left pulses of red-colored sediment everywhere on the western half of the Black Sea basin.

During the Bølling/Allerød warming period, ~15-13 kyr before present, the Black Sea-Lake regressed below the Bosporus outlet. It is also during this period that the sill became filled with sediments and was no longer deep but shallow, closer to its modern elevation of ~35 mbsl. The change of the depth of the sill prevented any salt water from entering the Black Sea-Lake until the global ocean reached the new threshold depth of the Bosporus sill.

The delayed breaching of the sill occurred at a time when the Black Sea-Lake regressed to a depth as low as 165 mbsl during the Preoboreal period and occurred at 9.3 kyr BP before present. The transgression that followed was caused by the inflow of Mediterranean water, and occurred rapidly, on the order of a few decades or less. Salinification of the surface water then occurred in two steps. An initial salinification, in which a small fraction of marine water mixed with shallow freshwater, also occurred within decades. The complete transition of Black Sea water to a sufficiently high salinity that exclusively marine fauna could tolerate, took ~1,500 calendar years.

Table of contents

List of Tables

Chapter 1: Black Sea-Lake during the last glacial period: cold, wet, partially isolated from outflow to the global ocean, and briefly frozen

Chapter 2: Megaflood delivery of meltwater from the Alps and Fennoscandinavian Ice Sheet into the Black Sea-Lake

List of figures

Chapter 1: Black Sea-Lake during the last glacial period: cold, wet, partially isolated from outflow to the global ocean, and briefly frozen

Chapter 2: Megaflood delivery of meltwater from the Alps and Fennoscandinavian Ice Sheet into the Black Sea-Lake

Chapter 3: Rapid transgression and gradual salinification of the Black Sea from inflow of Mediterranean water in the early Holocene

Chapter 4: The dynamic nature of the Bosporus sill and its implications for water exchange between the Black Sea and the Mediterranean Sea

Acknowledgements

This thesis could not have been possible without the guidance and collaboration of many individuals. Most and foremost, I would like to thank two of my advisors, Bill Ryan and Jerry McManus. Bill Ryan first got me interested and introduced me to the questions that were still plaguing the deglacial history of the Black Sea. This region has always been dear to my heart as it is where I first learned how to swim and spent all of our family vacations when growing up. I could not have asked for a better dissertation topic and one I would spend four years on. Bill Ryan's guidance has been indispensable to my learning to appreciate the importance of every sample and how each sample holds an interesting piece of the puzzle to understand the evolution of the Black Sea. Jerry McManus, whom I had the honor of working with as an undergraduate summer fellow at the Woods Hole Oceanographic Institute (WHOI) and with whom I first started working with at Lamont Doherty Earth Observatory (LDEO) as a graduate student, has also been just as an amazing source of information and support. Even when away on sabbatical during the last months of the preparation of my thesis he has continued to be an active source of information and guidance.

A large fraction of the dissertation relies on samples collected on the *R/V Akademik* during 2009 and 2011 expeditions. I would like to thank all of the crew who were involved in these expeditions. I also want to acknowledge specifically Petko Dimitrov, Dimitar Dimitrov, and Krasimira Slavova from the Institute of Oceanology—Bulgarian Institute of Sciences and Mariana Filipova-Marinova from the Varna Regional Museum of History. The expeditions and the success of my thesis would not have been possible without their contributions.

I would like to acknowledge Leo Pena, now a professor at the University of Barcelona, who has worked very closely with me to do the $^{87}Sr/^{86}Sr$ and ε_{Nd} analyses. He also introduced

me to amazing graphing software to develop figures to visualize my work. I owe almost all of the analytical skills I have obtained at LDEO to him. The analyses would not have been also possible without the help of Louise Bolge who helped me with running the samples on the mass spectrometers and taught me to be patient with these instruments when they malfunctioned.

I would like to thank Tim Kenna who worked closely with me to make X-ray fluorescence analyses on sediments and also closely reviewed my dissertation; Peter DeMenocal for serving as a valuable member of my committee, an amazing professor, source of guidance during the last months at LDEO as a graduate student, and allowing me to use his wet lab to process my sediment samples; Bob Anderson for introducing me to two fascinating cores from the core repository at LDEO that became part of my thesis; Nichole Anest at the core lab who helped me sample numerous cores, make the carbonate analyses and always an amazing resource for any questions that I have had; and Steve Goldstein, Martin Fleischer, and Will Jacobsen for help with learning to process carbonate for U/Th analyses; Liviu Giosan for hosting me at WHOI to give a seminar and for careful review of my dissertation; and Frank Wesselingh for species identification and collaboration.

This thesis would not have been possible without the collaboration with scientists nationally and internationally. I would like to thank Tony Nicholas and Allan Chivas from University of Wollongong who have sent samples from core 342 retrieved from the northern Black Sea shelf; Andrei Briceag from the National Institute of Research and Develoment of Marine Geology and Geoecology with whom I have collaborated to make $\delta^{18}O$, $\delta^{13}C$, ε_{Nd}, and ^{14}C measurements from 09-SG-13; Marius Stoica from Bucharest University who has provided me samples from MD04-2790, Marco Coolen from the Woods Hole Oceanographic Institution who has provided me samples from GGC18; Candace Major and Dan Cohen, earlier students of

Bill Ryan, who made a lot of the initial ^{14}C, $\delta^{18}O$, $\delta^{13}C$, and $^{87}Sr/^{86}Sr$ on carbonate; Naci Görür and Mehme Sakinç from the Istanbul Technical University for sending samples from the Sakaraya coastal plain; and Gilles Lericolais from the Institut français de recherché pour l'exploitation de la mer and Seda Okay from Institute of Marine Sciences and Technology at Dokuz Eylül University for BLaSON chirp profiles.

This list is just a few of those who have contributed and heavily impacted my work and success. Last but not least I would like to thank my little brother, Anton Yanchilin, who has been the most supportive family and friend I could ask for and has inspired me to keep pushing when times got tough. I must thank all of my extended family in Moscow: aunt Valeria Akimova, cousing Kristina Akimova, grandparents Roza and Valerey Kuznetsov, and grand uncle Lev Kuznetsov. I also must thank five of my best friends who have been the family to me and kept me on the right track, Nazish Alam, Edith De La Torre, Lumari Pardo, Stephanie Henry, and Anna Janas. I additionally would like to thank my two cycling teams, Houlihan Lokey and Columbia, who were also always a source of support and guidance and my coach, Michael Sencenbough.

"Life is like riding a bicycle.
To keep your balance you must keep moving"
- Albert Einstein

Introduction

This dissertation investigates the evolution of the Black Sea from a freshwater environment during the last glacial period to a marine environment upon its connection with the Mediterranean Sea in the early Holocene. This dissertation is unique in that it compiles a large fraction of prior Black Sea research, both in the form of measurements but also ideas. This dissertation seeks to reconcile the remaining mysteries about its deglacial evolution. In the following chapters I tackle questions that address the level and hydrological balance of the Black Sea-Lake during the glacial period, the source and volume of meltwater delivery into the basin during the disintegration and melting of the Fennoscandinavian and Alpine ice sheets, the level of the lake prior to its connection of the Mediterranean Sea in addition to its timing and rapidity, and the dynamic nature of the Bosporus sill that was lowered to its bedrock during the last glacial period but subsequently filled up sufficiently to delay the connection of the Black Sea-Lake with the Mediterranean until the early Holocene.

The first chapter focuses on the recognition of a deep Bosporus sill during the glacial period. This idea was introduced for the first time but not thoroughly discussed in a recent publication of Nicholas and Chivas, (2014). Major et al., (2002) also contemplated on the idea of a deep Bosporus sill but discounted it, as a deep Bosporus sill would not explain the delayed reconnection of the Black Sea with the Mediterranean. This chapter clearly shows that the Black Sea-Lake was pinned at the paleoshoreline, inferred to be located at ~95 meters below sea level (mbsl), and was predominantly outflowing to the Marmara Sea-Lake during this time. It is observed that the Black Sea-Lake must have outflowed during this period from the observation of similar $^{87}Sr/^{86}Sr$ and $\delta^{18}O$ composition of water in the two basins and also from active river activity in the Black Sea-Lake. It is also observed that, although predominantly outflowing, the

Black Sea-Lake did briefly freeze. This has never been suggested before and arises from the observation of a hiatus in the growth of Sofular Cave speleothems that are dependent on groundwater seepage. This hiatus occurred during a stadial period corresponding to the Heinrich Event 2 (HE 2) North Atlantic iceberg-discharge episode. There is a related observation of coarse dropstones in Black Sea cores during this period.

The second chapter focuses on explaining the source of deglacial floods that were delivered into the Black Sea-Lake at the time of the Heinrich Event 1 (HE1) North Atlantic iceberg-discharge episode. Chepalyga, (2007) proposed that these floods were derived from the overflow of the Caspian Lake into the Black Sea over the Manych depression whereas Soulet et al., (2013) proposed that these floods were exclusively sourced from a periodic draining of Lake Disna in the north. This chapter includes additional ε_{Nd} measurements to show that the floods were not sourced from one location but appear instead to be sourced from multiple locations, including both the Alpine and the Fennoscandinavian ice sheets. The chapter combines a calculation of the volume of red sediment observed on the Black Sea floor from a number of cores with $^{87}Sr/^{86}Sr$ measurements to estimate the range of volume of the delivered meltwater. The chapter also uses ^{14}C measurements and XRF data to show that the delivery of meltwater thoroughly ventilated the entire Black Sea-Lake and was so large as to change the $^{87}Sr/^{86}Sr$ composition of the Marmara Sea-Lake, a basin that received the downstream meltwater.

The third chapter focuses on revisiting some questions that have not yet been conclusively answered regarding the early Holocene transgression of the Black Sea. The questions this chapter addresses include: (1) What was the level of the Black Sea-Lake prior to transgression? (2) Was the Black Sea a freshwater lake prior to the transgression? (3) Was the transgression caused by the reconnection of the Black Sea with the Mediterranean Sea? (4) How

rapid was the initial transgression? (5) How rapid was the initial salinification of the surface water? (6) How rapid was the complete salinification of the Black Sea water to its modern salinity level? This chapter uses earlier published measurements but also new ^{14}C, $\delta^{18}O$, $\delta^{13}C$, and $^{87}Sr/^{86}Sr$ measurements from cores retrieved from the Black Sea from a number of expeditions, with a specific focus on the coquina found everywhere on the Black Sea shelf dating to this questionable period, to answer these questions. It builds upon the initial ideas set by Ryan et al., (1997), Ryan et al., (1997), Ryan et al., (2003), and Ryan, (2007).

The fourth and last chapter is a concluding chapter. This chapter revisits the idea introduced by Nicholas and Chivas, (2014) that the depth of the Bosporus sill does not remain the same through a deglaciation period but can change through time. This chapter ties the first three chapters together and also focuses on the deglaciation period after the delivery of meltwater into the Black Sea at approximately the time of HE1 and before the early Holocene transgression of the Black Sea. This chapter proposes that there was a deglacial interval when the Bosporus sill likely shallowed and considers possible explanations for this shoaling. This chapter also touches upon the changing ^{14}C reservoir of the Black Sea-Lake during the Bølling/Allerød, Younger Dryas, and Preboreal periods since the last ice age. It also extends farther back in time to interpret observations for periods including marine isotope stages 6, 5, and 3, representing the penultimate glaciation, last peak interglacial interval, and the glacial interval preceding the last glacial maximum, respectively.

Chapter 1 will be submitted to Palaeogeography, Palaeoclimatology, and Palaeocology and chapter 2 will be submitted to Quaternary Science Reviews. Chapter 3 is submitted to Marine Geology.

Future work will include explaining the evolution of the Black Sea after its reconnection to the Mediterranean and global ocean, especially in the context of the development of the sapropel and the coccolithosphore facies in the Black Sea basin. Future work will explore the U/Th dating of mollusks, work that has been started last year at LDEO, but will continue at the lab of Stephen Eggins at the Australian National University this spring. This lab allows the exploration of variations of U and Th isotopes through a shell of the mollusk in part to distinguish sources of contamination, a technique that has been explored before in Eggins et al., (2005) but never yet applied to the mollusks from the Black Sea. Another possible avenue would be to make ε_{Nd} measurements at several sources of riverine inflow and to evaluate the strength and variability of riverine flux through the deglacial history of the Black Sea, not just during the delivery of meltwater into the Black Sea. One of the cores from this thesis dissertation contains red sediment that was delivered prior to the meltwater event and it would be interesting to see whether the mechanisms for its deposition may have had some similarity with those during the HE1.

References

Chepalyga, A., 2007. The late glacial great flood in the ponto-caspian basin. In: V. Yanko-Hombach, A. Gilbert, N. Panin and P. Dolukhanov (Eds.), The Black Sea flood Question: Changes in Coastline, Climate, and Human Settlement. Springer, Dordrecht, The Netherlands, 119-148.

Eggins, E. M., R. Grün, M. T. McCulloch, A. W. G. Pike, J. Chappell, L. Kinsley, , G. Mortimer, M. Shelley, C. V. Murray-Wallace, C. Spötl and L. Taylor, 2005. In situ U-series dating by laser-ablation multi-collector ICPMS: new prospects for Quaternary geochronology. Quaternary Science Reviews 24, 2523-2538.

Karakilcik, H., U. Can Unlugenc and M. Okyar, 2014. Late glacial-Holocebe shelf evolution of the Sea of Marmara west of Istanbul. Journal of African Earth Sciences 100, 365-378.

Major, C. O., W. B. F. Ryan, G. Lericolais and I. Hajdas, 2002. Constraints on Black Sea outflow to the Sea of Marmara during the last glacial-interglacial transition. Marine Geology 190, 19-34.

Nicholas, W. A. and A. R. Chivas, 2014. Late Quaternary sea-level change on the Black Sea shelves. In: F. L. Chiocci and A. R. Chivas (Eds.), Continental Shelves of the World: Their Evolution During the Last Glacio-Eustatic Cycle. The Geological Society, London, 199-212.

Ryan, W. B. F., 2007. Status of the Black Sea flood hypothesis. In: V. Yanko-Hombach, A. S. Gilbert, N. Panin and P. M. Dolukhanov (Eds.), The Black Sea Flood Question: Changes in Coastline, Climate, and Human Settlement. Springer, Dordrecht, The Netherlands, 63-88.

Ryan, W. B. F., C. O. Major, G. Lericolais and S. L. Goldstein, 2003. Catastrophic flooding of the Black Sea. Annual Reviews of Earth and Planetary Sciences 31, 525-554.

Ryan, W. B. F., W. C. Pitman, C. O. Major, K. M. Shimkus , V. Moscalenko, G. A. Jones, P. Dimitrov, N. Görür, M. Sakinç and H. Y. Seyir, 1997. An abrupt drowning of the Black Sea shelf at 7.5 kyr BP. Geo-Eco-Mar. 2, 115-125.

Ryan, W. B. F., W. C. I. Pitman, C. O. Major, K. Shimkus, V. Moskalenko, G. A. Jones, P. Dimitrov, N. Gorür, M. Sakiniç and H. Yüce, 1997. Abrupt Drowning of the Black Sea Shelf. Marine Geology 138, 119-126.

Soulet, G., G. Menot, G. Bavon, F. Rostek, E. Ponsevera, S. Toucanne, G. Lericolais and E. Bard, 2013. Abrupt drainage cycles of the Fennoscandian Ice Sheet Proceedings of the National Academy of Sciences 110, 6682-6687.

CHAPTER 1

Black Sea-Lake during the last glacial period: cold, wet, partially isolated from outflow to the global ocean, and briefly frozen

Abstract

The elevation of the surface of the Black Sea-Lake and whether its outflow to the global ocean during the last glacial period was persistent or intermittent are not clear. Multiple studies report evidence of a paleoshoreline at a modern depth of 95 mbsl everywhere on the Black Sea shelf during the last glacial period suggesting that the lake level was predominantly at this water depth. Additional evidence in the form of carbonate fossil $\delta^{18}O$ and $^{87}Sr/^{86}Sr$ indications of the isotopic compositions of water in the Black Sea-Lake and Marmara Sea-Lake basins suggests that the Black Sea-Lake was generally outflowing to the Marmara Sea-Lake and potentially, also to the global ocean. Yet, the two-way exchange between the Black Sea-Lake and Sea of Marmara was not established until early Holocene, at a time when the global sea level reached 35 meters below modern sea level (mbsl), the level of the modern Bosporus sill. This paper compiles seismic profiles and sedimentary data, including stable and radiogenic isotopes, radiocarbon measurements, and elemental concentrations in order to reconcile the conflicting evidence and to propose that the level of the Bosporus sill was at its bedrock of 80 mbsl during the last glacial period. This kept the Black-Sea Lake within this upper threshold and allowed for the formation at that level of the observed paleoshoreline, which has subsequently been depressed by loading to its current elevation. This paper shows that the Black Sea-Lake was predominantly in a positive hydrological balance during the glacial period with the exception of

Heinrich Event 2 when the climate cooled so much that the lake completely froze over and its outflow to the Sea of Marmara was cut off.

1. Introduction

The Black Sea was shown to previously be a freshwater lake before it transformed into a modern sea (Arkhangel'skiy and Strakhov, 1938). This conclusion is derived from observations of seabed and sub-seabed sediments containing mollusks that also lived in rivers, estuaries, and deltas. The Black Sea-Lake faunal assemblage constituted *Dreissena rostriformis*, *Unio pictorum*, *Vivipirus vivipirus*, and was distinct from that of modern shelf environment composed of *Modiolus phaseolina*, *Cardium edule*, and *Mytilus galloprovincialis* (Fedorov, 1963; Nevesskaya, 1965), with no overlap between the two. Dinoflagellate evidence showed that the freshwater conditions lasted from glacial and into early Holocene (Wall and Dale, 1973; Wall and Dale, 1974). In addition to the fresh faunal composition, the decrease of the interstitial porewater salinity with increasing burial depth (Smirnow, 1958; Manheim and Stoffers, 1969; Soulet et al., 2010) and $\delta^{18}O$ measurements on bulk carbonate (Deuser, 1972) point that before its connection to the global ocean, Black Sea-Lake was fresh or at the most, slightly brackish. This set of observations poses the question: what mechanisms freshened the Black Sea-Lake from previous interglacial states when it had become salty after reconnection with the global ocean as today (Schrader, 1979; Badertscher et al., 2011; Shumilovskikh et al., 2013)?

The most likely scenario for freshening would occur through the loss of a supply of salt water from the Mediterranean as the global sea level decreased below that of the level of previous Dardanelles and Bosporus inlets. Yet under these conditions, the lake would only have freshened if it were capable of expelling its prior salty water composition. Based on existing

knowledge of the global eustatic sea level in the past (Milliman and Emery, 1968), the elevation of the Bosporus sill was originally proposed to be at 50 meters below modern sea level (mbsl) so as to agree with the change of the of the water from fresh to marine between 9 to 7 kyr ^{14}C years (Deuser, 1972; Ross and Degens, 1974). The surplus freshwater input to the Black Sea that is required for the full desalinification to occur is presumed to come from an excess of precipitation and river input relative to evaporation. Based on these hydrologic reasonings, the Pleistocene lake had a permanent outlet and was always outflowing (Kvasov, 1975; Kvasov and Blazhchishin, 1978; Chepalyga, 1984). Additional dating of the Holocene salinification later suggested that the Bosporus sill and lake level were at 30 mbs at the time of the reconnection to the global ocean that allowed saline waters to re-enter the Black Sea (Major et al., 2002; Nicholas et al., 2011).

However, the idea of continuous outflow was challenged by the discovery of a lowstand shoreline at depths of 90 to 110 mbsl below present global sea level (Kuprin et al., 1974; Scherbakov et al., 1978; Scherbakov, 1983; Kaplin and Shcherbakov, 1986). This observation led to the idea that the Black Sea-Lake remained at this depressed eleveation during most of the previous glacial period. The magnitude of the lowstand was fortified by over-incision of river valleys (Ostrovskiy et al., 1977; Ostrovskiy et al., 1977) and discovery of bed of the Don river at an elevation of 60 mbsl beneath the Kerch Strait (Popov, 1973; Skiba et al., 1976), and buried river channels extending across the shelf to deltas at an elevation of ~90 mbsl. Further support comes from observations of wave-cut terraces (Shimkus et al., 1980) and a belt of dunes landward of the lowstand shoreface (Ryan et al., 1997; Popescu et al., 2004). Reflection profiles identified an exposed margin of the lake landward of the paleoshoreline identified on Ukraine (Ryan et al., 1997), Romanian (Lericolais, 2001; Lericolais et al., 2003; Popescu et al., 2004;

Lericolais et al., 2007), Bulgarian (Genov, 2004b; Coleman and Ballard, 2007), Turkish (Okyar et al., 1994; Demirbag et al., 1999; Okyar and Ediger, 1999; Algan et al., 2002; Aksu et al., 2002a; Algan et al., 2007), and Caucasian (Ivanova et al., 2007) margins. Cores landward of this paleoshoreline were found to penetrate below the Holocne cover into aeolian, fluvial, and alluvial deposits as well as into exposures of Neogene and Mesozoic clay. Exposure of the shelf of the former marine sea would also explain observations of reworked marine dinoflagellates (Wall and Dale, 1973), coccoliths (Bukry et al., 1970), and redeposited carbonate (Deuser, 1972) in the lacustrine sediments of glacial and early postglacial age.

A shallow sill at the time of the connection and a paleoshoreline well below the elevation of such a shallow sill creates a dilemma. Either the regression that created this paleoshoreline was a short-lived phenomena that did not significantly interrupt the freshening, or the glacial age outlet lay far below the elevation of modern sill permitting continuous freshening. Yet, if the lowstand was short lived, most of the sediment deposited during the period that the lake was outflowing should have remained on the shelf. Kuprin and Sorokin, (2007) adopted an idea of a lowstand that occurred during the latest glacial, just after the last glacial maximum, and Kuprin et al., (1974) interpreted the shelf-wide coarse-grained coquina deposit reaching an elevation of 30 to 25 mbsl as a freshwater transgressive deposit. Kuprin and Sorokin, (2007) assigned a Neoeuxine age to this transgression that occurred from 15 to 8.50 kyr ^{14}C years. This interpretation is not consistent with recent observations. The ^{14}C dates on mollusks from supposedly transgressive coquina have a narrow span of ^{14}C ages that are limited to 8.50 kyr ^{14}C years and the $^{87}Sr/^{86}Sr$ composition of the mollusks rises abruptly from fresh to marine values (Major et al., 2006). Soulet et al., (2011a) suggested that the Black Sea was at the 30 mbsl sill

and outflowing sometime before the last glacial maximum (~30 to 26 kyr BP) and during the deposition of deglacial floods near the time of the Heinrich 1 event (~18 to 15 kyr BP).

Since all but the inner shelf would be submerged during a highstand that brought the lake to its 30 mbsl outlet, the discussion above implies that sediment of glacial and deglacial age should be present on the shelf below the observed coquina deposit. As will be shown in this study, sediments of glacial and deglacial age are not encountered on the shelf landward of the paleoshoreline. The only way for the lake to have maintained an outlet during a period of positive hydrologic balance that allowed the lake to freshen without any mid and inner shelf deposits would be an outlet at the same elevation as the observed paleoshoreline, which also happens to be near the depth of the bedrock of the Bosporus sill. Such an interpretation has never yet been proposed before and thus needs substantial documentation.

2. Methods

2.1 Core recovery & reflection profiles

The cores used in this study include a compilation from cruises spanning 1987 to 2011 and were recovered using gravity, borehole, vibracoring, and piston methods. The full compilation of cores, location, and respective cruises on which cores were collected is listed in Appendix A. The cores cover a broad area of the Black Sea (**Figure 1-1**) that includes northwest Black Sea slope and basin interior in addition to Russian, Ukrainian, Romanian, Bulgarian, and Turkish shelves from 0 to 2210 mbsl. Two of the cores, BLKS9830 and BLKS9834, were recovered from the fill of the meandering fluvial channel landward of the paleoshoreline on the inner Black Sea shelf (44°00.640 N, 29°53.710 E) and (44°41.970 N, 28°47.550 E) at 57 and 67 mbsl, respectively. These cores sample those sediments located in the fill of the channel

preserved in the substrate beneath the depressions of interior dunes. Four cores that include KSK-20, KSK-18, KSK-16, and KSK-4, are boreholes drilled on the adjacent coastal plane of the Sakaraya River by the Turkish State Waterworks (Görür et al., 2001). Boreholes drilled into the Dniprovs'ko Buhs'kyi liman from the Ukrainian coast sampled sediments in its fill to the above bedrock (Naukova, 1984). Three cores are recovered from the eastern Black Sea shelf. These include 721 form the Georgian coast (Apakidze and Burchuladze, 1987; Nicholas et al., 2011) and AK-500 and AK-521 from the Russian coast (Ivanova et al., 2007).

Chirp profiles from a series of cruises are presented to complement the sedimentation history reconstructed from the core recovery. Profile WC-6-13_0850-2040 was taken during the Aquanaut 1993 expedition, profile B008 during the BlaSON 1998 expedition, and profiles B2ch049 and B2ch007 during the BlaSON2 2002 expedition (**Figure 1-1**). Profile WC-6-13_0850-2040 cuts across a sedimentary wedge that is sampled by AK93-06, AK93-01, AK93-02, AK93-03-2, AK93-04, and AK93-05; profile B008 cuts across a sedimentary wedge that is sampled by BLKS98-09, 09-SG-13, BLKS98-08, BLKS98-07, BLKS98-06; B2ch049 cuts across a sedimentary wedge that is sampled by AKAD09-19, AKAD01-AB18&20, AKAD01-AB17, and AKAD09-28; and B2ch007 cuts across a sedimentary wedge that is sampled by Medex05-13.

2.2 Radiocarbon dating and chronology

The chronology of the cores was established by correlating sediment lithology and ^{14}C dates that were taken from carbonate material. The material used for radiocarbon dating included mollusks, ostracods, and occasional pieces of wood. Those shells analyzed for this study were sonicated for 30s in Quartz Distilled and methanol to remove contaminating surface

detrital matter. Samples were run using carbonate hydrolysis and CO_2-reduction at Woods Hole Oceanographic Institution and ETH-Zurich. Additional dates were acquired from prior published results (Apakidze and Burchuladze, 1987; Görür et al., 2001; Major et al., 2002; Major et al., 2006; Ivanova et al., 2007; Konikov et al., 2007; Lericolais et al., 2007; Nicholas et al., 2011; Soulet et al., 2011a).

Three types of cores with different lithologic history were recovered from the Black Sea bottom: (1) slope and basin, (2) shelf and seaward of the 90 mbsl paleoshoreline, and (3) shelf and landward of the 90 mbsl paleoshoreline. Those cores recovered from the slope and basin record the full sedimentation history of the Black Sea-Lake, although there are sections identified that have lithologic breaks either by detrital input or removal of sediments by activities such as winnowing, slides, and slumping. Generally, these cores have lithologic history that features a lacustrian record in the form of light and dark grey lutite during the Glacial period and Younger Dryas, red colored pulses during the Heinrich 1 event (HE 1), and white calcium carbonate rich sediment during Bølling Allerød and Preboreal interstadials. The lacustrian record is followed by sapropelic and coccolithophore rich sediments during mid to late Holocene. The ^{14}C dates are used to constrain the location of these lithologic boundaries.

Those cores that are collected from the shelf area of the Black Sea and are located seaward of the paleoshoreline exhibit a different type of sedimentation pattern. These cores also have glacial, meltwater, Younger Dryas, and mid and late Holocene sediment but sediment from Bølling/Allerød and Preboreal is absent and is separated from the bracketing lithologies by a coquina. The lithologic sections that are present are correlated with each other. The ^{14}C ages are used to constrain both unconformities and lithologic boundaries. Those cores that are collected

from the shelf, but landward of the paleoshoreline, only feature mid to late Holocene sediment that sit upon a coquina deposit, below which material dates to the glacial period and older.

2.4 ^{14}C reservoir and age model

The ^{14}C dates are used to derive a ^{14}C reservoir change from 40 kyr BP to the late Holocene. This is accomplished from compiling a number of independent records and methods. The first method comes from the work of Nowaczyk et al., (2013) who applied magnetostatigraphy to approximate calendar ages in addition to a thorough ^{14}C dating of their core. To get the ^{14}C reservoir for each calendar date, the calendar date was converted to the atmospheric ^{14}C date at the time and subtracted from the measured ^{14}C age, that taken to be of the lake water. The second method comes from detailed U/Th and stable isotope records from a stacked speleothem record of Sofular Cave in Northern Turkey, a record shown to reflect Black Sea precipitation from evaporated lake surface water, is matched to a stable isotope record of mollusks from the outer shelf of the Black Sea (Badertscher et al., 2011). The speleothems allow for determining calendar ages, conversion of calendar ages to atmospheric ^{14}C ages, and a derivation of the ^{14}C reservoir age as a function of time. The third method calculates the difference between ^{14}C ages of wood and mollusk from one of the shelf cores, AKAD09-28, where the wood is taken to represent the atmospheric ^{14}C age and the mollusk the ^{14}C age of the water. These reservoir ages are supplemented by those derived by dating tephra layers (Kwiecen et al., 2008), comparison of XRF Ti/Ca, $CaCO_3$, and TOC records from the northwesten Black Sea slope to Hulu $\delta^{18}O$ speleothem record (Soulet et al., 2011b), and comparison of Black Sea lithologic unit boundaries with GRIP $\delta^{18}O$ ice-core record from Greenland (Ryan, 2007).

2.5 Sedimentation rates

The sedimentation rate is calculated from dividing the amount of sediment accumulated between bracketing lithologic boundaries and corresponding calendar dates. Gaps in sedimentation are also noted. For those lithologic boundaries for which no ^{14}C measurements are made, a corresponding calendar age is ascribed to that lithologic boundary. The lithologic boundaries for which the sedimentation rates are calculated include Glacial (> 16.35 kyr BP), deposition of red layers near the time of the Heinrich 1 Event (16.35 to 15 kyr BP), Older Dryas (15 to 14.80 kyr BP), Bølling/Allerød (14.80 to 12.90 BP), Younger Dryas (12.90 to 12.10 kyr BP), Preboreal (12.10 to 9.30 kyr BP), Unit 2/Sapropel (9.30 to 3.00 kyr BP), and Unit 1/Coccolithophore ooze (3.00 kyr BP to present). The calendar ages assigned to lithologic boundaries belonging to the different periods of deposition from Glacial to the Preboreal are taken from the U/Th dated $\delta^{18}O$ and $\delta^{13}C$ records from the Sofular Cave in which the variation of the stable isotopes clearly identifies the distinct climates under which each sedimentary strata was deposited. The calendar date for the Unit 2/ 1 boundaries is taken from (Ross and Degens, 1974).

2.6 $\delta^{18}O$ and $\delta^{13}C$

Stable isotopes were measured by gas-sourced mass spectrometry at the Department of Earth and Planetary Sciences at Rutgers University (Mortlock, 2010) and at Rensselaer Polytechnic Institute (RPI) (Cohen and Ryan, 2011). Approximately 700 to 1200 μg of shell material was chosen from each mollusk specimen. Prepared samples were loaded onto a Multi-prep device attached to a Micromass Optima Stable Isotope Mass Spectrometer and reacted in 100% phosphoric acid at 90°C for 800 seconds. Values are reported versus V-PBD through the

analysis of an internal laboratory standard that is routinely calibrated against NBS-19. The errors associated with the measurements are 0.04 and 0.06 ‰ for $\delta^{13}C$ and $\delta^{18}O$, respectively. Major et al., (2002) and Major et al., (2006) provide additional $\delta^{13}C$ and $\delta^{18}O$ measurements.

2.7 $^{87}Sr/^{86}Sr$

For $^{87}Sr/^{86}Sr$ isotope analyses, mollusk shells were leached using a procedure modified from Bailey et al., (2000). The first leach consisted of a one-minute sonification of the sample in 0.1 N hydrochloric acid. The isotope ratios were measured by a dynamic multi-collector on a VG Sector 54 thermal ionization mass spectrometer (TIMS) at Lamont-Doherty Earth Observatory. The $^{87}Sr/^{86}Sr$ ratios were corrected for mass fractionation through normalizing to $^{86}Sr/^{88}Sr=0.1194$. Beam size was maintained at close to 4.5 x 10^{-11} A for ^{88}Sr. The measurements were further corrected for instrumental drift by analysis of NBS987 which gave $^{87}Sr/^{86}Sr=0.710255 \pm 2.31143E\text{-}05$, 2σ external reproducibility, n=7). All $^{87}Sr/^{86}Sr$ ratios are further corrected relative to the standard's $^{87}Sr/^{86}Sr$ value of 0.71024. The errors presented in this paper are the in-run 2σ error of the mean. Prior $^{87}Sr/^{86}Sr$ measurements supplement those made in this study (Major et al., 2006).

2.8 XRF

The bulk intensities of major elements were measured by a field portable-XRF spectrometer at LDEO on dry sediments. The sediment was prepared by homogenization with agate mortar and packed into sample cups equipped with Mylar polyester supports every 2 cm. Prepared cups were positioned in a sampling test stand supplied by the manufacturer. The intensities (in counts per second) were related to ppm by correlation with Standard Reference

Materials (Kenna et al., 2011). The full discussion of the measurements is given in Kenna et al., (2011). The results reported here are acceptable to within ±20% of the standards measured for each respective element and measurement precision is also, within 20%. The average error for each measured element is calculated individually. Results are also reported as ratios (i.e., Ti/Ca and Zr/Rb). Ti/Ca is calculated to emphasize differences in the relative distribution of terrigenous material relative to carbonate sedimentation (Bahr et al., 2005) and Zr/Rb was previously shown to represent changes in grain size (Dypvik and Harris, 2001).

3. Results

3.1 Bathymetry and Reflection Profiles

3.1 Reflection Profiles

3.1.1 Ukraine margin

Between 75 and 85 mbsl (**Figure 1-2**), lies a belt that consists of 1-2 km-wide wide ridges and tens of km-long belts that consist of 100 to 200 m wide ridges with heights of 1 to 5 m. The ridges have both linear and barchan shapes that have been interpreted as coastal dunes (Ryan et al., 1997; Naudts et al., 2006). Those dunes located at ~92 mbsl along the crest of an incline are interpreted to have been proximal to a paleo-shoreline (Ryan et al., 1997). A shelf-wide erosion surface, α (Aksu et al., 2002a), truncates the splay of filled channel terminations located below the dunes, landward of the paleo-shoreface feature. Seaward of it, a smooth ramp delineates a former shelf-edge pro-delta and where the erosion surface α truncates seaward dipping reflectors below it. A thin (1 to 2 m thick) sedimentary drape rests on the α erosion surface and is present everywhere across the shelf. This drape thins seaward and is composed of two internal layers.

Those cores retrieved landward (i.e., AK93-03-2 at 49 m and AK93-05 at 44 m) of the paleoshoreline, penetrated the drape and recovered sediments belonging to the drape and the underlying coquina deposit below it. The youngest sediment is dated to a period encompassing after the basin's connection with the Mediterranean (i.e., *Dreissena polymorpha* with a ^{14}C date of 8.33 kyr ^{14}C years in the coquina of AK93-03-2). Those cores retrieved from the top of dunes often sample material belonging to the dune and those cores retrieved from the top of an impenetrable hardground, sometimes retrieve the material of the eroded substrate in core catchers, that component of the coring device that scoops up material from the base of the cores. Those cores retrieved seaward of the paleoshoreface (i.e., AK93-08 at 99 m, AK93-10 at 106 m), penetrated below the coquina and the erosion surface and sampled sediment belonging to the set of seaward dipping reflectors (**Figure 1-2**). The sediment immediately below the erosion surface dates to the beginning of the Younger Dryas stadial at this water depth.

3.1.2 Romanian margin

Chirp profile B008 from the middle Romanian shelf and upper slope (**Figure 1-3**) spreads from 125 to 300 mbsl. The thin, 1 to 2 m thick, surficial sedimentary drape that covers the Ukrainian Shelf also covers the Romanian inner and middle shelf and upper slope (Popescu, 2008; Lericolais et al., 2009). On the outer shelf, between 135 and 200 mbsl, this drape becomes very thin. This observation is confirmed by poor recovery of this drape in BLKS98-06 at 135 mbsl, BLKS98-07 at 163 mbsl, BLKS98-08 at 186 mbsl, and 09-SG-13 at 200 mbsl. The drape is completely absent in BLKS98-07 and composes only 11 cm in 09-SG-13. On the slope, the sediments of equivalent age to the drape progressively thickens to >0.5 m. This observation is confirmed by BLKS98-09 at 240 mbsl and BLKS98-10 at 378 mbsl. A thin coquina and a

period of non-deposition and/or erosion is present between sediment belonging to Younger Dryas and the mid/late-Holocene in 09-SG-13. This feature of erosion or non-deposition between the Younger Dryas and the Holocene is also found from the sedimentary strata on the outer shelf as interpreted from BLKS98-06 and BLKS98-07. Landward of the paleoshoreline, a chirp profile collected from the Assemblage-1 cruise in 2004 reveals buried river channels (**Figure 1-4**) that were once filled, then partly eroded and upon which a uniform sedimentary drape was subsequently deposited.

3.1.3 Bulgarian margin

Chirp profile BlaSON2-B2ch049 (**Figure 1-5**) from the Bulgarian middle and outer shelf off Cape Emine extends from 30 to 170 mbsl. Several of the distinguishing features of the Ukrainian and Romanian margins (i.e., the α erosion surface, the subsequent coquina deposit, and, and the surficial drape) are also observed on the Bulgarian margin. The erosion surface is highlighted red. A row of ridges at 110 mbsl is observed that is similar to those interpreted as subaerial coastal dunes on Ukraine (Ryan et al., 1997) and Romanian (Lericolais et al., 2007) margins. These dunes rest on the α erosion surface that truncates clinoforms composed of topset, foreset, and bottomset beds. Two cores, AKAD09-19 and AKAD01-AB18, retrieved sediment belonging to these dunes, consisting of pulverized shells, quartz sand, sand-sized rounded and frosted lithic fragments. This dune material is mud free.

The chirp profile B2ch049 and the corresponding cores recovered along it are also located off Cape Emine (**Figure 1-5**). Profile B2ch049 crosses the inferred paleoshoreline at 95 mbsl. The cores have been projected upon two boomer-source reflection profiles (XXIV and

XV) obtained in 1998 with the Bulgarian navy ship Hydrograph (Fig. 7) (Genov and Slavova, 2004).

The dunes rest on the foreset beds and are separated from them by the α-erosion surface. Landward of the dune, the gently-seaward-dipping older strata beneath the foreset and bottomset beds are also truncated by the α-erosion surface. Cores AKAD01-AB17 and AKAD09-28 on Cape Emine sample the bottomset beds (**Figure 1-10**). The youngest bottomset beds are post-glacial as confirmed by ^{14}C dates of AKAD01-AB17 and AKAD09-28 at 126 mbsl.

The two coquina, observed in strata seaward of the paleshoreline, are interpreted as indications of the same brief hiatuses observed on the Ukrainain and Romanian margins. The sediment below the oldest coquina was observed to be very stiff during the on-board examination with a water content <15 %. The dry mud on the split core revealed desiccation crack, filled and then covered with a 0.12 m thick deposit of pulverized and bleached shell debris and fragments of wood. The dry sediment is red-colored and dated to 14.15 kyr ^{14}C years. The red-color is unique to sediments deposited during the meltwater event at HE1 and is also observed on Ukrainian and Romanian margins (Major et al., 2002; Bahr et al., 2006; Major et al., 2006; Soulet et al., 2011a). The sedimentary deposit that sits in between the two coquina deposits is composed of light gray mud with *Dreissena r*. mollusks, often articulated, that are preserved in sandy lenses. It is dated to Younger Dryas from the ^{14}C, $\delta^{18}O$, and $\delta^{13}C$ of the *Dreissena r*. The surficial drape recovered at this depth is 0.25 m thick.

3.1.4 NW Turkish margin

Chirp profile B2ch007 from the outermost Turkish shelf and upper slope (**Figure 1-11**) extends from 125 to 300 mbsl. Similar to the surficial drape observed on the Ukrainian,

Romanian, and Bulgarian margins, this drape is also observed in this chirp profile. It likewise, thins seaward. There are a number of features unique to this profile not found on other margins. First, a highly reflective deposit located between 150 and 125 mbsl, chaotically bedded and belonging to shelf branching channels. This deposit is thought to have formed during inflow of Mediterranean saltwater from the Bosporus (Flood et al., 2009; Hiscott et al., 2013; Ryan et al., 2013). Core MedEX05-13 at 118 mbsl, recovered sediment belonging to the seaward-dipping reflectors, identified as soft shale, indurated mud. Radiocarbon measurements from *Dreissena r.* retrieved from these sediments are >50 kyr ^{14}C. This strata is separated from the surficial drape by an α erosion surface and a 0.15 m thick mud-free coquina deposit composed of abraded, polished, bleached shells ^{14}C dated largely to the last glacial period and on occasion, to Younger Dryas.

Another feature unique to the bathymetry offshore of the Bosporus Strait is the near-absence of oblique clinforms below the α-erosion surface that are omni-present on the Ukrainian, Romanian, and Bulgarian margins seaward of the paleoshoreline (Aksu et al., 2002a). Core MAR98-04 and corresponding chirp profile B2ch013 (**Figure 1-14**) is the only available evidence from this part of the Turkish margin of sediments that belong to the foreset and bottomsets dating to the last glacial period.

3.2 Ukrainian limans

Sediment deposition history of the Dniprovs'ko-Buhs'lyi Liman (**Figure 1-15**) in northern Black Sea at the tributary of Dniepr, records a series of downcutting and deposition events from the last glacial through the Holocene (Naukova, 1984). Unconformities separate each successive layer of deposition. The first sediment that lies upon incised bedrock, identified

as of Neogene age, is interpreted as belonging to fluvial deposits and dates to 17.76±0.20 kyr ^{14}C. The two successive sediment deposits are interpreted as river flood deposits and identified as clay with *Monodacna* and *Dreissena sp*., respectively. Holocene deposits comprise the topmost deposits in the liman and date from 7.52±0.12 kyr ^{14}C onwards.

3.3 Radiocarbon calibrated Wheeler diagrams

Wheeler diagrams constructed for the three Black Sea shelves illustrate changes in sedimentation across the shelf area (**Figure 1-14**). Cores retrieved from the Ukrainian shelf do not reach below that sediment belonging to the meltwater event. Sediment belonging to the Old Black Sea and lower New Black Sea is non-existent at depths near 160 mbsl. Sediment belonging to Younger Dryas and the very beginning of the Preboreal are constrained to depths from 95 mbsl to 140 mbsl. Cores retrieved from the Romanian shelf cover periods belonging from the glacial to the New Black Sea. At 160 mbsl, similar to that feature identified in the wheeler diagram of the Ukrainian shelf, the sediment belonging to Unit 2 and Unit 1 thins out. Below 160 mbsl but above the paleoshoreline, sediment belonging to Younger Dryas and the very beginning of Preboreal, is present. In cores located between 200 and 95 mbsl below the unconformity, identified to have formed during the Bølling/Allerød warming, lies sediment belonging to Older Dryas and older. Cores retrieved from the Bulgarian margin record similar features described for Ukrainian and Romanian margins. There is no sediment of glacial age found, with the exception of dune formation and channel fills, landward of the paleoshoreline.

3.4 ^{14}C reservoir of Black Sea water

The ^{14}C age of the water is often different from the ^{14}C age of the atmosphere due to the hard-water effect in which older ^{14}C age material is dissolved in the lake water and gives an apparent older ^{14}C age offset of the water, different from the ^{14}C age of the atmosphere (Siani et al., 2000). The ^{14}C age of the water during the glacial period increased from 40 kyr BP until the onset of the meltwater event at 16.35 kyr BP (**Figure 1-15**). Using the derived calendar ages from Nowaczyk et al., (2013) the ^{14}C age of the surface water was low, possibly even zero, from 40 to 30 kyr BP. From 29.56 to 17.00 kyr BP, the ^{14}C age of the surface water rose from 1,150 to 2,247 ^{14}C years. At 14.56 kyr BP, the ^{14}C age of surface water is measured to be 1,700 ^{14}C years. This measurement is derived from the comparison of ^{14}C ages of wood and mollusk in the same sediment interval. Using the alignment between the stable isotope records of Sofular Cave and surface Black Sea water, the ^{14}C age prior to the onset of the Meltwater event is 1,956 ^{14}C years at 16.35 kyr BP. The adopted ^{14}C reservoir age for the glacial period is taken as a compromise between the ^{14}C age derived by (Soulet et al., 2013), and that described above (dashed red line in **Figure 1-15**).

3.5 Sedimentation rates

Sedimentation rates during the glacial period are higher relative to those in the post-connection Holocene period (**Figure 1-16**) but smaller relative to the deglacial period (i.e., meltwater to connection of the Black Sea with the Mediterranean). During the glacial period, sedimentation rates in all cores range from ~10 to 200 cm/kyr whereas during Units 1 and 2 are <50 cm/kyr. On the outer shelf, cores located landward of the shelf break but seaward of the paleoshoreline (AKAD09-28, AKAD09-30, AKAD11-01, and AKAD11-07), the sedimentation

rate ranges from 7 to 19 cm/kyr. Sedimentation rates from cores on the slope, MD04-2790 and 09-SG-13, are calculated to be 104 and 18 cm/kyr, respectively.

3.6 $\delta^{18}O$ and $\delta^{13}C$

The $\delta^{18}O$ of the stalagmites in the Sofular Cave ranges from -13 to -11.5 ‰ in the period spanning from 50 to 16.35 kyr BP (**Figure 1-17a**). Four Heinrich events (HE5 to HE2) and 10 D/O events (D/O13 to D/O03) are evident. The $\delta^{18}O$ decreases by ~0.5 ‰ during the Heinrich events and increases by ~0.5 to 1 ‰ during the D/O events. The increase during the D/O events is more pronounced and dramatic than the decrease during the Heinrich events. Four Heinrich events (5-2) and 10 D/O events (13-3) are noted. A period without stalagmite growth begins at 24.115 kyr BP and continues to 21.645 kyr BP.

The $\delta^{13}C$ of the Sofular Cave stalagmites ranges from -9.5 to -7.5 ‰ in the period spanning from 50 to 16.35 kyr BP (**Figure 1-17b**). The $\delta^{13}C$ increases by 1 to 2 ‰ during the Heinrich events and decreases by 0.5 to 4 ‰ during D/O events. The most dramatic HE to D/O transition occurs from HE4 to D/O 8 where the $\delta^{13}C$ drops from -6 to -10 ‰. The $\delta^{13}C$ of the lacustrine mollusks also varies by similar amplitides, 0.5 to 5 ‰, during the same time period.

3.7 $^{87}Sr/^{86}Sr$

The $^{87}Sr/^{86}Sr$ in the mollusk shells from the Bl ack Sea shows little variation from 50 to 16.35 kyr BP with a consistent value of ~0.7088 (**Figure 1-18**). The standard deviation of the variability during the glacial is 0.00018, a value that is barely larger than the error associated with the measurements (<0.0015). Mollusks from the Sea of Marmara have the same average

$^{87}Sr/^{86}Sr$ of 0.7088 but the variability is much greater than the error associated with the measurements.

Seawater (currently $^{87}Sr/^{86}Sr$ = 0.709155 for the global ocean (Henderson et al., 1994); 0.709157 for the Aegean Sea; 0.709150 for the Marmara Sea) has a significantly different Sr isotope ratio from the average river water feeding the Black Sea ($^{87}Sr/^{86}Sr$ = ~0.7088) (Palmer and Edmond, 1989). The average $^{87}Sr/^{86}Sr$ of mollusks in the marine sediments of the Black Sea is 0.709133 (±0.0002) indicating a slightly greater influence of riverine Sr than the simple 1:1 mixture prediction. The $^{87}Sr/^{86}Sr$ for Danube, Dniepr, Don, and Sakaraya are 0.7089, 0.7085, 0.7085, and 0.7089, respectively.

3.8 Logging

Water content (%) varies from 25 to 40 % and acoustic impedance covaries from 2500 to 500 $10^3 kg^{-2}s^{-1}$ in KN134-GC01 (**Figure 1-19**). There are three occurrences of decreased water content to below 30% during the glacial period. These periods are also characterized by increased magnetic susceptibility, wet bulk density, and partially, concentration of coarse fraction. Magnetic susceptibility is high relative to the rest of the glacial period, especially at 220 cm in the core. There is also a slight increase at 230 cm. Wet bulk density increases from 1.05 g/cc to 1.42 g/cc at 220 cm and 1.22 g/cc at 230 cm. Coarse fraction increases above 0 only at 220 cm in the core.

3.8 XRF

There are two intervals that are characterized by anomalous XRF-element distribution in the glacial period (180 to 245 cm) recovered in KN134-GC01 and are labeled K1 and K2 that

occur at 200 and 223 cm (**Figure 1-20**). Both are characterized by increased Ti/Ca, increased Zr/Rb, decreased Mn, and decreased Fe relative to the rest of the glacial record. K is depressed in K1 but not K2. The anomalies identified in K1 are also identified in the core photograph (**Figure 1-21**) at 223 cm but the anomalies identified in K2 are not present. At 223 cm, there is a large and distinct sand/silt bed, similar to those that are identified in this core during the deposition of the meltwater red layers (70 to 180 cm in KN134-GC01). There are no apparent changes in S, Mo, and Se in this deposit. The geochemical anomalies in the glacial silt layer are not identical to those in the red layers (i.e., Fe is increased in the meltwater silt deposits but it is decreased in the glacial silt deposit).

There are three intervals that are characterized by anomalous XRF-element distribution in the glacial record (245 to 400 cm) in AKAD11-17 and are labeled A1, A2, and A3 that occur at 342, 303, and 246 cm (**Figure 1-22**). Although there are no clear increases in Ti/Ca in these layers, the concentration of Ti relative to Ca does increase. The intervals are also characterized by increased Zr/Rb, decreased Mn, decreased, decreased K, prominent increases in S, Fe, and Co, and decreases in Zn. Certain anomalies in these intervals relative to the rest of the record are significantly larger than others. All of these geochemical signatures with the exception of changes in Mn and S are identical to those observed in the red layer meltwater events in KN134-GC01. Changes in S are completely absent during the deposition of the red layers and are also not observed in the glacial record of KN134-GC01. The pronounced increases in S and Fe occur in the same locations as do black bands in the core, identified as monosulfides (**Figure 1-23**).

3.9 Observation of anomalies in outer shelf cores

Cores from the outer shelf preserve a series of interesting features which include numerous coquina, pebbles, red sediment deposits, and quartz, amphibole, and quartz minerals (**Figure 1-24** and Table 1). Two coquina are identified in AKAD11-01 at 125 mbsl dated at 31.524 and 35.773 kyr BP, four coquina are identified in AKAD11-05 at 125 mbsl dated at 33.841, 34.618, 35.901, 37.274 kyr BP, two coquina are identified in AKAD11-07 at 153 mbsl dated at 26.295 and 23.198 kyr BP, one coquina is identified in AKAD09-28 at 18.041 kyr BP, and five coquina are identified at a range of 22.273 to 15.576 kyr BP. A transition to red colored sediment is noted in AKAD11-07 dated to 33.341 kyr BP, pebbles are noted in AKAD09-28 at 21.964 kyr BP, and minerals such as amphibole and quartz are observed in AKAD11-01 at 16.569 and 19.840 kyr BP. The coquina in AKAD11-01 at 324.5 cm in the core is very similar to those identified during the deglacial period in all of the cores of the outer shelf landward of the paleoshoreline that formed following the Bølling/Allerød and Preboreal warming events.

4. Discussion

The compilation of reflection profiles, core profiles, and corresponding Wheeler Diagrams for Ukrainian, Romanian, and Bulgarian shelves indicate an absence of glacial-age lacustrine sediment above the elevation of the paleoshoreline at 95 mbsl. The only recognizable and sampled sediments of glacial age at higher elevations belong to the fill of the subsurface fluvial channels. These channels extend across the shelf from today's coastal limans to the vicinity of the paleoshoreline (Ryan et al., 1997; Naudts et al., 2006; Popescu, 2008). These observations are consistent with a lake surface at the level of the observed shoreline but not shallower.

Similar ostracode $\delta^{18}O$ and $^{87}Sr/^{86}Sr$ measurements and their temporal variations in both the Black Sea and Sea of Marmara indicate that the Black Sea's glacial-age lake expelled its excess freshwater to the downstream Marmara lake more or less continuously during the last glacial period. Hence, the floor of the Bosporus Strait, then a river a valley, must have been at its current bedrock elevation. Previously, Ross and Degens, (1974) and Lane-Serff et al., (1997) argued that the lake was continuously outflowing whereas Aksu et al., (2002a) argued that the observation of the lake at 100 mbsl, a depth below the modern date of the Bosporus sill, suggested the lake was regressed and at a lowstand. A lake level at the bedrock sill and outflowing is consistent with all of the observations leading to these arguments. This interpretation was earlier also proposed by Nicholas and Chivas, (2014). The difference between the depth of the inferred paleoshoreline and the bedrock of the Bosporus sill is attributed to the removed weight load of the water during the glacial period, which would have lifted the Black Sea basin relative to its modern depth.

The sedimentation rates on the outer shelf, seaward of the paleoshoreline, basin, and slope were higher relative to those in the Holocene. This suggests a closer proximity of any one location in the Black Sea to the source of the sediment, consistent with a shoreline near the shelf edge and/or higher river activity. Additional evidence for high river activity comes from cores BLKS9830 and BLKS9834, that were cored from depressions in the inner Bulgarian shelf. Sediments below the Holocene coquina date to the glacial periods indicating active river discharge from the glacial-age Danube.

Contrary to the environments from which BLKS9830 and BLKS9834 cores were retrieved, cores such as AKAD09-27 and AKAD11-19 were retrieved from locations of pre-existing dunes. Lericolais, (2001) previously noted these features above the 100 mbsl water

depth. Foredunes and parallel dunes, beach ridges and cheniers are long, linear, ridge-forming formations representing the locations of ancient shorelines (Meldahl, 1995). These occur on low-level relief coastal plains, standing with several meters of relief above their surroundings. Enclosed depressions like those in the surveyed corridor are characteristic of windy and arid environments (Shaw and Thomas, 1997). The cavities are eroded into the substrate by deflation processes, with the magnitude of excavation ultimately limited by the groundwater table (Laity, 1994).

If the level of the Bosporus sill was at 80 mbsl during the glacial period, a question arises, was it always at this elevation and if no, when was this elevation established? It is suggested that the depth of the sill during the Eemian interglacial was close to 10 mbsl (Shumilovskikh et al., 2013). A plausible explanation for this is that the in-filled sediment that built up and shallowed the sill during the previous lowstand was subsequently removed from the sill by persistent outflow from the Black Sea-Lake to the Marmara Sea-Lake. This occurred with the onset of glacial conditions during which river activity was high and the lake was in a positive hydrological balance.

During the period spreading 30 to 16.35 kyr BP, the ^{14}C reservoir age of the surface Black Sea water increased from ~0 to 2,500 ^{14}C years. This is potentially explained by establishment of permanent ice cover that prevented the communication of the Black Sea with the atmosphere. Svendsen et al., (2004) note that the front of the Scandinavian Ice Sheet moved 1000 km southwards during only 7,000 to 8,000 years from 26 kyr BP years to LGM. Lunkka et al., (2001) estimated that the ice sheet advanced more than 125 m per year. The expansion of the ice sheet at this period likely decreased the temperature everywhere in Europe. The period of its expansion is exactly the time period during which the ^{14}C age of the surface water increased.

Methane hydrates are present in many locations in the Black Sea today (Reitner et al., 2005; Schmale et al., 2005; Naudts et al., 2006). It is also plausible that the activity of methane hydrates was increased during this period as a result of lower lake level, leading to decreased stability of methane hydrates on the shelf and increased methane gas with an old radiocarbon reservoir dissolving in the water column. It is also plausible that it was both of these mechanisms that were involved in increasing the ^{14}C reservoir age of the surface water. The establishment of ice cover and subsequent discharges is supported by evidence of dropstones and ice rafted debris (IRD) dated to this time period. IRD in the North Atlantic is associated with binge/purge oscillations of the Laurentide Ice Sheet (Alley and MacAyel, 1994). It it is possible that the IRD found in the Black Sea could also record oscillations and ice berg discharge in the Black Sea-lake.

It is likely that the gradual decrease of $\delta^{18}O$ in the shells from ~-5.5 ‰ to -6.5 ‰ during the passage from 50 to 16.35 kyr BP represents an evolving composition of $\delta^{18}O$ to more negative values in atmospheric precipitation (Major et al., 2006). The $\delta^{18}O$ composition in shells from Marmara Sea-Lake follows an identical trend. However, there is a brief period around 22 kyr BP when the $\delta^{18}O$ in Marmara Sea shells increases rather than decreases. A departure at the same time is observed in the $^{87}Sr/^{86}Sr$ composition between both lakes and is coincident with the halt in the growth of stalagmites in the Sofular Cave from 24.115 kyr to 21.645 kyr BP. If the gap in stalagmite growth, caused by a cessation of moisture percolating through the strata above the cave, indicates a seal by a cover of permafrost in northern Turkey, this gap corresponds to an especially cold interval coincident with the climax of HE2. Sediments deposited at this time on the Black Sea outermost shelf host gravel-sized pebbles that are rounded and flattened and similar in shape to beach gravel. Such single pebbles in the absence of sand have an appearance

of drop stones from melting ice. Thus there may have been a brief arrest of outflow of the Black Sea-Lake water to the Marmara Sea-Lake during this extreme cold period.

Two of the specimens, identified as belonging to a *Didacna* and a *Glycemeris*, have an enriched $^{87}Sr/^{86}Sr$ composition, suggesting it is possible they lived in a marine rather than a lacustrine environment. These polished, abraded, and stained specimens are dated to 33.90 and 30.60 kyr ^{14}C, respectively. The Black Sea was not marine during this period as there are a number of intact *Dreissena rostriformis* specimens of similar ages (e.g., in cores AKAD11-01 and AKAD11-05) whose very negative $\delta^{18}O$ composition indicates the Black Sea-Lake was fresh throughout that entire time. The conflicting ^{14}C age is ascribed to post-depositional incorporation of young ^{14}C into the shell lattice. This type of diagenesis is previously reported in Busschers et al., (2014). Comparing the $^{87}Sr/^{86}Sr$ composition of these mollusks to the global seawater in the past 30 Myr (McArthur et al., 2001) gives an approximate age to these mollusks of 6 and 4 Myr, respectively. This interpretation is consistent with their $\delta^{18}O$ composition when the global ocean $\delta^{18}O$ was depressed relative to the modern global ocean $\delta^{18}O$ as much less water was locked up in ice sheets during that period. These mollusks, *Didacna* and *Glycemeris* were additionally identified as belonging to Middle Pleistocene and Karangatian[1] (Wesselingh, 2015).

The $\delta^{13}C$ of the carbonate precipitated in Sofular Cave is similar to the $\delta^{18}O$ precipitated in Hulu Cave, a signal that is interpreted to respond to East Asian monsoon cycles. It is possible that the millennial changes in monsoon activity lead to changes in moisture and temperature distribution that altered the ratio of C_3 to C_4 plants. The $\delta^{13}C$ of the dissolved carbonate that is

[1] Karangatian age: 130,000 to 30,000, Eeimian Marine Isoptope Stage 5 (Shumilovskikh et al., 2012).

precipitated in Sofular Cave also is fed into the Black Sea-Lake, giving the surface water an identical $\delta^{13}C$ signature. The $\delta^{13}C$ of the bottom water of the Black Sea does not record the surface or the Sofular Cave but instead, reflects the reminiralization of organic matter. The oscillation of the $\delta^{13}C$ responds to changes in D/O events. These climate oscillations are abrupt warming periods in the Northern Hemisphere. The multiple coquina in the cores on the outer shelf are possibly regressions of the lake as a response to D/O events. It was previously shown that the Black Sea-Lake regresses during warming events, Bølling/Allerød and Preboreal (Major et al., 2006) so periods of minor regression during interstadial D/O events are also possible.

Analysis of sedimentological and geochemical parameters during the glacial period suggests a relatively stable climate regime with little significant variability (Bahr et al., 2005; Bahr et al., 2006; Major et al., 2006). In addition to possible regressions of the Black-Sea Lake during this period and a decreased/arrested outflow to the Sea of Marmara during LGM, a record of turbiditic processes, such as from KN134-GC01, suggests that possible increased river discharges, such as that recorded near the timing of HE1 in form of red layers, also occurred. These increased discharges of river water may have occurred during other HE events. A conclusion regarding these events would require more detailed dating of glacial sediments.

The formation of monosulfide layers in cores such as AKAD11-17 is attributed to changes in sedimentation rates. The concentration of sulfate in the bottom waters of Black Sea-lake was low at the time of the deposition of the dark layers (Berner, 1974). A high sedimentation rate would lead to a decreased bacterial sulfate reduction and production of H_2S, leading to complete removal of sulfate from the interstital waters and limiting the elemental sulfur necessary for the metamorphosis of monosulfide into pyrite. The pyrite is observed in the gray sediments that are not black in color. The concretion and formation of iron sulfide crystals

is attributed to the migration of iron and sulfur within anaerobic sediments early during diagenesis (Berner, 1969). The changes in sedimentation rate likely occurred during either increased river activity or short regressions of the lake level as a response to global climate variability in the form of Heinrich and D/O events.

5. Conclusions

During the last glacial period, 50 to 16.35 kyr BP, an interval of time that is recorded in ^{14}C dates and geochemical proxies (XRF element concentrations, $\delta^{18}O$, $\delta^{13}C$, and $^{87}Sr/^{86}Sr$ of mollusks and ostracodes), show that the Black Sea-Lake level remained pinned at the elevation of its ancient paleoshoreline. The observation of glacial-age lacustrine sediments everywhere on the Black Sea shelf seaward of the shoreline but complete absence landward suggests the lake surface remained at this level throughout the last glacial period. The lake surface would only stay at a constant elevation if its surface was pinned there by its outlet, spillway, in this case a stream in the Bosporus Strait flowing to the Sea of Marmara.

Rain and river water continuously fed the Black Sea-Lake and kept not only its isotopic composition largely unchanged at a $\delta^{18}O$ of -6.5 ‰ and $^{87}Sr/^{86}Sr$ of 0.7088, but also the composition of the downstream Marmara Sea-Lake. However, around 22 kyr BP, the isotopic composition of the two lakes diverged. The divergence is coincident with a gap in the growth of stalagmites in the Sofular cave in northern Turkey. The cessation of precipitation commenced during the later part of HE2 and occurred at a time when drop stones with the shape of beach gravel appear in the sediments on the outermost Black Sea shelf. Extreme cold accounts for the cessation of stalagmite growth by the arrival of permafrost in northern Turkey and can account for ice-rafted drop stones.

References

Aksu, A. E., R. N. Hiscott, M. A. Kaminski, P. J. Mudie, H. Gillespie, T. Abrajano and D. Yasar, 2002a. Last glacial-Holocene paleoceanography of the Black Sea and Marmara Sea: stable isotopic, foraminiferal and coccolith evidence. Marine Geology 190, 119-149.

Algan, O., M. Ergin, S. Keskin, E. Gokasan, B. Alpar, E. Kirci and D. Ongan, 2007. The sea level changes during the late Pleistocene-Holocene on the southern shelves of the Black Sea. In: V. Yanko-Hombach, A. S. Gilbert, N. Panin and P. M. Dolukhanov (Eds.), The Black Sea Flood Question: Changes in Coastline, Climate, and Human Settlement. Dordrecht, The Netherlands, Springer.

Algan, O., E. Gokasan, C. Gazioglu, Z. Y. Yucel, B. Alpar, C. Guneysu, E. Kirci, S. DEmirel and D. Ongan, 2002. A high-resolution seismic study in Sakarya delta and submarine canyon, southern Black Sea shelf. Cont. Shelf Res. 22, 1511-1527.

Alley, R. B. and D. R. MacAyel, 1994. Ice-rafted debris associated with binge/purge oscillations of the Laurentide Ice Sheet. Paleoceanography 9, 503-511.

Apakidze, A. M. and A. A. Burchuladze, 1987. Radiouglerodnoe datirovanie arkheologicheskikh i paleobotanicheskikh abraztsov Gruzii (Radiocarbon dating of archaeological and paleobotanical samples in Georgia). In (Eds.). Metsniereba, Tbilisi, Georgia.

Arkhangel'skiy, A. D. and N. M. Strakhov, 1938. Geological structure and history of the evolution of the Black Sea. Izv. Akad. Nauk SSSR 10, 3-104.

Badertscher, S., D. Fleitmann, H. Cheng, R. L. Edwards, O. M. Göktürk, A. Zumbühl, M. Leuenberger and O. Tüysüz, 2011. Pleistocene water intrusions from the Mediterranean and Caspian seas into the Black Sea. Nat. Geosci. 4, 236-239.

Bahr, A., H. Arz, F. Lamy and G. Wefer, 2006. Late glacial to Holocene paleoenvironmental evolution of the Black Sea, reconstructed with stable oxygen isotope records obtained on ostracod shells. Earth Planet. Sc. Lett. 241, 863-875.

Bahr, A., F. Lamy, H. Arz, H. Kuhlmann and G. Wefer, 2005. Late glacial to Holocene climate and sedimentation history in the NW Black Sea. Marine Geology 214, 309-322.

Bailey, T. R., J. M. McArthur, H. Prince and M. F. Thirwall, 2000. Dissolution methods for strontium isotope stratigraphy: Whole rock analysis. Chemical Geology 167, 313-319.

Berner, R., 1974. Iron sulfides in Pleistocene deep Black Sea sediments and their paleo-oceanographic significance. In: E. T. Degens and D. A. Ross (Eds.), The Black Sea-Geology, Chemistry and Biology, Am. Assoc. Petrol. Geol. Memoir 20**,** 523-531.

Berner, R. A., 1969. Migration of iron and sulfur within anaerobic sediments during early diagenesis. American Journal of Science 267, 19-42.

Bukry, D., S. A. King, M. K. Horn and F. T. Manheim, 1970. Geological Significance of Coccoliths in Fine-grained Carbonate Bands of Postglacial Black Sea Sediments. Nature 226, 156-158.

Busschers, F. S., F. P. Wesselingh, R. H. Kars, V. Verslujis-Helder, J. Wallinga, J. H. A. Bosch, J. Timmer, K. Nierop, G,J.;, T. Meijer, F. P. M. Bunnik and H. De Wolf,2014. Radiocarbon dating of late Pleistocene marine shells from the Southern North Sea. Radiocarbon 56, 1151-1166.

Chepalyga, A. L., 1984. Inland sea basins. In: A. A. Velichko, H. E. J. Wright and W. Barnosky-Cathy (Eds.), Late Quaternary environments of the Soviet Union. Mineapolis, MN, United States, Univ. Minn. Press.,229-247.

Cohen, D. and W. B. F. Ryan, 2011. Black Sea low stands during the Holocene and Pleistocene and reconnection with the global ocean, Columbia University.

Coleman, D. F. and R. D. Ballard, 2007. Southern and Western Black Sea-Implications for Inundated Prehistoric Archaeological Sites. In: V. Yanko-Hombach, A. S. Gilbert, N. Panin and P. M. Dolukhanov (Eds.), Black Sea Flood Question: Changes in Coastline, Climate, and Human Settlement. Netherlands, Springer, 671-696.

Demirbag, E., E. Gökasan, F. Y. Oktay, M. Simsek and H. Yüce, 1999. The last sea level changes in the Black Sea: evidence from the seismic data. Marine Geology 157, 249-265.

Deuser, W. G., 1972. Late-Pleistocene and Holocene history of the Black Sea as indicated by stable isotope studies. Jour. Geophys. Res. 77, 1071-1077.

Deuser, W. G., 1972. Late-Pleistocene and Holocene history of the Black Sea as indicated by stable-isotope studies. Journal of Geophysical Research 77, 1071-1077.

Dypvik, H. and N. B. Harris, 2001. Geochemical facies analysis of fine-grained siliclastics using Th/U, Zr/Rb, and (Zr+Rb)/Sr ratios. Chemical Geology 181, 131-146.

Fedorov, P. V., 1963. Statigrapfiya Chetvertichnikh otlozhenii Krymskogo-Kavkazkogo poberezhia nekotoroye voprosy geologicheskoy istorii Chernogo morya (Statigraphy of Quaternary sediments on the coast of the Crimea and Caucasus and some problems connected with the geological history of the Black Sea). Skad. Nauk SSSR Geol. Trudy 1, 159.

Flood, R. D., R. N. Hiscott and A. E. Aksu, 2009. Morphology and evolution of an anastomosed channel network where saline underflow enters the Black Sea. Sedimentology 56, 807-839.

Genov, I. D., 2004b. Way and time of swell formation near the Bulgarian Black Sea shelf. CR. Acad. Bulg. Sci. 57, 95-98.

Genov, I. D. and K. R. Slavova, 2004. Chronostatigraphy scheme correlation of Neoeuxine and Holocene sediments of Black Sea deepwater and shelf Review of the Bulgarian Geological Society 65, 25-35.

Görür, N., M. N. Çagatay, Ö. Emre, B. Alpar, M. Sakinç, Y. Islamoğlu, O. Algan, T. Erkal, M. Keçer, R. Akkök and G. Karlik, 2001. Is the abrupt drowning of the Black Sea shelf at 7150 yr BP a myth? Mar. Geol. 176, 65-73.

Henderson, G. M., D. J. Martel, R. K. O'Nions and N. J. Shackleton, 1994. Evolution of seawater Sr-87/Sr-86 over the last 400-ka - the absence of glacial interglacial cycles. Earth and Planetary Science Letters 128.

Hiscott, R. N., A. E. Aksu, R. D. Flood, V. Kostylev and D. Yaşar, 2013. Widespread overspill from a saline density-current channel and its interaction with topography on the south-west Black Sea shelf. Sedimentology 60, 1639-1667.

Ivanova, E. V., I. O. Murdmaa, A. L. Chepalyga, T. M. Cronin, I. V. Pasechnik, O. V. Levchenko, H. S.S, A. V. Manushkina and E.A.Platonova, 2007. Holocene sea-level oscillations and environmental changes on the Eastern Black Sea shelf. Palaeogeogr. Palaeoclimatol. Palaeoecol. 246, 228-259.

Kaplin, P. A. and F. A. Shcherbakov, 1986. Reconstructions of paleogeographic environments on the shelf during the late Quaternary time. Oceanology 26, 736-738.

Kenna, T. C., F. O. Nitsche, M. M. Herron, B. J. Maillouv, D. Peteet, S. Sritrairat, E. Sands and J. Baumgarten ,2011. Evaluation and Calibration of a Field Portable X-Ray Fluorescence Spectrometer for quantitative analysis of siliclastic soils and sediments. Journal of Analytic Atomic Spectrometry 26, 10.

Konikov, E., O. Likhodedova and G. Pedan, 2007. Paleogeographic reconstructions of sea-level change and coastline migration on the northwestern Black Sea shelf over the past 18kyr. Quatern. Int. 167-168, 49-60.

Kuprin, P. N., F. A. Scherbakov and I. I. Morgunov, 1974. Correlation, age and distribution of the postglacial continental terrace sediments of the Black Sea. Baltica 5, 241-249.

Kuprin, P. N. and V. M. Sorokin, 2007. On the post-glacial changes in the level of the Black Sea. In: V. Yanko-Hombach, A. Gilbert, N. Panin and P. Dolukhanov (Eds.), Black Sea Flood Question: Changes in Coastline, Climate, and Human Settlement. Netherlands, Springer**,** 205-220.

Kvasov, D. D., 1975. Late Quaternay History of Major Lakes and Inland Seas of Eastern Europe. Leningrad, Naula Press.

Kvasov, D. D. and A. I. Blazhchishin, 1978. The key to sources of the Pliocene and Pleistocene glaciation is at the bottom of the Barents Sea. Nature 273, 138-140.

Kwiecen, O., H. W. Arz, F. Lamy, S. Wulf, A. Bahr, U. Röhl and G. H. Haug, 2008. Estimated reservoir ages of the Black Sea since the Last Glacial. Radiocarbon 50, 99-118.

Laity, J. E., 1994. Landsforms of aeolian erosion. In: A. D. Abrahams and A. J. Parsons (Eds.), Geomorphology of Desert Environments. London, Chapman & Hall**,** 506-535.

Lane-Serff, G. F., E. J. Rohling, H. L. Bryden and H. Charnock, 1997. Post-glacial connection of the Black Sea to the Mediterranean and its relation to the timing of sapropel formation. Paleoceanography 12, 169-174.

Lericolais, G., 2001. La catastrophe du Bosphore. Pour la Science 284, 30-37.

Lericolais, G., C. Bulois, H. Gillet and F. Guichard, 2009. High frequency sea level fluctuations recorded in the Black Sea since the LGM. Global Planet Change 66, 65-75.

Lericolais, G., I. Popescu and F. Guichard, 2007. A Black Sea lowstand at 8500 yr BP indicated by a relict coastal dune system at a depth of 90 m below sea level. In: J. Harff, W. W. Hay and D. M. Tetzlaff (Eds.), Coastline Changes: Interrelation of Climate and Geological Processes., GSA Books; Allen Press, Inc. 426**,** 171-188.

Lericolais, G., I. Popescu, N. Panin, F. Guichard, S. M. Popescu and L. Manolakakis, 2003. Could the last rapid sea level rise of the Black Sea evidence by oceanographic surveys have been interpreted by Mankind? CIESM Workshop series, Fira, Santorni, Greece.

Lunkka, J. P., M. Saamisto, V. Gey, I. Demidov and V. Kiselova, 2001. Extent and age of the Last Glacial Maximum in the southeastern sector of the Scandinavian Ice Sheet. Global and Planetary Change 31, 407-425.

Major, C., S. Goldstein, W. Ryan, G. Lericolais, A. M. Piotrowski and I. Hajdas, 2006. The co-evolution of Black Sea level and composition through the last deglaciation and its paleoclimatic significance. Quatern. Sci. Rev. 25, 2031-2047.

Major, C. O., W. B. F. Ryan, G. Lericolais and I. Hajdas, 2002. Constraints on Black Sea outflow to the Sea of Marmara during the last glacial-interglacial transition. Marine Geology 190, 19-34.

Manheim, F. T. and P. Stoffers, 1969. Abstracts of the Annual Meetings of the Geological Society of America, 141.

McArthur, J. M., R. J. Howarth and T. R. Bailey, 2001. Strontium isotiope statigraphy: LOWESS Version 3: best fit to the marine Sr-isotope curve for 0-509 Ma and accompanying look-up table for deriving numerical age. The Journal of Geology 109, 155-170.

Meldahl, K. H., 1995. Pleistocene shoreline ridges from tide-dominated and wave-dominated coasts: Northern Gulf of California and western Baja California, Mexico. Marine Geology 123, 61-72.

Milliman, J. D. and K. O. Emery, 1968. Sea levels during the past 35,000 years. Science 162, 1121-1123.

Mortlock, R., 2010. Description of stable isotope analysis at the Department of Earth and Planetary Sciences.

Naudts, L., J. Greinert, Y. Artemov, P. Staelens, J. Poort, P. V. Rensbergen and M. De Batist,2006. Geological and morphological setting of 2778 methane seeps in the Dnepr paleodelta, northwestern Black Sea. Marine Geology 227, 177-199.

Naudts, L., J. Greinert, Y. Artemov, P. Staelens, J. Poort, P. Van Rensbergen and M. De Batist, 2006. Geological and morphological setting of 2778 methane seeps in the Dnepr paleo-delta, northwestern Black Sea. Marine Geology 227, 177-199.

Naukova, D., 1984. Radioulerodnoe datirovanie (Radiocarbon dating). In: Y. F. Shnyukov (Eds.), Geologiia shel'fa USSR**,** 38-40.

Nevesskaya, L. A., 1965. Late Quaternary bivalve mollusks of the Black Sea: Their systematics and ecology. Akad. Nauk SSSR Paleont. Inst. Trydy 105, 1-390.

Nicholas, W. A. and A. R. Chivas, 2014. Late Quaternary sea-level change on the Black Sea shelves. In: F. L. Chiocci and A. R. Chivas (Eds.), Continental Shelves of the World: Their Evolution During the Last Glacio-Eustatic Cycle. London, The Geological Society 41**,** 199-212.

Nicholas, W. A., A. R. Chivas, C. V. Murray-Wallace and D. Fink, 2011. Prompt transgression and gradual salinisation of the Black Sea during the early Holocene constrained by amino acid racemization and radiocarbon dating. Quatern. Sci. Rev. 30, 3769-3790.

Nowaczyk, N. R., U. Frank, J. Kind and H. W. Arz, 2013. A high-resolution paleointensity stack of the past 14 to 68 ka from Black Sea sediments. Earth and Planetary Science Letters 384, 1-16.

Okyar, M. and V. Ediger, 1999. Seismic evidence of shallow gas in the sediment on the shelf off Trabzon, southeastern Black Sea. Continental Shelf Research 19, 575-587.

Okyar, M., V. Ediger, M. Ergin and I. Erdemli,1994. Seismic stratigraphy of the southeastern Black Sea shelf from high resolution seismic records,. Marine Geology, 121, 213 -230.

Ostrovskiy, A. B., Y. A. Izmaylov, I. P. Balabanov, S. I. Skiba, N. G. Skryabina, S. A. Arslanov, N. A. Gey and N. I. Suprunova, 1977. New data on the paleohydrological regime of the Black Sea in the Upper Pleistocene and Holocene. In: P. A. Kaplin and F. A.

Shcherbakov (Eds.), Paleogeography and Deposits of the Pleistocene of the Southern Seas of the USSR. Moscow, Nauka Press**,** 131-141.

Ostrovskiy, A. B., Y. A. Izmaylov, A. P. Scheglo, K. A. Arslanov, V. Y. Shchelinskiy, I. P. Balabanov and S. I. Skiba, 1977. New data on the stratigraphy and geochronology of Pleistocene marine terraces of the Black Sea coast, Caucasus, and Kerch-Taman region. In: P. A. Kaplin and F. A. Shcherbakov (Eds.), Paleogeography and Deposits of the Pleistocene of the Southern Seas of the USSR. Moscow, Nauka Press**,** 61-69.

Palmer, M. R. and J. M. Edmond, 1989. The strontium budget of the modern ocean. Earth and Planetary Science Letters 92, 11-26.

Popescu, I., 2008. Processus sédimentaires récents dans l'éventail profond du Danube (Mer Noire). Geo-Eco-Mar 15-2.

Popescu, I., 2008. Processus sédimentaires récents dans l'éventail profond du Danube (Mer Noire). Geo-Eco-Marina Special Publication No. 2.

Popescu, I., G. Lericolais, N. Panin, Ç. N., A. Normand, C. Dinu, DC and E. Le Drezen, 2004. The Danube Submarine Canyon (Black Sea): morphology and sedimentary processes. Marine Geology 206, 249-265.

Popov, G. I., 1973. New data on the stratigraphy of Quaternary marine sediments of the Kerch Strait. Doklady Akademii Nauk SSSR 213, 84-86.

Reitner, J., J. Peckmann, M. Blumenberg, W. Michaelis, V. Reimer and V. Thiel,2005. Concretionary methane-seep carbonates and associated microbial communities in Black Sea sediments. Palaeogeography Palaeoclimatalogy Palaeoecology 227, 18-30.

Ross, D. and E. Degens, 1974. Recent Sediments of Black Sea, Sediments.

Ross, D. A. and E. T. Degens, 1974. Recent sediments of the Black Sea. In: E. T. Degens and D. A. Ross (Eds.), The Black Sea - Geology, Chemistry and Biology. Tulsa, Amer. Assoc. Petrol. Geol. Mem. 20**,** 183-199.

Ryan, W. B. F., 2007. Status of the Black Sea flood hypothesis. In: V. Yanko-Hombach, A. S. Gilbert, N. Panin and P. M. Dolukhanov (Eds.), The Black Sea Flood Question: Changes in Coastline, Climate, and Human Settlement. Dordrecht, The Netherlands, Springer**,** 63-88.

Ryan, W. B. F., W. C. Pitman, III, C. O. Major, K. Shimkus, V. Moskalenko, G. Jones, P. Dimitrov, N. Gorur, M. Sakinc and H. Yuce, 1997. An abrupt drowning of the Black Sea shelf. Marine Geology 138, 119-126.

Ryan, W. B. F., W. C. I. Pitman, C. O. Major, K. Shimkus, V. Moskalenko, G. A. Jones, P. Dimitrov, N. Gorür, M. Sakiniç and H. Yüce, 1997. An abrupt drowning of the Black Sea shelf at 7.5 kyr BP. GEO-ECO-MARINA, Special Publication 2/1997, 115-125.

Ryan, W. B. F., D. Vachtman, C. McHugh, M. N. Çagatay and Y. Mart, 2013. A channeled shelf fan initiated by flooding of the Black Sea. In: S. Gofredo and Z. Dubinsky (Eds.), The Mediterranean Sea: Its history and present challenges**,** 11-27.

Scherbakov, F. A., 1983. Continental margins in the Late Pleistocene and Holocene. Nauka, 123.

Scherbakov, F. A., P. N. Kuprin, L. I. Potapova, A. S. Polyakov, E. K. Zabelina and V. M. Sorokin, 1978. Sedimentation on the Continental Shelf of the Black Sea. Nauka, 211.

Schmale, O., J. Greinert and G. Rehder, 2005. Methane emission from high-intensity marine gas seeps in the Black Sea into the atmosphere. Geophysical Research Letters 32.

Schrader, H., J., 1979. Quaternary paleoclimatology of the Black Sea basin. Sedimentary Geology 23, 165 -180.

Shaw, P. A. and D. S. G. Thomas, 1997. Pans, playas and salt lakes. In: D. S. G. Thomas (Eds.), Arid Zone Geomorphology: Process, Form and Change in Drylands. New York, John Wiley & Sons Ltd.**,** 293-317.

Shimkus, K. M., Y. D. Evsyukov and R. N. Solovjeva, 1980. Submarine terraces of the lower shelf zone and their nature. In: Y. P. Malovitsky and K. M. Shimkus (Eds.), Geological and Geophysical Studies of the Pre-Oceanic Zone. Moscow, P.P. Shirshov Inst. of Oceanology Acad. Sci. USSR, 81-92.

Shumilovskikh, L. S., F. Marret, D. Fleitmann, H. W. Arz, N. Nowaczyk and H. Behling, 2013. Eemian and Holocene sea-surface conditions in the southern Black Sea: Organic-walled dinoflagellate cyst record from core 22-GC3. Marine Micropaleontology 101, 146-160.

Siani, G., M. Paterne, M. Arnold, E. Bard, B. Métivier, N. Tisnerat and F. Bassinot, 2000. Radiocarbon reservoir ages in the Mediterranean Sea and Black Sea. Radiocarbon 42, 271-280.

Skiba, S. I., F. A. Scherbakov and P. N. Kuprin, 1976. Paleogeography of the Kerch-Taman region during the late Pleistocene and Holocene. Oceanology 15, 575-578.

Smirnow, L. P., 1958. Black Sea Basin: Its position in the alpine structure and its richly organic quaternary sediments: typical modern basins. SP 18: Habitat of Oil, 982-994.

Soulet, G., G. Delaygue, C. Vallet-Coulomb, M. E. Böttcher, C. Sonzogni, G. Lericolais and E. Bard, 2010. Glacial hydrologic conditions in the Black Sea reconstructed using geochemical pore water profiles. Earth and Planetary Science Letters 296.

Soulet, G., G. Menot, G. Bavon, F. Rostek, E. Ponsevera, S. Toucanne, G. Lericolais and E. Bard, 2013. Abrupt drainage cycles of the Fennoscandian Ice Sheet Proceedings of the National Academy of Sciences 110, 6682-6687.

Soulet, G., G. Ménot, V. Garreta, F. Rostek, S. Zaragosi, G. Lericolais and E. Bard, 2011a. Black Sea "Lake" reservoir age evolution since the Last Glacial — Hydrologic and climatic implications. Earth Planet. Sc. Lett. 308, 245-258.

Soulet, G., G. Ménot, G. Lericolais and E. Bard, 2011b. A revised calendar age for the last reconnection of the Black Sea to the global ocean. Quaternary Science Reviews 30.

Svendsen, J. I., H. Alexanderson, V. I. Astakhov, M. Jakobsson, K. H. Kjær, E. Larsen, H. Lokrantz, J. P. Lunkka, A. Lysa, J. Mangerud, A. Matiouchkov, A. Murray, P. Möller, F. Niessen, O. Nikolskaya, L. Polyak, M. Saarnisto, C. Siegert, M. J. Siegert, R. F. Spielhagen, I. Demidov, A. Dowdswell, S. Funder, V. Gataullin, M. Henriksen, C. Hjort, M. Houmark-Nielsen, H. W. Hubberten, O. Ingólfsson and R. Stein, 2004. Late Quaternary ice sheet history of northern Eurasia. Quaternary Science Reviews 23, 1229-1271.

Wall, D. and B. Dale, 1973. Of the Blac Sea-A Summary. Contribution No. 2733 of the Woods Hole Oceanographic Institution, 95-102.

Wall, D. and B. Dale, 1974. Dinoflagellates in Late Quaternary Deep-Water Sediments of Black Sea. Tulsa, Amer. Assoc. Petrol. Geol.

Wesselingh, F. P., 2015. Mollusk identification.

Tables

Table 1-1: List of intervals with coquina, black minerals, amphibole, basalt, quartz and red/brown layers

Core Name	Core Depth	Depth in Core (cm)	Feature	^{14}C date	Calendar Date
AKAD11-01	125	146-152	Black Mineral	15,211	16,569
		166-190	Amphibole, Basalt, Quartz	18,216	19,840
		259-262	Coquina Deposit	27,008	31,524
		323-326	Coquina Deposit	31,528	35,773
AKAD11-05	125	262-265	Coquina Deposit	29,511	33,841
		279-291	Coquina Deposit	30,318	34,618
		306-309	Coquina Deposit	31,663	35,901
		332-342	Coquina Deposit	33,106	37,274
AKAD11-07	153	263-268	Coquina Deposit	23,021	26,295
		319-325	Coquina Deposit in Black Dense Clay	28,819	23,198
		325	Transition to Brown	28,974	33,341
AKAD09-28	126	166-170	Coquina Deposit	16,630	18,041
		235-238	Pebbles	19,750	21,964
AKAD09-30	115	147	Coquina Deposit	15,576	16,516
		161	Coquina Deposit	17,234	18,667
		192	Coquina Deposit	17,344	18,789
		258-260	Coquina Deposit	19,820	22,051
		293-298	Coquina Deposit	22,273	25,279

Figure captions

Figure 1-1: Location of the cores used in this study. The different color of the dots refers to the different cruises on which the cores were collected. The cores are listed in Appendix A, Table 1. The red dotted contour refers to the inferred 95 mbsl paleoshoreline. The red circle refers to the BLKS9830 and BLKS9834 cores. The yellow circle refers to the location of the Dniprovs'ko-Buhs'kyi Liman. The black dotted contours refer to the locations of the WC-6-13, B008, B2ch049, and B2ch007 chirp profiles.

Figure 1-2: Passage in the seaward direction across the outer Ukraine shelf, zoom into WC-6_13_0200-2040 from 120 to 75 mbsl, from a narrow belt of dunes to steep paleo-shoreface to a terrace above truncated seaward-dipping reflectors.

Figure 1-3: The BLASON1-B008 chirp profile from the outer Romanian margin with superimposition of cores BLKS98-09, 08, 07 and 06.. The ^{14}C dates of mollusk shells from different levels in the cores are noted. This chirp profile covers -300 to -125 mbsl water depth.

Figure 1-4: Chirp profile across the Danube channel fill from Assemblage-1 cruise in 2004.

Figure 1-5: The B2ch049 chirp profile with superimposition of cores AKAD09-19, AKAD01-AB18, AKAD01-AB20, AKAD01-AB17, AKAD09-28. The red contour traces the erosion surface α from the middle shelf to the uppermost slope.

Figure 1-6: Location of cores and reflection profiles on the Bulgarian margin. The cores are grouped into five transects.

Figure 1-7: The Cape Emine and Varna transect bathymetry with location of cores and reflection profiles.

Figure 1-8: Reflection profile XXIV belonging to the Cape Emine transect. Here color is used to outline the dune interiors (yellow), the surficial drape (green), foreset clinoforms (blue) of presumed previous interglacial age. Cores are projected a few km at most onto this profile, with their ^{14}C dates and lithologies, including the coquina deposit. Pebbles are present in sediment of late glacial age.

Figure 1-9: The B2ch007 chirp profile from the Turkish margin with superimposition of cores MedEx05-13. This chirp profile covers 200 to 100 mbsl water depth. The location of the Holocene marine drift, shelf channeled-fan deposit, α erosion surface, and presumed last glacial sediment are noted. The ^{14}C dates on carbonate from MedEx05-13 are included and presented relative to the type of fossilized fauna from which they were obtained.

Figure 1-10: B2ch013 chirp profile on the outermost Turkish margin north of the Bosporus Strait. Here core MAR98-04 sampled mollusk shells dated at 33.5 kyr BP (^{14}C) from strata just below reflector α.

Figure 1-11: Dniprovs'ko-Bush'kyi Liman (Naukova, 1984). Rf: translated as watered down; Q^4_{III} ant, pt: Fluvial during regression and dated between 15 and 22.5 kyr; pr-st: Alluvial, flood and streambed deposits and dated between 12 and 14.5 kyr; nev: Neoeuxine, clay with *Monodacna caspia* and *Dreissena sp.* Dated between 9.5 and 12 kyr; Q^1_{IV}: unconformity and Bugaz dated between 9.5 and 7.5 kyr; Q^2_{IV}: Old Black Sea dated between 7.5 and 2.5 kyr; Q^3_{IV}: New Black Sea dated between 2.5 and 0 kyr.

Figure 1-12: Wheeler diagrams for the sedimentation record typical of Ukrainian, Romanian, and Bulgarian shelves in the Black Sea. The dashes highlight non-deposition and unconformities in the record. The diamonds refer to specific dated mollusks from each individual core with a calibrated calendar age.

Figure 1-13: The ^{14}C age of the surface water as a function of calendar age from multiple records: Derivation from work of Nowaczyk et al., (2013) (light blue dashed line); ash from deep cores published in Kwiecen et al., (2008) (navy blue diamonds); Comparison between ^{14}C dated wood and *Dreissena rostriformis* in AKAD09-28 (brown diamond); Published ^{14}C age from (gray dashed line) Ryan, (2007); published ^{14}C age from Soulet et al., (2011a), Soulet et al., (2011b) (purple dashed line); ^{14}C age calculated from alignment of stable isotope records from surface mollusk record to that of Sofular Cave (solid red line); Adopted ^{14}C age of the water in the manuscript (dashed red line).

Figure 1-14: Sedimentation rate (cm/kyr) for cores spanning from 2210 mbsl to 17.7 mbsl for which there are measured ^{14}C dates (calibrated to calendar ages based on the adopted ^{14}C

reservoir correction) and/or clear lithologic boundaries that allow to assign calendar ages to different deposition periods in Black Sea history.

Figure 1-15: (a) ^{14}C reservoir corrected $\delta^{18}O$ record of the surface Black Sea water from ^{14}C dates of individual mollusk specimens (diamonds) and U/Th dated Sofular cave $\delta^{18}O$ record (gray contour); (b) Same as (a) but $\delta^{13}C$ records from the ^{14}C reservoir age corrected mollusk and cave records. Pink bars highlight Heinrich events and yellow bars D/O events.

Figure 1-16: $^{87}Sr/^{86}Sr$ measurements for the Black Sea and Marmara Sea as a function of calendar age. Each color represents a different core. The glacial period is highlighted.

Figure 1-17: From top to bottom: (1) Water content (%) and superimposed acoustic impedance (10^3 $kgm^{-2}s^{-1}$), (2) Natural log of magnetic susceptibility, (3) Wet bulk density (g/cc), and (4) Coarse Fraction (>63 μm) (%) on KN134-GC01.

Figure 1-18: From top to bottom: Ti/Ca, Ti (ppm), Ca (ppm) and $CaCO_3$ (%), Zr/Rb, Mn (ppm), K (ppm), S (ppm), Fe (ppm), Mo (ppm), Se (ppm).

Figure 1-19: KN134-GC01 from 160 cm to 250 cm of the core, that part of the core interpreted as pre-red layer / meltwater deposition.

Figure 1-20: From top to bottom: Ti/Ca, Ti (ppm), Ca (ppm) and $CaCO_3$ (%), Zr/Rb, Mn (ppm), K (ppm), S (ppm), Fe (ppm), Co (ppm), Zn (ppm).

Figure 1-21: AKAD11-17 with the focus on that part of the core that is characterized by monosulfide and silt/sand concentrations. Monosulfides are identified at 246 and 272-273 cm and the silt/sand lenses at 265-266 cm and 275-277 cm.

Figure 1-22: Photographs of outer shelf cores and indicated features noted in Table 1 (a) AKAD11-01; (b) AKAD11-07; (c) AKAD09-28, and (d) AKAD09-30. The red dotted lines highlight the features of interest in the core photographs.

Figure 1-1

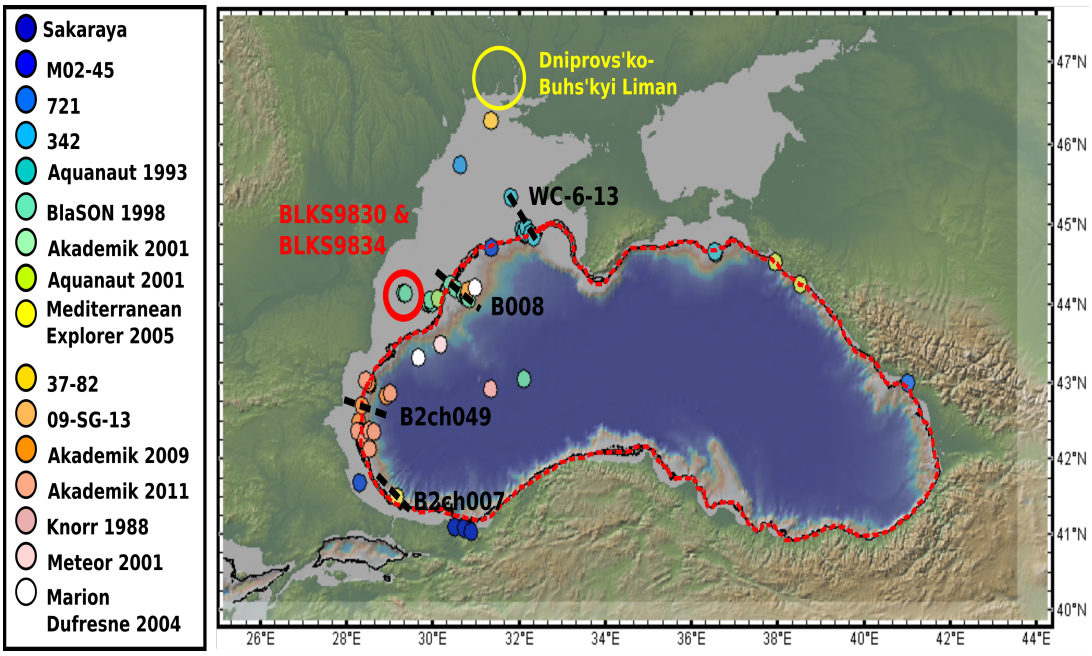
Sakaraya
M02-45
721
342
Aquanaut 1993
BlaSON 1998
Akademik 2001
Aquanaut 2001
Mediterranean Explorer 2005
37-82
09-SG-13
Akademik 2009
Akademik 2011
Knorr 1988
Meteor 2001
Marion Dufresne 2004
Dniprovs'ko-Buhs'kyi Liman
WC-6-13
BLKS9830 & BLKS9834
B008
B2ch049
B2ch007
47°N
46°N
45°N
44°N
43°N
42°N
41°N
40°N
26°E
28°E
30°E
32°E
34°E
36°E
38°E
40°E
42°E
44°E

Figure 1-2

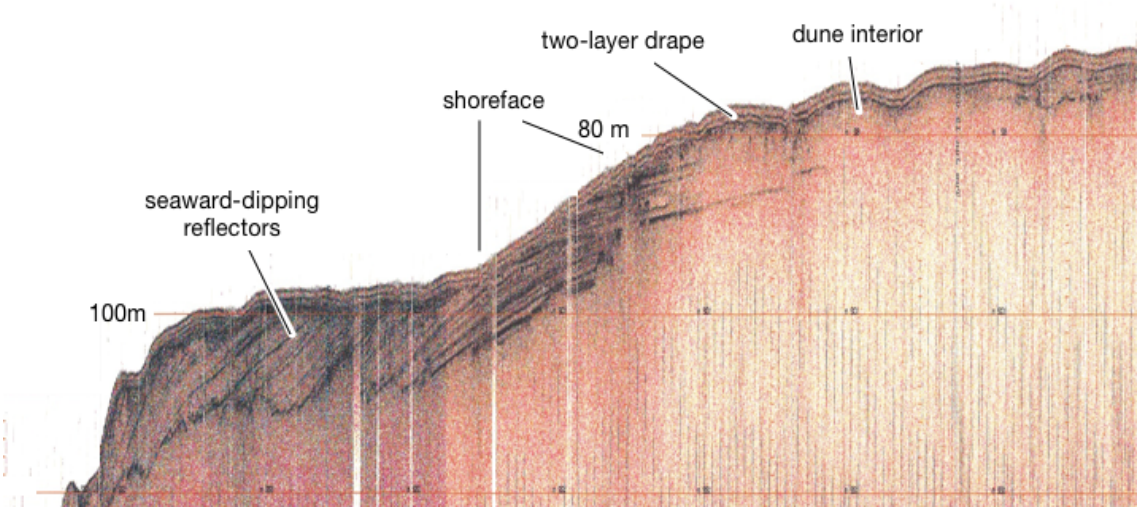
two-layer drape
dune interior
shoreface
80 m
seaward-dipping
reflectors
100m

Figure 1-3

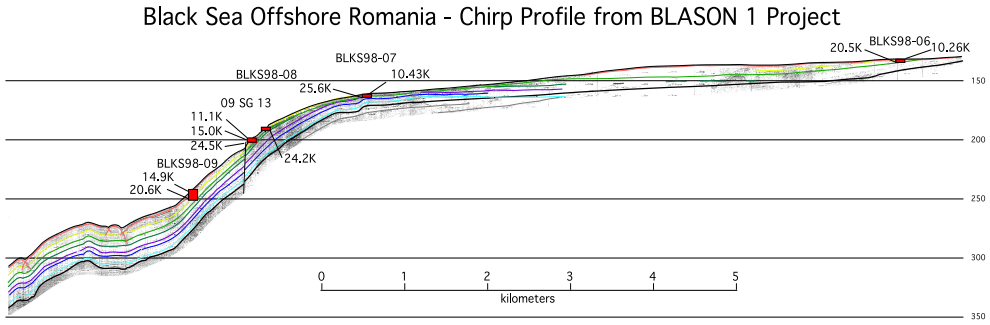
Black Sea Offshore Romania - Chirp Profile from BLASON 1 Project
20.5K
BLKS98-06
10.26K
BLKS98-07
10.43K
BLKS98-08
25.6K
09 SG 13
11.1K
15.0K
24.5K
24.2K
BLKS98-09
14.9K
20.6K
150
200
250
300
350
0
1
2
3
4
5
kilometers

Figure 1-4

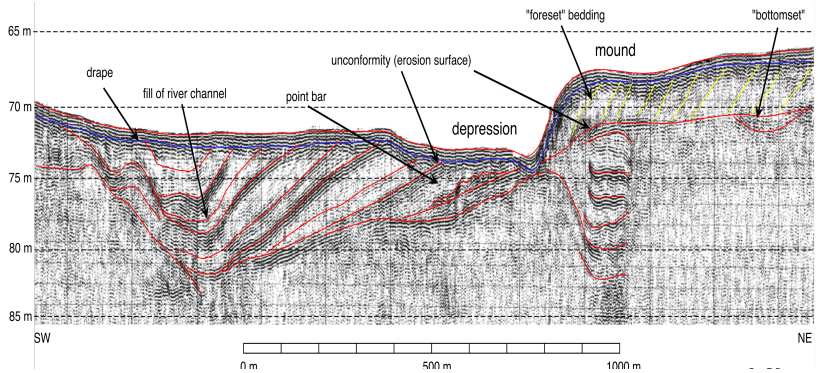
"foreset" bedding
"bottomset"
mound
unconformity (erosion surface)
drape
fill of river channel
point bar
depression
65 m
70 m
75 m
80 m
85 m
SW
NE
0 m
500 m
1000 m

Figure 1-5

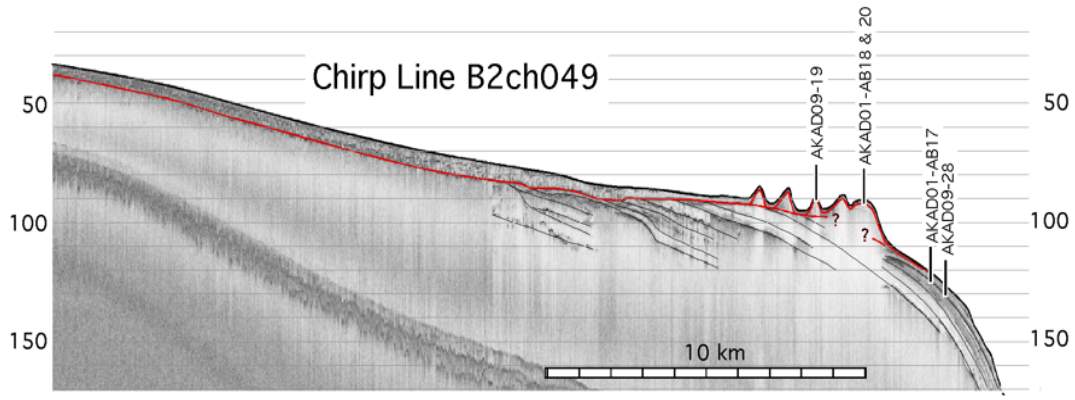
Chirp Line B2ch049
AKAD09-19
AKAD01-AB18 & 20
AKAD01-AB17
AKAD09-28
50
100
150
10 km

Figure 1-6

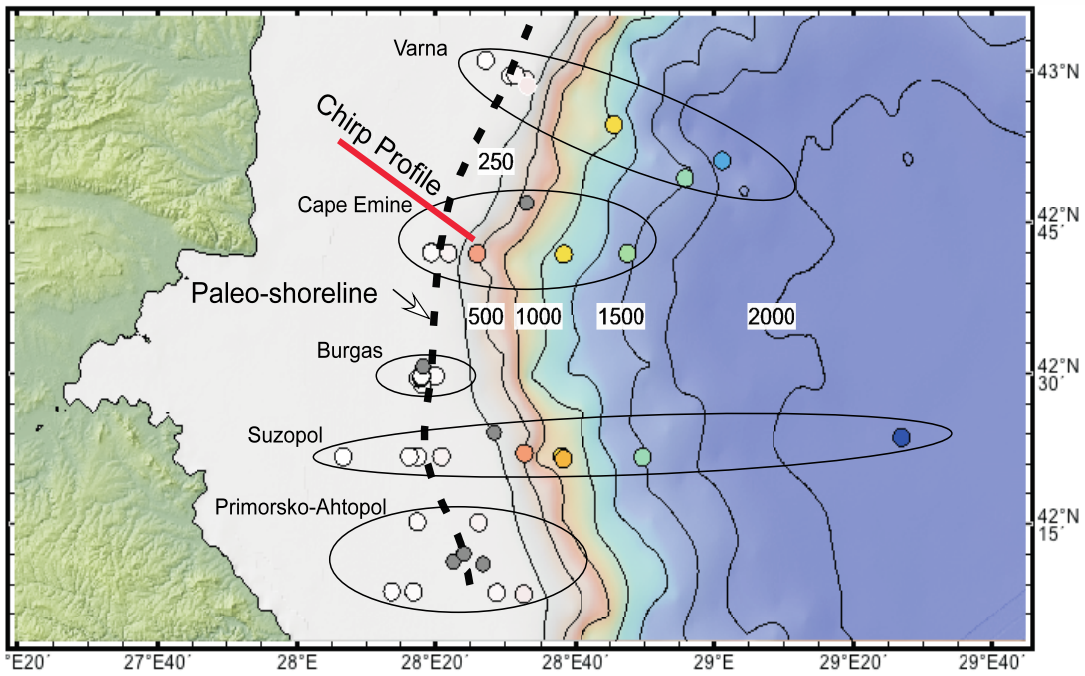
Varna
Chirp Profile
250
Cape Emine
Paleo-shoreline
500
1000
1500
2000
Burgas
Suzopol
Primorsko-Ahtopol
43°N
42°N
45´
42°N
30´
42°N
15´
°E20´
27°E40´
28°E
28°E20´
28°E40´
29°E
29°E20´
29°E40´

Figure 1-7

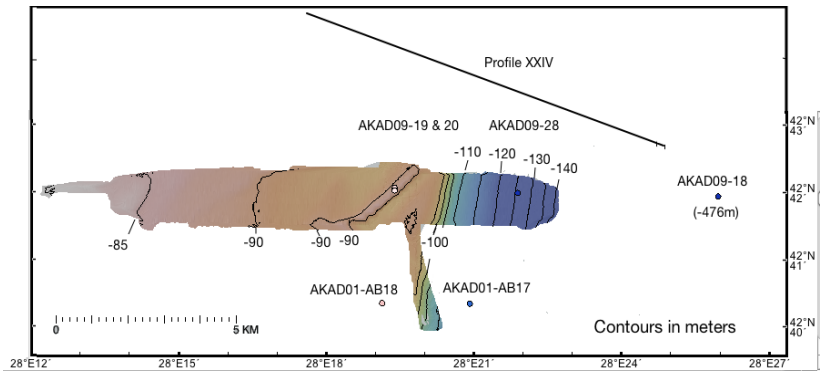
Profile XXIV
AKAD09-19 & 20
AKAD09-28
-110
-120
-130
-140
AKAD09-18
(-476m)
-85
-90
-90
-90
-100
AKAD01-AB18
AKAD01-AB17
0
5 KM
Contours in meters
42°N 43'
42°N 42'
42°N 41'
42°N 40'
28°E12'
28°E15'
28°E18'
28°E21'
28°E24'
28°E27'

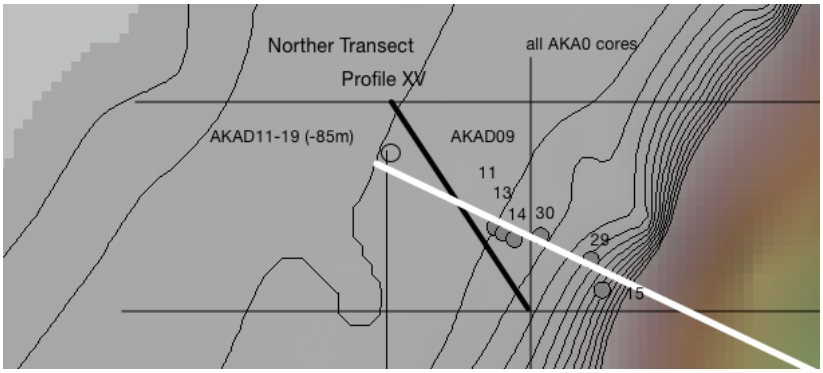
Norther Transect
Profile XV
all AKA0 cores
AKAD11-19 (-85m)
AKAD09
11
13
14
30
29
15

Figure 1-8

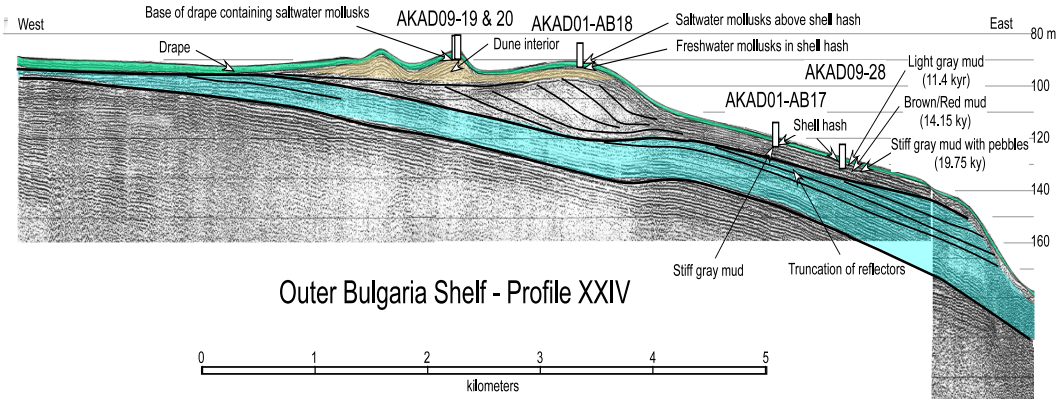
West
East
Base of drape containing saltwater mollusks
AKAD09-19 & 20
AKAD01-AB18
Saltwater mollusks above shell hash
Drape
Dune interior
Freshwater mollusks in shell hash
AKAD09-28
Light gray mud
(11.4 kyr)
AKAD01-AB17
Brown/Red mud
(14.15 ky)
Shell hash
Stiff gray mud with pebbles
(19.75 ky)
80 m
100
120
140
160
Stiff gray mud
Truncation of reflectors
Outer Bulgaria Shelf - Profile XXIV
0
1
2
3
4
5
kilometers

Figure 1-9

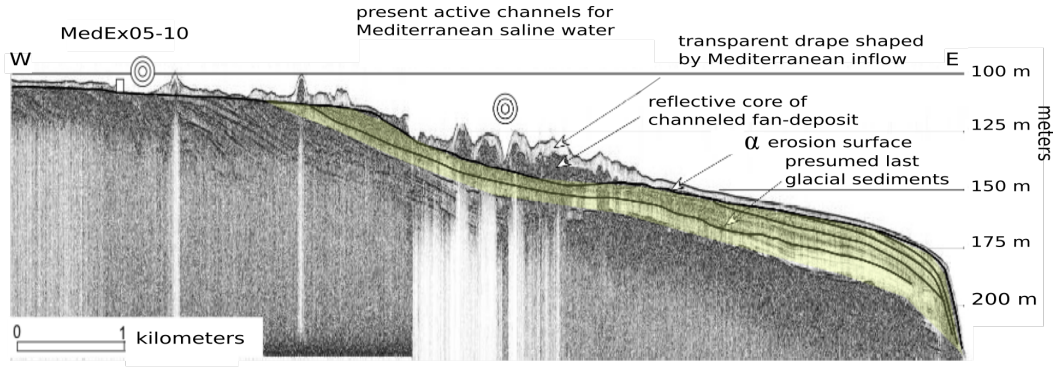
MedEx05-10
present active channels for
Mediterranean saline water
W
transparent drape shaped
by Mediterranean inflow
E
100 m
reflective core of
channeled fan-deposit
125 m
α erosion surface
presumed last
glacial sediments
150 m
175 m
200 m
meters
0
1
kilometers

Figure 1-10

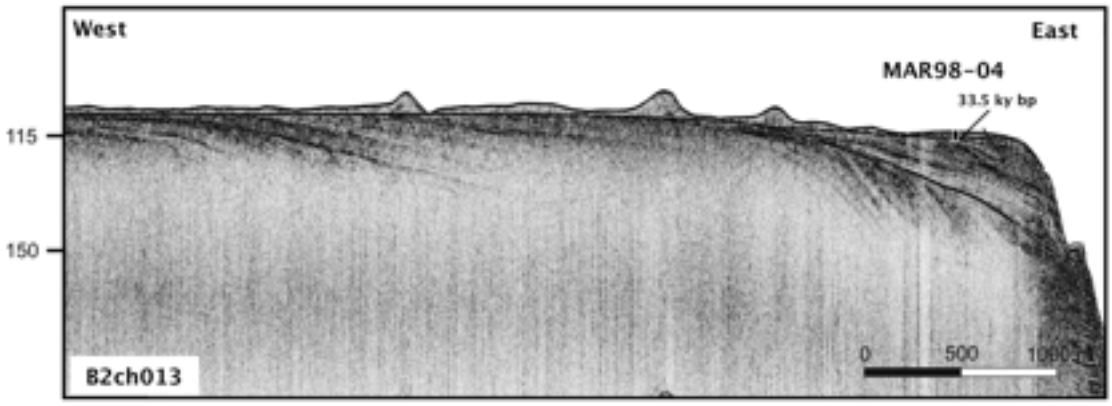

Figure 1-11

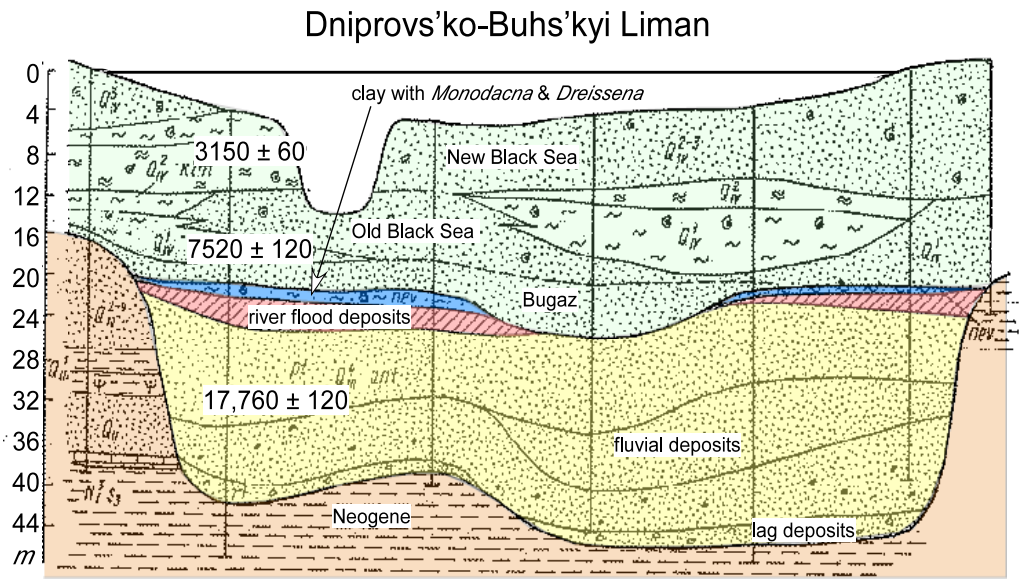
Dniprovs'ko-Buhs'kyi Liman
0
4
8
12
16
20
24
28
32
36
40
44
m
clay with *Monodacna* & *Dreissena*
3150 ± 60
New Black Sea
Old Black Sea
7520 ± 120
Bugaz
river flood deposits
17,760 ± 120
fluvial deposits
Neogene
lag deposits

Figure 1-12

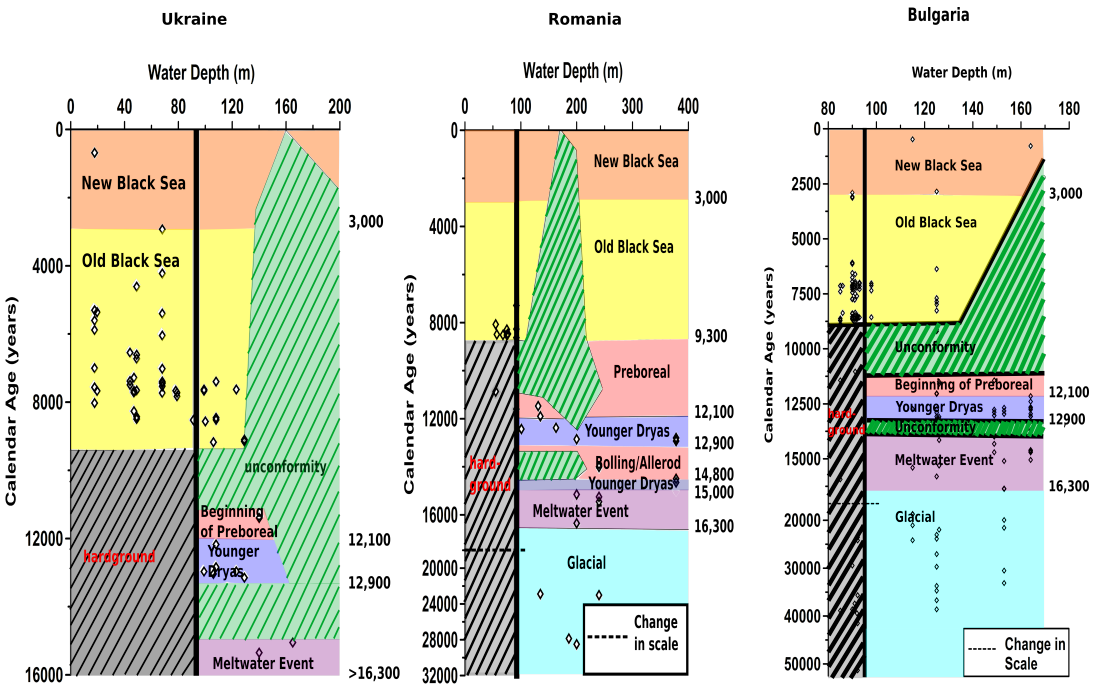
Ukraine
Water Depth (m)
0
40
80
120
160
200
Calendar Age (years)
New Black Sea
Old Black Sea
unconformity
Beginning of Preboreal
Younger Dryas
Meltwater Event
hard-ground
3,000
12,100
12,900
>16,300
Romania
Water Depth (m)
0
100
200
300
400
Calendar Age (years)
New Black Sea
Old Black Sea
Preboreal
Younger Dryas
Bolling/Allerod
Younger Dryas
Meltwater Event
Glacial
hard-ground
Change in scale
3,000
9,300
12,100
12,900
14,800
15,000
16,300
Bulgaria
Water Depth (m)
80
100
120
140
160
180
Calendar Age (years)
New Black Sea
Old Black Sea
Unconformity
Beginning of Preboreal
Younger Dryas
Unconformity
Meltwater Event
Glacial
hard-ground
Change in Scale
3,000
12,100
12900
16,300

Figure 1-13

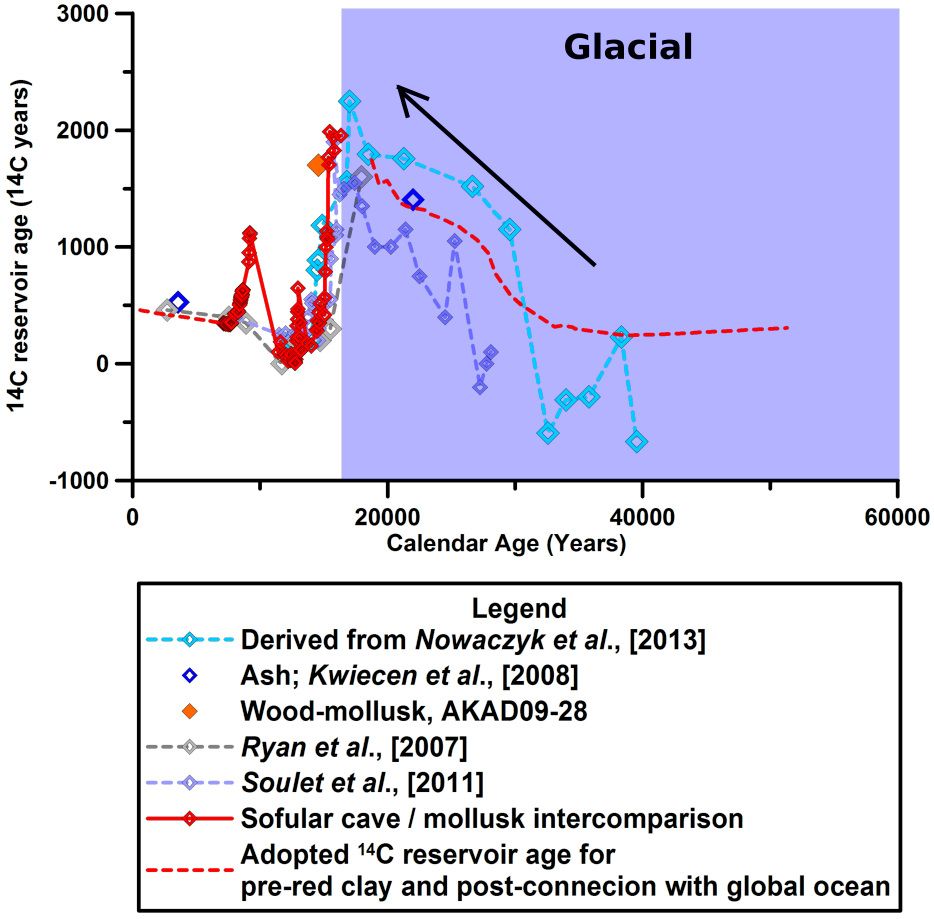
Glacial
14C reservoir age (14C years)
Calendar Age (Years)
3000
2000
1000
0
-1000
0
20000
40000
60000
Legend
Derived from Nowaczyk et al., [2013]
Ash; Kwiecen et al., [2008]
Wood-mollusk, AKAD09-28
Ryan et al., [2007]
Soulet et al., [2011]
Sofular cave / mollusk intercomparison
Adopted 14C reservoir age for
pre-red clay and post-connecion with global ocean

Figure 1-14

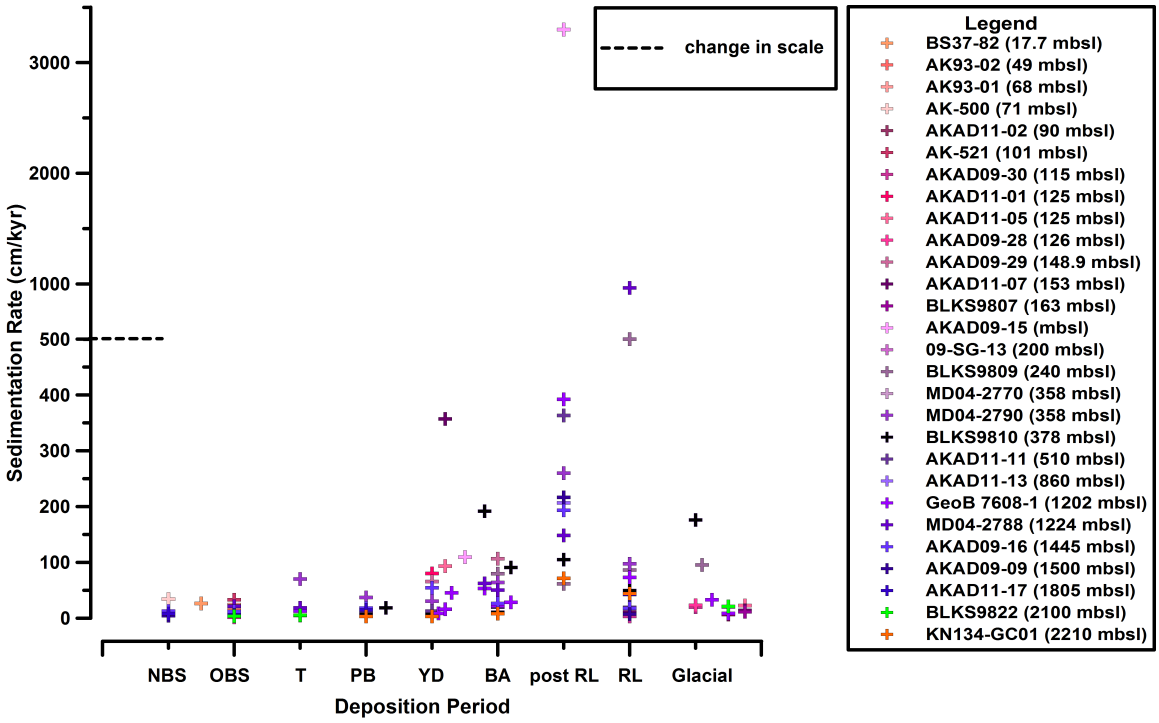
change in scale
Legend
BS37-82 (17.7 mbsl)
AK93-02 (49 mbsl)
AK93-01 (68 mbsl)
AK-500 (71 mbsl)
AKAD11-02 (90 mbsl)
AK-521 (101 mbsl)
AKAD09-30 (115 mbsl)
AKAD11-01 (125 mbsl)
AKAD11-05 (125 mbsl)
AKAD09-28 (126 mbsl)
AKAD09-29 (148.9 mbsl)
AKAD11-07 (153 mbsl)
BLKS9807 (163 mbsl)
AKAD09-15 (mbsl)
09-SG-13 (200 mbsl)
BLKS9809 (240 mbsl)
MD04-2770 (358 mbsl)
MD04-2790 (358 mbsl)
BLKS9810 (378 mbsl)
AKAD11-11 (510 mbsl)
AKAD11-13 (860 mbsl)
GeoB 7608-1 (1202 mbsl)
MD04-2788 (1224 mbsl)
AKAD09-16 (1445 mbsl)
AKAD09-09 (1500 mbsl)
AKAD11-17 (1805 mbsl)
BLKS9822 (2100 mbsl)
KN134-GC01 (2210 mbsl)
Sedimentation Rate (cm/kyr)
0
100
200
300
400
500
1000
2000
3000
NBS
OBS
T
PB
YD
BA
post RL
RL
Glacial
Deposition Period

Figure 1-15

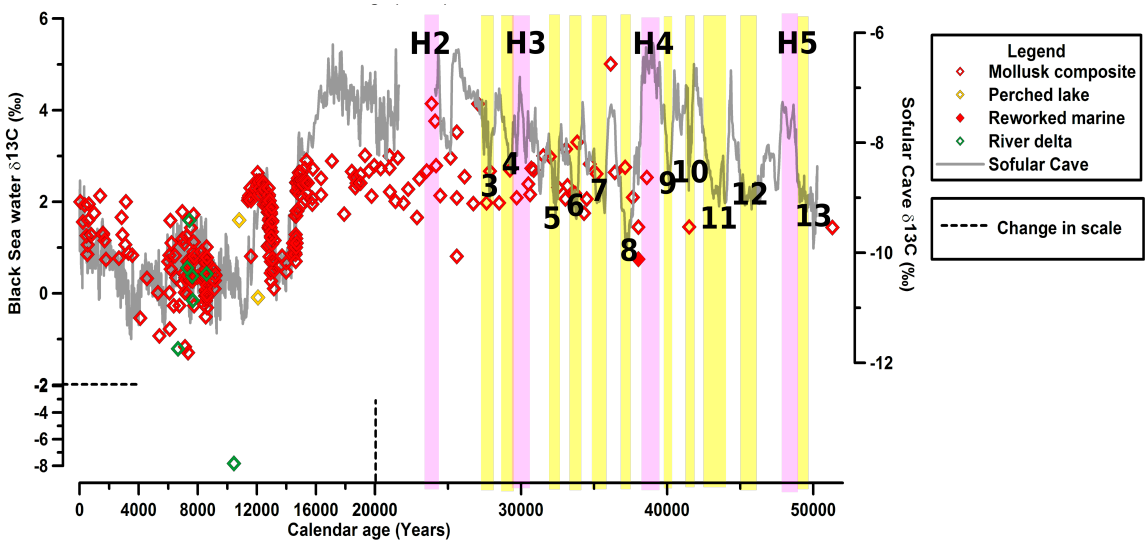
H2
H3
H4
H5
3
4
5
6
7
8
9
10
11
12
13
Black Sea water δ13C (‰)
Sofular Cave δ13C (‰)
Calendar age (Years)
0
4000
8000
12000
16000
20000
30000
40000
50000
6
4
2
0
-2
-4
-6
-8
-6
-8
-10
-12
Legend
Mollusk composite
Perched lake
Reworked marine
River delta
Sofular Cave
Change in scale

Figure 1-16

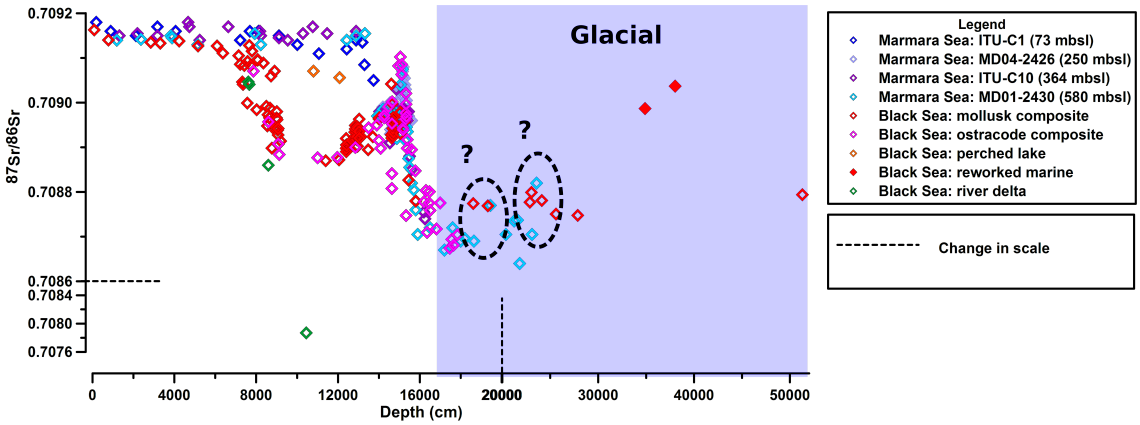
Glacial
?
?
87Sr/86Sr
0.7092
0.7090
0.7088
0.7086
0.7084
0.7080
0.7076
0
4000
8000
12000
16000
20000
30000
40000
50000
Depth (cm)
Legend
Marmara Sea: ITU-C1 (73 mbsl)
Marmara Sea: MD04-2426 (250 mbsl)
Marmara Sea: ITU-C10 (364 mbsl)
Marmara Sea: MD01-2430 (580 mbsl)
Black Sea: mollusk composite
Black Sea: ostracode composite
Black Sea: perched lake
Black Sea: reworked marine
Black Sea: river delta
Change in scale

Figure 1-17

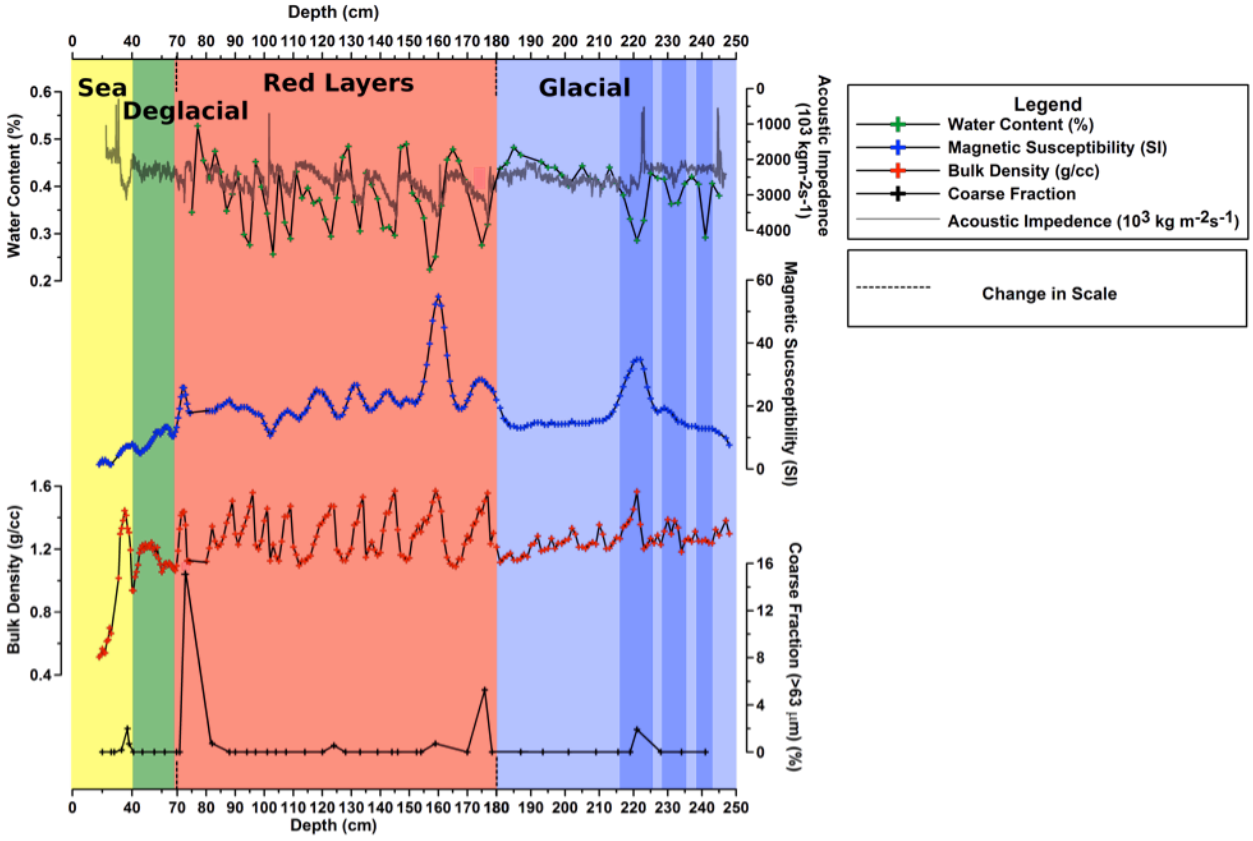
Depth (cm)
Sea
Deglacial
Red Layers
Glacial
Water Content (%)
Acoustic Impedence (10³ kgm⁻²s⁻¹)
Magnetic Susceptibility (SI)
Bulk Density (g/cc)
Coarse Fraction (>63 μm) (%)
Legend
Water Content (%)
Magnetic Susceptibility (SI)
Bulk Density (g/cc)
Coarse Fraction
Acoustic Impedence (10³ kg m⁻²s⁻¹)
Change in Scale

Figure 1-18

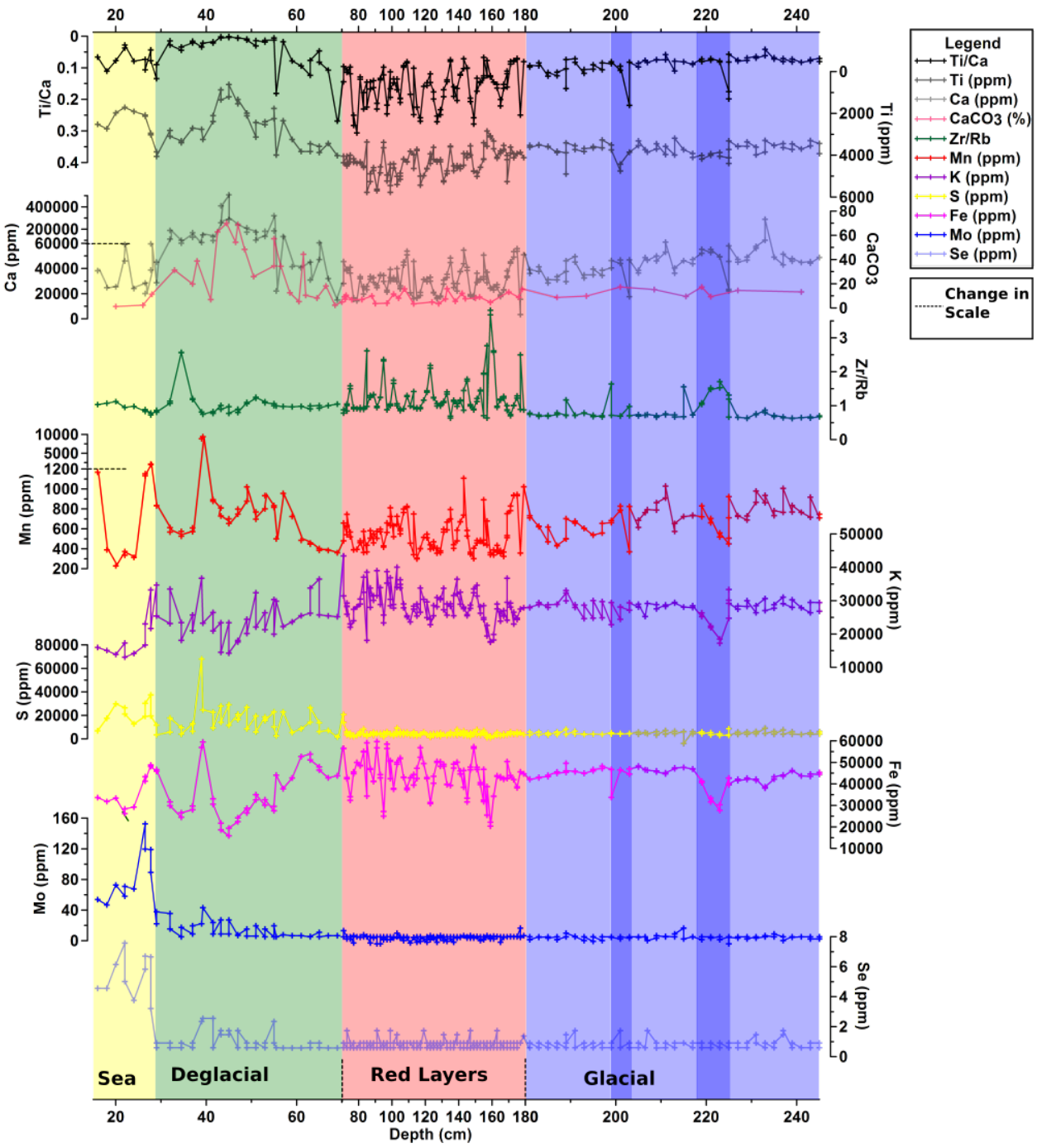
Legend
Ti/Ca
Ti (ppm)
Ca (ppm)
CaCO3 (%)
Zr/Rb
Mn (ppm)
K (ppm)
S (ppm)
Fe (ppm)
Mo (ppm)
Se (ppm)
Change in Scale
Sea
Deglacial
Red Layers
Glacial
Depth (cm)

Figure 1-19

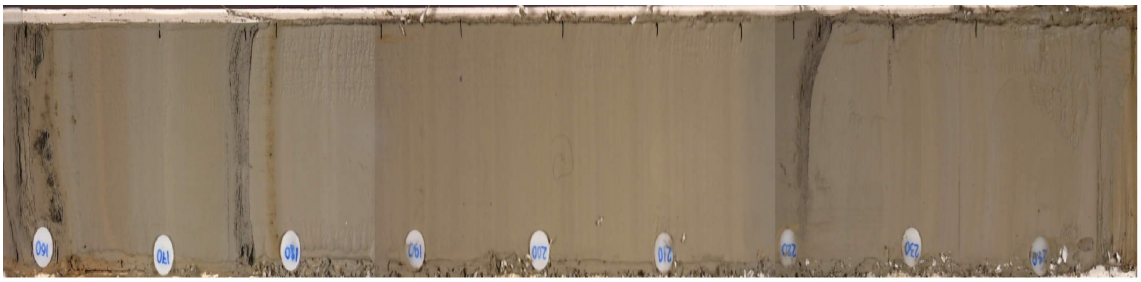

Figure 1-20

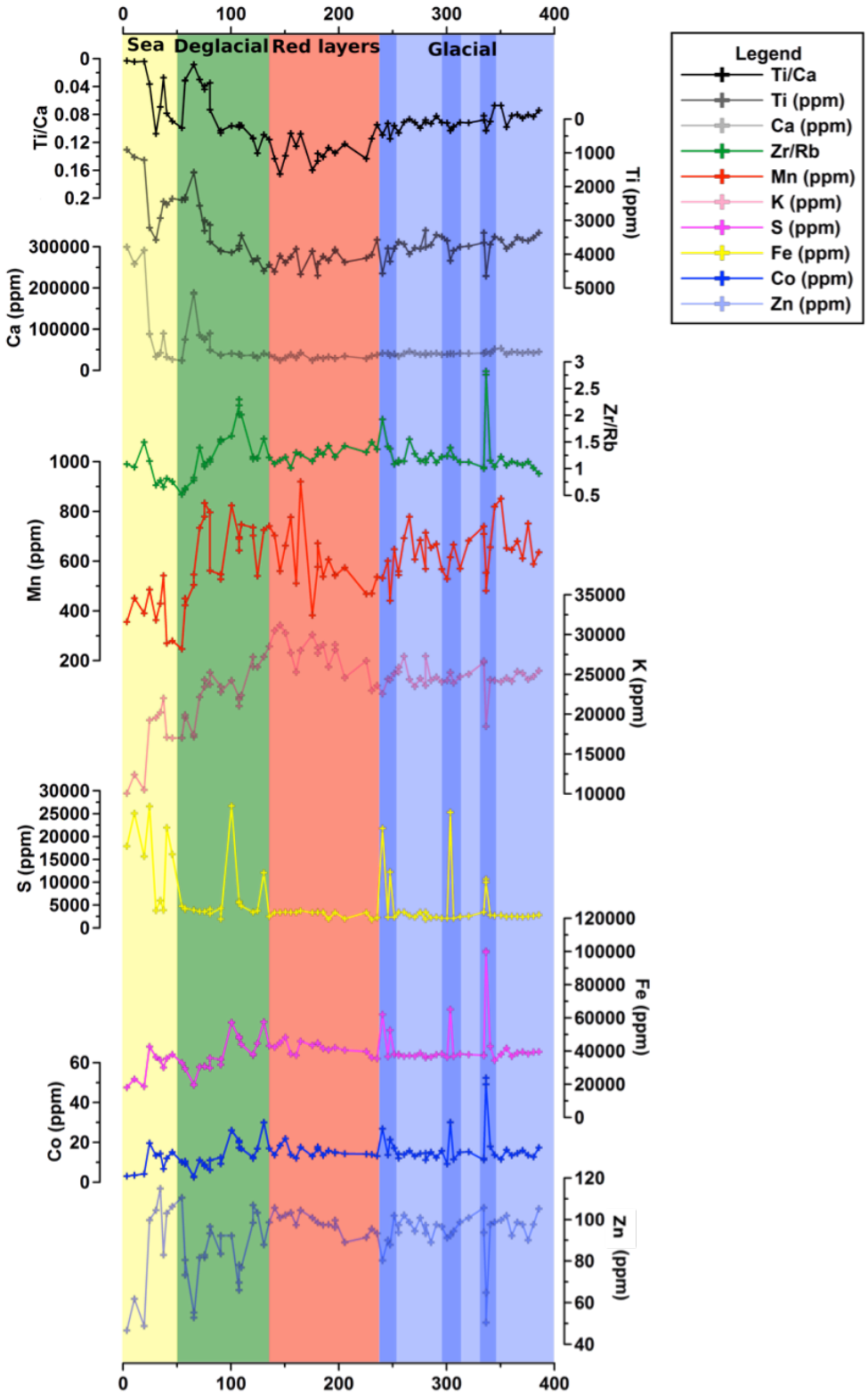
Sea
Deglacial
Red layers
Glacial
Legend
Ti/Ca
Ti (ppm)
Ca (ppm)
Zr/Rb
Mn (ppm)
K (ppm)
S (ppm)
Fe (ppm)
Co (ppm)
Zn (ppm)
0
100
200
300
400

Figure 1-21

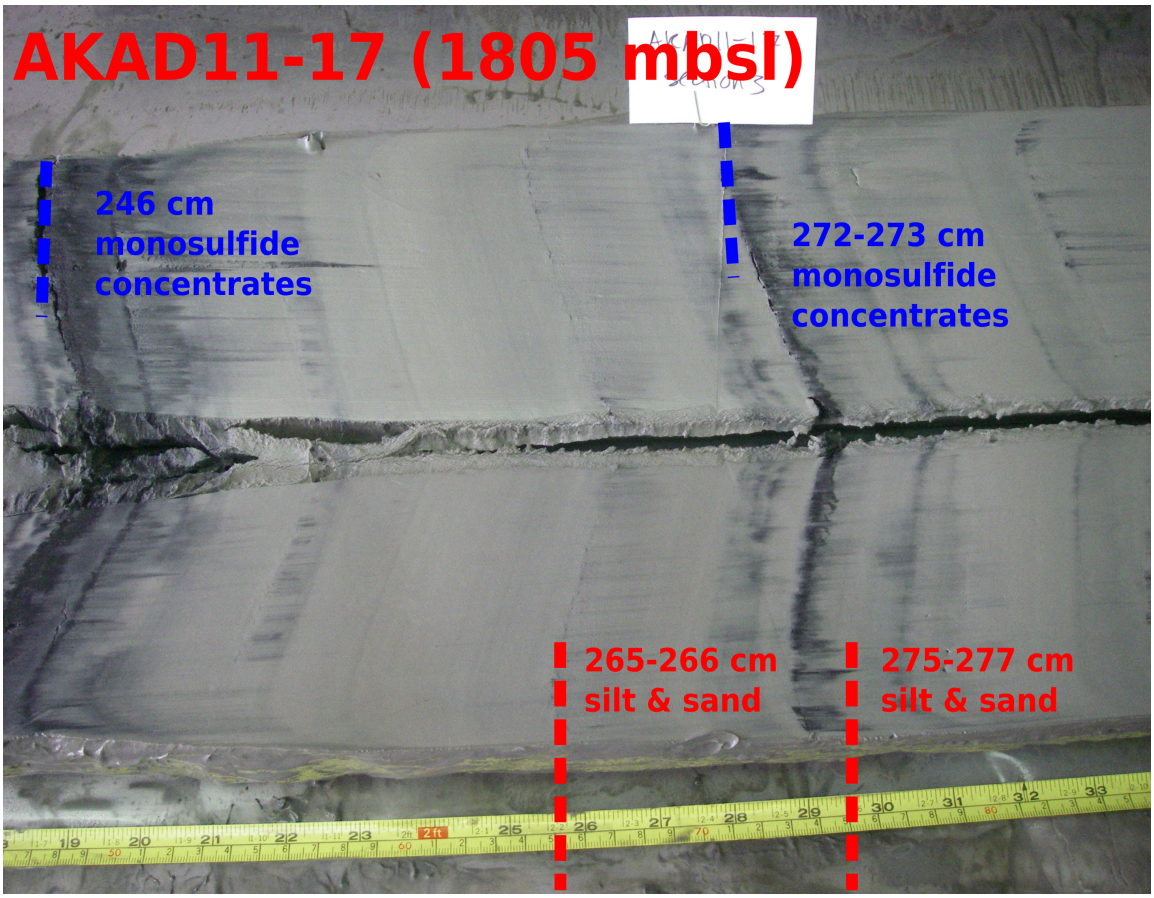
AKAD11-17 (1805 mbsl)
246 cm
monosulfide
concentrates
272-273 cm
monosulfide
concentrates
265-266 cm
silt & sand
275-277 cm
silt & sand

Figure 1-22

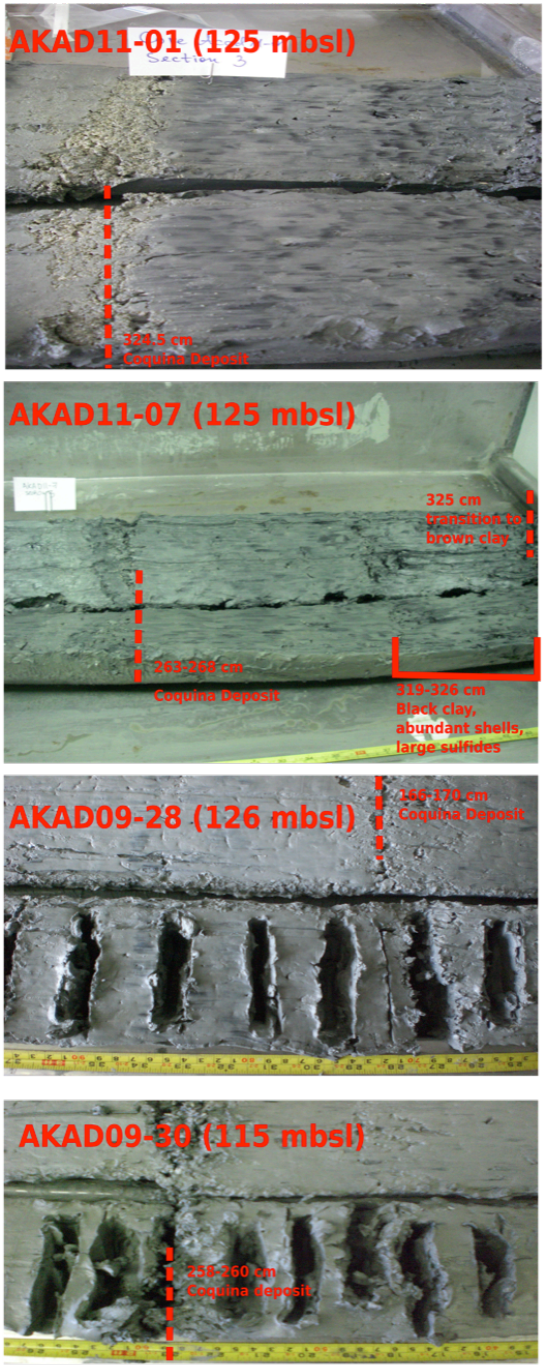
AKAD11-01 (125 mbsl)
321.5 cm
Coquina Deposit
AKAD11-07 (125 mbsl)
325 cm
Transition to
brown clay
263-282 cm
Coquina Deposit
319-326 cm
Black clay,
abundant shells,
large sulfides
AKAD09-28 (126 mbsl)
166-170 cm
Coquina Deposit
AKAD09-30 (115 mbsl)
258-260 cm
Coquina deposit

Appendix 1-1

Core name	Lat (N)	Lon (E)	Core Depth (m)	Cruise and/or first reference
KSK-20	41.06	30.74	0	Turkish State Waterworks, *Görür et al.*, 2001
KSK-18	41.01	30.70	0	Turkish State Waterworks, *Görür et al.*, 2001
KSK-16	41.01	30.52	0	Turkish State Waterworks, *Görür et al.*, 2001
KSK-4	41.04	30.90	0	Turkish State Waterworks, *Görür et al.*, 2001
M02-45TWC	41.69	28.32	-69	Trigger core; *Hiscott et al.*, 2007
M02-45P	41.69	28.32	-69	Piston core; *Hiscott et al.*, 2007
45B	44.71	31.37	-107	Ukrainian HERMES Cruise; *Nicholas et al.*, 2011
721	42.99	41.04	-14.9	Apakidze and Burchuladze, 1987
342	45.74	30.64	-30	Ukrainian Geological Survey of Black Sea region
				Nicholas et al., 2011
AQ93-01	44.95	32.08	-68	Aquanaut 1993
AQ93-3-2	45.35	31.82	-49	Aquanaut 1993
AQ93-07	44.88	32.15	-108	Aquanaut 1993
AQ93-08	44.90	32.13	-99	Aquanaut 1993
AQ93-09	44.88	32.15	-123	Aquanaut 1993
AQ93-10	44.89	32.15	-106	Aquanaut 1993
AQ93-11	44.91	32.13	-91	Aquanaut 1993
AQ93-12	44.97	32.18	-78	Aquanaut 1993
AQ93-13	44.88	32.28	-165	Aquanaut 1993
AQ93-14	44.85	32.35	-140	Aquanaut 1993
AQ93-22	44.65	36.58	129	Aquanaut 1993
AQ93-24	44.67	36.56	-110	Aquanaut 1993
BLKS9801	44.25	30.42	-92	BlaSON, 1998
BLKS9804	44.20	30.54	-101	BlaSON, 1998
BLKS9806	44.13	30.73	-135	BlaSON, 1998
BLKS9807	44.10	30.79	-163	BlaSON, 1998
BLKS9808	44.10	30.79	-186	BlaSON, 1998
BLKS9809	44.09	30.81	-240	BlaSON, 1998
BLKS9810	44.07	30.85	-378	BlaSON, 1998
BLKS9814	44.14	29.33	-55	BlaSON, 1998
BLKS9815	44.14	29.37	-55	BlaSON, 1998
BLKS9822	43.04	32.13	-2100	BlaSON, 1998
BLKS9830	44.01	29.90	-57	BlaSON, 1998
BLKS9831	44.02	29.92	-75	BlaSON, 1998
BLKS9834	44.04	29.95	-67	BlaSON, 1998
BLKS9837	44.02	29.99	-68	BlaSON, 1998
BLKS9838	44.06	29.96	-77	BlaSON, 1998
AKAD01-AB8	44.08	30.13	-90	Akademik, 2001

CHAPTER 2

Megaflood delivery of meltwater from the Alps and Fennoscandinavian Ice Sheet into the Black Sea-Lake

Abstract

The manifestation of the late Pleistocene deglaciation in the Black Sea occurs in the form of allochthonous pulses of red sediment, synchronous with the catastrophic North Atlantic iceberg phenomenon, global Heinrich Event 1 (HE1), 16.35 to 15 kyr BP. The spatial coverage of these sediments exceeded ~75,000 km^2 and their volume is estimated to be >50 km^3. The deposits reveal a decreased $\delta^{18}O$ and radiogenic strontium in the shells of in situ planktonic fossils, consistent with allochtonous glacial meltwater, and increases in Ti/Ca, kaolinite, and illite within the sediments themselves, indicating a continentally derived, likely Eurasian source. The magnitude of the $^{87}Sr/^{86}Sr$ shift and the drop in the radiocarbon age of the lake water from ~2300 ^{14}C years to near zero indicate that these were huge megafloods that vigorously ventilated the water in the lake and potentially replaced all of it. The shift in ε_{Nd} shift indicates that the meltwater was sourced from both the Fennoscandinavian ice sheet and the Alps. Examination of redox-sensitive elements (i.e., Mn, Se, and Mo) shows that the bottom water was oxic, suggesting that the water column was not stratified. The deposits vary from a single layer to more than eleven in individual cores from different locations.

1. Introduction

The record of deglaciation and disintegration of the Eurasian Ice Sheet Complex (EISC) during the late Pleistocene as the Earth was coming out of its last glacial period have been

extensively studied, yet is still not fully understood (Grosswald, 1980; Forman et al., 1999; Siegert and Dowdeswell, 2004; Spielhagen et al., 2004; Svendsen et al., 2004; Ménot et al., 2006; Gyllencreutz et al., 2007). Important questions remain about the sequence of icecap and ice sheet disintegration and the pathways followed by the meltwater that drained from the ice sheets. The Black Sea serves as one of the best locations with potential to record melting events of the EISC as it is a drainage basin for a number of European and Asian rivers. In its modern configuration, the Black Sea receives runoff from over 2 million km^2 of Eastern Europe and Western Asia (Major et al., 2006) (Fig.1). This is roughly 20% of the total area of these regions (~ 10 million km^2). Rivers currently account for about a third of water input into the Black Sea, with Mediterranean inflow and precipitation accounting for the remainder (Ünlüata et al., 1990). In its lake configuration, prior to its present connection with the global ocean, rivers would have contributed to about half the water balance.

More than 50% of the riverine input to the northwestern Black Sea continental margin derives from the Danube (Bondar et al., 1991; Panin and Jipa, 2002). The Danube is the second largest river in Europe and drains over 817,000 km^2 of southeastern Europe (Panin and Jipa, 2002). The contribution from the Dniepr and Don rivers that empty into the Black Sea from the north is smaller and is approximately 21% (Palmer and Edmond, 1989). The Sakarya contributes an additional 4% from the south (Major et al., 2006). The input of these rivers during the last glacial period, together with reduced evaporation rates, led to a positive hydrological balance and outflow of lake water downstream into the Marmara and Aegean Seas (Kvasov, 1968; Yanchilina et al., to be submitted). This also led to freshening of the lake by flushing out saltwater delivered during the Eemian marine connection (Wegwerth et al., 2014).

During the last ice age the EISC blocked the rivers flowing into the Arctic Ocean, diverted them to the south, and dammed extensive lakes in northern Siberia (Mangerud et al., 2001; Grosswald and Hughes, 2002). Based on the location of moraines, the leading edge of the Scandinavian Ice Sheet advanced into the watersheds of the Dniepr River (Kalicki and Sanko, 1998) and rerouted smaller rivers (previously flowing northward to the Baltic and Arctic Seas) into the Black Sea and Caspian Sea-Lakes (Kvasov, 1968; Grosswald, 1980). The Barents-Kara ice sheet was restricted to the shelf areas of the Arctic Ocean and unable to block northward flowing rivers (Mangerud et al., 2002). The Scandinavian Ice Sheet reached its maximum extent at ca. 17-18 kyr BP and rerouted rivers and meltwater from the Baltic Basin into the Caspian Sea via the Volga River (Mangerud et al., 2004). Concurrent with the timing of Heinrich Event 1 (HE1) (Bond et al., 1992; Bond et al., 1993; McManus et al., 1998; Hemming, 2004), retreat of the ice sheets led to changes in the drainage basins of the rivers and release of water from proglacial lakes (Soulet et al., 2013). Ménot et al., (2006) show that the rivers, upon disintegration of the Fennoscandian and British ice sheets, that previously formed the Channel River and drained into Bay of Biscal were rerouted elsewhere. Toucanne et al., (2010) and Toucanne et al., (2015) noted the cessation of channel river activity at 16.70 kyr. Denton et al., (1999) suggested that instead of drainage primarily into the Caspian Sea, the rapid retreat of ice sheets and glaciers in northern Europe and the Alps would have led to a burst of meltwater via the Dniepr and Danube rivers that occurred in less than two millennia.

A record of red sediments in the Black Sea dates close to the time of the disintegration of the EISC (Major et al., 2002; Bahr et al., 2005; Major et al., 2006; Chepalyga, 2007; Ryan, 2007; Soulet et al., 2013). These sediments have been suggested to come from either the overflow of the Caspian Sea via the Manych Strait (Chepalyga, 2007), the Fennoscandinavian Ice sheet, or

the Alps. The pulse history is often reported in the form of three to more than ten oscillations, each lasting 500-600 years and potentially grouped into 3 superflood waves (Chepalyga, 2007). This paper takes a closer look at where the meltwater originated, how large the superflood events were, and the consequences these events had on the Black Sea isotopic composition, salinity, and ventilation.

2. Background and prior research

The deposition of the red layers in the Black Sea is linked chronologically to the timing of the high latitude climate variations as they correspond to periods of decreased $\delta^{18}O$ during GS-2 (Greenland Stadial 2) in the GRIP and NGRIP ice-record between 20.5 and 16 kyr BP (Andersen et al., 2004) and to the time of the HE1 iceberg discharge into the subpolar North Atlantic Ocean, 16.8 to 15 kyr BP (Bond et al., 1992; Bond et al., 1993; McManus et al., 1998; Hemming, 2004). The Black Sea red layers are detrital in nature and are 100-200 cm thick (Major et al., 2002). Elevated Ti/Ca (Bahr et al., 2005), BIT and C_{25}-alkane/total organic carbon (TOC) (Soulet et al., 2013) identify that the layers are composed of terrestrial material. Increases in illite and kaolinite clay minerals indicate their northern provenance (Major et al., 2002). Each of the red layers is noted to have a complex internal structure and mm-scale laminations interpreted to represent interannual/ annual pulses of meltwater discharge (Bahr et al., 2005). The incorporation of these sediments into the load carried by rivers is likely to be linked to a combination of the abundance of unconsolidated soil from melting of permafrost, scarce vegetation cover, and the higher transport capacity of these meltwater-bearing rivers.

The $\delta^{18}O$ of surface biogenic carbonate drops by 1.6 ‰ within the sequence of the red sediments from -6.5 to -8.1 ‰. The decrease of $\delta^{18}O$ is noted to mark the input of the $\delta^{18}O$-

depleted meltwater into the Black Sea from the north. The large increase in freshwater input into the Black Sea is argued to raise the Black Sea-Lake water level by 100 m to the depth of the Bosphorus sill at 35 mbsl, flooding the northwestern shelf (Soulet et al., 2013). The amount of freshwater discharge carried into the lake is thought to be so high as to fill the basin entirely and also overflow into the Marmara and Aegean Seas. The $^{87}Sr/^{86}Sr$ of biogenic carbonate in these red layers spikes from 0.70896 to 0.7091. This increase is primarily attributed to water of allochtonous origin. It is also possible that the incorporation of the more radiogenic $^{87}Sr/^{86}Sr$ resulted from greater erosion and river sediment load during deglaciation (Hinderer, 2001) and/or that the radiogenic $^{87}Sr/^{86}Sr$ was released during early stages of weathering that followed deglaciation (Blum and Erel, 1995). The increase of $^{87}Sr/^{86}Sr$ in the Black Sea-Lake is not likely to be explained by the $^{87}Sr/^{86}Sr$ of the modern Caspian Sea, which is 0.7082 (Clauer et al., 2000), a value much lower than that recorded in the red layers. This observation suggests that either the red layers were not sourced from the Caspian or that the process that was responsible for their deposition in the Black Sea also was also responsible for their deposition in the Caspian (i.e., meltwater delivered by rivers in floods from the north).

Using ε_{Nd}, (Soulet et al., 2013) identified that the meltwater was sourced entirely and exclusively from the draining of proglacial Lake Disna, formed at the edge of the Fennoscandian Ice Sheet and delivered to the Black Sea via Dniepr. This meltwater was released cyclically and linked to the occurrence of HE 1, a period during which a switch occurred from meltwater first routed towards the North Atlantic through the "English Channel megariver," also known as the Fleuve Manche (Toucanne et al., 2010; Toucanne et al., 2015) to its diversion southward (Toucanne et al., 2015) as a consequence of the rapid motion of a Fennoscandian ice tongue over the present North Sea. The release of this cold and fresh water into the lake was inferred to

stratify the Black Sea water column and thus lead to bottom water reducing conditions (Bahr et al., 2005). As reducing conditions lead to increased solubility of Mn in the water column, the decrease of Mn in these red sediments has been interpreted to indicate a depletion of oxygen in the Black Sea-Lake formed during this enhanced freshwater input (Bahr et al., 2005).

3. Materials and Methods

3.1 Core descriptions

The cores used in this paper are compiled from a set of research cruises in the Black Sea during the 1980's to 2000's that geographically encompass its western basin, slope, and shelf (**Figure 2-1** and **Table 2-1**). The red layers were searched for in cores recovered from the eastern slope and basin but were not observed. Two of the slope and basin cores (i.e., 09-SG-13, and KN134-11-GC01) are studied in detail through application of geochemical analyses. The remaining set is used to calculate the thickness of red sediments and geographical extent, and to characterize changes in sediment composition as a function of their location. The WC-6_18_1210 chirp profile was taken during the Aquanaut 19993 cruise (**Figure 2-2**). Core AK93-14 was retrieved from the NE corner of the chirp transect.

Core 09-SG-13 was recovered from just beyond the slope break on the Romanian margin north of the Danube Fan (44°07.204 N, 30°48.087 E) at a depth of 200 m during the 2009 Mare Nigrum cruise (**Figure 2-3a**, 53 cm to 104 cm). This core features sedimentation from the glacial period to the beginning of the Holocene sapropel and contains 90 cm of red sediments. The coring site is located near that of MDO4-2790 core previously described and studied by (Soulet et al., 2011a; Soulet et al., 2011b; Soulet et al., 2013). These cores do not feature a silt layer at their base that grades into clay but instead (**Figure 2-3c**), as pointed out by (Soulet et al.,

2013), each red lamination is characterized by high amounts of scattered silts and sands (largely quartz) that are disseminated within a reddish clayey matrix. This is clear from the >63 micron fraction of red pulses (**Figure 2-3b**).

KN134-11-GGC01 was recovered from the southwest quadrant of the Black Sea basin (42°54.730 N, 31°21.700 E) at a depth of 2210 m during the 1988 Knorr cruise. KN134-11-GGC01 features a number of lithologic units that include the sapropel, Preboreal, Younger Dryas, meltwater/ red sediment unit and the end of the glacial period, Marine Isotope Stage 2 (MIS 2). The section containing red sediments is 110 cm thick and is located from 70 to 180 cm in the core. The red sediments comprise 11 pulses of silt grading into clay (**Figure 2-4**). In some of the pulses, the silt is grey in color but grades into red clay. Thin sulfide layers are often superimposed on the red clay deposits.

3.2 Core Scanning

Bulk density (g/cc), magnetic susceptibility (SI), and acoustic impedance were measured at mm-scale resolution from a freshly split core sections using a Geo Tek Multi Sensor Core Logger, Serial #47 at the Core Lab of Lamont Doherty Earth Observatory (LDEO) on KN134-11-GGC01 (Geotek, 2014). Bulk density was calculated from gamma ray attenuation measurements. Acoustic impedance was measured as a function of P-wave velocity (m/s) and bulk density (g/cc) in 10^3 $kgs^{-1}m^{-3}$ adjusted to a measurement temperature of 20°C. Magnetic susceptibility was measured as volume-specific magnetic susceptibility and is presented as the natural log of magnetic susceptibility (From now on, referred to as magnetic susceptibility). Discrete water-content measurements to supplement estimates from acoustic impedance were made every 2 cm by differencing sample weights before and after freeze-drying.

3.3 X-Ray Fluorescence (XRF)

The bulk intensities of major elements were measured by a field portable-XRF spectrometer at LDEO on dry and wet sediments. The measurements presented in this study were all made on dry sediment to avoid any dilutions from water. Sediment samples were taken every 2 cm, homogenized with agate mortar and pestle, and packed into sample cups equipped with Mylar polyester supports with every 2 cm. Prepared cups were positioned in a sampling test stand supplied by the manufacturer. The measured intensities (in counts per second) were related to ppm by correlation with Standard Reference Materials (Kenna et al., 2011). The full discussion of the measurements and error propagation is given in Kenna et al., (2011). Errors reported for each XRF measured element are given as an average error of all of the samples run, for simplicity. Results are reported as concentrations (ppm) (i.e., Ca, Ti, Mn, K, Fe, S, Mo, and Se) and elemental ratios (i.e., Ti/Ca and Zr/Rb). The elemental ratios are calculated to emphasize differences in the relative distribution of terrigenous material relative to carbonate sedimentation (Bahr et al., 2005). Ca, Ti, K, Mn, and Fe are interpreted to reflect the difference in the terrigenous character of the red sediments from the beginning of the pulse to its end and S, Mo, and Se are presented to interpret the effect these meltwater events had on the ventilation of the Black Sea water column as these elements are redox-sensitive. Zr is normalized to Rb as this was shown to represent changes in grain size (Dypvik and Harris, 2001).

3.4 Neodymium

The measurement of ε_{Nd} followed the protocol of Gutjahr et al., (2007). Approximately 300 mg of coarse (>63 μm) and fine (<63 μm) sediment was prepared for authigenic and detrital

separates. The sediment was treated with 1 M Na acetate to remove carbonate, leached with 1M $MgCl_2$ to remove the exchangeable fraction, and with 0.05 M hydroxalamine hydrochloride 15% acetic acid-0.03 M Na-EDTA to remove the authigenic component. The authigenic component was prepared for both fine and detrital fraction. The remainder of the detrital fraction was digested in a mixture of HF and HNO_3. The biogenic carbonate was treated with HNO_3 until complete dissolution was reached. After full dissolution, all of the samples were passed through TRU Spec columns for separation of REEs and Ln-Spec columns to remove Sm. Nd isotopes were measured on the Neptune Plus High Resolution Multicollector ICP-MS at Lamont Doherty Earth Observatory with a standard error of 6.4 ppm and corrected to Jndi, La Jolla, and CHUR standards (Jacobsen and Wasserburg, 1980).

3.5 $^{87}Sr/^{86}Sr$

The $^{87}Sr/^{86}Sr$ measurements on carbonate samples composed of mollusk and ostracode shells were sonified and subsequently leached following a modified procedure from (Bailey et al., 2000). The $^{87}Sr/^{86}Sr$ ratio was measured on a dynamic multi-collector on a VG Sector 54 thermal ionization mass spectrometer (TIMS) at Lamont-Doherty Earth Observatory. The $^{87}Sr/^{86}Sr$ isotope ratio was corrected for mass fractionation by normalizing the ratio to 0.1194. The beam size specific to ^{88}Sr chosen was maintained at approximately 4.5×10^{-11} A. Instrumental drift was corrected for by analysis of NBS987 and gave an average value of $^{87}Sr/^{86}Sr$ equivalent to 0.710255 ± 2.31143E-05 with 2σ external reproducibility and n=7. The final correction involved correction of the $^{87}Sr/^{86}Sr$ relative to the NBS987 value of 0.71024. The results presented include prior $^{87}Sr/^{86}Sr$ measurements (Major et al., 2006; Vidal et al., 2010) and unpublished measurements (Major et al., 2006; Cohen and Ryan, 2011). The unpublished

$^{87}Sr/^{86}Sr$ measurements include those from four cores from the Sea of Marmara: ITU-C1 at 73 mbsl, MD04-2426 at 250 mbsl, ITU-C10 at 364 mbsl, and MD01-2430 at 580 mbsl. Age control on the $^{87}Sr/^{86}Sr$ measurements is provided by the AMS ^{14}C dates and the subsequent correction to calendar ages, discussed below.

3.6 Age Model and ^{14}C Reservoir Age

Calendar ages were calculated by aligning the $\delta^{18}O$ and $\delta^{13}C$ compositions of mollusks as a function of their measured ^{14}C age from all of the available shelf cores to $\delta^{18}O$ and $\delta^{13}C$ measurements in the nearby U/Th dated stalagmites in the Sofular Cave (Fleitmann et al., 2009; Badertscher et al., 2011). The justification for this methodology is found in Fleitmann et al., (2009), Badertscher et al., (2011), and Yanchilina et al., (submitted). This alignment is applied specifically to the deglaciation period (20 to 7 kyr BP) of the Black Sea paleoceanographic history as this is where most of the shelf core records preserve a sediment history and where the $\delta^{18}O$ and $\delta^{13}C$ of both the surface calcium-carbonate and cave deposits have the most structure. The ^{14}C reservoir age offsets for this time period were calculated by converting the aligned calendar age to the respective ^{14}C atmospheric age at the time and subtracting it from the measured ^{14}C age of the mollusks.

The results presented by this alignment are supplemented by previous work. The ^{14}C reservoir ages can be calculated from the work of Nowaczyk et al., (2012). These are calculated by finding ^{14}C measurements that are converted from their derived calendar ages to corresponding ^{14}C ages and subtracting the measured ^{14}C age from the measured ^{14}C age. The ^{14}C reservoir age prior to 18 kyr BP is adopted between those ^{14}C reservoir ages presented by Soulet et al., (2011a) and Nowaczyk et al., (2012). This is a compromise between modest

differences of the two methodologies. The calendar age assigned to the $^{87}Sr/^{86}Sr$ records from the Marmara Sea-Lake are calculated from the alignment of the Marmara Sea-Lake $^{87}Sr/^{86}Sr$ to the calendar age of the Black Sea-Lake $^{87}Sr/^{86}Sr$ during the deglaciation periods (i.e., 20 to 7 kyr BP).

3.7 Volume Estimations

Water content in KN134-GC01 was calculated by measuring the difference in weight before and after freeze-drying samples. The water content ranges between ~20 to 30 % in the silty base of each red layer and ~50 to 55% in clay deposit that is superimposed on the silty base. The lower values are an anomalous relative to the rest of the record. The water content of sediment deposited prior to the red layers is characterized by much less variability and is ~50 to 55%. It should be noted that the mud and finer silts are found on the western Black Sea slope while turbidites are found on the Danube Fan. The average thickness of red sediments that drape the western fraction of the Black Sea bottom (**Figure 2-5**) is calculated to be 100 cm with a standard deviation of ± 84 cm, a value derived from the existing cores with red sediment (**Table 2-1**). It should also be noted that this is a minimum estimate, as some of the cores did not recover the full sedimentary deposit belonging to that of the red layers. This deposit is spread over at least an area of 75,000 km^2 (**Figure 2-1**) and amounts to a volume of 75 km^3. For water content of 30%, the remaining 70% is sediment. This mean ratio of sediment to water is applied to all of the red layer deposits for a rough estimate. This calculates to ~50 km^3 of pure sediment. The deposit is identified as a turbidite based on the size grading of each layer. In this particular location, the sediment deposits are well graded, from sand in the lower part of the unit through silts to clay in the upper portion. This sequence is a defining characteristic of turbidites and sets

these deposits apart from other subaqueous sedimentary density flows (Bouma, 1962; Mulder and Alexander, 2001). Turbidites result from flow with concentrations 0.5 to 9% by volume (Bell, 1942; Bagnold, 1962; Syvitski and Schafer, 1996; Mulder and Alexander, 2001). The estimation of the amount of sediment deposited by turbidite activity allows the back-calculation of the minimum amount of meltwater that would have been released to the Black Sea-Lake. The results are presented and discussed in Section 4.1.

The red layer deposit on the East Rim of the Dniepr Canyon (**Figure 2-6**) covers the entire shelf to slope transition from 140 to 550 mbsl. Core AK93-14 is retrieved from 140 mbsl on the northeast corner of the transect. A ^{14}C date from the red layer deposit at 215 cm gives an age of 14.70 kyr ^{14}C (15,350 kyr BP). The clinoform at this depth is identified by yellow contours and is followed from the shelf to slope. The maximum thickness of this deposit occurs around 400 m and is estimated to be as large as 25 m.

A second method for estimating the amount of meltwater that entered into the Black Sea carrying the red sediments is from measurements of $^{87}Sr/^{86}Sr$ on biogenic carbonate using an isotope water mass mixing equation:

$$\left(\frac{^{87}Sr}{^{86}Sr}\right)_{mixture} = \frac{\left(\frac{^{87}Sr}{^{86}Sr_{F1}} \cdot C_{F1} \cdot F_{F1} + \frac{^{87}Sr}{^{86}Sr_{F2}} \cdot C_{F2} \cdot F_{F2}\right)}{\left(C_{F1} \cdot F_{F1} + C_{F2} \cdot F_{F2}\right)} \qquad \text{(Eq. 1)}$$

where the $^{87}Sr/^{86}Sr$ of the mixture is the $^{87}Sr/^{86}Sr$ composition of the Black-Sea Lake after the entry of the meltwater and its mixing with the lake, $^{87}Sr/^{86}Sr_{F1}$ the $^{87}Sr/^{86}Sr$ composition of the original lake water, C_{F1} the concentration of Sr of the original lake water, F_{F1} the fraction of original lake water relative to the entering meltwater, $^{87}Sr/^{86}Sr^{F2}$ the $^{87}Sr/^{86}Sr$ composition of the

meltwater, C_{F2} the concentration of Sr of the meltwater, and F_{F2} the fraction of the entering meltwater upon it mixing with the lake.

The $^{87}Sr/^{86}Sr$ composition of the original Black Sea-Lake water before the onset of the melting events is taken as 0.70867 (Major et al., 2006) and the Sr concentration of the original Black Sea-Lake water is taken to be 0.25 ppm (Palmer and Edmond, 1989; Major et al., 2006). This is the mean concentration of Sr that is flowing into the Black Sea from rivers and would reflect that of the Black Sea-Lake at that time if the lake given that the lake was hydrological balance. The lake is shown to be in this configuration as it was outflowing to the Sea of Marmara at this time (i.e., precipitation and delivery of water by rivers was equivalent to evaporation and outflow to the Sea of Marmara) (Yanchilina et al., to be submitted). The final composition of the mixture between the Black Sea and the delivered meltwater is 0.7091 (Bahr et al., 2005; Major et al., 2006). It should be noted that the meltwater was delivered in individual pulses, from three to more than eleven, that progressively brought the altered composition of the water to 0.7091 progressively. To estimate the original volume of the meltwater that was delivered by these floods, it is necessary to determine values for the $^{87}Sr/^{86}Sr$ composition of the incoming meltwater and the concentration of Sr of this water. This information then allows the estimation of the fraction of the water that entered the Black Sea-Lake relative to the lake's original volume and mixed with the initially present lake water to increase its $^{87}Sr/^{86}Sr$ composition to 0.7091.

Determining the likely original $^{87}Sr/^{86}Sr$ composition and Sr concentration of the meltwater is not straightforward. It has been previously inferred that the origin of the meltwater is exclusively from the north (Soulet et al., 2013). The northern rivers in the Precambrian Shielf area to the north of the Baltic Sea have low Sr concentrations of 0.015 to 0.05 ppm and $^{87}Sr/^{86}Sr$

composition of 0.73 to 0.75 while those that drain the Mesozoic-Paleozoic terrain south of the Baltic Sea have high Sr concentrations of 0.1 to 0.5 ppm and $^{87}Sr/^{86}Sr$ composition of 0.71 (Löfvendahl et al., 1990). The isotopic composition and Sr concentration reflect the geochemistry of the terrain that is drained: the more radiogenic composition is derived from rocks that are not as easily weathered whereas the less radiogenic is derived from rocks that are more easily weathered (Löfvendahl et al., 1990) so the scenario of water incoming with a high concentration of Sr that also happens to be highly radiogenic is unlikely. The ε_{Nd} of the two drainage systems are -20 and -14, respectively (Andersson et al., 1992; Andersson et al., 1994). Since the ε_{Nd} that characterized the detrital matter associated with the delivery of the red layers was ~-14 (Soulet et al., 2013), it is possible that the $^{87}Sr/^{86}Sr$ composition was that of the rivers draining into the Baltic Sea from the south. On the other hand, the $^{87}Sr/^{86}Sr$ composition of the bulk red sediment clays is 0.75093 suggesting that an origin of the waters from farther north cannot be completely ruled out. The isotopic water-mixing model explores both options for a range of mixtures between lake water and meltwater (**Figure 2-9** in Section 4.4).

4. Results & Discussion

4.1 Core logging and measurements (moisture, coarse fraction)

The numerous independent measurements on KN134-11-GC01 (**Figure 2-7**) allow the consideration of the synchronous variations of geochemical and acoustic properties of red layers and to determine whether or not these deposits are turbiditic. This multiproxy approach in a single core avoids the age-depth uncertainties inherent in the comparison of different proxies and their interpretation at different locations (Fritz, 2008). The application of multiple parameters at the same temporal resolution further enables the determination of a common time frame for

changes in the elemental distribution of the sediments and their physical properties (Brisset et al., 2013). The combination of these two kinds of data makes the resulting interpretations of their changes more robust.

Acoustic and physical properties of unconsolidated, marine sediments are closely related to sediment composition and reflect changes in grain-size distribution and/or the ratio of terrigenous (quartz and clay) and biogenic (carbonate and opal) components (Weber et al., 1997). The wet-bulk density in KN134-11-GC01 decreases from ~1.5 to 1.6 g/cc to 1.0 g/cc through each consecutive pulse (**Figure 2-7**). There are approximately eleven of these oscillatory changes in the increase in bulk density. The changes in bulk density are accompanied by opposite changes in water content (**Figure 2-7**) in which the amount water increases from a water content of 20 to 30% at the silty base of each pulse to a water content of 50 to 55 % in the fine red clay sediment that is deposited after. Each cycle reflects higher sediment content per amount of volume at the onset of each pulse relative to the amount of water. The higher value of ~1.5 g/cc correlates with the base of each pulse, composed primarily of silt and sand. The bulk density sharply decreases and reflects that the composition of the sediment returns predominantly to clay. The changes in wet bulk density and water content reflect the changing porosity of the sediment; this observation can be interpreted as a change in size of the predominating sediment fraction.

Acoustic Impedance is a logging proxy for water content that is often used and is used as a proxy for changes in water content for that location in the core for which no water content was measured. This parameter demonstrates that the variability during the deposition of the red layers is higher than either during the post-connection Holocene or the glacial period prior to the meltwater event. There are two intervals during red sediment layer deposition in which the

amount of coarse sediment increases in the red sediments and is found in the silty bases of the layers (**Figure 2-7**). The documentation of the coarse sediment indicates that this silty base deposit occasionally also contains sand and possibly gravel. These occur at 176 and 87 cm in KN134-GC01. It is possible that each episodic meltwater event was different in strength and hence, some of the coarser sediment settled out closer to the source during some events than others.

P-wave velocity is also higher in coarse-grained sediments as a result of their grain to grain contact (Weber et al., 1997). The magnetic properties of sediment are most often related to the composition and proportion of detrital fraction, as well as changes in particle size (Dearing et al., 2001; Oldfield et al., 2003). The natural log of magnetic susceptibility (from now on referred to as magnetic susceptibility) drastically increases at the onset of each red layer, reaching well above background sediment levels. This spike reflects high textural and bulk density changes. The magnetic susceptibility near the base of each turbidite varies directly with relative sediment density and sand content, reflecting the pronounced textural layering within that each successive red layer deposit. The occurrence of multiple layers, overlying one another, suggests that these layers were deposited in a pulse-like manner, one after the other, possibly reflecting the delivery of water related to a cyclic mechanism.

4.2 X-Ray Fluorescence

The distribution and concentration of elements in the Black Sea-Lake red-layer sediments is an integrated result of a variety of factors and processes that include the composition of source rocks and sediment provenance, how efficient the sediments and allocthonous water are transported, sedimentation and deposition processes, and response of the Black Sea-Lake water

column during their deposition. The absolute (Ti, Ca, Zr, Mn, K, Fe, Mo, and Se) in ppm and relative (i.e., Ti/Ca) distributions of elements are presented (**Figure 2-8**). The average error associated with the XRF-measurements for Ti, Ca, Zr, Mn, K, Mo, and Se are 5%, 3%, 8.5%, 5.7%, 3.5%, 20%, 17.6%.

Titanium is related to the terrigenous-siliclastic component (i.e., clay minerals) whereas calcium reflects the carbonate component (i.e., that calcium deposited as an elemental component of calcite and aragonite) (Toucanne et al., 2009) as well as Ca from detrital and other continental input. Ti is presented as absolute concentrations (ppm) (**Figure 2-8**). Ca is also presented as absolute concentrations (ppm), as the directly measured $CaCO_3$ (%) (**Figure 2-8**), and as a ratio of Ti relative to the concentration of Ca (i.e., Ti/Ca). The concentration of Ca and $CaCO_3$ is inversely related to that of Ti. The resolution of the $CaCO_3$ record is less than the XRF measurements and hence the lack of direct correlation between the $CaCO_3$ and Ca (ppm) (**Figure 2-9**). The correlation between $CaCO_3$ and Ca (ppm) varies from 0.35 to 0.7 between different periods of deposition (i.e., Sapropel/ Unit 2, deglacial deposit that includes Preboreal and end of Younger Dryas, red layers, and glacial) but is 0.8 when all of the data is combined. This indicates that most of the Ca that is deposited in the sediment is in the form of $CaCO_3$. The concentration of XRF-Ca is high at each silty base, 40,000 to 50,000 ppm, and decreases in the clay deposit to a value between 0 and 20,000 ppm. $CaCO_3$ rises from 4 % to 16% through each pulse.

Ti is inert against digenetic alterations, exhibits conservative nature during transport and weathering, and is not subject to biological activity (Kylander et al., 2011). The ratio of Ti to Ca (**Figure 2-8**) is typically used as a representative indicator for variations in the relative proportion of terrigenous to carbonate sedimentation. As in Bahr et al., (2005), each time the

concentration of Ti concentration increases, the concentration of Ca decreases. However, the changes in Ti/Ca may not be representative of changes in the relative proportions of carbonate and detrital sedimentation during the deposition of the red layers but instead to changing mineralogical composition and grain size of the coarse silica rich sediment to finer clay sediment as all of the sediment during the red sediment layer deposition is essentially detrital in nature. We therefore reinterpret the identification of red layers via the Ti/Ca and suggest instead that the application of Ti/Ca is related to the nature of the deposition environment. In this particular core, the Ti/Ca refers to the fining upwards sequence of the red layers and the onset of each red layer is where the Ti/Ca is the lowest. Hence, the Ti/Ca signature of the meltwater deposits is unique to different deposition environments. For cores located in the activity of the rim current, such as MD07-2790, reveal a Ti/Ca that peaks in the red deposits whereas for the cores located downstream of river activity, record the changes in mineralogy and size grading, characteristic of turbidity deposits.

Zr/Rb was shown to be a reliable proxy for grain size changes (Dypvik and Harris, 2001; Kylander et al., 2011). Hence, it is applied to study the structure of the red layers in KN134-GC01 (**Figure 2-8**). Generally, Zr/Rb ratio increase with the increases in grains size. Ti, Rb, and K are often associated with clay mineral assemblages while Zr and Si are generally linked to coarser silt and sand sized fractions (Dypvik and Harris, 2001). Ti and Rb are present in several common minerals including mica and clay minerals and displays low environmental mobility mainly due to its very strong sorption to clay minerals, particularly at high pH. Zr is normally enriched in medium coarse silts and is associated with heavy minerals like zircon (Kylander et al., 2011). The largest relative proportion of Zr/Rb is found in the section of coarser sediment at the onset of each pulse and represents the higher proportion of sand and silt relative to clay.

4.3 Increase in water column ventilation

Fe content increases in each pulse as the sediment composition changes from coarse to fine (**Figure 2-8**). Changes in Fe can be indicative of redox conditions in the lake, of detrital inputs, and/or changes in sediment source (Davison, 1993). Moreover, Mn and Fe may react together in an anoxic environment but Fe can also be more associated with K, Ti, and Rb and indicative instead of detrital input (Kylander et al., 2011). In this case, increases in Fe occur at the same time as increases in Ti (but not Zr/Rb) which are attributed to higher Fe content of the clay. Mn is depressed in each pulse (**Figure 2-8**) and behaves opposite to that of Fe and Ti but identical to Ca and Si. It is possible that the increases in Fe are related to diagenetic processes after deposition as the red layers do exhibit darker layers and spots. The absence of changes in the concentration of sulfur, however, does not support this interpretation, and hence additional measurements, perhaps in the form of XRD analyses and other methods for isolating different mineralogical constituents, are necessary.

Bahr et al., (2005) previously attributed the lower concentrations of Mn to its decreased precipitation in a reducing environment. Reducing conditions makes Mn^{2+} more soluble (Peinerud, 2000; Tekiroğlu et al., 2001) whereas Mn precipitation is a sign of increased oxygen of the bottom waters instead of its absence. The close relationship with the increased concentration of coarser grained sediment suggests that the changes of Mn during the deposition of red sediments is more likely to be related to changes in grain size and mineralogy of the sediments and has little to do with ventilation. In fact, the correlation factor of Mn and Ca is 0.75 (**Figure 2-10b**). This is similar to the relationship of Ca and Mn during the glacial period (**Figure 2-10c**) where the correlation factor is 0.69. The relationship breaks down during the

Preboreal period (**Figure 2-10a**), where high $CaCO_3$ is precipitated from assimilation of CO_2 by phytoplankton (Major et al., 2006), and the $CaCO_3$ deposited is no longer detrital in nature but is biogenic. The vigorous and thorough ventilation of the water column is supported by the dramatic drop in radiocarbon at the onset of red layer deposition and its persistence until the end of the meltwater entrance (Soulet et al., 2011a; Yanchilina et al., to be submitted). Additionally, there is no supporting evidence of any deglacial increase in the concentration of Mo and Se, elements that also respond to changes in anoxia. These elements only increase above background levels in the early Holocene, once the Black Sea connected to the Mediterranean and the bottom water becomes anoxic (Piper and Calvert, 2011).

The $^{87}Sr/^{86}Sr$ composition of the Black Sea-Lake and the Marmara Sea-Lake (**Figure 2-11**) rises identically, at the same time, and at the same rate from ~0.7087 to 0.7091 in ~<100 years at 16 kyr BP. Following this rise, the $^{87}Sr/^{86}Sr$ composition of the Black Sea-Lake drops to 0.70875 at 14.80 kyr BP. A similar drop also occurs in the Marmara Sea-Lake although it is not as prominent. The $^{87}Sr/^{86}Sr$ composition of both lakes then stabilizes at 0.7089 until connection with the Mediterranean (13.80 kyr BP for the Marmara Sea-Lake and 9.30 kyr BP for the Black Sea-Lake).

4.4 Observations from core distributions

The distribution of cores shows two types of red sediment deposition. The sediment retrieved from the direction of prior river activity (i.e., KN134-11-GC01) features sediment with a predominance of silt and often sand and gravel, at the base of the red layers, grading to clay, and the sediment retrieved from the direction of the Rim Current (i.e., SG-09-30 and MD04-2790) features pulses of cross-bedded laminated clay.

The red sediments that are found downstream of a previously flowing Danube (i.e., KN134-11-GC01) are identified as turbidites from their fining up sequence. This is concluded from the gradation of silt to clay that is found within each pulse. Similar turbidic deposits are identified in other lake systems (Gilli et al., 2012; Zhang et al., 2014; Dhivert et al., 2015). The turbidite layer is defined as classically well graded, from sand in the lower part of the unit through silts to clay in the upper portion (Weber et al., 1997). A number of cores (i.e., BLKS98-21, BLKS98-22, BLKS98-23, BLKS98-24, BLKS98-25, BLKS98-27) taken from the Danube Fan and analyzed by Popescu et al., (2004) have similar pulses of red sediments that have sandy bases and grade up to silt and clay. Hyperpycnal flow at the Danube mouth was likely encouraged, a consequence of Black Sea being a freshwater lake. This type of environment favored the development of hyperpycnal flow of turbid waters entering at the Danube mouth, since only minor density differences prevailed between lake water and fresh river water.

The red deposits from those cores that are retrieved north of the Danube Fan and south of the Dniepr Fan (i.e., MD04-2790 and 09-SG-13) do not have similar fining up sequence and instead are largely composed of clay with scattered silts and sands. Hence, the mud delivered to these locations is not exclusively derived from the Danube but also from northern rivers (i.e., Dniepr and Don). Soulet et al., (2013) previously interpreted these red layers as the result not of turbidic processes but instead representing the springtime expulsion of anchor ice by deglacial meltwater discharges. We presented an example of the coarse component of this unconsolidated sediment with silt and sand in **Figure 2-2b**. Our interpretation acknowledges that these are not classically standard turbidite deposits, but nevertheless does attribute them to turbidic processes, which may yield a wide range of sedimentary deposits. The spatial distribution of these deposits (**Figure 2-5**) is also consistent with that typically associated with turbitite deposits. The absence

of graded beds in the individual pulses is likely to be a consequence of the settling out of coarser sediment closer to the source location (i.e., river channel) whereas the finer sediment would have been carried by the Rim Current and deposited farther from the original source on shelf and upper slope. Those red sediments that are found south of these northerm and northwestern river systems such as on the Turkey shelf and slope, are also characterized by the absence of grading in the individual pulses. Each channel fan has an individual expression of turbidites of that channel whereas sediments that are far from the source incorporate all the finer sediment carried by the Rim Current and allowed to settle out. The amount of sand found in each pulse is interpreted to reflect an inverse relationship with the distance from the channel axis. These interpretations are supported by those of Oguz et al., (1990) who hypothesized that the shelf-parallel Rim Current advects a dilute suspended sediment-cloud from the channel axis across the adjacent shelf.

4.5 Volume of Meltwater Delivery

Applying a set of original volume concentrations, from 0.5 to 9%, of the amount of sediment carried by turbidites, estimated to be 52.5 km^3, provides a range of volume estimates from ~10,500 km^3 to 580 km^3 of meltwater delivered to the Black-Sea Lake. This is a minimum estimate and only refers to the water that was delivered by the turbiditic processes, observed in the spatial distribution of cores collected in the Black Sea with the red sediments. The entire amount of water that was drained from the EISC and was delivered to the Black Sea-Lake draining from the EISC has potential to be much larger and would likely be delivered additionally, following each individual turbidite deposit, as a cyclic drainage of proglacial lakes. The full quantity of water that would have been delivered to the Black Sea-Lake can be

calculated from changes in $^{87}Sr/^{86}Sr$ of the Black Sea-Lake water during this period. The application of the results from modeling $^{87}Sr/^{86}Sr$ composition of the water by different original composition of the meltwater are illustrated and discussed below (**Figure 2-12**).

The range of $^{87}Sr/^{86}Sr$ as a function of the fraction of meltwater that would compose the final mixture implies that the there are two possible endmembers of meltwater delivery into the Black Sea-Lake. If the meltwater that entered was more radiogenic (i.e., $^{87}Sr/^{86}Sr$ of 0.73 to 0.75) its potential contribution to the Black Sea Lake water would be 5 to 10%. On the other hand, if the meltwater that was entered less radiogenic (i.e., $^{87}Sr/^{86}Sr$ of 0.71) its potential contribution would be a minimum of 20%. These calculations are both highly dependent also on the respective Sr concentration of the meltwater. If the incoming water had a lower Sr concentration, the observed shift in $^{87}Sr/^{86}Sr$ implies the replacement of a significantly larger fraction of the original Black Sea-Lake water, possibly up to 90%. A contribution of 5% is equivalent to ~20,000 km^3 and 90% equivalent to ~400,000 km^3 at the time the lake level was depressed by a 100 m relative to the present (that volume is estimated to be ~450,000 km^3). The $^{87}Sr/^{86}Sr$ composition of bulk sediment suggests that it is more likely that 5 to 10% of meltwater was delivered to the Black Sea. The lower estimation of 5% is close to the upper estimation of the water that entered with the turbidites, if the sediment concentration carried in the meltwater is on the order of 0.5%. The employment of two independent methods to estimate the amount of meltwater that entered the Black Sea-Lake with the turbiditic events and that which was delivered additionally, potentially even replacing all of the water in the basin. These calculations show that these were substantial flooding events and that the Black Sea served as an important catchment basin through which water from the northern ice sheets was routed during the latter part of the deglaciation at the time of HE1.

The $^{87}Sr/^{86}Sr$ evolution curves of the Marmara Sea-Lake and the Black Sea-Lake (**Figure 2-11**) indicate that the amount of water that entered the Black Sea-Lake was so large during this period that it overflowed into the Marmara Sea-Lake and changed the $^{87}Sr/^{86}Sr$ composition of the Marmara Lake-Sea as well. A feature identified earlier (Major et al., 2006) but not previously thoroughly discussed in the $^{87}Sr/^{86}Sr$ composition of the Black Sea-Lake is the drop in $^{87}Sr/^{86}Sr$ at 14.8 kyr BP. This may indicate the continued addition of meltwater to the Black Sea-Lake but from another source with a lower $^{87}Sr/^{86}Sr$ composition. Potential alternatives include the Dniepr and Don, with a modern $^{87}Sr/^{86}Sr$ composition of 0.7085 and drainage from the north. The corresponding volume of water that would have entered into the Black Sea-Lake with this composition, estimated from the mixing equation 1, is 22,500 km^3. The drop in $^{87}Sr/^{86}Sr$ occurred in less than 100 years and would correspond to a volumetric flux rate of 225 km^3/year. In comparison with the modern flow rate of ~75 km^3/year, this would be a three fold increase in Dniepr and Don discharge.

The size of the Eurasian ice sheets (Scandinavian Ice Sheet, Barents-Kara Ice Sheet, and British Ice Sheet) is estimated to be between 4.5 and 8 million km^3 at the time of the LGM (Siegert et al., 2001; Svendsen et al., 2004). The Barents-Kara Ice Sheets were getting progressively smaller during the successive Pleistocene glaciations, whereas the dimensions of the Scandinavian Ice Sheets increased through time (Svendsen et al., 2004). At the LGM, the Barents-Kara Ice Sheets are estimated to make up 30% of the total volume of the Eurasian Ice Sheet (Svendsen et al., 2004). The largest European ice sheets at this time are documented to have existed over Scandinavia (>2 km thick) and W. Barents Sea (>0.75 km thick). The vast size of these ice sheets suggests their huge potential for meltwater delivery to drainage areas, such as the Black Sea-Lake. The Alpine glaciers are estimated to have reached a volume of 120

thousand km^3 (Kelly et al., 2004; Ivy-Ochs et al., 2008). Despite their smaller size, the Alpine glaciers also have potential to deliver a significant amount of meltwater to the Black Sea-Lake.

During the LGM and just after the ice sheet had retreated from the Kubenskoye basin, extensive lakes are documented to have formed in front of the ice (Mangerud et al., 2004). The water level of these lakes, reconstructed from shorelines and deltas, was above sea level, as high as 130 m. Wide straits linked these lakes (Mangerud et al., 2004; Svendsen et al., 2004). Alternatively, meltwater may have escaped from the north in the form of jökulhlaups. Evatt et al., (2006) proposed that the drainage of lakes occurred beneath the ice sheets during the decomposition of the Laurentide Ice Sheet during the last ice age in a time-periodic manner and that these meltwater discharges could reach size of severe magnitude.

4.6 Origin of Red Layers

The minimal contribution of meltwater delivered to the Black Sea-Lake from these lakes would be a very small percentage of the ice sheets' volume. The application of ε_{Nd} to the detrital and authigenic components of the sediments provides a further constraint on the potential source of the meltwater that deposited these red layers in the Black Sea-Lake. The results from ε_{Nd} analysis are presented in the discussion and illustration below (**Figure 2-13**).

The ε_{Nd} results for authigenic and detrital fraction are illustrated together with ^{14}C, $\delta^{18}O$, and $\delta^{13}C$ data (surface and lake bottom). The ^{14}C and $\delta^{18}O$ constrain the deposition of the red layers to the time of the HE 1 and show that this interval in the core can be correlated to all of the other red layer deposits across the entire Black Sea sediment record. The ^{14}C dates were measured on juvenile *Dreissena r.* mollusks in the core at 159 and 59 cm and gave ^{14}C ages of 15 and 13.8 kyr BP, respectively (**Figure 2-13**). These convert to 16.35 and 15.00 kyr BP

(Yanchilina et al., submitted). The $\delta^{18}O$ of surface water is -6.87 ‰ at the onset of the red layers and falls to -7.852 ‰ at the end (the surface water $\delta^{18}O$ is derived from juvenile *Dreissena* shells). The $\delta^{13}C$ of *Dreissena r.* additionally constrain that this sediment was deposited during an environment in which the regional climate returned to glacial conditions. This is concluded from the $\delta^{13}C$ composition of mollusks in these sediments with a value of 2 ‰. Applying the simplest assumption of linear sedimentation between dated intervals yields a mean sedimentation rate of 14 calendar years/cm. This allows the assignment of calendar ages to the three intervals on which ε_{Nd} was analyzed: 16.35, 15.97 and 15.35 kyr BP.

The detrital values for ε_{Nd} are -10.1±0.08, -15.6±0.07, and -13.7±0.08 and the authigenic values for the two later pulses are -13.1±0.08 and -14.0±0.11. These results are not identical to those published by Soulet et al., (2013), who showed that all of the red layers had ε_{Nd} of -13 and belowThe explanation for the difference in isotope values is more likely to be ascribed to multiple sources of meltwater into the Black Sea at this time and that not any single meltwater event to be recorded identically everywhere on the basin bottom. The deposition of these red layers across the basin floor is known to regionally vary. Bahr et al., (2005) documents that the number of layers varies from 1 to 4 whereas in this manuscript, close examination of KN134-GC01 documents 11 layers.

It is possible that meltwater from an Alpine source was delivered to the Black Sea-Lake first and was subsequently followed by meltwater delivered from the EISC source afterwards as the east sourced ε_{Nd} was recorded first in the sequence of red layers in 09-SG-13. The red sediment delivered by the Danube was carried by the Rim Current across the Black Sea shelf and deposited in the current's downstream direction. It should be noted that red colored sediments are also deposited in some of the Romanian lakes such as Lake Preluca Tiganului (Wohlfarth et

al., 2001). Some of these red sediments are documented to remain exposed as glaciolacustrine kame terraces, such as those in Lithuania; these terraces spread up to 4 km long and are 400-700 m in width and 50 m in height (Bitinas et al., 2004). As meltwater was carried in rivers, draining to various basins, it likely picked up a substantial amount of the glacial loess along its way, such as that documented in deposits in western Europe. Haase et al., (2007) show that substantial loess deposits and loess derivatives of >5 m thickness occur in the northern drainage area of the Black Sea. This suggests a potential additional approach to constrain the sources and drainage of meltwater into various basins, namely the measurement of $^{87}Sr/^{86}Sr$ and ε_{Nd} within multiple red clay/silt deposits at different location, all dated to the HE 1 time period in Europe.

The meltwater that was derived from the Fennoscandianavian Ice Sheet came in such a large volume that the ε_{Nd} of meltwater was imprinted upon that of the Black Sea-Lake as is evident from the authigenic component of ε_{Nd}. The authigenic ε_{Nd} may be geographically biased towards the ε_{Nd} of the inflowing water, however. One way to test the realistic extent of the meltwater and its contribution, similar to the application of $^{87}Sr/^{86}Sr$ isotopes, is to test the authigenic component of the Black Sea water in cores that are farther offshore (i.e., KN134-11-GC01 and AKAD09-16).

The different values for ε_{Nd} in the red layers point to multiple sources of meltwater to the Black Sea. Bahr et al., (2005) stated that alpine meltwater can only potentially account for the deposition of red layers between 18 and 17.3 kyr BP, not for the entire period of 2,500 years during the deposition of the red layers. Bahr et al., (2005) applied a 1,000 reservoir age to all of their ^{14}C ages before converting to calendar ages whereas in this manuscript, a varying ^{14}C reservoir, details of which are presented in Yanchilina et al., (to be submitted), is subtracted from all of the ^{14}C measurements before converting them to calendar ages. Hence, it is more

appropriate to compare observations as a function of measured uncorrected ^{14}C ages rather than from absolute calendar ages as this parameter has evolved through the publication record as each publication presents a new age model specific to their work and interpretations. Denton et al., (1999), on the other hand, showed that the Swiss Alps experienced massive deglaciation during Oldest Dryas time, defined as to have occurred between 12 to 11.8 kyr ^{14}C (i.e., 13.84-13.69 kyr BP), hence deglaciation from the Alpine source could have taken place at some point during the deposition of these red layers and not necessarily at the very beginning of HE1.

Furthermore, Toucanne et al., (2009) identify prior existence of a Fleuve Manche (**Figure 2-14**), a glacially fed river that delivered meltwater along the southern margin of the ice sheets to the Bay of Biscay. Thorough ε_{Nd} measurements in a core from this specific location documented the delivery of meltwater and revealed that the meltwater was not exclusively sourced from a single location but have come from a series of locations. The source of the turbidites alternated between the Scandinavian ice-sheet (SIS) and British-Irish ice-sheet (BIIS) (Toucanne et al., 2015) (SIS and BIIS are shown as one EISC (Svendsen et al., 2004). It is therefore likely that the meltwater to the Black Sea was not exclusively sourced from one location the entire time but from multiple sources and even, potentially, in an episodically varying manner. A clear decrease of glacially derived inflowing water is documented to occur after 17 kyr BP, an observation that is consistent with a substantial reduction of seaward transfer of continentally derived sediment onto the Armorican margin (Toucanne et al., 2009; Toucanne et al., 2010; Toucanne et al., 2015). If the delivery of water to the Bay of Biscay was reduced, even as the Fennoscandinavian ice sheet continued to melt, the meltwater had to be transported elsewhere.

It is therefore likely that this meltwater made its way south to basins such as the Black Sea, the Caspian Sea, and various lakes in Europe via Danube, Dniestr, Dniepr, Don, and Volga

as the retreat of the ice sheets continued and the initial drainage framework changed (**Figure 2-14**). The volume of Lake Disna, the exclusive source of meltwater to the Black Sea suggested by (Soulet et al., 2013) is only ~4,000 km^3. It is not likely that the entire lake drained and that all of the water reached the Black Sea. If the amount of original water that did make it to the Black Sea is assumed to be 10% from Lake Disna, there would have to be 25 flood events to add up to the minimum estimated amount of meltwater that was delivered to the Black Sea during this period. Since the largest amount of layers is documented to be 11, and that it is possible that all of the water in the Black Sea was replaced by the delivery of meltwater based on $^{87}Sr/^{86}Sr$ mixing calculations, it is much more likely that meltwater was not exclusively sourced from Lake Disna but from multiple locations during the deglaciation process.

The possibility that meltwater outflowed to the Caspian Sea cannot be dismissed. The modern $^{87}Sr/^{86}Sr$ cannot be used to argue that the $^{87}Sr/^{86}Sr$ remained constant through the entire time in the deglaciation history of the Black Sea. It is possible that meltwater from the north also was delivered into the Caspian. Judging by the size of the meltwater delivered to the Black Sea, that meltwater delivered to the Caspian would have high potential for overflowing into downstream basins (i.e., Black Sea). A straightforward way to test this argument would be the generation of $^{87}Sr/^{86}$ and complementary ε_{Nd} measurements in the Caspian from the red layers identified there.

4.6 Sequence of disintegration of EISC

The proposed sequence of disintegration of the EISC and Alpine Ice Caps is broken up into four stages (**Figure 2-15**). During stage 1, 18.2 to 16.7 kyr BP, the southern margin of the EISC was retreating with the meltwater delivered to the Bay of Biscay (Toucanne et al., 2009;

Toucanne et al., 2015) via Fleuve Manche (aka Channel River) (**Figure 2-15a**). During stage 2, 16.70 to 16.35 kyr BP, EISC broke up into two smaller ice sheets, SIS and BIIS. Following the primary retreat of the southern margin, the meltwater is proposed to escape north to the Arctic via Fleuve Norde positioned in between the two ice sheets (**Figure 2-15b**). During stage 3, 16.35 to 15.00 kyr BP, after the EISC has retreated more to the north, Don and Dniepr deliver meltwater to drainage basins located to the south, such as the Black Sea (**Figure 2-15c**). The contribution of meltwater from the Alps is proposed to take place during stages 1-3. During stage 4, 15 to ~12.90 kyr BP (Mangerud et al., 2004), the meltwater from the SIS is proposed to resume its drainage north to the Arctic via Fleuve Norde (II) (**Figure 2-15d**). It is also likely that water from the northeastern margin of SIS drained south to the Caspian Sea via Volga River as red layer deposits are documented in this basin as well (Bahr et al., 2006). From the north, the water was likely sourced either from proglacial lakes that formed at the margin of the ice sheets and/or from jökulhaups escaping from lakes formed underneath melting ice sheets. From the west, it is likely that the meltwater initially ponded in the Hungarian basin. Then, it catastrophically drained through the Iron Gates via the Danube, similar to the catastrophic drainage of Lake Missoula (Baker, 1973). Those deposits formed in the core of the rivers were turbidites whereas those that formed in the direction of the Rim Current, were laminated scattered silts and clays. It cannot be dismissed that meltwater did not drain to the Black Sea-Lake from the Caspian Sea, as red layers are also identified in this basin dating to this time period and invites further research.

The meltwater delivered to the Black Sea-Lake did not necessarily raise the lake level as the lake level was already at its outlet to the global ocean via the Bosporus sill at -80 m (Nicholas and Chivas, 2014; Yanchilina et al., submitted). The increased inflow and therefore

outflow would have reduced the residence time of water within the basin. At least some of the meltwater descended to depths as turbid hyperpycnal flows, and some even reached the bottom of the Black Sea-Lake in the form of the documented turbidite deposits, thoroughly ventilating the entire water column and eradicating any prior glacial stratification. These megafloods are similar to those that have formed the Channeled Scabland of the western US (Bretz, 1923; Baker et al., 1978). Gupta et al., (2007) previously described a similar relict channel network produced by Pleistocene megafloods that now have submerged beneath the waters of the North Sea. These megafloods are highly erosive and their channels are deeply incised, into both superficial material and bedrock (Baker et al., 1978; Gupta et al., 2007). The water delivered to the Black Sea was of large volume and overflowed into the Marmara Sea, and potentially also into the Agean Sea, as is clearly shown for the dual spike in $^{87}Sr/^{86}Sr$ in both the Black Sea and Sea of Marmara biogenic carbonate (Vidal et al., 2010; Soulet et al., 2013; Yanchilina et al., to be submitted).

5. Conclusions

The results presented here identify meltwater events as episodic events, megafloods that entered the Black Sea-Lake during the deglacial period in Earth's late Pleistocene history between 16.35 and 15.00 kyr BP. These deposits are not identical everywhere and vary between a composition exclusively clay and scattered silts to fining-up sequences from silt to clay. This variation in their character is location-based, and a fining-up structure to the deposits is more likely to occur closer to the source location. This sequence of meltwater events is similar to others that have occurred during the deglaciation period such as the Channeled Scabland of the western United States. This is a regional manifestation of a global phenomenon in which water

previously locked up in massive ice sheets was released into downstream basins in the form of huge floods. It is estimated that the maximum amount of water descended into the abyss as turbidity currents is ~10,500 km^3 and that water delivered additionally as part of cyclic megaflood activity ranges from 20,000 km^3 to 400,000 km^3, a number that is equivalent to the entire volume of the lake at that time. These floods were not exclusively sourced from Lake Disna, but more likely came from meltwater escaping from a series of dammed proglacial lakes the EISC and the Alps. The megafloods delivered water to the basin bottom in the form of hyperpycnal flows and turbidity currents, vigorously ventilating and delivering oxygen to the entire water column, bringing the ^{14}C age of the water at all depths to zero. As the lake was already at its outflow sill prior to this period, there was no significant rise in lake level, leaving it its paleoshoreline of 95 mbsl. The excess water outflowed to a network of basins connected to the Black Sea Lake (i.e., Sea of Marmara and the Aegean Sea).

References

Andersen, K., N. Azuma, J.-M. Barnola, M. Bigler, P. Biscaye, N. Caillon, J. Chappellaz, B. Clausen, D. Dahl-Jensen, H. Fischer, J. Flückiger, D. Fritzsche, Y. Fujii, K. Goto-Azuma, K. Grønvold, N. S. Gundenstrup, M. Hansson, C. Huber, C. S. Hvidberg, J. Johnsen, U. Jonsell, S. Kipfstuhl, A. Landais, M. Leuenberger, R. Lorrain, V. Masson-Delmotte, H. Miller, ;, H. Motoyama, H. Narita, T. Popp, S. O. Rasmussen, D. Raynaud, R. Rothlisberger, U. Ruth, D. Samyn, J. Schwander, H. Shoji, M.-L. Siggard-Andersen, J. P. Steffensen, T. Stocker, A. E. Sveinbjörnsdóttir, A. Svensson, M. Takata, J.-L. Tison, T. Thorsteinsson, ;, O. Watanabe, F. Wilhems and J. W. C. White, 2004. High-resolution record of Northern Hemisphere climate extending into the last interglacial period. Nature 431, 147-151.

Andersson, P. S., G. J. Wasserburg and J. Ingri, 1992. The sources and transport of Sr and Nd isotopes in the Baltic Sea. Earth and Planetary Science Letters 113, 459-472.

Andersson, P. S., G. J. Wasserburg, J. Ingri and M. C. Stordal, 1994. Stronitium, dissolved and particulate loads in fresh and brackish waters: The Baltic Sea and Mississippi Delta. Earth and Planetary Science Letters 124, 195-210.

Badertscher, S., D. Fleitmann, H. Cheng, R. L. Edwards, O. M. Göktürk, A. Zumbühl, M. Leuenberger and O. Tüysüz, 2011. Pleistocene water intrusions from the Mediterranean and Caspian seas into the Black Sea. Nat. Geosci. 4, 236-239.

Bagnold, R. A., 1962. Auto-suspension of transported sediment; turbidity currents. Proceedings of the Royal Society of London. Series A, Mathematical and Physical Sciences 265, 315-319.

Bahr, A., H. Arz, F. Lamy and G. Wefer, 2006. Late glacial to Holocene paleoenvironmental evolution of the Black Sea, reconstructed with stable oxygen isotope records obtained on ostracod shells. Earth Planet. Sc. Lett. 241, 863-875.

Bahr, A., F. Lamy, H. Arz, H. Kuhlmann and G. Wefer, 2005. Late glacial to Holocene climate and sedimentation history in the NW Black Sea. Marine Geology 214, 309-322.

Bailey, T. R., J. M. McArthur, H. Prince and M. F. Thirwall, 2000. Dissolution methods for strontium isotope stratigraphy: Whole rock analysis. Chemical Geology 167, 313-319.

Baker, E. W., S. E. Palmer and W. Y. Huang, 1978. Early and intermediate chlorophyll diagenesis of Black Sea sediments; sites 379, 380, and 381. . In: Leg 42B, Istanbul, Turkey, to Istanbul, Turkey, May June 1975. 42 Part 2.

Baker, V. R., 1973. Paleohydrology and sedimentology of Lake Missoula flooding in eastern Washington. Geol. Soc. America Special Paper 144, 79.

Bell, H. S., 1942. Density currents as agents for transporting sediments. Journal of Geology 50, 512-547.

Bitinas, A., D. Karmazien and A. Jusien, 2004. Glaciolacustrine kame terraces as an indicator of conditions of deglaciation in Lithuania during the Last Glaciation. Sedimentary Geology 165, 285-294.

Blum, J. D. and Y. Erel, 1995. A silicate weathering mechanism linking increases in marine 87Sr/86Sr with global glaciation. Nature 373, 415-418.

Bond, G., W. Broecker, S. Johnsen, J. McManus, L. Labeyrie, J. Jouzel and G. Bonani, 1993. Correlations between climate records from North Atlantic sediments and Greenland ice. Nature 365, 143-147.

Bond, G., H. Heinrich, W. Broecker, L. Labeyrie, J. McManus, J. Andrews, S. Huon, R. Jantschik, S. Clasen, C. Simet, K. Tedesco, M. Klas, G. Bonani and S. Ivy, 1992. Evidece for massive discharges of icebergs into the North Atlantic ocean during the last glacial period. Nature 360, 245-249.

Bondar, C., I. State, D. Cernea and E. Harabagiu, 1991. Water flow and sediment transport of the Danube River at its outlet into the Black Sea. Meterol. Hydrol. 21, 21-25.

Bouma, A. H., 1962. Sedimentology of some flysch deposits. A graphic approach to facies interpretation. Amsterdam, Elsevier.

Bretz, J. H., 1923. The Channeled Scabland of the Columbia Plateau. Jour. Geology 31, 617-649.

Brisset, E., C. Miramont, F. Guiter, E. J. Anthony, K. Tachikawa, J. Poulenard, F. Arnaud, C. Delhon, J.-D. Meunier, E. Bard and F. Suméra, 2013. Non-reversible geosystem destablisation at 4200 cal. BP: Sedimentological, geochemical and botanical markers of soil erosion recorded in a Mediterranean alpine lake. The Holocene 23, 1863-1874.

Chepalyga, A., 2007. The late glacial great flood in the ponto-caspian basin. In: V. Yanko-Hombach, A. Gilbert, N. Panin and P. Dolukhanov (Eds.), The Black Sea flood Question: Changes in Coastline, Climate, and Human Settlement. Dordrecht, The Netherlands, Springer**:** 119-148.

Clauer, N., S. Chaudhuri, T. Toulkeridis and G. Blanc, 2000. Fluctuations of Caspian Sea level: Beyond climatic variations? Geology 28, 1015-1018.

Cohen, D. and W. B. F. Ryan, 2011. Black Sea low stands during the Holocene and Pleistocene and reconnection with the global ocean.

Davison, W., 1993. Iron and manganese in lakes. Earth-Science Reviews 34, 119-163.

Dearing, J., Y. Hu, P. Doody, P. A. James and A. Brauer, 2001. Preliminary reconstruction of sediment-source linkages for the past 6000 yr at the Petit Lac d'Annecy, France, based on mineral magnetic data. Journal of Paleolimnology 25, 245-258.

Denton, G. H., C. J. Heusser, T. V. Lowell, P. I. Moreno, B. G. Anderson, L. E. Heusser, C. Schlüchter and D. R. Marchant, 1999. Interhemispheric linkage of paleoclimate during the last glaciation. Geografiska Annaler 81, 107-153.

Dhivert, E., C. Grosboi, A. Coynel, I. Lefèvre and M. Desmet, 2015. Influences of major flood sediment inputs on sedimentary and geochemical signals archived in a reservoir core (Upper Loire Basin, France). Catena 126, 75-85.

Dypvik, H. and N. B. Harris, 2001. Geochemical facies analysis of fine-grained siliclastics using Th/U, Zr/Rb, and (Zr+Rb)/Sr ratios. Chemical Geology 181, 131-146.

Evatt, G. W., A. C. Fowler, C. D. Clark and N. R. Hulton, 2006. Subglacial floods beneath ice sheets. Philosophical transactions of the Royal Soceity A 364, 1769-1794.

Fleitmann, D., H. Cheng, S. Badertscher, R. L. Edwards, M. Mudelsee, O. M. Göktürk, A. Fankhauser, R. Pickering, C. C. Raible, A. Matter, J. Kramers and O. Tüysüz, 2009. Timing and climatic impact of Greenland interstadials recorded in stalagmites from northern Turkey. Geophysical Research Letters 36.

Forman, S. L., Ó. Ingólfssonl, V. Gataullin, W. F. Manley and H. Lokrantz, 1999. Late Quaternary stratigraphy of western Yamal Peninsula, Russia: New constraints on the configuration of the Eurasian ice sheet. Geology 27, 807-810.

Fritz, S., 2008. Deciphering climatic history from lake sediments. Journal of Paleolimnology 39, 5-16.

Geotek, I., 2014. Multi-sensor core logger manual (version 17-02-14). Available from World Wide Web, http://www.geotek.co.uk/sites/default/files/MSCLmanual.pdf.

Gilli, A., F. S. Anselmetti, L. Glur and S. B. Wirth, 2012. Lake sediments as archives of recurrence rates and intensities of past flood events. In: M. Schneuwly-Bollschweiler, M. Stoffel and F. Rudolf-Miklau (Eds.), Dating Torrential Processes on Fans and Cones. Dordrecht, Springer Netherlands. 47**:** 225-242.

Grosswald, M. G., 1980. Late Weichselian ice sheet of Northern Europe. Quaternary Research 13, 1-32.

Grosswald, M. G. and T. J. Hughes, 2002. The Russian component of an Arctic ice sheet during the Last Glacial Maximum. Quaternary Science Reviews 21, 121-146.

Gupta, S., J. S. Collier, A. Palmer-Felgate and G. Potter, 2007. Catastrophic flooding origin of shelf valley systems in the English Channel. Nature 448, 342-345.

Gutjahr, M., M. Frank, C. H. Stirling, V. Klemm, T. van de Flierdt and A. N. Halliday, 2007. Reliable extraction of a deepwater trace metal isotope signal from Fe-Mn oxyhydroxide coatings of marine sediments. Chemical Geology 242, 351-370.

Gyllencreutz, R., J. Mangerud, J.-I. Svendsen and O. Lohne, 2007. Dated - a GIS-based reconstruction and dating database of the Eurasian Deglaciation. Geological Survey of Finland, 113-120.

Haase, D., J. Fink, G. Haase, R. Ruske, M. Pécsi, H. Richter, M. Altermann and K.-D. Jäger, 2007. Loess in Europe-its spatial distribution based on a European Loess Map, scale 1:2,500,000. Quaternary Science Reviews 26, 1301-1312.

Hemming, S. R., 2004. Heinrich events: massive late Pleistocene detritus layers of the north Atlantic and their global climate imprint. Reviews of Geophysics 42, RG1005.

Hinderer, M., 2001. Late Quaternary denudation of the Alps, valley and lake fillings and modern river loads. Geodinamica Acta 14, 231-263.

Ivy-Ochs, S., H. Kerschner, A. Reuther, F. Preusser, K. Heine, M. Maisch, P. W. Kubik and C. Schlüchter, 2008. Chronology of the last glacial cycle in the European Alps. Journal of Quaternary Science 23, 559-573.

Jacobsen, S. B. and G. J. Wasserburg, 1980. Sm-Nd isotopic evolution of chondrites. Earth and Planetary Science Letters 50, 139-155.

Kalicki, T. and A. F. Sanko, 1998. Palaeohydrological changes in the Upper Dneper Valley, Belarus, during the last 20,000 years. In: G. Benito, V. R. Baker and K. J. Gregory (Eds.), Palaeohydrology and Environmental Change. Chichester, England, John Wiley & Sons, Ltd.**:** 125-135.

Kelly, M. A. l., J.-F. Buoncristiani and C. Schlüchter, 2004. A reconstruction of the last glacial maximum (LGM) ice-surface geometry in the western Swiss Alps and contiguous Alpine regions in Italy and France. Swiss Journal of Geosciences 97, 57-75.

Kenna, T. C., F. O. Nitsche, M. M. Herron, B. J. Maillouv, D. Peteet, S. Sritrairat, E. Sands and J. Baumgarten, 2011. Evaluation and Calibration of a Field Portable X-Ray Fluorescence Spectrometer for quantitative analysis of siliclastic soils and sediments. Journal of Analytic Atomic Spectrometry 26, 10.

Kvasov, D. D., 1968. Paleohydrology of eastern Europe in late Quaternary time. Yezhegodnkkh Chetniyakh Pamyati L.S. Berga Doklady Izd. Nauka, Leningrad, 65-81.

Kylander, M., L. Ampel, B. Wohlfarth and D. Veres, 2011. High-resolution X-ray fluorescence core scanning analysis of Les Echets (France) sedimentary sequence: new insights from chemical proxies. Journal of Quaternary Science 26, 109-117.

Löfvendahl, R., G. Aberg and P. Joseph, 1990. Strontium in rivers of the Baltic Basin. Aquatic Sciences 52, 315-329.

Major, C., S. Goldstein, W. Ryan, G. Lericolais, A. M. Piotrowski and I. Hajdas, 2006. The co-evolution of Black Sea level and composition through the last deglaciation and its paleoclimatic significance. Quatern. Sci. Rev. 25, 2031-2047.

Major, C., W. Ryan, G. Lericolais and I. Hajdas, 2002. Constraints on Black Sea outflow to the Sea of Marmara during the last glacial–interglacial transition. Marine Geology.

Mangerud, J., V. Astakhov, M. Jakobsson and J. I. Svendsen, 2001. Huge Ice-age lakes in Russia. Journal of Quaternary Science 16, 773-777.

Mangerud, J., V. Astakhov and J.-I. Svendsen, 2002. The extent of the Barents-Kara ice sheet during the Last Glacial Maximum. Quaternary Science Reviews 21, 111-119.

Mangerud, J., M. Jakobsson, H. Alexanderson, V. Asyakhov, G. K. C. Clarke, M. Henriksen, C. Hjort, G. Krinner, J.-P. Lunkka, P. Moller, A. Murray and O. Nikolskaya, 2004. Ice-dammed lakes and rerouting of the drainage of northern Eurasia during the Last Glaciation. Quaternary Science Reviews 23, 1313-1332.

McManus, J. F., D. W. Oppo and J. L. Cullen, 1998. A 0.5-million-year record of millenial scale climate variability in the North Atlantic. Science 283, 971-975.

Ménot, G., E. Bard, F. Rostek, J. W. H. Weijers, E. C. Hopmans, S. Schouten and J. S. Sinninghe Damsté, 2006. Early reactivation of European rivers during the last deglaciation. Science 313, 1623-1625.

Ménot, G., E. Bard, F. Rostek, J. W. H. Weijers, E. C. Hopmans, S. Schouten and J. S. Sinninghe Damsté, 2006. Early reactivation of European rivers during the last deglaciation. Science 313, 1623-1625.

Mulder, T. and J. Alexander, 2001. The physical character of subaqueous sedimentary density flows and their deposits. Sedimentology 48, 269-299.

Nicholas, W. A. and A. R. Chivas, 2014. Late Quaternary sea-level change on the Black Sea shelves. In: F. L. Chiocci and A. R. Chivas (Eds.), Continental shelves of the world: their evolution during the last glacial-eustatic cycle. London, Geological Society. 41**:** 199-212.

Nowaczyk, N. R., H. W. Arz, U. Frank, J. Kind and B. Plessen, 2012. Dynamics of the Laschamp geomagnetic excursion from Black Sea sediments. Earth and Planetary Science Letters 351-352, 54-69.

Oguz, T., E. Özsoy, M. A. Latif, H. I. Sur and Ü. Ünlüata, 1990. Modelling of hydraulically controlled exchange £ow in the Bosphorur Strait. J. Phys. Oceangr. 20, 945-965.

Oldfield, F., R. Wake, J. Boyle, S. Nolan, Z. Gibbs, P. Appleby, E. Fisher and G. Wolff, 2003. The late-Holocene history of Gormire Lake (NE England) and its catchment: a multiproxy reconstruction of past human impact. The Holocene 13, 677-690.

Palmer, M. R. and J. M. Edmond, 1989. The strontium budget of the modern ocean. Earth and Planetary Science Letters 92, 11-26.

Panin, N. and D. Jipa, 2002. Danube river sediment input and its interaction with the north-western Black Sea. Estuarine, Coastal, and Shelf Science 54, 551-562.

Peinerud, E. K., 2000. Interpretation of Si concentrations in lake sediments: three case studies. Environmental Geology 40, 64-72.

Piper, D. and S. Calvert, 2011. Holocene and late glacial palaeoceanography and palaeolimnology of the Black Sea: Changing sediment provenance and basin hydrography over the past 20,000 years. Geochim. Cosmochim. Acta 75, 5597-5624.

Popescu, I., G. Lericolais, N. Panin, Ç. N., A. Normand, C. Dinu, DC and E. Le Drezen, 2004. The Danube Submarine Canyon (Black Sea): morphology and sedimentary processes. Marine Geology 206, 249-265.

Ryan, W. B. F., 2007. Status of the Black Sea flood hypothesis. In: V. Yanko-Hombach, A. S. Gilbert, N. Panin and P. M. Dolukhanov (Eds.), The Black Sea Flood Question: Changes in Coastline, Climate, and Human Settlement. Dordrecht, The Netherlands, Springer**:** 63-88.

Siegert, M. J. and J. A. Dowdeswell, 2004. Numerical reconstructions of the Eurasian Ice Sheet and climate during the Late Weichselian. Quaternary Science Reviews 23, 1273-1283.

Siegert, M. J., J. A. Dowdeswell, M. Hald and J.-I. Svendsen, 2001. Modelling the Eurasian Ice Sheet through a full (Weichselian) glacial cycle. Global and Planetary Change 31, 367-385.

Soulet, G., G. Menot, G. Bavon, F. Rostek, E. Ponsevera, S. Toucanne, G. Lericolais and E. Bard, 2013. Abrupt drainage cycles of the Fennoscandian Ice Sheet Proceedings of the National Academy of Sciences 110, 6682-6687.

Soulet, G., G. Ménot, V. Garreta, F. Rostek, S. Zaragosi, G. Lericolais and E. Bard, 2011a. Black Sea "Lake" reservoir age evolution since the Last Glacial — Hydrologic and climatic implications. Earth Planet. Sc. Lett. 308, 245-258.

Soulet, G., G. Ménot, G. Lericolais and E. Bard, 2011b. A revised calendar age for the last reconnection of the Black Sea to the global ocean. Quaternary Science Reviews 30.

Spielhagen, R. F., K.-H. Baumann, H. Erlenkeuser, N. R. Nowaczyk, N.-P. N., C. Vogt and D. Weiel, 2004. Arctic Ocean deep-sea record of northern Eurasian ice sheet history. Quaternary Science Reviews 23, 1455-1483.

Svendsen, J.-I., H. Alexanderson, V. Astakhov, I. Demidov, J. A. Dowdeswell, S. Funder, V. Gataullin, M. Henriksen, C. Hjort, M. Hounmark-Nielsen, H. W. Hubberten, Ó. Ingólfssonl, M. Jakobsson, K. H. Kjæri, E. Larsen, H. Lokrantz, J. P. Lunkka, A. Lysa, J.

Mangerud, A. Matiouchkov, A. Murray, P. Möller, F. Niessen, O. Nikolskaya, L. Polyak, M. Saarnisto and C. Siegert, 2004. Late Quaternary ice sheet history of northern Eurasia. Quaternary Science Reviews 23, 1229-1271.

Syvitski, J. P. M. and C. T. Schafer, 1996. Evidence for an earthquake-triggered basin collapse in Saguenay Fjord, Canada. Sedimentary Geology 104, 127-153.

Tekiroğlu, S. E., V. Ediger, S. Yemenicioğlu, S. Kapur and E. Akça, 2001. The experimental analysis on the Late Quaternary deposits of the Black Sea. Oceanologica Acta 24, 51-67.

Toucanne, S., G. Soulet, N. Freslon, S. R. Jacinto, B. Dennielou, S. Zaragosi, F. Eynaurd, J.-F. Bourillet and G. Bayon, 2015. Millenial-scale fluctuations of the European Ice Sheet at the end of the last glacial, and their potential impact on global climate. Quaternary Science Reviews 123, 113-133.

Toucanne, S., S. Zaragosi, J.-F. Bourillet, M. Cremer, F. Eynaud, B. Van Vilet-Lanoë, A. Penaud, C. Fontanier, J.-L. Turon, E. Cortijo and P. L. Gibbard, 2009. Timing of massive 'Fleuve Manche' discharges over the last 350 kyr: insights into the European ice-sheet oscillations and the European drainage network from MIS 10 to 2. Quaternary Science Reviews 28, 1238-1256.

Toucanne, S., S. Zaragosi, J.-F. Bourillet, V. Marieu, M. Cremer, M. Kageyama, B. V. Vliet-Lanoë, F. Eynaud, J.-L. Turon and P. L. Gibbard, 2010. The firts estimation of Fleuve-Manche palaeoriver discharge during the last deglaciation: Evidence for Fennoscandian ice sheet meltwater flow in the English Channel 20-18 ka ago. Earth and Planetary Science Letters 290, 459-473.

Ünlüata, Ü., T. Oguz, M. A. Latif and E. Özsoy, 1990. On the physical oceanography of the Turkish Straits. In: L. J. Pratt (Eds.), The Physical Oceanography of Sea Straits. Deventer, The Netherlands, Kluwer**:** 25-60.

Vidal, L., G. Ménot, C. Joly, H. Bruneton, F. Rostek, M. N. Çağatay, C. Major and E. Bard, 2010. Hydrology in the Sea of Marmara during the last 23 ka: Implications for timing of Black Sea connections and sapropel deposition. Paleoceanography 25.

Weber, M. E., F. Niessen, G. Kuhn, ; and M. Wiedicke, 1997. Calibration and application of mairne sedimentary physical properties using a multi-sensor core logger. Marine Geology 136, 151-152.

Wegwerth, A., O. Dellwig, J. Kaiser, G. Ménot, E. Bard, L. Shumilovskikh, B. Schnetger, I. C. Kleinhanns, M. Wille and H. W. Arz, 2014. Meltwater events and the Mediterranean reconnection at the Saalian-Eemian transition in the Black Sea. Earth and Planetary Science Letters 404, 124-135.

Wohlfarth, B., G. Hannon, A. Feurdean, L. Ghergari, B. P. Onac and G. Possnert, 2001. Reconstruction of climatic and environmental changes in NW Romania during the early

part of the last deglaciation (~15,000-13,6000 cal yr BP). Quaternary Science Reviews 20, 1897-1914.

Yanchilina, A. G., W. B. F. Ryan, J. F. McManus, P. Dimitrov, D. Dimitrov, K. Slavova and M. Filipova-Marinova, submitted. Rapid transgression and gradual salinification of the Black Sea from inflow of Mediterranean water in the Holocene. Marine Geology.

Yanchilina, A. G., W. B. F. Ryan, J. F. McManus, T. C. Kenna, M. Filipova-Marinova, D. Dimitar and P. DImitrov, to be submitted. Black Sea-Lake during the last glacial period: cold, wet, partially isolated from outflow to the global ocean and briefly frozen. Quaternary Science Reviews.

Zhang, X., C. A. Scholz, R. E. Hecky, D. A. Wood, H. J. Zal and C. J. Ebinger, 2014. Climatic control of the late Quaternary turbidite sedimentology of Lake Kivu, East Africa: Implications for deep mixing and geologic hazards. Geology 42, 811-814.

Table 2-1

Table 1

Core name	Latitude (N)	Longitude (E)	Core Depth (m)	Red Sediment Thickness (cm)	Cruise and/or Reference
09-SG-13	44°07.204	30°48.087	200	105	Mare Nigrum, 2009 & *Briceag et al.*, 2014
A96	42°47.200	28°33.500	630	25	*Khrischev and Georgiev*, 1991
AKAD09-09	42°49.500	28°55.800	1500	24	Akademik 2009
AKAD09-16	42°41.970	28°47.550	1445	35	Akademik 2009
AKAD09-10	42°54.800	28°45.600	1000	20	Akademik 2009
AKAD09-18	42°41.948	28°25.965	476	50	Akademik 2009
AKAD09-28	42°42.001	28°21.889	126	6	Akademik 2009
AKAD09-30	42°59.714	28°31.433	115	8	Akademik 2009
AKAD11-11	42°22.097	28°32.705	510	52	Akademik 2011
AKAD11-13	42°21.527	28°38.277	820	168	Akademik 2011
AKAD11-17	42°51.225	29°01.142	1805	93	Akademik 2011
AKAD11-07	42°08.080	28°32.604	125	>10	Akademik 2011
BLKS98-09	44°05.238	30°47.986	240	195	BLaSON 1998 & *Major et al.*, 2002
BLKS98-10	44°04.040	30°50.680	378	112	BLaSON 1998 & *Major et al.*, 2002
BLKS98-22	43°02.271	32°07.492	2100	34	BLaSON 1998 & *Major et al.*, 2002
BLKS98-23	43°05.730	32°04.227	2090	134	*Popescu et al.*, 2008
BLKS98-24	43°31.338	31°33.670	1862	>178	*Popescu et al.*, 2008
D2DP 42-380	42°05.940	29°36.822	2107	150	DSDP 42 & *Ross and Degens*, 1974
GC01	41°53.320	28°49.210	649	20	Knorr 1988 & *Arthur and Dean*, 1998
GC014	43°04.680	34°01.620	2218	51	Knorr 1988 & *Piper and Calvert*, 2011
GC08	41°55.900	28°55.190	901	50	Knorr 1988 & *Arthur and Dean*, 1998
GC09	41°56.220	29°02.110	1258	50	Knorr 1988 & *Arthur and Dean*, 1998
GC19	42°52.480	31°22.460	2096	50	Knorr 1988 & *Arthur and Dean*, 1998
GC20	43°06.980	32°00.850	2088	50	Knorr 1988 & *Arthur and Dean*, 1998
GeoB 7604-2	42°56.200	30°01.900	1977	55	RV Meteor 2001 and *Bahret al.*, 2005
GeoB 7607-2	43°09.700	29°57.700	1562	100	RV Meteor 2001 and *Bahret al.*, 2005
GeoB 7608-1	43°29.200	30°11.800	1202	195	RV Meteor 2001 and *Bahret al.*, 2005
GeoB 7609-1	43°32.800	30°09.200	941	170	RV Meteor 2001 and *Bahret al.*, 2005
GeoB 7610-1	43°38.900	30°04.100	456	200	RV Meteor 2001 and *Bahret al.*, 2005
KN134-11-GC01	42°54.730	31°21.700	2086	74	Knorr 1988
MD04-2762	42°38.870	32°45.973	2210	270	Assemblage-1 2004 & *Lericolais et al.*, 2001
MD04-2770	44°12.800	30°59.600	358	300	Assemblage-1 2004 & *Stoica* 2013
MD04-2790	44°12.790	30°59.610	352	305	Assemblage-1 2004 & *Soulet et al.*, 2011
GH-18	43°46.000	31°06.000	1217	159	Mare Nigrum 2004 & *Opreanu et al.*, 2003
P824GC	44°50.000	32°02.000	1014	70	RV Poseidon 2004 & *Knabet al.*, 2009

Figure captions

Figure 2-1: Map of the Black Sea drainage area (Danube, Sakaraya, Anatolia, Kuban, Volga, Don, Dniper, Bug and Dniestr), location of proglacial lakes (blue), and the maximim expansion of the EISC at ~20 kyr as reconstructed from .

Figure 2-2: Map of the Black Sea with the distribution of cores that contain the red sediment (colored circles) [Composed via Geomap Ap]. The color of the circles corresponds to the depth of the core that range from dark blue (-2000 m) to white (<-200 m) with the complementary legend on the left side of the figure. The bright red circle points to the location of the two mid shelf cores that sample the fill of the paleorivers, BLKS98-30 and BLKS98-34. The dotted red contour points to the location of WC-6_18_1210 chirp profile.

Figure 2-3: (a) 53 to 104 cm of core 09-SG-13; (b) Sieved >63 μm sediment fraction of red sediment from 09-SG-13, 80 to 85 cm in the core; (c) Figure 4 of *Soulet et al*., [2013] that illustrates the section of the MD04-2790 core with the deglacial red sediments in x-ray, thin section, and natural light at 1cm, 2 mm, and 1 mm resolution, respectively with the first two both at 1 cm resolution.

Figure 2-4: KN134-11-GGC01, truncated to show sediment from 70 to 180 cm in the core that highlights the location of the red sediments and the grading from silt to clay in each pulse.

Figure 2-5: Scatter plot of cores used in this study from Figure 1 and Table 1 with the minimum thickness of red sediments (cm) plotted as a function of water depth (m).

Figure 2-6: Chirp profile WC-6_18_1210 from Ukraine Shelf. The deposits belonging to the meltwater events are inside the yellow contours. AK93-14 was retrieved from 140 mbsl. A ^{14}C date at 215 cm in the core gives an age of 14,700 ^{14}C years, identifying the beginning of the meltwater deposit in this core.

Figure 2-7: Logging and direct measurements (water content and coarse fraction) for KN134-11-GGC01 from top to bottom: Water content (%) and Acoustic Impedence (10^3kgm-^{2}s-1), Magnetic Susceptibility (SI), Bulk Density (g/cc), and Coarse Fraction (> 63 μm).

Figure 2-8: Carbonate and dry XRF measurements for KN134-11-GGC01 from top to bottom: Ti/Ca, Ti (ppm), Ca (ppm) and CaCO3 (%), Zr/Rb, Mn (ppm), K (ppm), S (ppm), Fe (ppm), Mo (ppm), Se (ppm).

Figure 2-9: Scatter plot of XRF measured Ca (ppm) in dry bulk sediment as a function of CaCO3 (%) for four different time periods in KN134-GC01: (a) Sapropel and post-connection Holocene (Unit 2), (b) Deglacial period that includes the end of Younger Dryas and beginning of Preboreal, (c) Red layer deposits, (d) Glacial period and pre-red layer deposition, (e) all of the depositional data combined.

Figure 2-10: Mn (ppm) as a function of Ca (ppm) for (a) Preboreal and high $CaCO_3$ deposition; (b) Red layer deposition, and (c) Glacial period and pre-red layer deposition.

Figure 2-11: $^{87}Sr/^{86}Sr$ composition of ostracode and mollusk shells in the Sea of Marmara (upper plot) and the Black Sea (lower plot). The two contours indicate the adopted $^{87}Sr/^{86}Sr$ curves for the Sea of Marmara (red) and the Black Sea (blue).

Figure 2-12: $^{87}Sr/^{86}Sr$ of the composite Black Sea-Lake and meltwater mixture plotted as a function of the fraction of meltwater entered. The different lines represent the different compositions of the meltwater used in the water mixing equations in the form of Sr concentration (ppm) and $^{87}Sr/^{86}Sr$.

Figure 2-13: Core SG-09-13 with different colors representing different lithologic sections. The brown sediments are located from 58 to 159 cm in three pulses and are indicated by brown color. ^{14}C dates are superimposed on the core as are $\delta^{18}O$ of bottom and surface water for reference. The ε_{Nd} measurements are indicated at the top, with (d) referring to the detrital and (b) to the authigenic components.

Figure 2-14: Location of (1) Fleuve Manche (blue), (2) EISC and Alpine ice sheets (red), (3) Danube, Dniestr, Dniepr, Don, and Volga rivers (black) with Volga dotted to differentiate its drainage to the Caspian Sea, and (4) Adriatic, Black, and Aegean Seas (dark grey), (5) Manych Strait (green).

Figure 2-15: Sequence of deglaciation events for the EISC: (a) Meltwater drainage via Channel River to the east; (b) meltwater drainage north to the Arctic via Fleuve Norde; (c) meltwater drainage south via Don and Dniper to the Black Sea; (d) meltwater drainage north to the Arctic via Fleuve Norde (II) and east.

Figure 2-1

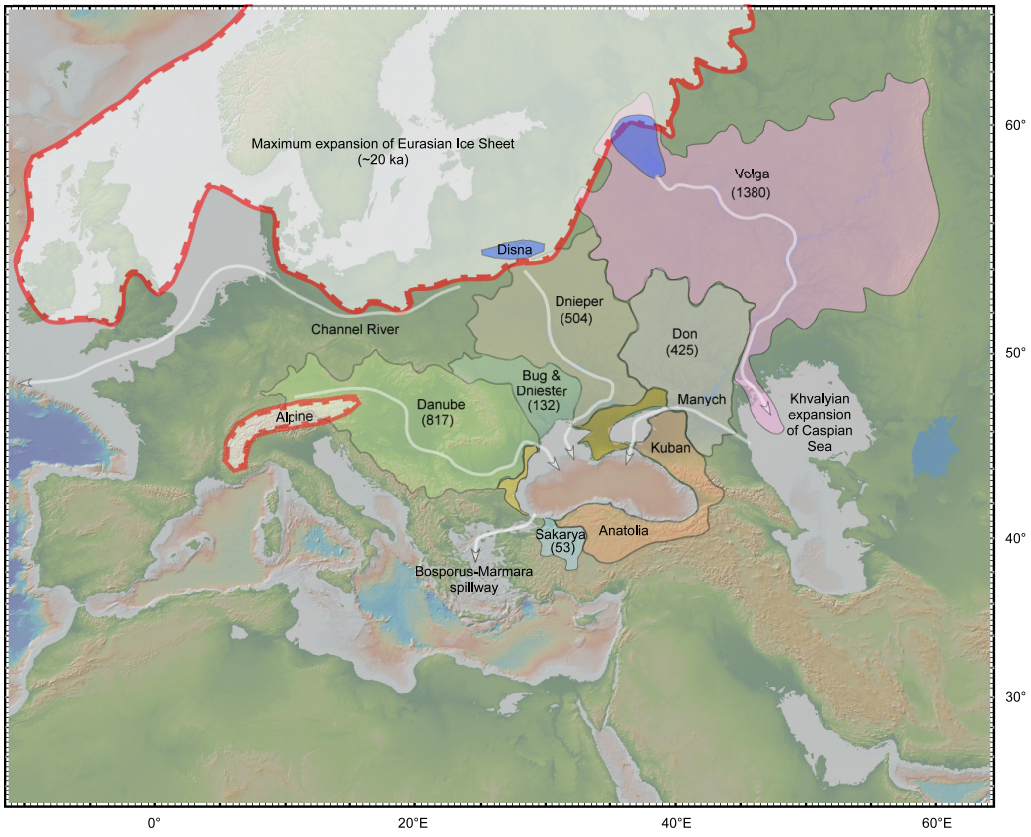
Maximum expansion of Eurasian Ice Sheet
(~20 ka)
Volga
(1380)
Disna
Dnieper
(504)
Channel River
Don
(425)
Bug &
Dniester
(132)
Danube
(817)
Manych
Khvalyian
expansion
of Caspian
Sea
Alpine
Kuban
Sakarya
(53)
Anatolia
Bosporus-Marmara
spillway
60°
50°
40°
30°
0°
20°E
40°E
60°E

Figure 2-2

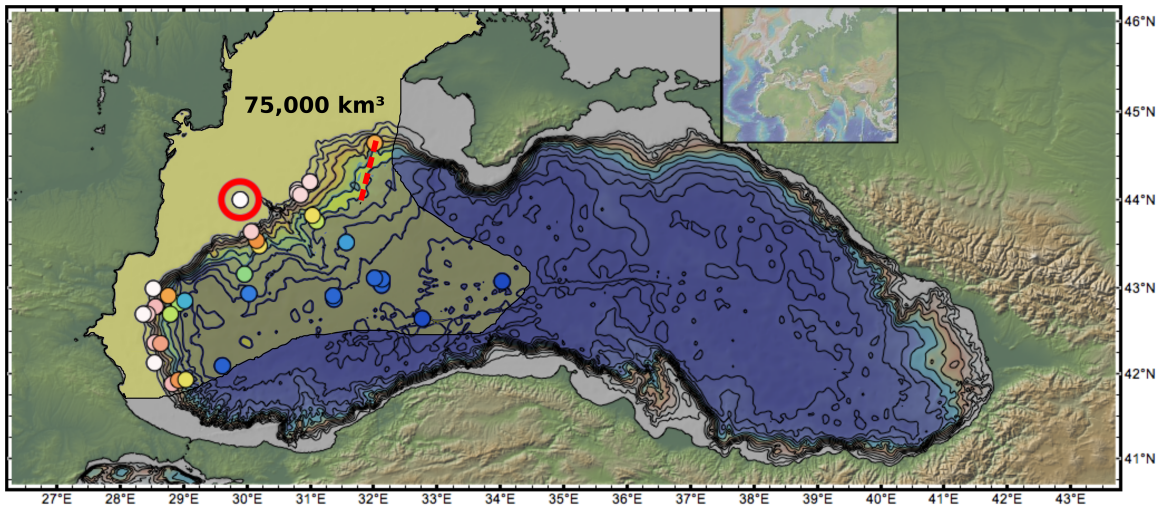
75,000 km³
46°N
45°N
44°N
43°N
42°N
41°N
27°E
28°E
29°E
30°E
31°E
32°E
33°E
34°E
35°E
36°E
37°E
38°E
39°E
40°E
41°E
42°E
43°E

Figure 2-3

(a)

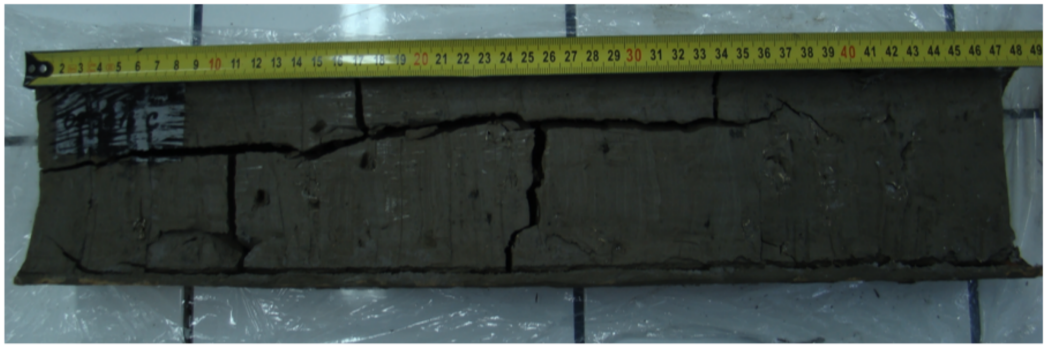

(b)

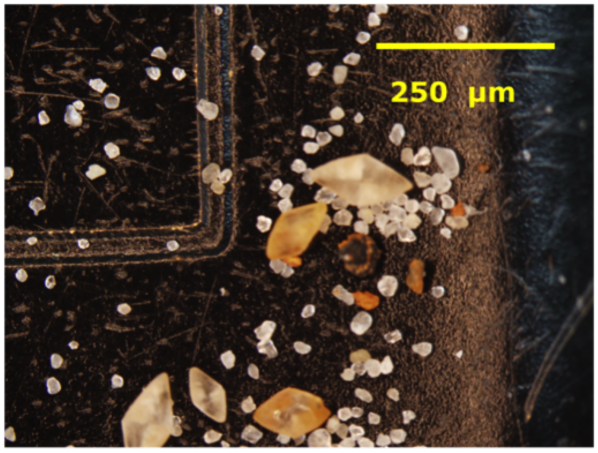

(c)

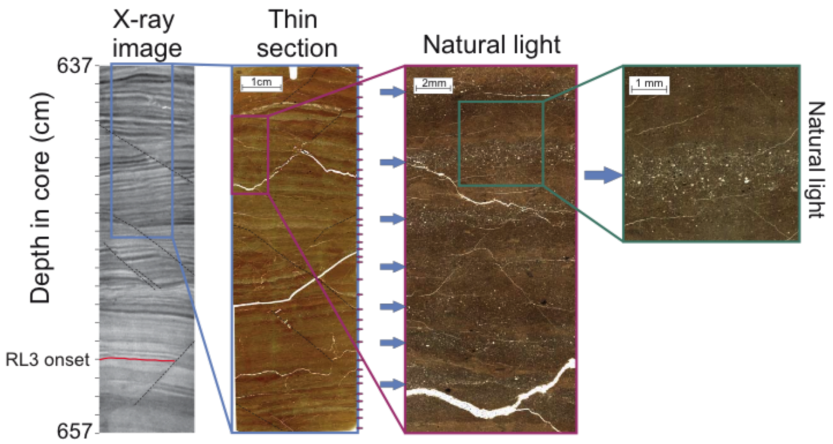

Figure 2-4

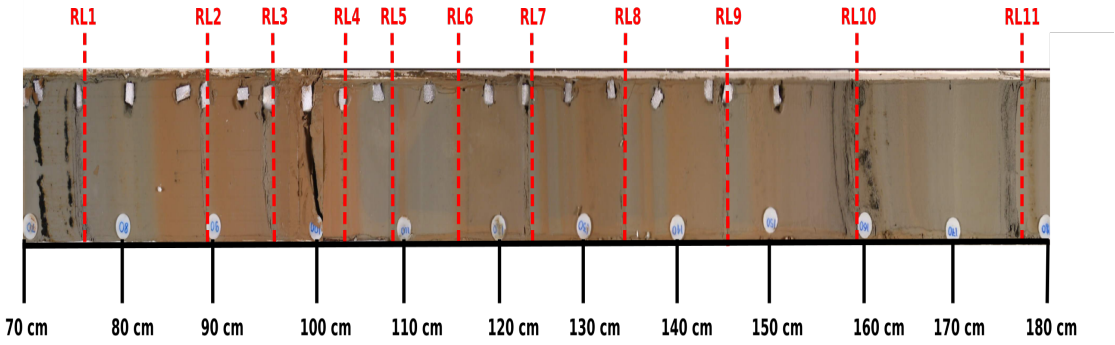
RL1
RL2
RL3
RL4
RL5
RL6
RL7
RL8
RL9
RL10
RL11
70 cm
80 cm
90 cm
100 cm
110 cm
120 cm
130 cm
140 cm
150 cm
160 cm
170 cm
180 cm

Figure 2-5

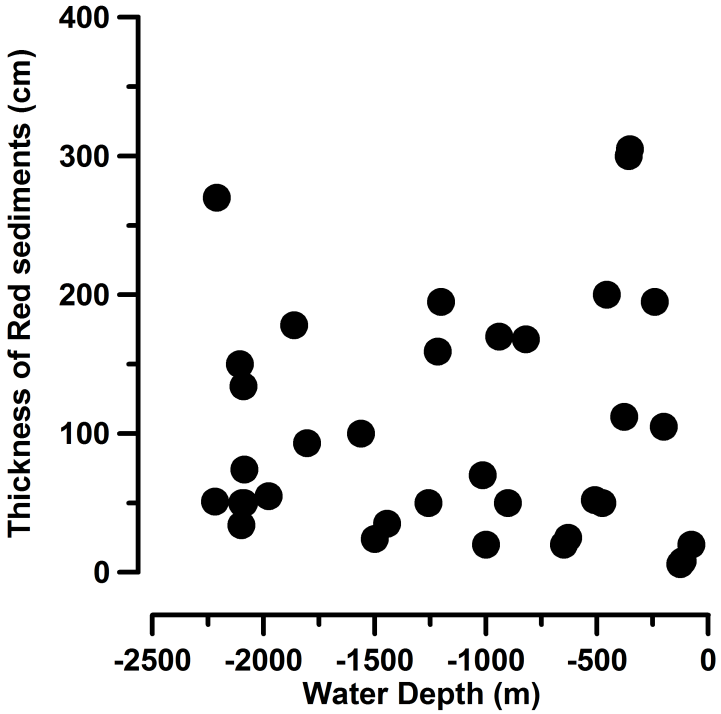
Thickness of Red sediments (cm)
400
300
200
100
0
-2500
-2000
-1500
-1000
-500
0
Water Depth (m)

Figure 2-6

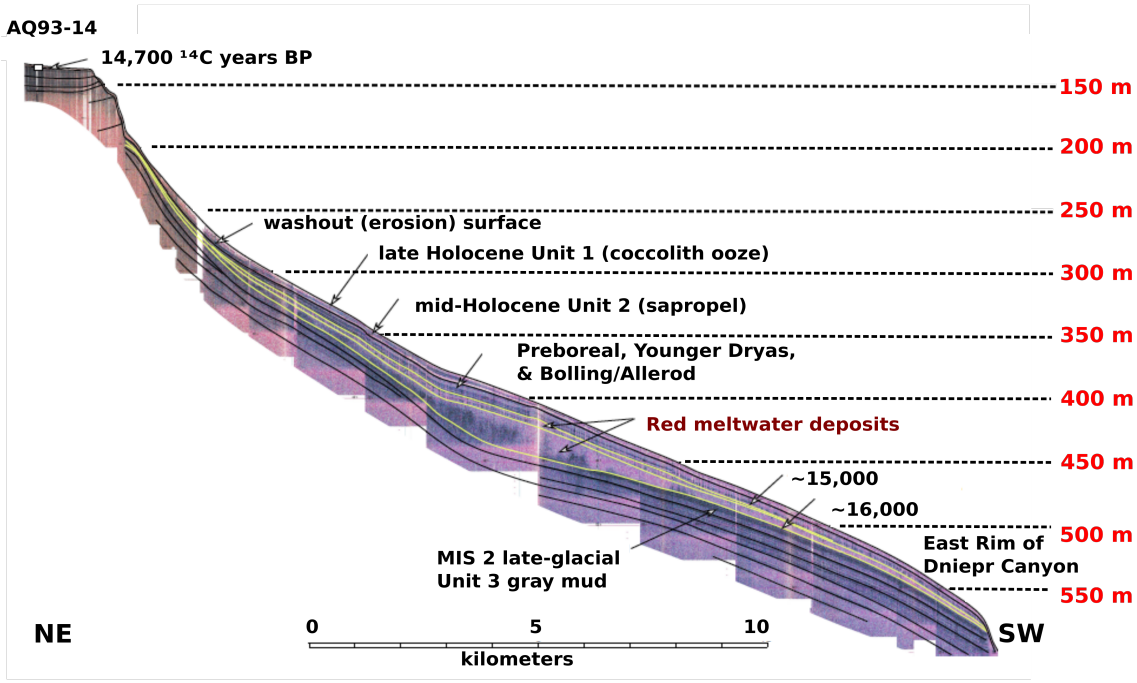
AQ93-14
14,700 ¹⁴C years BP
150 m
200 m
250 m
washout (erosion) surface
late Holocene Unit 1 (coccolith ooze)
300 m
mid-Holocene Unit 2 (sapropel)
350 m
Preboreal, Younger Dryas,
& Bolling/Allerod
400 m
Red meltwater deposits
450 m
~15,000
~16,000
500 m
East Rim of
Dniepr Canyon
MIS 2 late-glacial
Unit 3 gray mud
550 m
NE
0
5
10
kilometers
SW

Figure 2-7

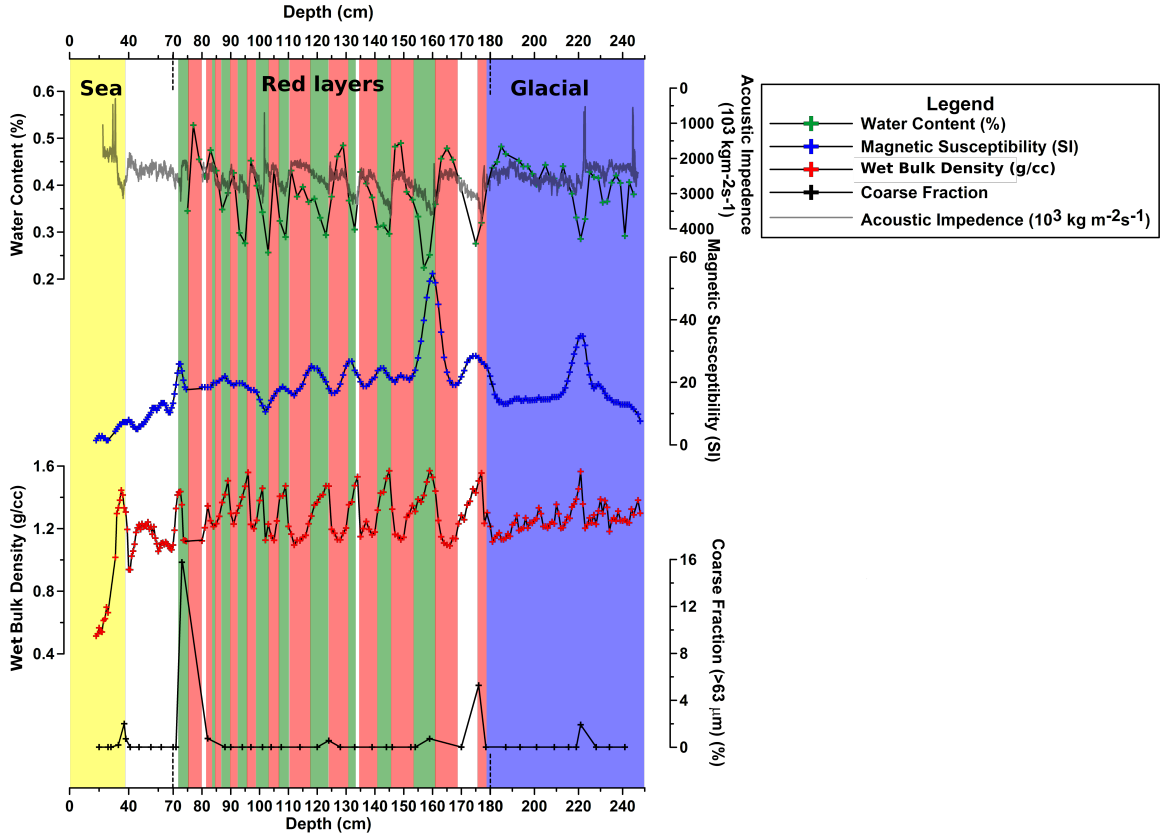
Depth (cm)
Sea
Red layers
Glacial
Water Content (%)
Wet Bulk Density (g/cc)
Acoustic Impedence (10³ kgm⁻²s⁻¹)
Magnetic Susceptibility (SI)
Coarse Fraction (>63 μm) (%)
Legend
Water Content (%)
Magnetic Susceptibility (SI)
Wet Bulk Density (g/cc)
Coarse Fraction
Acoustic Impedence (10³ kg m⁻²s⁻¹)

Figure 2-8

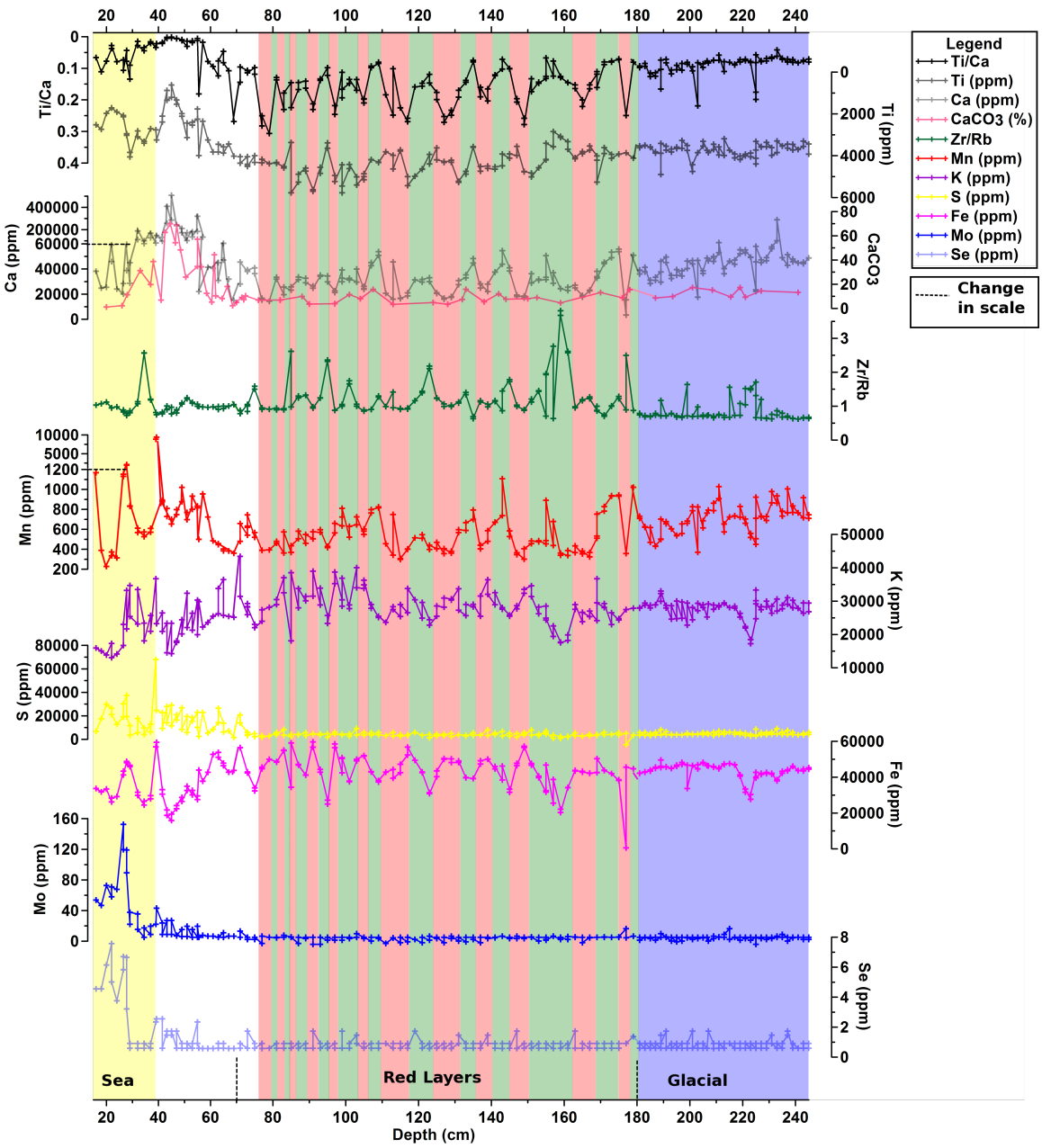
Legend
Ti/Ca
Ti (ppm)
Ca (ppm)
CaCO3 (%)
Zr/Rb
Mn (ppm)
K (ppm)
S (ppm)
Fe (ppm)
Mo (ppm)
Se (ppm)
Change in scale
Ti/Ca
Ti (ppm)
Ca (ppm)
CaCO3
Zr/Rb
Mn (ppm)
K (ppm)
S (ppm)
Fe (ppm)
Mo (ppm)
Se (ppm)
Sea
Red Layers
Glacial
Depth (cm)

Figure 2-9

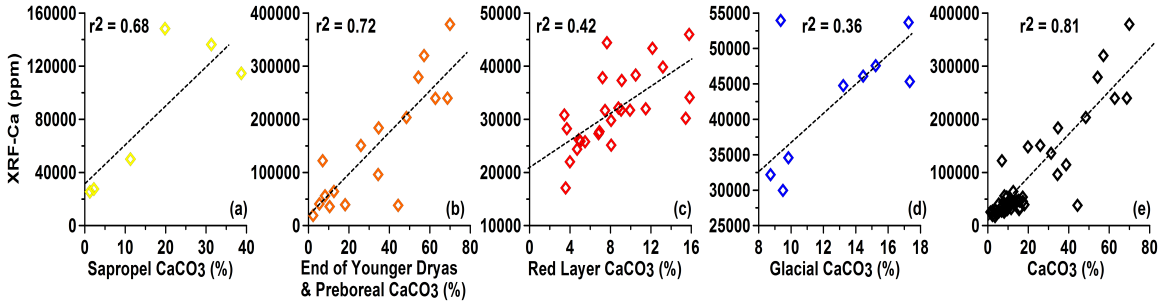
XRF-Ca (ppm)
r2 = 0.68
(a)
Sapropel CaCO3 (%)
r2 = 0.72
(b)
End of Younger Dryas & Preboreal CaCO3 (%)
r2 = 0.42
(c)
Red Layer CaCO3 (%)
r2 = 0.36
(d)
Glacial CaCO3 (%)
r2 = 0.81
(e)
CaCO3 (%)

Figure 2-10

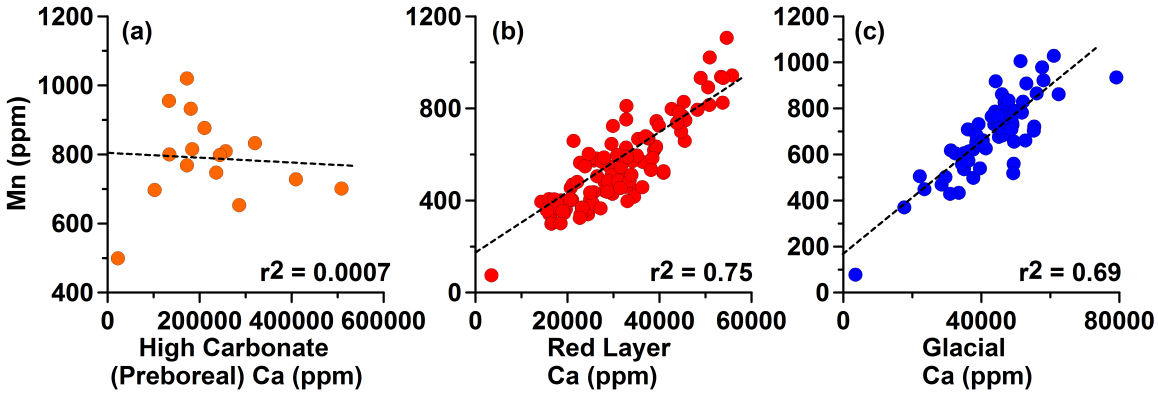
(a)
(b)
(c)
Mn (ppm)
1200
1000
800
600
400
200
0
r2 = 0.0007
r2 = 0.75
r2 = 0.69
0
200000
400000
600000
20000
40000
60000
80000
High Carbonate
(Preboreal) Ca (ppm)
Red Layer
Ca (ppm)
Glacial
Ca (ppm)

Figure 2-11

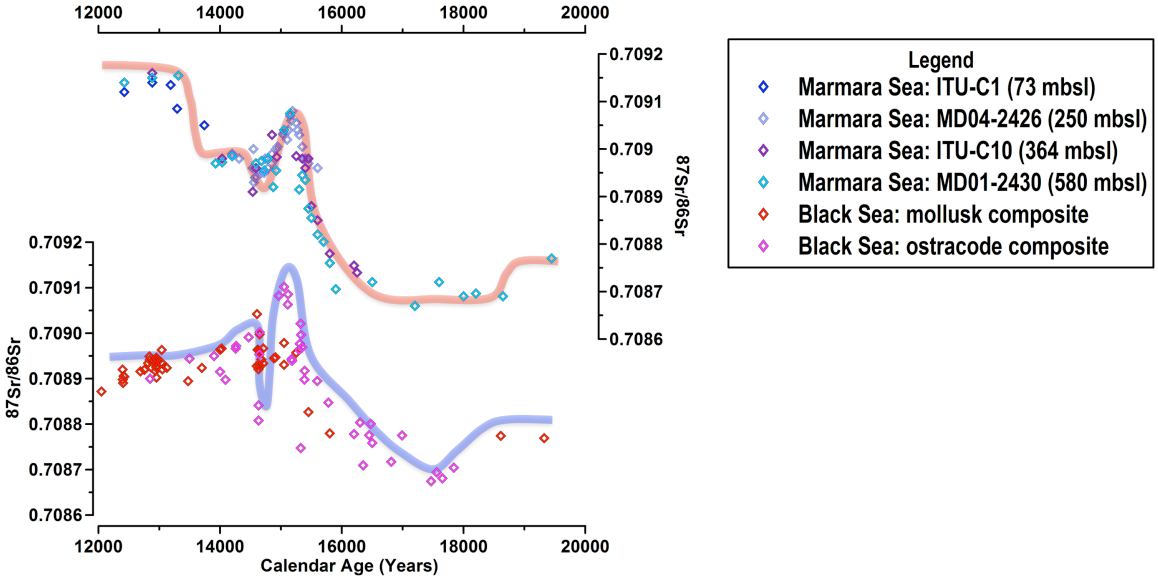
12000
14000
16000
18000
20000
0.7092
0.7091
0.709
0.7089
0.7088
0.7087
0.7086
87Sr/86Sr
Calendar Age (Years)
Legend
Marmara Sea: ITU-C1 (73 mbsl)
Marmara Sea: MD04-2426 (250 mbsl)
Marmara Sea: ITU-C10 (364 mbsl)
Marmara Sea: MD01-2430 (580 mbsl)
Black Sea: mollusk composite
Black Sea: ostracode composite

Figure 2-12

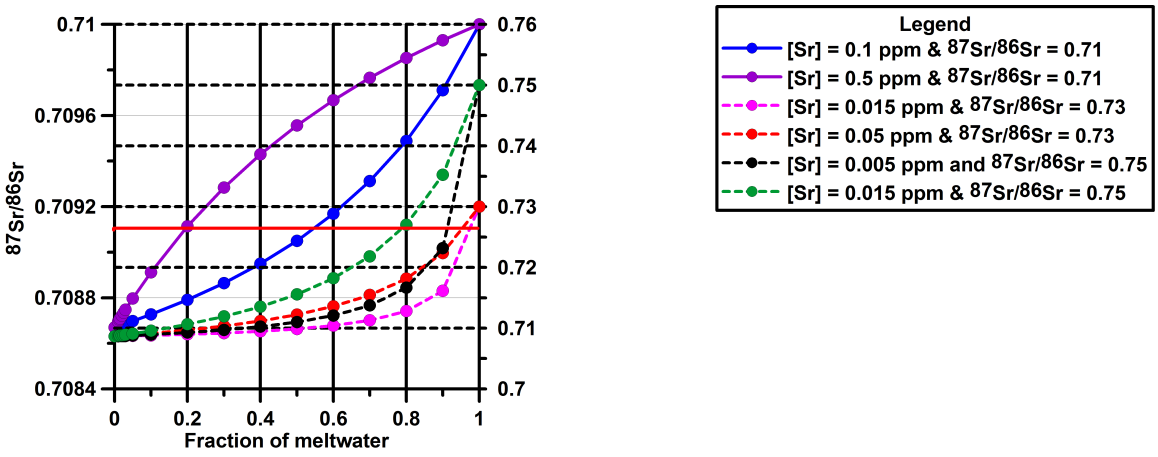
0.71
0.7096
0.7092
0.7088
0.7084
87Sr/86Sr
0.76
0.75
0.74
0.73
0.72
0.71
0.7
0
0.2
0.4
0.6
0.8
1
Fraction of meltwater
Legend
[Sr] = 0.1 ppm & 87Sr/86Sr = 0.71
[Sr] = 0.5 ppm & 87Sr/86Sr = 0.71
[Sr] = 0.015 ppm & 87Sr/86Sr = 0.73
[Sr] = 0.05 ppm & 87Sr/86Sr = 0.73
[Sr] = 0.005 ppm and 87Sr/86Sr = 0.75
[Sr] = 0.015 ppm & 87Sr/86Sr = 0.75

Figure 2-13

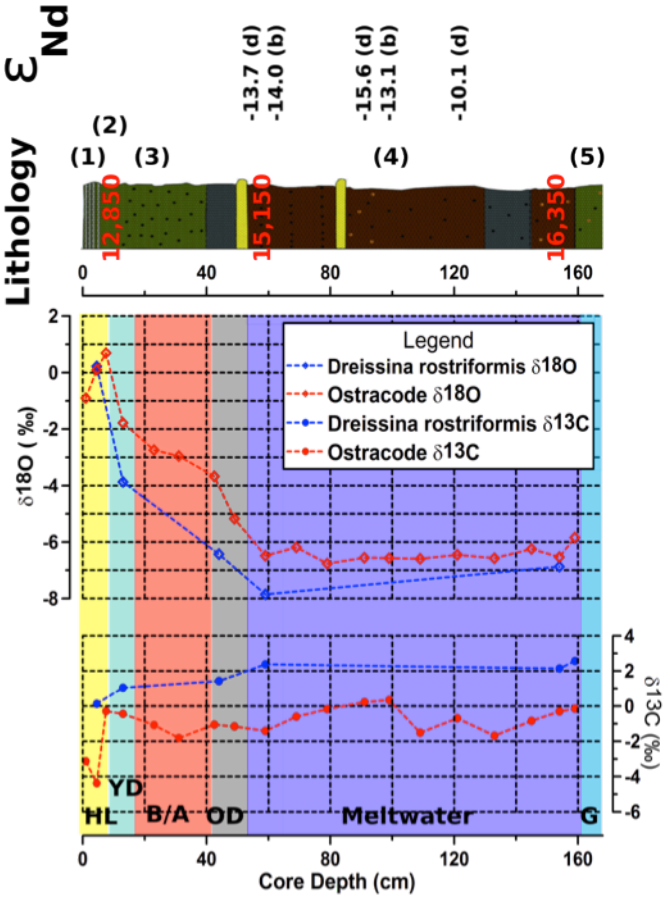
εNd
-13.7 (d)
-14.0 (b)
-15.6 (d)
-13.1 (b)
-10.1 (d)
Lithology
(1)
(2)
(3)
(4)
(5)
12,850
15,150
16,350
0
40
80
120
160
Legend
Dreissina rostriformis δ18O
Ostracode δ18O
Dreissina rostriformis δ13C
Ostracode δ13C
δ18O (‰)
δ13C (‰)
YD
HL
B/A
OD
Meltwater
G
Core Depth (cm)

Figure 2-14

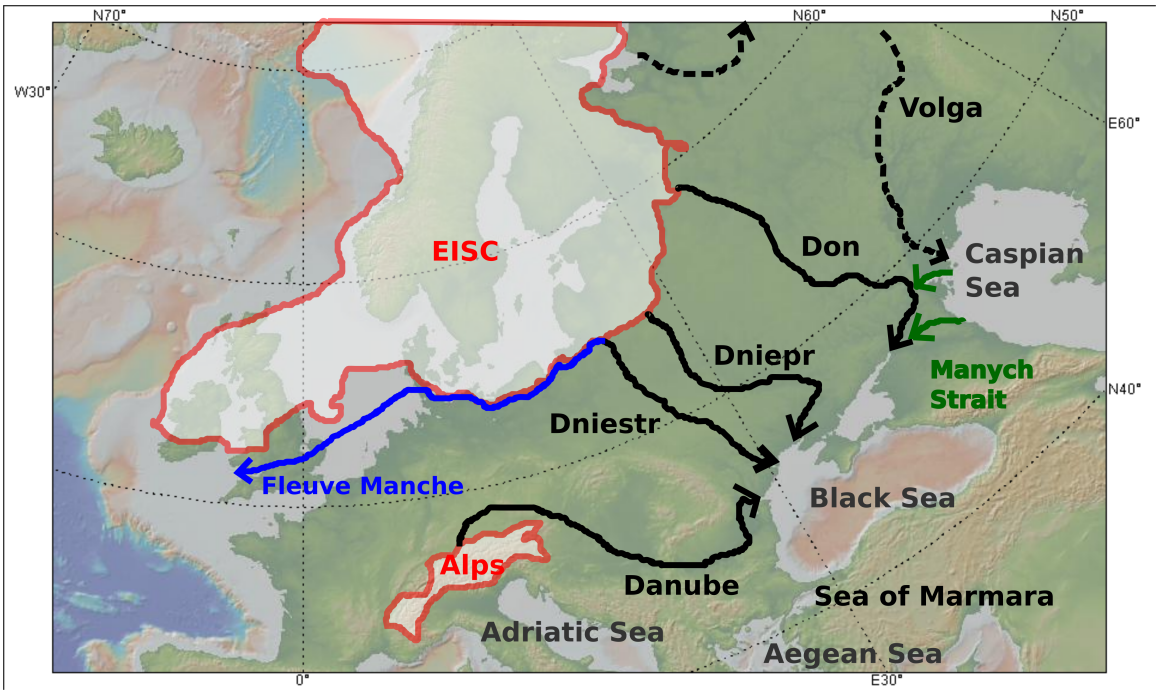
N70°
N60°
N50°
W30°
E60°
N40°
0°
E30°
Volga
EISC
Don
Caspian Sea
Dniepr
Manych Strait
Dniestr
Fleuve Manche
Black Sea
Alps
Danube
Sea of Marmara
Adriatic Sea
Aegean Sea

Figure 2-15

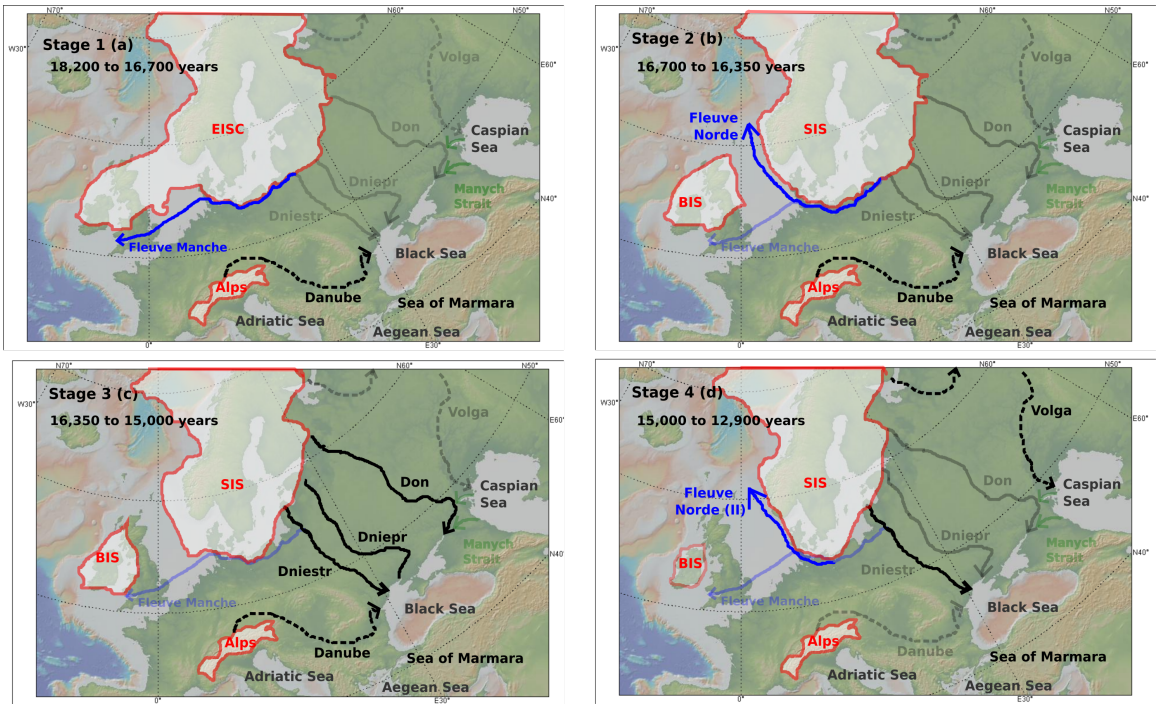
Stage 1 (a)
18,200 to 16,700 years
EISC
Fleuve Manche
Volga
Don
Caspian Sea
Dniepr
Manych Strait
Dniestr
Black Sea
Alps
Danube
Sea of Marmara
Adriatic Sea
Aegean Sea
Stage 2 (b)
16,700 to 16,350 years
Fleuve Norde
SIS
BIS
Stage 3 (c)
16,350 to 15,000 years
Stage 4 (d)
15,000 to 12,900 years
Fleuve Norde (II)

Chapter 3

Rapid transgression and gradual salinification of the Black Sea from inflow of Mediterranean water in the Holocene

Abstract

A number of important and unanswered questions remain regarding the early Holocene transgression and salinification of the Black Sea: (1) its timing and duration; (2) its cause, climate, and relationship with global eustacy; (3) and the elevation of the lake surface prior to its onset. To address these questions, cores were collected in transects across the Black Sea shelves of Ukraine, Romania, Bulgaria, and Turkey. The analysis of sediment density, presence of desiccation features, and plant remains below a shelf-wide coquina deposit shows that the lake was largely regressed to ~165 mbsl, possibly even lower, prior to the onset of the arrival of saltwater from the Mediterranean and subsequent salinification. The coquina extends all the way from today's shelf edge to 25 mbsl across the shelf and into coastal limans and estuaries. Individual specimens from the coquina, many still articulated and unabraided with original coloring intact, are examined for $^{87}Sr/^{86}Sr$, $\delta^{18}O$, $\delta^{13}C$, and ^{14}C.

The $^{87}Sr/^{86}Sr$ measurements show that all of the analyzed specimens have shell compositions that indicate an introduction of salt water from the external global ocean into a prior Black Sea freshwater lake. *Dreissena-Dreissena rostriformis*, a common stenohaline freshwater mollusk with a fully lacustrine $^{87}Sr/^{86}Sr$ composition in deposits beneath the coquina, has an isotope signature with an already identifiable and distinct marine composition when sampled from the coquina. The more brackish species, *Monodacna caspia* and *Dreissena polymorpha*, appear with younger ^{14}C ages. Their $^{87}Sr/^{86}Sr$ composition indicates a growing

fraction of Mediterranean water and their $\delta^{18}O$ composition approaches that of the external surface ocean. *Cardium edule* and *Mytilus galloprovincialis*, a common saltwater clam and mussel, found *in situ* and with their two valves still together in the sediment immediately above the coquina, have $^{87}Sr/^{86}Sr$ and $\delta^{18}O$ compositions that indicate water composition nearly identical to that of the Mediterranean and therefore with a salinity no longer able to support the previous lake fauna.

An alignment is made of the $\delta^{18}O$ and $\delta^{13}C$ trends when plotted against their ^{14}C age obtained from Black Sea mollusks with similar trends for the same isotopes measured from the Sofular Cave in northern Turkey dated by U/Th methods. This alignment derives a history of decreasing Black Sea reservoir ages and shows that the introduction of Mediterranean water upon the breaching of the Bosporus sill began at 9.30 kyr uncorrected ^{14}C (8.20 corrected kyr ^{14}C and 9.30 kyr BP). The rapid decrease in measured ^{14}C ages towards younger values in the coquina indicates that the reservoir age of the Black Sea diminished as additional Mediterranean—radiocarbon—equilibrated water arrived. The rise of lake level and transgression of the Black Sea shelf, derived from the observation of $^{87}Sr/^{86}Sr$ and ^{14}C age of *Dreissna-Dreissena rostriformis* mollusks, is estimated to be rapid. This is supported by hydraulic calculations. The subsequent evolution from a freshwater lake to a saltwater sea was accomplished in 1,500 years.

1. Introduction

The Black Sea is a large and deep meromictic body of water connected to the global ocean via a system of straits and intermediate seas. Currently, the water exchange that controls the basin's salinity is estuarine across the Strait of Bosporus at 35 mbsl, allowing for water

exchange with the Mediterranean Sea. This configuration is dynamic, and changes between glacial and interglacial periods. During glacial periods, when global sea level falls below the level of the Black Sea's outlet, its lake level cannot rise above the elevation of the outlet sill and is controlled by the regional hydrologic budget. As a consequence, the sea remains isolated from the global ocean and evolves over time into a lake (Arkhangel'skiy and Strakhov, 1938; Brujevich, 1952). When the deglaciation raises the external sea level above the level of the outlet, the lake reverts to a sea for the duration of the interglacial highstand.

The most recent reconnection of the Black Sea with the Mediterranean has been placed, with broad consensus, in the early Holocene, between 7 and 8 kyr ^{14}C (Ross et al., 1970; Strakhov, 1971; Kuprin et al., 1974; Scherbakov and Babak, 1979; Degens et al., 1980 ; Dimitrov, 1982; Jones and Gagnon, 1994; Ryan et al., 1997; Aksu et al., 2002a; Aksu et al., 2002b; Dimitrov and Dimitrov, 2004; Major et al., 2006; Dimitrov, 2010; Nicholas et al., 2011; Soulet et al., 2011b; Filipova-Marinova et al., 2013; Nicholas and Chivas, 2014). Prior to the connection, it is widely agreed that the Black Sea-Lake experienced a significant regression, exposing most of its shelf and turning it into a terrestrial landscape out to a shoreline between 80 to 100 mbsl (Kuprin et al., 1974; Scherbakov and Babak, 1979; Konikov et al., 2007). This regression is supported by pervasive erosion observed in reflection profiles that cross the Ukraine, Romanian, Bulgarian, Russian, and Turkish shelves (Ryan et al., 1997; Demirbag et al., 1999; Hiscott et al., 2002; Aksu et al., 2002b; Algan et al., 2007; Glebov and Shel'ting, 2007; Lericolais et al., 2007; Dimitrov, 2010). Despite overall consensus, the element of disagreement arises from interpretation of data regarding the level of the water surface in the Black Sea-Lake at the time of the introduction of Mediterranean water. Was the lake surface below the level of

the inlet such that it involved a transgression? Or was the lake already at the elevation of the inlet?

Four different propositions for the Black Sea-Lake level currently exist (**Figure 3-1**). One school assigns the maximum regression to 18 kyr (^{14}C years), followed by a gradual transgression to the Black Sea outlet (placed at 35 mbsl) and completed before entry of saltwater (Kuprin et al., 1974; Kaplin and Shcherbakov, 1986; Pirazzoli, 1996; Kaplin and Selivanov, 2004; Balbanov, 2007; Sorokin and Kuprin, 2007). A second school places the maximum regression at 11 kyr ^{14}C years, recognized as the Younger Dryas period of the late Pleistocene, followed by a rapid freshwater transgression ending at ~10 kyr ^{14}C years to the level of the outlet (Bosporus sill) and also completed prior to the connection of the Mediterranean Sea with the Black Sea-Lake (Hiscott et al., 2002; Aksu et al., 2002b; Hiscott et al., 2007a; Hiscott et al., 2007b). A third school also recognizes a regression in the Younger Dryas period but one that persists into the Preboreal and that ends with an abrupt transgression exclusively caused by a cascade of Mediterranean saltwater that begins when the rise of external eustatic sea level reaches the inlet (Lericolais et al., 2007; Nicholas et al., 2011; Nicholas and Chivas, 2014). A fourth school recognizes a significant regression in the Preboreal period, immediately before the rapid transgression from the entry of Mediterranean water (Dimitrov, 1982; Ryan et al., 1997; Major et al., 2002; Ryan et al., 2003; Dimitrov and Dimitrov, 2004; Ryan, 2007; Dimitrov, 2010). The interpretations that contribute to each of the individual schools of thought do not use comprehensive geochemical data, suffer from applying poorly constrained radiocarbon reservoir ages to ^{14}C measurements and/or interpret ^{14}C measurements without any reservoir corrections at all, and do not interpret data comprehensively from a number of Black Sea shelves. This paper re-evaluates each of these hypotheses with additional ^{14}C, δ^{18}O, δ^{13}C, and ^{87}Sr/^{86}Sr

measurements from mollusks from all of the Black Sea margins together with complementary chirp and multibeam data to establish a consensus that agrees with all of the prior observations.

2. Materials and methods

Reflection profiles were acquired on the 1993 Aquanaut, 1998 BLaSON1, 2002 BLaSON2 expeditions, and 1998 Bulgarian navy ship *Hydrograph* (**Figure 3-2**). Chirp profile WC-6_13_0200-2040 was retrieved from the Ukrainian margin during the 1993 Aquanaut expedition; chirp profile B008 was retrieved from the Romanian margin during the 1998 BLaSON1 expedition; chirp profile B2ch049 and B2ch007 was retrieved during the 2002 BLaSON2 expedition from the Bulgarian margin; chirp profiles XXIV and XV were retrieved during the 1998 expedition with the Bulgarian navy ship Hydrograph from the Bulgarian margin; chirp profiles B2ch007, B2ch0036, B2ch013 were retrieved during the 2002 BLaSON2 expedition from the Turkish margin.

Cores collected to complement reflection profiles were collected on transects across the Black Sea shelf include: (1) joint Russian-US expedition, AK93, in 1993 on board the *R/V Aquanaut* that surveyed western Crimea and Kerch region of the outer continental shelf, (2) a joint French-Romanian BlaSON1 expedition in 1998 that surveyed Romanian region of the inner and outer continental shelf aboard the *R/V Suroit*, (3) a 1998 survey of the Bulgarian shelf with the R/V Hydrograph, (4) a 2001 expedition aboard R/V Akvanavt across the Russian shelf, (5) a French-Romanian BLaSON2 survey in 2002 that surveyed the Bulgarian and Turkish regions of the outer continental shelf, (6) a collaborative Israel, Turkey, and US expedition in 2005 aboard the *R/V Mediterranean Explorer* on the western Turkish margin, and (7) expeditions in 2009 and

2011 on the Bulgarian margin aboard the *R/V Akademik* (**Figure 3-2**). A full list of cores used in this study is listed in Appendix A, Table 1.

When penetrating the seabed the cores encountered a distinct coquina that rests directly on a shelf-wide erosion surface called reflector α (Hiscott et al., 2002; Aksu et al., 2002b). This erosion surface extends landward from beyond the shelf edge into coastal limans (Naukova, 1984). Mollusks in the coquina along with ostracods in the earlier deglacial and glacial age sediment, and specimens from the younger cover were analyzed for radiocarbon, stable isotopes, and strontium isotopes. Analyses were also made on material from boreholes in the Sakarya coastal plain (Görür et al., 2001) and a vibra-core on the inner Ukrainian shelf (Konikov et al., 2007).

Water content measurements of sediment sampled from cores collected on the *R/V Aquanaut* were made by a resonance probe and converted to water content by complementary measurements of weighing sediments before and after freeze-drying. The bulk density of the sediments was measured by weighing the sediments in a pre-measured and pre-weighed container.

The mollusks and ostracod shells were sonicated for 30s in quartz distilled water and methanol to remove contaminating surface detrital matter. Samples were analyzed following carbonate hydrolysis and CO_2 reduction at Woods Hole Oceanographic Institution and ETH-Zurich. Additional ^{14}C dates were acquired from prior published results (Apakidze and Burchuladze, 1987; Görür et al., 2001; Major et al., 2002; Major et al., 2006; Ivanova et al., 2007; Konikov et al., 2007; Lericolais et al., 2007; Nicholas et al., 2011; Soulet et al., 2011a).

Stable isotopes were measured by gas-source mass spectrometry at the Department of Earth and Planetary Sciences at Rutgers University (Mortlock, 2010) and at Rensselaer

Polytechnique Institute (RPI) (Cohen and Ryan, 2011). A fragment weighing approximately 700 to 1200 μg of shell material was taken from each mollusk specimen. Prepared samples were loaded onto a Multi-prep device attached to a Micromass Optima Stable Isotope Mass Spectrometer and reacted in 100% phosphoric acid at 90°C for 800 seconds. Values are reported versus V-PBD through the analysis of an internal laboratory standard that is routinely calibrated against NBS-19. The errors associated with the measurements are 0.04 and 0.06 ‰ for $\delta^{13}C$ and $\delta^{18}O$, respectively. Additional $\delta^{13}C$ and $\delta^{18}O$ are supplemented to the existing stable isotope records from earlier work (Major et al., 2002; Major et al., 2006).

For $^{87}Sr/^{86}Sr$ isotope analyses, mollusk and ostracode shells were leached using a procedure modified from Bailey et al., (2000) following the sonification treatment. The first leach consisted of a one-minute sonification of the sample in 0.1 N hydrochloric acid. The isotope ratios were measured by a dynamic multi-collector on a VG Sector 54 thermal ionization mass spectrometer (TIMS) at Lamont-Doherty Earth Observatory. The $^{87}Sr/^{86}Sr$ ratios were corrected for mass fractionation through normalizing to $^{86}Sr/^{88}Sr = 0.1194$. Beam size was maintained at close to 4.5×10^{-11} A for ^{88}Sr. The measurements were further corrected for instrumental drift by analysis of NBS987 which gave $^{87}Sr/^{86}Sr = 0.710255 \pm 2.31143E\text{-}05$, 2σ external reproducibility, n=7). All $^{87}Sr/^{86}Sr$ ratios are further corrected relative to the NBS987 standard's $^{87}Sr/^{86}Sr$ value of 0.71024. The errors presented in this paper are the in-run 2σ error of the mean. Our investigation also includes previous $^{87}Sr/^{86}Sr$ measurements from some of the same cores (Major et al., 2006; Cohen and Ryan, 2011). Age control of the isotopic measurements is provided by AMS ^{14}C dates on the same shell material.

The age model for assembling all of the isotope measurements in chronological order is created by deriving ^{14}C reservoir ages for the late Pleistocene and Holocene stages of the Black

Sea history, and then using the ^{14}C reservoir ages to convert the measured ^{14}C dates into calendar ages (Reimer et al., 2013). This chronology is developed for the history of the Black Sea surface water from the last glacial period to the present. The time-varying ^{14}C reservoir ages are obtained by comparing the $\delta^{18}O$ and $\delta^{13}C$ compositions of mollusks as a function of their measured ^{14}C age from all of the available shelf cores to $\delta^{18}O$ and $\delta^{13}C$ measurements in nearby U/Th dated stalagmites in the Sofular Cave (Fleitmann et al., 2009; Badertscher et al., 2011). The alignment of the mollusk $\delta^{18}O$ to the Sofular Cave $\delta^{18}O$ is supported by known studies showing that the $\delta^{18}O$ composition precipitated in the carbonate of the cave reflects the evaporated surface water $\delta^{18}O$ of the Black Sea-Lake (Fleitmann et al., 2009; Badertscher et al., 2011). The alignment of the mollusk $\delta^{13}C$ to the Sofular Cave $\delta^{13}C$ is supported by an identical source of dissolved carbonate, one that responds to a change in the distribution of C_3 and C_4 plants and that feeds both the carbonate precipitation in the Sofular Cave and the surface Black Sea. Meltwater, Older Dryas, Bølling/Allerød, Younger Dryas, and Preboreal periods are identified, as specifically reflecting changes in Black Sea climate, to correspond to 16.30 to 15.00 kyr BP, 15.000to 14.80 kyr BP, 14.80 to 12.90 kyr BP, 12.90 to 11.90 kyr BP and 11.90 to 9.30 kyr BP, respectively. Younger Dryas is identified as a peak in $\delta^{13}C$ whereas Bølling/Allerød and Preboreal as troughs in $\delta^{13}C$.

This methodology of alignment works best during the deglaciation period as this is the period where most stable isotopic data from mollusks are available and also where the $\delta^{18}O$ and $\delta^{13}C$ changes in both the mollusk and the cave record have more defined structure. Mollusks with ^{14}C dates taken from Sakarya coastal plain and sediment ascribed to have been deposited in shallow lakes and ancient river beds, are tentatively given a zero ^{14}C reservoir correction since

freshwater came predominantly from river-water with permanent exposure to the atmosphere and hence, immediate equilibration to the atmospheric ^{14}C age.

The resulting time-variations in reservoir age generally agree with those previously published (Jones and Gagnon, 1994; Ryan, 2007; Kwiecien et al., 2009; Soulet et al., 2011a; Nowaczyk et al., 2012) but provide greater detail for the time period just before and just after the reconnection of the Mediterranean with the Black Sea. The ^{14}C reservoir ages from Nowaczyk et al., (2012) are calculated from finding values that convert their derived calendar ages to ^{14}C ages and subtracting the calculated ^{14}C ages from their measured ^{14}C age in the same sediment sample. For the glacial period prior to 18 kyr BP, our adopted ^{14}C reservoir ages are set approximately between those of Soulet et al., (2011a) and Nowaczyk et al., (2012) as a compromise between modest differences. For the Holocene period post connection, the ^{14}C reservoir adopted in this paper is set to rise progressively to that of the modern surface ^{14}C reservoir of the Black Sea of 460 ^{14}C years (Jones and Gagnon, 1994).

3. Results

The results presented include (1) reflection profiles from the Ukrainian, Romanian, Bulgarian, and Turkish margins, (2) description of sediments on the shelf in terms of their lithology, faunal distribution, and sediment water content and bulk density, (3) geochemical composition of the coquina, (4) geographical trends in the geochemical composition of the coquina, (5) changes in the geochemistry of water as a function of time during the formation of the coquina, and (6) liman record of the early Holocene.

3.1 Reflection Profiles

3.1.1 Ukraine Margin

Chirp profile WC-6_13_0850-2040 (**Figure 3-2** and **3-3**) descends from 45 to 140 mbsl across the middle and outer Ukraine shelf and all the way to the uppermost slope. The shelf is not entirely smooth, but instead is populated by a mesa separated by depressions. Numerous buried channels are encountered between the adjacent mesas (**Figure 3-3-B, C, D**).

A belt consisting of 100 to 200 meter wide ridges spans an area that is 1-2 km-wide and tens of km-long between 75 and 85 mbsl (**Figure 3-2** and **3-4**). Ryan et al., (1996) and Naudts et al., (2006) interpret these ridges as coastal dunes that display symmetric and barchan shapes. The dunes are situated in front of an incline interpreted as a paleo-shoreface (Ryan et al., 1996). Beyond, a smooth ramp delineates a former shelf-edge pro-delta (Naudts et al., 2006). The dunes rest above a splay of filled channel terminations whose strata are truncated by the shelf-wide erosion surface, α (Aksu et al., 2002b). A thin (1 to 2 m thick) sedimentary drape rests on this erosion surface and is present everywhere across the shelf. The drape thins seaward and is composed of two internal layers.

The erosion surface truncates all of its substrate reflectors. These features include concave-upwards strata belonging to fill in the channels (**Figure 3-5**). Landward of the dunes, the substrate beneath the erosion surface attenuates acoustic energy, thereby limiting sub-bottom penetration except in regions of buried channels.

The cores located landward of the dunes penetrate the drape and recover sediments comprising the drape and the underlying coquina that rests on the erosion surface. Some material of the eroded substrate is occasionally recovered in core catchers (that component of a coring device that retains material from falling out as the coring device is retrieved). The material derived from the hard ground is shell free, stiff, and deprived of water. Cores seaward of

the dunes and shoreface encounter two erosion surfaces. The older one is identified as α. The cores penetrate well below the two erosion surfaces and successfully sample sediment that belongs to the set of seaward dipping reflectors (**Figure 3-4**).

3.1.2 Romanian Margin

Chirp profile B008 from the Romanian shelf (**Figure 3-2** and **3-6**) extends from 125 to 300 mbsl. The sedimentary profile consists of three deposition units identified as the surficial drape, sediment dated to a range between 10.26 and 11.10 kyr ^{14}C, and sediment older than 14.90 kyr ^{14}C. A coquina separates each of these deposition units. The older coquina sits upon erosion surface α and the younger coquina upon the younger erosion surface. The surficial drape is a 1-2 m thick uniform cover that is also identified on the Ukrainian shelf (Popescu, 2008; Lericolais et al., 2009). This drape thins to <0.5 m on the outermost shelf based on recovery in BLKS98-06 (135 mbsl), BLKS98-07 (163 mbsl), BLKS98-08 (186 mbsl) and 09-SG-13 (200 mbsl). On the slope, the cover then thickens to >0.5 m as shown by $\delta^{18}O$ measurements on bulk carbonate in BLKS98-09 (240 mbsl) and BLKS98-10 (378 mbsl). In 09-SG-13, this surface has mollusks identified as *Modiolus phaeseolinuse*.

3.1.3 Bulgarian Margin

Chirp profile BLASON2-B2ch049 (**Figure 3-2** and **3-7**) crosses the Bulgarian middle and outer shelf off Cape Emine from 30 to 170 mbsl. The same surficial drape as observed on the Ukraine and Romanian margins is also omni-present and thins seaward. The drape rests on the α erosion surface, here colored red. Above 90 mbsl the substrate is acoustically opaque due to strong attenuation of acoustic energy. Between 90 and 110 mbsl, there is a row of ridges that

are similar in shape, size, and orientation to those identified as subaerial coastal dunes on Ukraine (Ryan et al., 1996) and Romanian (Lericolais et al., 2007) margins. These dunes rest on the α erosion surface. Cores AKAD09-19 and AKAD01-AB18 penetrated a few cm into the dune interiors and recovered mud-free sand consisting mostly of pulverized shells, quartz grains rounded and with a frosty texture, and sand-sized lithic fragments. Core AKAD09-28, recovered from strata located seaward of the paleoshoreline, penetrated into three deposition units: the surficial drape, sediment dated to ~10.20 and older than 14.15 kyr ^{14}C with younger and older coquina separating each unit, respectively.

Chirp profile B2ch049 and cores retrieved along it are taken from the Cape Emine transect on the Bulgarian margin (**Figures 3-2**, **3-8**, and **3-9**). Also shown are two boomer-type reflection profiles (XXIV and XV) obtained in 1998 with the Bulgarian navy ship *Hydrograph* (Genov et al., 2004a) upon which cores have been projected (**Figures 3-2**, **3-9**, and **3-10**).

The greater acoustic penetration of the boomer sound source allows the dunes to be observed as superimposed on the truncated foreset beds. The internal reflectors of these beds can be traced seaward as bottom-set beds sampled in cores AKAD01-AB17 and AKAD09-28 on the cape Emine Transect (**Figures 3-2**, **3-10**, and **3-11**). On the west end of the profile, erosion has cut so deep as to expose much older conformable layers (blue) beneath the drape and the coquina bed. These conformable layers clearly predate the overlying clinoforms and are separated from the clinoforms by another erosion surface. They subcrop beneath the dunes with the older strata exposed at shallower depths relative to younger strata.

Where mapped in detail on the Emine Transect, the coastal dunes are oriented oblique to the shoreface (**Figures 3-2** and **3-12**). Gravity cores AKAD09-19 and -20 attempted to penetrate into the dune interior without success. Only the surficial drape with a thickness reaching 0.9 m

was recovered. However, core AKAD09-28 beyond the shoreface was able to sample late glacial and post-glacial sediments as well as the coquina deposit and its overlying drape with a thickness of 0.25 m.

The strata beneath the offshore ramp on the outermost shelf contain two hiatuses evident in the chirp profile. These two hiatuses are separating three deposition units in AKAD09-28: the surficial drape, that dated to 10.20 kyr ^{14}C, and that dated to 14,15 kyr ^{14}C and older. This is the exact same situation encountered beyond the paleo-shoreline on the outermost Ukraine shelf. The dark gray mud below the older hiatus is stiff, as observed during core splitting on board the Akademik 2009 cruise, and is characterized by an anomalous low water content (estimated at <15%). Mud cracks were observed in the top of this firm clay, and are filled and covered with a 0.12 m thick deposit of pulverized and bleached shell debris. The uppermost 0.1 m of the stiff mud contains pieces of wood. This mud overlies brown clay that is ^{14}C dated to 14.15 kyr ^{14}C and belongs to the same lithology as sampled on the Romanian margin and attributed to an episode of post-glacial melt-water flooding (Major et al., 2002; Bahr et al., 2006; Major et al., 2006; Soulet et al., 2011a). In turn the shell debris is overlain by light gray mud with articulated mollusks in sandy lenses and dated to the 10.20 kyr ^{14}C. This coquina sit upon the α erosion surface. Corresponding δ^{18}O and δ^{13}C composition of the carbonate is -4 ‰ and 2 ‰, respectively. On top of this mud is another bed of pulverized and bleached shell debris belonging to the coquina; this unit sits upon the shallower surface. The drape cover is just 0.25 m thick.

3.1.4 Turkish Margin

Chirp profile B2ch007 is located on the outermost Turkish shelf north of the entrance of the Bosporus Strait (**Figures 3-2** and **3-13**). This profile (**Figures 3-2** and **3-14**) is oriented west-to-east in the distal region of a network of branching channels that presently funnel highly saline Mediterranean water from the strait into the heads of submarine canyons (Di Iorio and Yüce, 1998; Flood et al., 2009; Hiscott et al., 2013).

An acoustically transparent drape is observed that thins seaward and reaches beyond the shelf break, similar to the behavior of the surficial cover on the previously described shelves (**Figure 3-14**). However, on this margin there are two notable differences. One difference is a somewhat chaotically bedded and highly reflective deposit in the center of the profile that belongs to the internal cores of the levees of branching channels formed beginning with the inflow of Mediterranean saltwater from the Bosporus (Flood et al., 2009; Hiscott et al., 2010; Ryan et al., 2013). The other is the wavy character of the transparent layer shaped and scoured by the inflowing more saline Mediterranean water that is currently traveling (into the page) through the two channels shown in the figure. Core MedEx05-10 sampled the transparent drape adjacent to one of the channels and confirmed that it is composed of mud with exclusively saltwater mollusks.

The a erosion surface beneath the drape truncates older seaward-dipping strata out to an abrupt change in gradient at 115 mbsl. Here are strata equivalent to those on the outer Bulgarian shelf that can be tentatively assigned to the previous glacial period (shown in yellow in **Figure 3-14**). These strata are also truncated by the a erosion surface right out to the shelf break at 180 mbsl. The most severe erosion has occurred beneath the highly reflection cores of the channel deposit in the center of the profile.

Chirp profile B2ch036 (**Figures 3-2** and **3-15**) illustrates widespread truncation of strata by the a erosion surface. This surface has been reached and penetrated by two cores (MedEx05-13 and MAR98-04) described in Ryan et al., (2013) and Aksu et al., (2002b), respectively. MedEx05-13 encountered a 0.15 m thick mud-free gravel and pebble deposit corresponding to the erosion surface. The gravel is predominately round and flat and consists mostly of mudstone and sandstone. However, the pebbles are angular. The latter consists of quartzite, schist and gabbro abundant in the Paleozoic bedrock of the Bosporus Strait. The sediment below the a erosion surface is a soft shale rich in intact specimens of *Mytilus galloprovincialis* with no remaining ^{14}C and thus belongs to an older marine highstand. Core MAR98-04 also penetrated through the a surface and retrieved a white mussel (presumably *Dreissena rostriformis*) with a ^{14}C age of 33.55 kyr ^{14}C (Aksu et al., 2002b). Thus, sediments of presumed glacial age (MIS 2 to MIS 4) are present at the very edge of the shelf here, and make their appearance at same depth as they do in profile B2ch007 on the Bulgarian margin.

The absence of sediments belonging to the last glacial cycle at depths shallower than 110 mbsl on the margin of Turkey north of the Bosporus Strait is further confirmed in chirp profile B2ch013 (**Figures 3-2** and **3-16**) where MAR98-04 is precisely placed on the profile. Thus, in summary, on all four margins (Ukraine, Romania, Bulgaria and Turkey), sediments belonging to the last glacial cycle are present only in a narrow belt on the outermost shelf. Where present, the strata are partly truncated and scoured at the level of the a erosion surface landward of the paleoshoreline and at the level of a younger erosion surface seaward of the paleoshoreline. This younger erosion surface is identified and thoroughly analyzed in the section 4.

3.2 Description of the Sediments

3.2.1 Lithology, faunal composition and ages

The surficial sediment drape in cores from the shelf consists of three lithologies. The upper is a light-colored olive-green mud with no silt or sand and especially rich in saltwater *Modiolus phaseolinuse*, commonly articulated when handled very carefully. The middle lithology is a dark-green mud, richer in organic carbon and without *Modiolus phaseolinuse*. This lithology is rich in saltwater *Mytilus galloprovincialis* (sometimes referred to as *Mytilus edulis*) and *Cardium edule* (also referred to as *Parvicardium exiguum* and *Cerastoderma edule*) and occasionally *Mytilaster lineatus*. Intact articulated specimens of all of these species with bright original coloring are abundant. The shells belonging to *Mytilus galloprovincialis* and *Mytilaster lineatus* are thin and especially fragile, showing signs of dissolution, except in cores deeper than 150 mbsl. The lower-most lithology is a lighter-colored gray-green mud with minor detrital silt and sand. The diagnostic feature of this layer is white specks on exposed surfaces that consist of tiny bleached fragments of shells belonging almost entirely to the freshwater *Dreissena-Dreissema rostriformis* (from now on used in the text as *Dreissena rostriformis*). In this layer there is an overlap of shells belonging to the salt-water environment and those of the fresh and brackish environments. The saltwater mussel specimens are often articulated whereas the freshwater specimens are often single valve or fragments of valves. Based on faunal composition, the upper layer belongs to the New Black Sea stage, the middle layer to the Old Black Sea stage, and the lower layer to the Bugaz stage (Fedorov, 1963; Nevesskaya, 1965). Nevesskaya (personal communication) composed a range of specimens diagnostic of the three lithologies from AK93-01 (**Figure 3-17**).

The sediments assigned to the Bugaz (**Figure 3-17**) directly overlie the afore-mentioned coquina. In previous publications, the coquina has been called a “shell-hash” or “hash layer”

because it is coarse-grained and made up almost entirely of fragmented shells (i.e. Dimitrov, 1982; Ryan et al., 1997; Major et al., 2002; Major et al., 2006; Lericolais et al., 2007; Lericolais et al., 2009; Dimitrov, 2010). The fragmented shells are a mixture of abraided black and bleached white *Dreissena sp*. The coquina often contains lithic sand, gravel, and small pebbles. These detrital components are usually rounded and the pebbles also flattened. The coquina is in the form of two units: a lower mud free unit and an upper, mud enriched unit. Heavily reworked specimens are absent in the coquina in cores on the middle and inner shelf and are limited to those cores in the vicinity of the paleoshoreline and seaward of it.

Intact and even articulated specimens are present in this coquina deposit. These specimens are identified as *Dreissena rostriformis distincta*, *Dreissena polymorpha*, *Monodacna caspia*, *Turricaspia caspia caspia*, *Theodoxus pallas*, and sometimes *Viviparus viviparus*. *Cardium edule* is also present, but usually only in the upper part of the coquina. When present, these specimens are often articulated. It should be noted that *Cardium edule* and *Monodacna caspia* are clams that burrow into and live within their substrate whereas mussels (such as *Dreissena sp.* and *Mytilus galloprovincialis*) are sessile and live on their substrate. *Mytilus galloprovincialis* and *Mytilaster lineatus* only appear in the Bugaz sediments and are never in the coquina.

The ranges of specimens and lithology change in core AKAD11-19 located at 85 mbsl on the crest of a dune on the Varna transect of the Bulgarian shelf (**Figure 3-18**). Here the coquina deposit is 0.13 m thick and begins at 0.43 m below the core top. It rests on a black band with wood and plant fragments belonging to Younger Dryas (i.e., a piece of wood has a ^{14}C date of 10.40 kyr ^{14}C) directly above mud-free sand, a facies attributed to the dune interior. The two units of the coquina, with mud and without mud, are also identified.

In core AKAD11-19, the Bugaz layer is composed of mud with minor sand and has a mixture of fresh, brackish and marine mollusks. The contact with the coquina occurs at 43 cm (**Figure 3-19**). An assemblage of *Dreissena sp*. with *Mytilus galloprovincialis* and *Mytilaster lineatus* from the Bugaz layer is shown in **Figure 3-18** (upper right). An unwashed sample from the coquina with selected specimens of *Dreissena sp*. and *Theodoxus pallasi* that live in both fresh and brackish water is located in a deposit with shell sand and mud (**Figure 3-19**). The fine pulverized shell material appears as white specks in the unwashed-mud adhering to the shells. Some *Dreissena sp*. shells are polished, stained black and otherwise abraded. No species tolerant of saltwater are present in the coquina except for *Cardium edule* that burrowed into the deposit.

A black band of mud occurs between 56 and 59 cm, containing pieces of wood, plant, and blackened fragments of *Dreissena rostriformis*. This layer is cut by a mud-crack (i.e., Neptunian dyke) that extends into the sand beneath. The opening is filled with sandy-mud and contains valves of *Dreissena rostriformis* (**Figure 3-19(d)**). The sand beneath is mud-free, coarse in texture, and consists mostly of *Dreissena rostriformis* shell detritus, minerals, and a few pebbles of indurated shale and sandstone.

Numerous cores were targeted in the vicinity of the paleo-shore-zone on the Burgaz transect across the Bulgarian outer shelf (**Figure 3-20**). Cores AKAD09-21 through AKAD09-26 reached and sampled the coquina deposit beneath 70 to 110 cm of the drape, but the material from the substrate was not recovered. Pebbles are present in all of the core-catchers, as well as wood fragments in AKAD09-23. An abraded fragment of *Didacna*, blackened *Cardium edule*, and coarse quartz sand were extracted from the catcher of AKAD09-26.

Core AKAD09-27 (**Figure 3-21**) sampled the interior side of the front-most coastal dune or barrier island located in the Burgas transect of the Bulgarian margin (**Figure 3-20**). This sampling effort used a vibra-coring device and sampled both the surficial sediment drape (i.e., New Black Sea, Old Black Sea, and Bugaz units), the coquina, and the material belonging to the dune or barrier island beneath. The device was inadvertently lowered into the seabed and then pulled back out before a second penetration that was then completed with turning on the vibrations. As a consequence the marine drape was recovered twice (first between 0 and 137 cm and second, below 137 cm). The analyses were carried out on the material below 137 cm.

The coquina contains exclusively lacustrine and brackish water species mixed in sandy mud with scattered small pebbles and pulverized shell debris. The substrate is even coarser-grained with mostly blackened, abraded, and polished shells mixed into coarse sand composed predominantly of shell debris. Sampled specimens of *Dreissena rostriformis* from the substrate have ^{14}C ages older than 20 kyr ^{14}C. *Dreissena sp*. from the coquina have a narrow range of ages from 8.20 to 8.80 kyr ^{14}C. The gap in ages between the coquina and its substrate corresponds to the sub-bottom level of the wide-spread erosion surface (reflector α) observed in the chirp profiles.

3.2.2 Sediment water content and bulk density

The water content in sediments that belong to a period after the Black Sea has submerged is consistently at 40 to 50% and the bulk density is 1.3 to 1.4 g/cm^3 (**Figure 3-22**). For the cores located landward of and in the vicinity of the paleoshoreline, AK93-11 at 91 mbsl and AK93-08 at 99 mbsl (**Figures 3-22 a and b**), the water content drops below 20% to as low as 10% and the bulk density increases to 1.85 g/cm^3. For the cores located seaward of the paleoshoreline the

water content drops to 30 % and the bulk density rises to a range between 1.8 and 1.9 g/ cm^3 in AQ93-24 at 110 mbsl, AQ93-09 at 123 mbsl, AQ93-22 at 129 mbsl, and AQ93-23 at 150 mbsl below the coquina, deposition with ^{14}C ages that range between 11 to 10 kyr ^{14}C years (**Figures 3-22 c, d, r, g**). The water content drops to 20% and bulk density rises to a range between 1.9 and 2.0 g/cm^3 in AQ93-14 and AQ93-15 (**Figures 3-22 f and h**) at 140 and 165 mbsl, respectively, below a lower coquina, deposition with ^{14}C ages of > 14.70 kyr ^{14}C. The water content is low and bulk density is high in all of the coquina.

3.3 Isotopic composition of the coquina

The $^{87}Sr/^{86}Sr$ composition of mollusks from the coquina and overlying Bugaz deposits in AKAD09-27 and AKAD11-19 cores ranges from 0.70875 to 0.70915 (**Figure 3-23**). *Monodacna caspia* and *Cardium edule* in the Bugaz interval of AKAD09-27 have $^{87}Sr/^{86}Sr$ compositions of 0.70908 and 0.709105, respectively. This *Cardium edule* specimen is dated to 6.60 kyr ^{14}C. *Dreissena rostriformis* from the Bugaz and the top of the coquina (that with the presence of sand) has $^{87}Sr/^{86}Sr$ compositions strictly around the value of 0.70895 with ^{14}C ages that range between 8.38 and 8.75 kyr ^{14}C. In the clean coquina unit, a *Dreissena rostriformis* has a $^{87}Sr/^{86}Sr$ value of 0.70875 in AKAD09-27 and 0.70891 in AKAD11-19. The bottom of the coquina and the top of the dune in AKAD09-27 features a polished *Dreissena sp.* with a $^{87}Sr/^{86}Sr$ composition of 0.70879. One of the *Dreissena rostriformis* mollusks in this interval, also reworked, gives a ^{14}C age of 22.50 kyr ^{14}C. This interval also features two significantly polished specimens identified as a *Didacna* of Middle Pleistocene age and *Glycemeris* of Karangatian age (Wesselingh, 2015). Both of these are marine bivalves. Curiously, both give ^{14}C ages in the 30

to 40 kyr ^{14}C age and this measurement. These mollusks have $^{87}Sr/^{86}Sr$ composition of 0.70899 and 0.70904, respectively.

The $\delta^{18}O$ composition of the mollusks in AKAD09-27 and AKAD11-19 ranges from ~-9.0 to 0.5 ‰ (**Figure 3-23**). In the Bugaz layer, the marine and transitional specimens (i.e., *Cardium edule*, *Mytilaster lineatus*, *Monodacna caspia*) have $\delta^{18}O$ compositions between -0.83 and 0.50 ‰ whereas *Dreissena rostriformis* and a *Turricaspia caspia* specimens give ~-2.0 ‰. A *Cardium edule* and *Mytilus galloprovincialis* in AKAD11-19 give ^{14}C dates of 6.580 and 6.590 kyr ^{14}C, respectively. In the top, muddy coquina unit section of the deposit, unreworked *Dreissena rostriformis* specimens have $\delta^{18}O$ compositions also consistently around -2 ‰. All of the *Turricaspia caspia* specimens in this layer in the AKAD09-27 have $\delta^{18}O$ composition that range between -6.0 and -9.0 ‰. This sedimentary layer also features a *Theodoxus heldreichi* specimen with a $\delta^{18}O$ composition of -4.0 ‰. The lower interval of the coquina deposit, that with a reduced amount of mud, features a number of *Theodoxus heldreichi* and *Turricaspia caspia* specimens with a $\delta^{18}O$ composition of -4.0 ‰. This interval also contains heavily reworked *Dreissena sp.* with a $\delta^{18}O$ composition of -6.0 and -8.6 ‰. The two bottom-most *Dreissena sp*. have ^{14}C dates of 31.40 and 48.10 kyr ^{14}C. One of the heavily reworked marine bivalves, identified as belonging to the *Glycemeris* family, has a $\delta^{18}O$ of -1.67 ‰.

3.4 Geographical trends in the isotopic composition of the coquina deposit

The analysis of $^{87}Sr/^{86}Sr$, $\delta^{18}O$, and ^{14}C composition in the coquina and Bugaz deposits as a function of water depth indicates several trends (**Figure 3-24**). The $^{87}Sr/^{86}Sr$ composition of the intact mollusks within the coquina deposit increases from 0.70890 to 0.70915 as the core sites shoal from 120 to 50 mbsl. From 50 to 20 mbsl, the $^{87}Sr/^{86}Sr$ composition then decreases to

0.70885. There are no *Dreissena rostriformis* specimens found in the coquina at water depths shallower then 22.50 mbsl. The specimens landward of 22.50 mbsl are all identified as inhabiting the Black Sea shelf after the initial transition from fresh to marine was completed.

A similar trend is identified in the $\delta^{18}O$ composition of mollusks. From 150 to 50 mbsl, the $\delta^{18}O$ composition of the intact mollusks within the coquina increases from -2.5 to -0.2 ‰. From 50 to 20 mbsl, the $\delta^{18}O$ composition retreats to -4 ‰. The ^{14}C composition of the mollusks also allows the recognition of when the various species inhabited the Black Sea-Lake during the transition from the lacustrine to marine environment. The ^{14}C ages of the *Dreissena rostriformis* are constricted to a time window from 9.30 to 8.10 kyr ^{14}, that of *Dreissena polymorpha* are constricted to a time window 8.70 to 7.90 kyr ^{14}C, that of the Monodacna caspia to a time window 8.10 to 6.50 ^{14}C years, and that of *Cardium edule* and *Mytilus galloprovincialis* from the Bugaz layer in the transgressive deposit to 7.90 to 6.10 kyr ^{14}C. These periods of colonization overlap each other successively. There is a slight trend of ^{14}C composition in the *Dreissena rostriformis* towards younger values with decreasing water depth.

3.5 Changes of ^{14}C reservoir, $\delta^{18}O$, $\delta^{13}C$, and $^{87Sr}/^{86}Sr$ during the change from lacustrine to marine

The presentation of measurements of the ^{14}C reservoir age, $\delta^{18}O$, $\delta^{13}C$, and $^{87}Sr/^{86}Sr$ in correspondence to calendar age for the interval from 40 kyr to the present is shown in **Figure 3-25**. This description will focus on the interval spanning the Bølling/Allerød interstadials to the mid-Holocene. During the Bølling/Allerød, the ^{14}C reservoir increases to 650 ^{14}C years. Likewise, during the Preboreal, the ^{14}C reservoir rises to at least 1,100 ^{14}C years. The estimation only has a lower bound as there are limited data available immediately before 9,300 years.

Following the Preboreal, the ^{14}C reservoir age drops from 1,100 ^{14}C years to 350 ^{14}C years. This change occurs in a time span of 1,500 calendar years. All measurements used single *Dreissena sp.* specimens for matching their signals to those derived from stalagmites in the Sofular Cave of Turkey.

The $\delta^{18}O$ rises from -2 ‰ to 0 ‰ in the time range of 9.30 to 7.80 kyr BP. However, the magnitude of this change varies by mollusk type. The $\delta^{18}O$ composition of *Dreissena sp.* rises from -2 ‰ to -1 ‰ in the time range of 9.30 to 8.30 kyr BP, the $\delta^{18}O$ of *Monodacna caspia* rises from -1.3 ‰ to -0.1 ‰ in the time span of 8.40 to 7.80 kyr BP, and the $\delta^{18}O$ composition of marine mollusks (e.g., *Cardium edule* and *Mytilus galloprovincialis*) varies ±-0.5 around 0 per ‰ through the rest of the Holocene. There are some additional data from Sakarya coastal plain. For a calendar age of around 9.20 kyr BP, a very well preserved and without any significant reworking, a *Dreissena sp*. has a $\delta^{18}O$ composition of -9.2 ‰.

The $\delta^{13}C$ rises from -0.5 to 1.8 ‰ in the time range of 9.30 to 7.80 kyr BP. As with the $\delta^{18}O$ composition, this change varies by mollusk type. The $\delta^{13}C$ composition of *Dreissena sp.* rises from -0.5 to 1 ‰. The $\delta^{13}C$ composition of other transitional (e.g., *Monodacna caspia*) and fully marine species (e.g., *Cardium edule* and *Mytilus galloprovincialis*) ranges from 1.8 to -1 ‰. It is possible that this is actually a drop in $\delta^{13}C$ composition, similar to that drop in $\delta^{13}C$ that occurs in the Sofular Cave at 6 kyr BP. In the mollusk record this change occurs in a time range of 7.70 to 6 kyr BP. The $\delta^{13}C$ composition of the *Dreissena sp.* from Sakarya coastal plain is, as with its $\delta^{18}O$ composition, very different from the rest of the mollusks. It is much more negative, -7.8 ‰, closer to the $\delta^{13}C$ composition of the calcite that is precipitated in the Sofular Cave, also in northern Turkey.

The $^{87}Sr/^{86}Sr$ composition rises from 0.70885 to 0.709104 in the time range of 9.30 to 7.80 kyr BP. As with $\delta^{18}O$ and $\delta^{13}C$, this change varies by mollusk. The $^{87}Sr/^{86}Sr$ composition *Dreissena sp.* rises from 0.70885 to 0.709104. The $^{87}Sr/^{86}Sr$ composition of transitional and marine mollusks varies around 0.709104 with a standard deviation of 0.00005 which is just outside 2 σ for the error associated with the measurements. There are a number of *Cardium edule* specimens that have an $^{87}Sr/^{86}Sr$ composition in the range of 0.70895 to 0.70905. Two of these specimens are from the Sakarya coastal plain and one other is from a shallow core, 37-82, that was taken from a water depth of 17.7 mbsl. A *Monodacna caspia* specimen from this same core and depth interval in the core, also has a lower $^{87}Sr/^{86}Sr$ composition. One of the Sakarya *Dreissena polymorpha* specimens gives a $^{87}Sr/^{86}Sr$ composition of 0.7079. This is the same specimen that has very different $\delta^{18}O$ and $\delta^{13}C$ compositions and records the composition of the river water. It should be noted that the $^{87}Sr/^{86}Sr$ composition of the ostracodes is identical to the $^{87}Sr/^{86}Sr$ composition of the mollusks.

3.6 Limans

A cross section of the Dniprovs'ko-Bush'kyi Liman on the Ukraine coast obtained by drill cores (**Figure 3-26**) illustrates a deep riverbed incision into Neogene sedimentary bedrock followed by episodes of infill and some re-incision, beginning in the late glacial times according to ^{14}C measurements reported in Naukova, (1984). The earliest fill is fluvial sand that blankets an initial gravel and pebble lag deposit. This fill is then covered by red-brown mud attributed to major river floods. A thin layer of Neoeuxine mud, with fauna identified as *Monodacna caspia* and *Dreissena sp*., covers the flood deposits. This layer (shaded blue in **Figure 3-26**) contains first indication of a salinity change. Then once the river transformed into an estuary colonized

by the typical marine mollusk assemblage of the Bugaz stage with *Mytilus galloprovincialis* there is a new incision removing some of the Neoeuxine and red mud in the center of the channel. The filling then continues to almost completely constrict to what is now the Dnieper River except for a modern narrow deep channel.

4. Discussion

The largest element of disagreement in the aforementioned four schools of thought, as it relates to the understanding of the Holocene transgression of the Black Sea-Lake, arises from the interpretation of data regarding the location of the lake level prior to the lake's connection with the Mediterranean Sea. The discussion reinterprets prior data with the new set of ^{14}C, $\delta^{18}O$, $\delta^{13}C$, and $^{87}Sr/^{86}Sr$ measurements presented to show that (1) the modern Black Sea shelf was exposed immediately prior to and at the time of the breaching of the Bosporus sill by Mediterranean water, (2) the composition of the Black Sea-Lake was fresh prior to the inflow of Mediterranean water, (3) the Black Sea-Lake level was regressed to at least 165 mbsl if not lower, (4) the transgression across the shelf was exclusively caused by the inflow of Mediterranean water, (5) the transgression was very fast, and (6) the initial salinization was fast and was followed by a slower one before fresh and brackish species could tolerate the increased surface water salinity.

4.1 The Black Sea shelf was a terrestrial landscape at the time of the initial inflow of Mediterranean saltwater

4.1.1 Evidence from widespread erosion

The discovery of a pervasive erosion surface, reflector a, documented in published reflection profiles and profiles presented above is entirely consistent with the deduction

formulated many decades ago that much of today's submerged Black Sea continental shelf was once a terrestrial landscape (Kuprin et al., 1974). Additional evidence comes from the observation of: 1) a paleo-shoreline close to the modern shelf edge based on the geometry of buried strata analogous to modern delta and pro-delta deposits (Aksu et al., 2002b; Dimitrov and Dimitrov, 2004; Genov et al., 2004a; Genov, 2004b; Lericolais et al., 2009); 2) meandering shelf-crossing river channels (Ryan et al., 1996; Popescu et al., 2004; Ryan, 2007; Popescu, 2008); 3) relic dunes diagnostic of wind-swept and coastal landscapes (Ryan et al., 1996; Naudts et al., 2006; Lericolais et al., 2007; Ryan, 2007); 3) meandering shelf-crossing river channels (Ryan et al., 1996; Popescu et al., 2004; Ryan, 2007; Ryan, 2007; Popescu, 2008; Dimitrov, 2010); 4) substantial increase in the density of the sediments below the erosion surface; 5) peat, grass, leaves, wood, and desiccation cracks at sites where the substrate below reflector a has been successfully sampled (Nicholas et al., 2011; Mudie et al., 2014; Nicholas and Chivas, 2014).

4.1.2 Paleo-rivers

The inclined strata that make up the substrate on the Bulgarian and Turkish margins are beveled uniformly with little differential resistance between layers (**Figures 3-7, 3-14, 3-15, and 3-16**). This observation is in contrast to the Ukraine margins (**Figures 3-4 and 3-5**) where the erosion surface is considerably more rugged. The difference may be explained by the abundance of shelf-crossing river channels on the northern margin and their sparseness on the southern margins. As the shoreline retreats during regression, rivers keep pace and cut into the new landscape as they adjust to lowered base level. Such incision created the Dniepr and Dniestr shelf valleys (Konikov et al., 2007; Yanko-Hombach et al., 2014). Interfluves are observed between the mesa in the reflection profiles.

River-bed infilling commences once a permanent lowstand paleoshoreline has been established. Rivers are then able to meander. Downstream, gradients decrease and flow velocities drop. This allows bedload to accumulate above an initial lag coarse deposit. On the Romanian shelf, cores BLKS98-30 and BLKS98-34 sample fill in a meandering channel between 70 and 76 mbsl that would presumably be fed by the paleo-Danube. The fluvial sediment below the coquina (dated to 8.30 kyr ^{14}C) is sandy, devoid of mollusks, and accumulated before 23.63 kyr ^{14}C. The fill of the entrenched Dniepr River is located beneath the floor of the Dniprovs'ko-Bush'kyi Liman (Naukova, 1984). The maximum incision was completed before 17.76 kyr ^{14}C (**Figure 3-27**).

4.1.3 Aeolian dunes

A survey on the mid-shelf (65 to 80 mbsl) off Romania imaged a field of dunes with transverse and barchan shapes (Lericolais et al., 2007). The dunes grew directly over the α erosion surface and its underlying river channels (Popescu, 2008). Measurements of dune height versus dune spacing are identical to terrestrial dunes in Colorado and SW Kalahari.

Between dunes are enclosed depressions likened to wind-blown hollows and desert pans. The walls of these depressions display bathtub rings indicative that they periodically filled with water to become ponds that occasionally over-spilled into neighboring ponds (Ryan, 2007). Core BLVK9814, located at 55 mbsl in one such depression between dunes on the inner Romanian shelf, contains dwarfed specimens of *Cardium edule* and *Adacna* from below the coquina. The *Cardium edule* with an age of 9.58 kyr ^{14}C has a $^{87}Sr/^{86}Sr$ composition of 0.709071 which is vastly more radiogenic than the composition of the Black Sea lake water at that time (0.708900). This discrepancy is ascribed to colonization of perched ponds at elevations high above the

paleoshoreline of the Black Sea-Lake (Major et al., 2006). Scherbakov and Babak, (1979) describe the same faunal assemblage in sediments from the Sea of Azov which they also interpret to be perched saline ponds during periods of lowered Black Sea level.

These inner and mid-shelf ponds formed during wetter intervals. As the climate became drier during the Preboreal, these ponds shrank, their solutes concentrated, and the environment became suitable only to species such as the *Cardids* that are tolerant of saltier water. The eventual desiccation of the ponds is demonstrated by the migration of dunes across them.

4.1.4 Coastal dunes

In the vicinity of the paleoshoreline, other dunes sit upon the α erosion surface. These dunes are smaller in size compared to those dunes located on the mid-shelf and are likened to Lake Superior shoreface and ridges (Lericolais et al., 2007). These features (**Figures 3-10, 3-11, 3-12**) are interpreted as coastal dunes. Those cores that penetrated into the interior of the coastal dunes, AKAD09-27 and AKAD11-19, recovered mud-free sand with pulverized shell material directly overlain by the coquina. The large shell fragments from within the dune belong to polished and bleached mollusk specimens (**Figure 3-19**) with ages that range from 21 to 48.10 kyr ^{14}C.

The ages of these mollusks indicate that some material in the dunes is very old. The material in the dunes is likely derived from wind ablation and coastal wave action along the paleo-shoreline. The dunes rest on truncated clinoforms, interpreted as forced-regression deposits (Lericolais et al., 2007). An age belonging to the last glacial period can be assigned by the continuity of foresets to bottomsets that have been sampled in cores seaward of the paleoshoreline. The clinoforms on the Bulgarian shelf (**Figure 3-10 and 3-11**) are similar in

geometry and depth below sea level to those on the southwest Turkey shelf identified as Δ_1 (Aksu et al., 2002). On both margins topset beds are missing and the seaward dipping foreset beds are truncated by reflector α.

4.1.5 High bulk density and low water content of the substrate

The substantial decrease in measured water content (<20%) and corresponding increase in bulk density to values exceeding 1.8 g/cm^3 (**Figure 3-22**) is attributed to emergence of the lake bed and exposure of the land surface that then after subsequent submersion and burial becomes the substrate below reflector α sampled in the cores. A firm and dry substrate is observed not only beneath reflector α everywhere landward and in the vicinity of the paleoshoreline, but for the sediment below both reflectors α1 and α, seaward of the paleoshoreline. Following the observations and using nomenclature of Aksu et al., (2002b), reflector α1 corresponds to the younger reflector that separates sediment of Younger Dryas age (and older) from the post-connection surficial drape and sits above the α erosion surface. This is only observed seaward of the paleoshoreline as reflector α1 is not present landward of the paleoshoreline.

Dry and dense sediment identified as the Younger Dryas is present at 110 mbsl in core AQ93-24, at 123 mbsl in core AQ93-08, and at 129 mbsl in core AQ93-22. Dry and dense sediment identified with glacial and meltwater deposits is present at 140 mbsl in core AQ93-14, at 150 mbsl in core AQ93-23, and at 165 mbsl in core AQ93-13.

The water content is high and bulk density is low in some, but not all, of the sediments identified with the Younger Dryas beneath the α1 (i.e., the water content decreases and bulk density increases for AQ93-23 but not AQ93-14). This observation may be explained in two

ways: (1) a briefer regression of the Black Sea-Lake at these depths relative to their shallower counterparts and hence, a shorter period of time for water content to have been lost before submergence by marine water and/or (2) thinner sedimentary Younger Dryas unit in AQ93-23 relative to AQ93-14 exposed to the atmosphere making it easier to loose moisture while exposed rather than retain it. The top of the Younger Dryas sediment in AQ93-14 does have a short drop in water content relative to the rest of the record. Yanko-Hombach et al., (2007) cite Soviet era publications and report that bluish-grey stiff clay that fills depressions and paleo-river valleys on the Ukrainian shelf has a density reaching 2.7 g/cm^3. The decrease in moisture could only have occurred during periods of regression, when the shelf was exposed to the atmosphere allowing for the evaporation of sediment pore water. Hence, the lake surface was below the exposed shelf during periods corresponding to Bølling/Allerød and Preboreal.

4.1.6 Peat, grass, leaves, wood, and desiccation cracks

Peat that forms in ponds, bogs, and coastal marshes has been observed in many cores from the Black Sea shelf where it is directly overlain by the coquina (Yanko-Hombach et al., 2007). Although dating of peat does not need prior knowledge of a ^{14}C reservoir age, as do lacustrine samples, analysis of bulk samples risks the incorporation of older material. Individual plant leaves and pieces of wood removes the ambiguity. Mudie et al., (2004) report ages of 8.45 kyr ^{14}C for a sedge leaf and 8.89 kyr ^{14}C for wood from a core at 33 mbsl on the Ukrainian shelf. Even though peat has not been found at elevations below 55 mbsl on any Black Sea shelves, plant roots and wood fragments are present at 99 mbsl associated with desiccation cracks in core AK93-08. Plant leaf fragments are present at 110 mbsl in core AK93-24 and at 126 mbsl in core

AKAD09-28. Roots occur again at 123 mbsl in core AK93-09. Plant material in its original setting is strongly suggestive of prior emergence.

4.2 Black Sea was a freshwater lake prior to entrance of Mediterranean water

The inference that that the Black Sea-Lake was fresh or only slightly brackish prior to the latest entrance of salt water from the Mediterranean is based on four lines of evidence: 1) benthic fauna, 2) planktonic fauna, 3) dinoflagellates, 4) pore-water chemistry, and 5) isotopic composition of shells and authigenic calcite.

4.2.1 Benthic fauna

The benthic mollusk faunal assemblage in samples below the coquina includes *Dreissena rostriformis distincta*, *Turricaspia caspia*, *Theodoxus pallasi*, *Viviparus viviparous*, and *Unio pictorum*. According to Nevesskaya, (1965) and Fedorov, (1963), the latter two species are exclusive to freshwater environments. *Theodoxus pallasi* lives today in Varna Lake, freshwater lagoons, and the most strongly-freshened regions of the Azov Sea. This freshwater mollusk assemblage is distinct and without any of the species belonging to the subsequent saltwater assemblage (e.g., *Cardium edule*, *Mytilus galloprovincialis*, *Mytilaster lineatus*, and *Modiolus phaseolina*).

The benthic foraminiferal assemblage in cores on the shelf is entirely composed of oligohaline species (1-5 ppt). *Ammonia caspia*, *P. martkobi tschaudicus*, *M. brotzkajae*, and *E. caspicum* today inhabit river deltas in the Black and Caspian Seas (Yanko-Hombach et al., 2007). Benthic foraminifera are absent (except for reworked specimens) in cores from the slope and basin floor. Therefore these foraminifera can only be used to estimate the prior salinity of

uppermost water column. On the other hand, deep-water salinity can be deduced from bottom-dwelling ostracods. The assemblage from sediment older than the shelf coquina (i.e., belonging to Unit 3 of Ross and Degens, (1974) consists of species encountered today in the Black and Caspian Sea deltas with low salinity (Ivanova et al., 2007; Schornikov, 2011). Just prior to the introduction of saltwater from the Mediterranean, diversity was highest and *Leptocytheridae* species dominated the assemblage (Briceag et al., in revision).

4.2.2 Planktonic fauna

The pelagic components in sediments older than the coquina are juvenile *Dreissena rostriformis distincta* and dinocysts (Nevesskaya, 1965; Wall and Dale, 1974; Mudie et al., 2001). The dinoflagellate assemblage is characterized by dominance of Pyxidinopsis psilata (now Tectodinium psilatum), and *Spiniferites cruciformis* accompanied by freshwater algae (*Pediastrum sp.* and *Botryoccocccus*) (Marret et al., 2008). *Spiniferites cruciformis* is considered freshwater taxa (Wall and Dale, 1974; Atanassova, 2005) and is abundant in the late glacial deposits of Lake Kastoria (Greece) (Kouli et al., 2001). Mudie et al., (2001) also associate *Spiniferites cruciformis* with very low salinities (3.5-7 ppt), but "probably not entirely freshwater". Although juvenile mollusks and dinoflagellate cysts occur in deep-water cores from the basin floors, they also are only indicators of surface-water salinity.

4.2.3 Dinoflagellates

The dinoflagellate cyst assemblage in the period preceding the connection is dominated by fresh- to brackish- water species (i.e., *Spiniferites cruciformis* and *Pyxidinopsis psilata*) (Filipova-Marinova et al., 2013). This assemblage reflects sea surface salinity of <7 p.s.u

(Deuser, 1972; Wall and Dale, 1974; Mudie et al., 2001; Chepalyga, 2002). This freshwater assemblage does not include any species belonging to the subsequent saltwater assemblage (i.e., *Lingulodinium machaerophorum*, *Spiniferites belerius*, *Spiniferites bentorii*, *Operculodinium centrocarpum*). *Spiniferites cruciformis* and *Pyxidinopsis psilata* are characteristic of water that is cold and is of low salinity. The former was observed in the sediments of Lake Kastoria northern Greece identified to accumulate during the Glacial Period (Kouli et al., 2001). This species is also common to the brackish Caspian and Aral Seas (Marret et al., 2004).

4.2.4 Pore-water chemistry

Fluid extracted from freshly-opened cores can be used to investigate the salinity of fossil water originally entrapped in the pores of now-buried sediment from deep-basin settings (Manheim and Chan, 1974). Brujevich, (1952) was the first to observe that the salinity and chlorinity decreased with depth in long piston cores from the Black Sea. This trend was first direct evidence that the interior of the Black Sea had been fresher in the past. Kvasov, (1968) linked the estimated timing of this freshening to the late glacial (Neoeuxine) regression and proposed that streambed erosion during a freshwater cascade through the Bosporus spillway to the Sea of Marmara was the causative agent for the lowering of the Black Sea-Lake level.

The measured salt concentrations are not the actual salinities of former Black Sea bottom water. The observed down-core freshening is the consequence of salt diffusing from higher salinity in modern seabed to regions of lower salinity in the pore-water of the deep interior. It is from the curvature of the diffusion profiles that actual paleosalinity can be calculated. In a collection of more than two dozen long piston cores examined by Manheim and Chan, (1974), the downward trend of decreasing chlorinity remained unabated. Thus, the minimum measured

interstital-chlorinity values of 5 to 6 g/kg at 12 m in the bottom of a core from 2,114 mbsl are maximum values for the prior bottom water. The calculated minima from modeling of diffusion is ~3.5 g/kg for chlorine and thus an equivalent of 6 g/kg for bottom-water salinity Manheim and Chan, (1974).

Soulet et al., (2010) measured the downward trend of chlorinity using an ultra-long piston core from 358 mbsl. The minimum measured value of dissolved chloride at 28 mbsf is 1.1 g/kg translates to a salinity of 2 ppt (psu). From a best fit of their observed diffusion profile to model calculations, these authors conclude that the late glacial Black Sea-Lake was a freshwater body during the glacial period and pose a possibility that the Black Sea-Lake remained fresh throughout the deglaciation until the moment of saltwater intrusion from the Mediterranean.

4.2.5 Inferences of water salinity from its isotopic composition

It is also possible to deduce the salinity of the Black Sea-Lake from the isotopic composition of carbonate shells of mollusks and ostracods. $^{87}Sr/^{86}Sr$ is exceptionally useful as the $^{87}Sr/^{86}Sr$ composition of water primarily reflects the contribution from sources that make up the water in any particular basin (e.g., Black Sea), whether that is rivers or water flowing in from another basin (e.g., Mediterranean), and largely excludes changes that would result from processes such as evaporation or precipitation (Stein et al., 1997; Krom et al., 1999). The application of the $^{87}Sr/^{86}Sr$ to fauna that colonized the Black Sea-Lake water prior to the connection of the Black Sea-Lake with the Mediterranean was shown to express the average value of river water feeding the Black Sea-Lake (Palmer and Edmond, 1989; Major et al., 2006; Bahr et al., 2008). These set of observations lead to an interpretation that the basin was predominantly composed of freshwater that kept the Black Sea-Lake fresh during the

deglaciation and there were no traces of marine water until its connection with the Mediterranean.

The stable oxygen isotope composition of the surface water, as measured in mollusk shells, increased during the deglacial period, 15 kyr BP to 9.30 kyr BP, from -7.5 to ~<-2 ‰. This is largely ascribed to progressive isotopic enrichment of meteoric water as the earth was coming out of the glaciation (Major et al., 2006; Bahr et al., 2008). The $\delta^{18}O$ isotopic value of the surface water prior to the connection reflected the combined processes of the isotopic composition of rivers flowing into the Black Sea and precipitation.

4.3 Lake was largely regressed immediately prior to its connection with the Mediterranean

The lake level immediately prior to the inflow of Mediterranean water is estimated from: (1) the observation of the hiatus between those sediments deposited prior to the inflow of Mediterranean water and those that are deposited after, (2) the depth extent across the shelf with a measured decrease of water content beneath the coquina, (3) the location of coastal dunes ^{14}C dated by mollusk shells, and (4) the location of the ^{14}C dated peat, wood, and plant remains (**Figure 3-27**). The hiatus extends from the inner shelf and onto the slope, beyond the shelf break. The yellow contour designates the lake level and is constrained by the presence of peat and mollusk data as a function of depth and time. The lake surface sits below the contemporary peat deposits, coastal and windblown interior dunes, which formed above water and above any deposits belonging to the Black Sea (in its lake and marine form).

Coquina lies above the hiatus. Its composition of concentrated shells and gravel-size shell debris generates the strong reverberant nature of reflectivity observed in the chirp profiles. Landward of the paleoshoreline, reflector α separates material of glacial age and older from those

deposited after the submergence of the Black Sea-Lake. Seaward of the paleoshoreline, α bifurcates into α and α1. As mentioned earlier, the reflector that corresponds to the younger gap is identified as α1 and that of the older gap is the continuation of reflector α. Reflector α1 separates material of Younger Dryas age and older from those deposited after the submergence of Black Sea-Lake. Reflector α sits below α1 and separates sediments belonging to the Younger Dryas from underlying gray glacial deposits and red muds delivered by enhanced meltwater discharge (Dimitrov, 1982; Major et al., 2002; Ryan et al., 2003; Dimitrov and Dimitrov, 2004; Bahr et al., 2006; Ryan, 2007; Bahr et al., 2008; Soulet et al., 2011a). Missing in the two gaps are sediments belonging to the Preboreal and the Bølling/Allerød stages.

The evaluation of the hiatuses and coquina suggests that the lake level stood at least at 165 mbsl at 9.30 kyr BP (8,200 corrected kyr ^{14}C). The 165 mbsl is a minimum estimate; the level of the lake prior to its transgression may have stood even lower. The more extreme estimate is derived from absence of sediment of Preboreal age from cores at 200 mbsl, 09-SG-13, and at 240 mbsl, BLKS9809. The core at 200 mbsl does not indicate any evidence of erosion or water deprivation but there is a layer of concentrated coquina that separates sediments of Younger Dryas and Holocene age. This deposit may have been formed during a depressed water level by enhanced wave action that washed out the mud and concentrated the coquina. Other than absence of sediment, there is no indication of any coquina deposits that separate sediment of deglacial age and post-connection for a core retrieved from 240 mbsl. Hence, it is not possible to confirm or refute whether the lake level regressed below 240 mbsl during the Preboreal.

Measurements of water content beneath the coquina support the observations made from hiatuses and the locations of the coquina that the regression was below the inferred level of the paleoshoreline at least to a depth of 150 mbsl (**Figure 3-22**). Absence of sediment belonging to

the Younger Dryas at deeper elevations does not support or refute a regression to a level at 165 mbsl and/or lower. This interpretation is a digression from the Black Sea-Lake level curves presented by the three schools of thought discussed in the introduction, none of which attributed the low stand exclusively to the Preboreal warm period. The compiled data makes the conclusion associated with the interpretation from the fourth school of thought much more robust.

A number of authors assert that the level of the Black Sea-Lake was already at the elevation of the current Bosporus Sill, 35-40 mbsl prior to the inflow of Mediterranean water (Görür et al., 2001; Aksu et al., 2002b; Kaplin and Selivanov, 2004; Yanko-Hombach et al., 2007; Hiscott et al., 2007a; Giosan et al., 2009; Marret et al., 2009; Hiscott et al., 2010; Yanko-Hombach et al., 2011; Mudie et al., 2014; Yanko-Hombach et al., 2014). In particular, Yanko-Hombach et al., (2014) and Mudie et al., (2014) interpret the wood, sedge-leaf, and co-deposited peat from core 342 from a depth of 30 mbsl as evidence that the Black Sea-Lake level was near this water depth prior to its connection with the Mediterranean at 8.90 ^{14}C years. Although the measured ^{14}C ages on wood and sedge leaf are 8.55±0.40 and 8.54±0.40 kyr ^{14}C, respectively, the authors use *Dreissena sp*. and *Cardium edule*, specimens found above the peat deposit, with measured ^{14}C ages of 9.140 and 9.620 kyr ^{14}C to infer an even earlier age of connection of 8.90 kyr ^{14}C. The authors attribute the older age of the specimens to the hardwater effect.

Hiscott et al., (2002) use mollusks dated between 8.57 and 9.07 kyr ^{14}C from a core at 69 mbsl on the Turkish shelf, M02-45, well above the lake level, to infer that the lake surface was at its outlet prior to connection. The specimens with ^{14}C dates that range from 8.57±0.70 to 8.840±0.70 kyr ^{14}C fall in the range of the specimens dated from the coquina, formed after the submergence of the Black Sea-Lake by the Mediterranean water to the elevation of the paleo-Bosporus sill. Other species with measured ^{14}C ages older than the connection of the Black Sea-

Lake with the Mediterranean, 9.37±0.70 ^{14}C and 9.070±0.70 ^{14}C years, are identified as *Dreissena rostriformis* and *Theodoxus pallasi*. Hiscott et al., (2007a) uses this observation together with an assumption of a 50 mbsl wave base to conclude that the lake level was at 30 mbsl prior to its connection with the Mediterranean. However, these strata are confined to a mid-shelf depression and are absent on the outer- and inner-most shelves. Hiscott et al., (2007a) explain that this absence is a consequence of wave action preventing any sediment deposition above the wave base. However, the absence of these from the outer-most shelf cannot be explained by wave-action and hence, another mechanism is needed, not commented upon by the authors.

These deposits that are found at depths shallower than the paleoshoreline on the middle and inner Black Sea-shelf and that also date to a period before the connection, are anomalous. Very few records exist. On the Romanian Shelf, two *Cardium edule* specimens from BLKS98-14 at a depth of 55 mbsl are dated at 9.58±0.80 and 9.58±0.90 kyr ^{14}C The latter specimen has a ^{87}Sr/^{86}Sr composition of 0.709071, a measurement that shows that these mollusks did not inhabit an environment submerged by the Black Sea-Lake and instead, inhabited an environment disconnected from it, such as a perched pond/lake. The mollusks from M02-45 with ^{14}C ages of 9.14 and 9.62 kyr ^{14}C interpreted as those belonging to a submerged lake in Yanko-Hombach et al., (2014), Mudie et al., (2014), Giosan et al., (2009), and Hiscott et al., (2007a) are hence, also much more likely to belong to previously existing perched lake/ pond environments. Hence, the arguments presented cannot be used to refute that the lake regressed below the paleoshoreline without additional analyses. ^{87}Sr/^{86}Sr and/or ε_{Nd} measurements would show whether or not these specimens inhabited an environment akin to a ponded lake.

Giosan et al., (2009) assert that the level of the Black Sea-Lake was ~30 mbsl from prior to the connection of the Black Sea-Lake with the Mediterranean Sea from an observation that the Danube was building an early Holocene delta at that time from radiocarbon measurements of *Dreissena polymorpha*. These specimens were dated to 8.66±0.45 kyr ^{14}C and 8.86±0.45 kyr ^{14}C from a drill core in the Danube delta. Given the measured ^{14}C ages of the mollusks, however, this observation is entirely consistent with the interpretation that the Black Sea was already at this level at this time. The Danube delta that was building up was doing so after the connection of the Black Sea-Lake with the Mediterranean Sea. $^{87}Sr/^{86}Sr$ and/or ε_{Nd} measurements would conclusively determine whether these *Dreissena polymorpha* speciments belonged to a marine of freshwater body of water.

Görür et al., (2001) assert that the Black Sea-Lake transgressed a large fraction of the shelf prior to its connection with the Mediterranean from an observation of a deposit with a *Dreissena polymorpha* specimens and co-depositional wood that is ^{14}C dated to 7.23±0.26 kyr ^{14}C BP from cores recovered from the Sakaraya river at 28 mbsl. The authors interpret that this indicates that the Black Sea-Lake was a freshwater lake with a water level of 28 mbsl and/or shallower prior to its connection with the Mediterranean Sea. However, the Black Sea was already connected to the Mediterranean Sea at this time and this fauna assemblage alone cannot be used to show that the Black Sea was fresh as it is shown that *Dreissena polymorpha* that date to a range of 8.20-8.80 ^{14}C ages has a $^{87}Sr/^{86}Sr$ composition with a marine signal. The deposit observed below, described by Görür et al., (2001) was likely formed prior to the connection of the Black Sea-Lake with the Mediterranean due to the identification of peat, a deposit that forms only above water with a ^{14}C date of 8.090±0.12 kyr ^{14}C. A specimen also found in this environment, identified as *Dreissena polymorpha*, was dated to 9.277±0.157 kyr ^{14}C and very

different $^{87}Sr/^{86}Sr$, $\delta^{18}O$, and $\delta^{13}C$ composition, interpreted here to have inhabited an environment of Sakaraya river water and not submerged by the Black Sea-Lake water.

Hiscott et al., (2002) observed a delta formed at the southern end of the Bosporus Sill. Its formation was originally ascribed to the Younger Dryas and formed as a consequence of outflow from the Black Sea into the Sea of Marmara, obliterating any arguments that asserted that the Black Sea was largely regressed prior to its connection with the Mediterranean. This interpretation, however, was not substantiated by any sampling. Eris et al., (2007) showed that the delta was formed later than asserted by Hiscott et al., (2002). Gökasan et al., (2005) showed that the delta instead, was fed by a river and was not connected to any outflow from the Bosporus into the Sea of Marmara. Hence, the evidence provided in Hiscott et al., (2002) cannot be used to support that the level of the Black Sea-Lake was above the Bosporus sill prior to the its connection with the Mediterranean Sea at 9.30 kyr BP.

4.4 The transgression was caused by the Mediterranean water breaching the Bosporus sill

The $^{87}Sr/^{86}Sr$ composition of every specimen in the coquina with ^{14}C dates 8.80 kyr ^{14}C and younger reflects the contribution of marine $^{87}Sr/^{86}Sr$. The *Dreissena rostriformis* all consistently have a $^{87}Sr/^{86}Sr$ composition of ~0.70895. Taking the pre-transgression $^{87}Sr/^{86}Sr$ composition of the water as 0.70890, this composition is equivalent to a 1% marine water that has mixed in with the fresh lake water. This indicates that the water that the *Dreissena rostriformis* colonized had, although small but highly distinguishable, fraction of marine water mixed in and refutes the possibility that the transgression was fresh, as argued by the first three schools listed in the introduction. It is clear that the increase in $^{87}Sr/^{86}Sr$ is related to a marine contribution and not a change in source of $^{87}Sr/^{86}Sr$ as the Sr concentration of carbonate also

increases significantly during this period (Bahr et al., 2008). During the colonization of the water by transitional mollusks (i.e., *Dreissena polymorpha* and *Monodacna caspia*), the marine water makes up of 2.5 % total surface Black Sea water. During the final stage of salinization, the $^{87}Sr/^{86}Sr$ composition of marine mollusks (i.e., *Cardium edule*), the marine water makes up 20% of total. The modern $^{87}Sr/^{86}Sr$ of Black Sea water is 0.709133 (Major et al., 2006). This is slightly lower than the modern $^{87}Sr/^{86}Sr$ composition of the global ocean, 0.709157, and gives a mixture of 75% freshwater and 25% marine.

The 2.0 to 3.0 ‰ change in the $\delta^{18}O$ composition of the carbonate also likely reflects the entry of water from the Mediterranean and mixing in with that of the Black Sea-Lake. Surface Mediterranean water during the Preboreal period in the Black Sea period was ~2 ‰ (Paul et al., 2001). The slight trend from lower to higher $\delta^{18}O$ with decreasing depth is consistent with this observation (**Figure 3-24**). This trend also shows, as does the $^{87}Sr/^{86}Sr$ and ^{14}C composition, that the three distinct mollusk populations are sampling different water and recording the progression of the salinification. Those mollusks from cores from shallower depth (<45 mbsl) have a lighter $\delta^{18}O$ composition, reflecting the greater influence of rivers. The $\delta^{13}C$ composition of *Dreissena rostriformis* and *Dreissena polymorpha* also increase during the transition period by 1.0 ‰. This rise can similarly be attributed to the mixing in of Mediterranean water, which had a $\delta^{13}C$ composition of ~2.0 ‰ during this period (Emeis et al., 2000).

4.5 Transgression was fast

The rapidity of the transgression is estimated from (1) the alignment of the stable carbonate composition in the ^{14}C dated mollusk record and the U/Th dated Sofular Cave to deduce a calendar age for its onset and progression, (2) the change in $^{87}Sr/^{86}Sr$ as a function of

corrected calendar age, and (3) observations from the chirp on the Ukrainian, Bulgarian, Romanian, and Turkish shelves. These observations are supported by hydraulic calculations. Aligning the change in the $\delta^{13}C$ and $\delta^{18}O$ composition in the mollusks with the change in the $\delta^{13}C$ and $\delta^{18}O$ of the precipitated carbonate of the Sofular Cave during the transition period of the Black Sea surface water allows to calculate that the ^{14}C reservoir of the surface water dropped significantly. Prior to the transgression, at 9.30 kyr BP, the ^{14}C reservoir age is estimated to be as large as 1,100 ^{14}C years.

$^{87}Sr/^{86}Sr$ measurements can be used to examine the changes in the sources of water that make up the water composition in any particular basin. $^{87}Sr/^{86}Sr$ of mollusks is employed here to constrain the volume and the flux of Mediterranean water into the Black Sea-Lake. The $^{87}Sr/^{86}Sr$ contribution of marine water to Black Sea-Lake water in the $^{87}Sr/^{86}Sr$ composition of mollusks shells is observed in every mollusk in the coquina across the depth range of 125 to 17.7 mbsl on the shelf. Those mollusks from coquina at depths below 125 mbsl were not analyzed for $^{87}Sr/^{86}Sr$ and hence, the absence of this information cannot be used to affirm or refute whether the marine $^{87}Sr/^{86}Sr$ contributed to their $^{87}Sr/^{86}Sr$ shell composition or not.

A transgression from 165 to 20 mbsl involves an addition of approximately 40,000 to 60,000 km^3 of water and would make up 10 % of the Black Sea-Lake water. If this amount of water came in and mixed in instantaneously with Black Sea-Lake water, the $^{87}Sr/^{86}Sr$ composition of the mollusks that initially colonized the coquina would be ~0.70905. This, however, is not observed. Instead, the $^{87}Sr/^{86}Sr$ composition measured is 0.70895 and reflects a contribution of only 1 % marine water. This observation suggests that the Mediterranean water much more likely first entered into the interior of the lake, similar to what occurs today. This phenomenon would be even more efficient and pronounced at the time of the transgression due

to the larger density contrast between the originally fresh lake water and the incoming Mediterranean water.

Similarly, the Mediterranean water would bring in ^{14}C-equilibrated water into the interior first. The Black Sea-Lake water on the shelf would remain old with the large ^{14}C reservoir age until the ^{14}C-equilibrated water would have mixed from below. Hence, the range of ^{14}C dates measured on the mollusks from the coquina cannot be exclusively used to derive its actual duration as was employed by Nicholas et al., (2011) and Nicholas and Chivas, (2014). The authors suggested an age of 400 years for the transgression to take place from the difference between ^{14}C dates of peat and uncorrected ^{14}C measurements of fauna as a function of depth on the shelf. The range of ^{14}C dates is rather a reflection of the evolution of the ^{14}C reservoir as more and more ^{14}C equilibrated marine water mixes into the surface from the interior.

Observation of the chirp profiles from the Black Sea shelf also suggests that the event was a faster one rather than a slower one and took only a few years. There is no observation of any coastal onlap in any of the chirp profiles. If the transgression were slow, a ravinement surface would be formed due to the heavy reworking of material by wave-action as the lake level rose. The preservation of shelf-edge river channels and sand dunes, however, does not indicate that these surfaces were subject to reworking that would otherwise appear from the destructive processes of the surf zone, as first pointed out by Ryan et al., (1997) and reaffirmed by Lericolais et al., (2007). Instead, the Holocene drape covers the surface beneath it uniformly and without any indication of reworking of material.

Hydraulic estimations also give a lower estimation for the rapidity of the transgression. Siddall et al., (2004) estimated the NW Shelf, comprising 94% of the total shelf area of the Black Sea, to have a water volume of ~62,000 km^3. Given this estimate and the modern inflow of

water from the Sea of Marmara through the Bosporus sill, ~315 km^3/year (Öszoy et al., 1986; Öszoy et al., 1988; Latif et al., 1991), the change in volume would take 200 years. This is a maximum estimate. Additional calculations suggest a faster period for the transgression. Siddall et al., (2004) use a mathematical model to show that the infill would take 34 years. Myers et al., (2003) estimate the infill would take approximately 8 years using estimations of the maximum amount of water flux through the Bosporus sill, 15 km^3/day (~5,475 km^3/year) for a volume change of 43,146 km^3. The flux through the Bosporus at the time of the transgression is much more likely to have been rapid rather than gradual as erosion, similar to phenomena observed during dam breakage, would increase the depth and width of the sill allowing more and more water to enter from the Mediterranean.

4.5 Rapidity of Salinification

At 8.40 kyr BP (7.60 kyr ^{14}C), the Black Sea crossed a threshold level of increased salinity such that lacustrine mollusks of Caspian affinity could no longer survive in the basin's waters. By the end of this initial salinification, the ^{14}C reservoir age dropped to 350 ^{14}C years. The substantial increase in surface water salinity is interpreted from absence of *Dreissena rostriformis* and *Dreissena polymorpha* specimens in AK93-05, 37-82, 37-82A cored from 44, 17.7 and 19.6 mbsl, respectively. A core at 47 m, AK93-04, has a *Dreissena polymorpha* specimen but no *Dreissena rostriformis*, also suggesting that at that location, the lake became salty enough that *Dreissena rostriformis* could no longer tolerate such an environment. The oldest specimen at 49 mbsl gives an age of 8.33 ± 0.70 kyr ^{14}C, at 47 mbsl gives an age of 7.930 ± 0.35 kyr ^{14}C, at 44 mbsl gives an age of 6.960 ±0.139 kyr ^{14}C, and at 27 mbsl gives an age of 7.610 kyr ^{14}C. The specimen retrieved from a core at 44 mbsl calibrates to a calendar age of 8.27

kyr BP and the specimen retrieved from a core at 17.7 calibrates to a calendar age of 8.03 kyr BP. Some fresher fauna do persist near rivers during the initial salinification as indicated by two *Dreissena rostriformis* specimens at 38 mbsl dated to 8.66-8.86 kyr ^{14}C from the subsurface of the Danube delta by Giosan et al., (2009).

A coquina of approximately 10 cm thickness and the successive Bugaz layer with its mixture of lacustrine, transitional and fully marine specimens, sits upon the α erosion surface everywhere on the shelf. The lacustrine fauna are those that are living in water with a small amount of marine water that has mixed in from the interior and can tolerate this initial but minor increase in surface salinity. These two deposition units occur from the outer to the inner shelf (**Figure 3-28**). In the vicinity of the paleoshoreline, the bottom-most composition of the coquina includes very old material from the substrate below, reworked from coastal dunes, also mud free. The top section of the coquina also has a large composition of old sediments (shells dating to the glacial period and ^{14}C dead), polished and bleached material but has higher mud content. Occasional pieces of wood of Younger Dryas age are also found (i.e., 10.40 kyr ^{14}C date from AKAD11-19).

All of the ^{14}C dates from *Dreissena rostriformis* have ages that range from 8.80 to 8.20 ^{14}C kyr BP, independent of depth from 165 to 38 mbsl, the shallower constraint taken from observation of *Dreissena rostriformis* with these ages from the subsurface water of the Danube delta (Giosan et al., 2009). The pulverized shell detritus in the coquina gives an age of 16.809 ± 0.319 kyr ^{14}C. If one takes the younger end-member as 8.60 kyr ^{14}C, a value representative of Black Sea water ^{14}C age immediately prior to inflow of Mediterranean, and the older member as 25 kyr ^{14}C, a value representative of the glacial period, the old-member makes up about 75% of the material in the coquina. The coquina that sits upon the hardground on the inner shelf does

not have reworked mollusks from the substrate below as that substrate is shell free. The coquina from cores retrieved seaward of the paleoshoreline has reworked mollusks from the sediments belonging to Younger Dryas and glacial period.

The coquina is interpreted as a colonization deposit on the newly submerged shelf. The sequence of post-connection lacustrine, transitional, and marine mollusks in the coquina is interpreted to be a consequence of their progressive appearance and disappearance during rising salinity. *Dreissena rostriformis*, fauna identified as traditionally inhabiting strictly freshwater environments, persisted from the prior lake environment to the new marine environment until its salinity tolerance was exceeded. On the other hand, the marine fauna such as *Cardium edule*, *Mytilus galloprovincialis*, and *Mytilaster lineatus* colonized water only after a threshold was reached. *Monodacna caspia* and *Dreissena polymorpha* lived in the interim period.

The presence of shells of *Monodacna caspia* and *Dreissena polymorpha* in the Bugaz layer is ascribed to bioturbation, a process that typically churns the upper ~10cm of the seabed. The Bugaz layer is rich in fragments of bleached shell debris. *Monodacna caspia* and *Dreissena polymorpha* are never found in an articulated condition. These species are present only as single valves and fragments.

Marine bivalves such as *Cardium edule* dig into the sediment and live beneath the sea-floor. Hence, these clams are occasionally found in the coquina deposit side-by-side with *Dreissena sp.* and *Monodacna caspia*, even though all three species lived at different times and in tolerance to different salinities as indicated by their diverse ^{14}C ages from the same sample. When found within the coquina, the specimens of *Cardium edule* are everywhere articulated.

Following the submergence of the shelf up to the 25 mbsl isobath, lacustrine fauna, able to tolerate the minor increased salinity of the lake surface, were the first to colonize the seabed.

Brackish species began to colonize the seabed after the lacustrine fauna could no longer adapt to the increasing surface water salinity. Once the salinity became so high as to exclude them, marine fauna took over (**Figure 3-18 and 3-21**). With the adjustment for evolving ^{14}C reservoir ages, this succession of lacustrine to marine spanned 1,500 calendar years. There may even have been an interval of several centuries between the last surviving brackish species (7.60 kyr ^{14}C) and the introduction of the first marine species (7.25 kyr ^{14}C).

It is most likely that the water that entered the Black Sea from the Mediterranean descended to the bottom as a consequence of their density differences between lake and seawater. The continuity of inflow of Mediterranean water gradually replaced the freshwater above, expelling it out of the basin. The salinity of the surface water increased as the interface between marine and fresh water rose and the mixing occurred between the two layers. The spread of ^{14}C ages and different isotope geochemistry (i.e., $^{87}Sr/^{86}Sr$, $\delta^{18}O$, $\delta^{13}C$) of the mollusks that recorded the transition illustrates this evolution of water.

The first deposit above the former terrestrial surface on the innermost shelf (i.e. < 20 mbsl) belongs to the Bugaz stage and immediately follows the period of the rapid salinification. From this time onward, sea level in the Black Sea rose in tandem with global (eustatic) sealevel. The landward limit of the coquina between 20 to 30 mbsl (Kuprin et al., 1974; Scherbakov and Babak, 1979) is in agreement with a proposed sill depth in the Bosporus Strait of ~35 mbsl at the time of the first entry of Mediterranean water (Major et al., 2002; Nicholas and Chivas, 2014).

Marine mollusks from cores at depths <25 mbsl (i.e., 37-82, 37-82A) have ^{14}C ages that indicate subsequent submergence after completion of the initial flooding. The apparent younger ^{14}C age of these mollusks is attributed to their proximity to river inflow and incorporation of water that reflects the ^{14}C age of the atmosphere, whereas the older apparent ^{14}C age of the

mollusks located farther from rivers and sources of ^{14}C equilibrated water is attributed to a greater influence of old ^{14}C water that characterized Black Sea surface water at that time (**Figure 3-25** and **Figure 3-27**).

The salinification of the Black Sea-Lake has been previously interpreted to last between 5 to 7 kyr BP, beginning with the initial connection of the lake with the Mediterranean and ending with the first permanent appearance of coccolithophore *E. huxleyi* (Bukry, 1974; Ross and Degens, 1974; Soulet et al., 2010). Yanko-Hombach et al., (2014) shorten this period to 3.60 kyr BP based on changes in isotopes and dinocyst data from core MAR02-45 at -69 m. However, the length of time assigned by Yanko-Hombach et al., (2014) does not take into account changes in the ^{14}C reservoir age of Black Sea water. Hence their duration is over-estimated.

By observing the rate of succession of mollusks in the coquina deposit using the evolving history of decreasing reservoir ages, the interval shortens to 1,500 years. This briefer span is consistent with the abrupt shift (and lack of overlap) in the dinoflagellate assemblage from fresh to marine in deep-water cores across the Unit 3/2 boundary of Ross and Degens, (1974), as first observed by Wall and Dale, (1974), and then by subsequent researchers. Also, the duration of 1,500 years is consistent with the estimate by Nicholas et al., (2011) of 1,000 years or more from the initial transgressive event, based on the difference between the ^{14}C ages between the oldest freshwater and the first marine mollusks to appear on the trangressive surface. A rapid salinification likewise fits the observations of (Giunta et al., 2007) that the early, although not pronounced appearance of *E. huxleyi* and *B. bigelowii*, in the base of Unit 2 sapropel indicates that the surface Black Sea water had already reached 17 psu (very close to its present value) by ~7 kyr ^{14}C.

The 1,500 year period for the salinification of the surface water of the Black Sea is supported by calculations of Myers et al., (2003) using a Bosporus channel width of 1,000 m. This channel width is supported by the observation of an erosion surface of the Bosporus strait interpreted to be formed by the inflow of water from the Mediterranean into the Black Sea (Gökasan et al., 2005).

5. Conclusions

The data and evidence in the form of stable isotopes, radiocarbon, $^{87}Sr/^{86}Sr$ measurements and chirp profiles from shelf cores on the Ukrainian, Romanian, Bulgarian, and Turkish margins presented in this manuscript allow the careful consideration of four competing schools of thought regarding the reconnection of the Black Sea to the Mediterranean and thus the global ocean following the last ice age. Three of these schools of thought are refuted as inconsistent with the observations taken as a whole. The evidence validates the fourth school indicating that a pronounced transgression and subsequent salinification at 9.30 kyr BP was a consequence of the inflow of Mediterranean water.

The data presented also allow the reconstruction of a detailed sequence of events related to the transgression: (1) The presence of an erosion surface up to a depth exceeding 165 mbsl dated to the Preboreal and absence of sediment up to a depth range between 240 and 378 mbsl indicates a serious regression immediately preceding the inflow of Mediterranean water into the Black Sea. (2) The alignment of $\delta^{18}O$ and $\delta^{13}C$ compositions of thoroughly U/Th-dated carbonate precipitated in stalactites from Sofular Cave and Black Sea mollusks shows that the Mediterranean water entered and transgressed the Black Sea shelf starting at 9.30 kyr BP. This transgression lasted a maximum of 200 years, given modern day rates of river and Mediterranean

inflow into the Black Sea. However, it likely was much faster, given greater flow rates at the time of the breaching, and may have been as brief as 5 to 10 years. The absence of detritus from strata below the α erosion surface in the initial coquina indicates that the transgression was a rapid flooding event and not a gradual ravinement. (3) It is most likely, given large density differences between fresh and marine water, that the dense salty inflowing water initially descended into the deep interior and the surface water then experienced a somewhat delayed evolution from fresh to marine as more and more salty water filled the interior and progressively mixed with the fresher water above.

The subsequent salinifcation took 1,500 years. This event is illustrated by a sequence of mollusks that tolerate progressively higher salinity water, leaving a record of the sequence of their respective appearance and disappearance everywhere on the shelf coquina extending from >165 to 25 mbsl. The transgression brought the level of the sea to ~25 mbsl. The sea level rise that followed occurred in tandem with global sea level since the initial transgression until the modern day.

References

Aksu, A. E., R. N. Hiscott, M. A. Kaminski, P. J. Mudie, H. Gillespie, T. Abrajano and D. Yasar, 2002a. Last glacial-Holocene paleoceanography of the Black Sea and Marmara Sea: stable isotopic, foraminiferal and coccolith evidence. Marine Geology 190, 119-149.

Aksu, A. E., R. N. Hiscott, P. J. Mudie, A. Rochon, M. A. Kaminski, T. Abrajano and D. Yasar, 2002b. Persistent Holocene outflow from the Black Sea to the eastern Mediterra- nean contradicts Noah's flood hypothesis. GSA Today 12, 4-10.

Aksu, A. E., R. N. Hiscott, D. Yasar, F. I. Isler and S. Marsh, 2002. Seismic stratigraphy of late Quaternary deposits from the southwestern Black Sea shelf: evidence for non-catastrophic variations in sea-level during the last ~10,000 yr. Marine Geology 190, 61-94.

Algan, O., M. Ergin, S. Keskin, E. Gokasan, B. Alpar, E. Kirci and D. Ongan, 2007. The sea level changes during the late Pleistocene-Holocene on the southern shelves of the Black Sea. In V. Yanko-Hombach, A. S. Gilbert, N. Panin and P. M. Dolukhanov (Eds.), The Black Sea Flood Question: Changes in Coastline, Climate, and Human Settlement. Dordrecht, The Netherlands, Springer.

Apakidze, A. M. and A. A. Burchuladze, 1987. Radiouglerodnoe datirovanie arkheologicheskikh i paleobotanicheskikh abraztzov Gruzii (Radiocarbon dating of archaeological and paleobotanical samples in georgia). Tbilisi, Georgia, Metsniereba.

Arkhangel'skiy, A. D. and N. M. Strakhov, 1938. Geological structure and history of the evolution of the Black Sea. Izv. Akad. Nauk SSSR 10, 3-104.

Atanassova, J., 2005. Palaeoecological setting of the western Black Sea area during the last 15,000 years. The Holocene 15, 576-584.

Badertscher, S., D. Fleitmann, H. Cheng, R. L. Edwards, O. M. Göktürk, A. Zumbühl, M. Leuenberger and O. Tüysüz, 2011. Pleistocene water intrusions from the Mediterranean and Caspian seas into the Black Sea. Nat. Geosci. 4, 236-239.

Bahr, A., H. Arz, F. Lamy and G. Wefer, 2006. Late glacial to Holocene paleoenvironmental evolution of the Black Sea, reconstructed with stable oxygen isotope records obtained on ostracod shells. Earth Planet. Sc. Lett. 241, 863-875.

Bahr, A., F. Lamy, H. W. Arz, C. Major, O. Kwiecien and G. Wefer, 2008. Abrupt changes of temperature and water chemistry in the late Pleistocene and early Holocene Black Sea. Geochem. Geophy. Geosy. 9.

Bailey, T. R., J. M. McArthur, H. Prince and M. F. Thirwall, 2000. Dissolution methods for strontium isotope stratigraphy: Whole rock analysis. Chemical Geology 167, 313-319.

Balbanov, I. P., 2007. Holocene sea-level changes of the Black Sea. In V. Yanko-Hombach, A. S. Gilbert, N. Panin and P. M. Dolukhanov (Eds.), The Black Sea Flood Question: Changes in Coastline, Climate, and Human Settlement. Netherlands, Springer.

Briceag, A., A. G. Yanchilina, W. B. F. Ryan, M. Stoica, G. Oaie and M. C. Melinte-Dobrinescu, in revision. Late Pleistocene - Holocene paleoenvironmental changes inferred by microfaunal and isotope fluctuations in the Romanian Black Sea shelf. Quaternary Research.

Brujevich, S. V., 1952. Buried fresh water beneath the recent sediments in the Black Sea. Dokl. Acad. Nauk SSSR 84, 575-577.

Bukry, D., 1974. Coccoliths as paleosalinity indicators—evidence from the Black Sea. In E. T. Degens and D. A. Ross (Eds.), The Black Sea-Geology, Chemistry and Biology. Tuksa, OK, Am. Assoc. Petrol. Geol., Memoir 20**,** 353-363.

Chepalyga, A. L., 2002. The Black Sea. In A. A. Velichko (Eds.), Dynamics of Terrestrial Landscape Components and Inner Marine Basins of Northern Eurasia during the last 130,000 years. Moscow, GEOS**,** 170-182.

Cohen, D. and W. B. F. Ryan, 2011. Black Sea low stands during the Holocene and Pleistocene and reconnection with the global ocean.

Degens, E. T., P. Stoffers and A. Hallam, 1980 Environmental events recorded in Quaternary sediments of the Black Sea. . In: Black shales. 137 Part 2, 131 138.

Demirbag, E., E. Gökasan, F. Y. Oktay, M. Simsek and H. Yüce, 1999. The last sea level changes in the Black Sea: evidence from the seismic data. Marine Geology 157, 249-265.

Deuser, W. G., 1972. Late-Pleistocene and Holocene history of the Black Sea as indicated by stable isotope studies. Jour. Geophys. Res. 77, 1071-1077.

Di Iorio, D. and H. Yüce, 1998. Observations of Mediterranean flow into the Black Sea. J. Geophys. Res. 104, 3091-3106.

Dimitrov, D., 2010. Geology and non-traditional resources of the Black Sea. Germany, Lambert Academik Publishing AG.

Dimitrov, P., 1982. Radiocarbon datings of bottom sediments from the Bulgarian Black Sea shelf. Bulgarian Academy of Sciences Oceanology 9, 45-53.

Dimitrov, P. and D. Dimitrov, 2004. The Black Sea, the Flood, and the Ancient Myths. Varna, Slavena.

Dimitrov, P. S., 1982. Radiocarbon datings of bottom sediments from the Bulgarian Black Sea Shelf. Bulg. Acad. Sci. Oceanology 9, 45-53.

Emeis, K. C., U. Struck, H. M. Schulz, R. Rosenberg, S. M. Bernasconi, H. Erlenkeuser, T. Sakamoto and F. Martinez-Ruiz, 2000. Temperature and salinity variations of Mediterranean Sea surface waters over the last 16,000 years from records of planktonic stable isotope and alkenone unsaturation ratios. Paleogeography, Palaeoclimatology, Paaeoecology 158, 259-280.

Eris, K. K., W. B. F. Ryan, M. N. Çağatay, U. Sancar and G. Lericolais, 2007. The timing and evolution of the post-glacial transgression across the Sea of Marmara shelf south of Istanbul. Marine Geology 243, 57-76.

Fedorov, P. V., 1963. Statigrapfiya chetvertichnikh otlozhenii Krymskogo-Kavkazkogo poberezhia nekotorye voprosy geologicheskoy istorii Chernogo Morya (Statigraphy of Quaternary sediments on the coast of the Crimea and Caucasus and some problems connected with the geological history of the Black Sea). Truda Geologii 8.

Filipova-Marinova, M., D. Pavlov, M. Coolen and L. Giosan, 2012. First high-resolution marinopalynological stratigraphy of Late Quaternary sediments from the central part of the Bulgarian Black Sea area. Quatern. Int. 293, 170-183.

Fleitmann, D., H. Cheng, S. Badertscher, R. L. Edwards, M. Mudelsee, O. M. Göktürk, A. Fankhauser, R. Pickering, C. C. Raible, A. Matter, J. Kramers and O. Tüysüz, 2009. Timing and climatic impact of Greenland interstadials recorded in stalagmites from northern Turkey. Geophysical Research Letters 36.

Flood, R. D., R. N. Hiscott and A. E. Aksu, 2009. Morphology and evolution of an anastomosed channel network where saline underflow enters the Black Sea. Sedimentology 56, 807-839.

Genov, I., K. Slavova and P. Dimitrov, 2004a. Geological events as result from the climatic changes in the Black Sea Region during the period 20000–7000 calendar years BP. In Proceedings of the International. Symposium of Earth System Science, Istanbul, Turkey, Kelebek and Grafika Grup, Istanbul.

Genov, I. D., 2004b. Way and time of swell formation near the Bulgarian Black Sea shelf. CR. Acad. Bulg. Sci. 57, 95-98.

Giosan, L., F. Filip and S. Constatinescu, 2009. Was the Black Sea catastrophically flooded in the early Holocene? . Quaternary Science Reviews 28, 1-6.

Giunta, S., C. Morigi, A. Negri, F. Guichard and G. Lericolais, 2007. Holocene biostratigraphy and paleoenvironmental changes in the Black Sea based on calcareous nannoplankton. Mar. Micropaleontol. 63, 91-110.

Glebov, A. Y. and S. K. Shel'ting, 2007. Sea-level changes and coastline migrations in the Russian sector of the Black Sea. In V. Yanko-Hombach, A. S. Gilbert, N. Panin and P. M. Dolukhanov (Eds.), The Black Sea Flood Question: Changes in Coastline, Climate, and Human Settlement. Netherlands, Springer**,** 731-773.

Gökasan, E., O. Algan, H. Tur, E. Meriç, A. Türker and M. Simsek 2005. Delta formation at the southern entrance of Istanbul Strait (Marmara sea, Turkey): a new interpretation based on high-resolution seismic stratigraphy. Geo-Mar. Lett. 25, 370-377.

Görür, N., M. N. Çagatay, O. Emre, B. Alpar, M. Sakinç, Y. Islamoglu, O. Algan, M. Erkal, R. Akkok and G. Karlik, 2001. Is the abrupt drowning of the Black Sea shelf at 7150 yr BP a myth? Marine Geology 176, 65-73.

Hiscott, R. N., A. E. Aksu, R. G. Flood, V. Kostylev and D. Yaşar, 2013. Widespread overspill from a saline density-current and its interaction with topography on the southwest Black Sea shelf. Sedimentology 60, 1639-1667.

Hiscott, R. N., A. E. Aksu, P. J. Mudie, T. A. Abrajano, P. J. Kaminski, J. Evans, A. İ. Çakiroğlu and D. Yaşar, 2010. Corrigendum to "A gradual drowning of the southwestern Black Sea shelf: Evidence for a progressive rather than abrupt Holocene reconnection with the eastern Mediterranean Sea through the Marmara Sea Gateway". Quaternary International 226.

Hiscott, R. N., A. E. Aksu, P. J. Mudie, P. J. Kaminski, T. A. Abrajano, D. Yaşar and A. ROchon, 2007b. The Marmara Sea Gateway since ~16 ky BP: Non-catastrophic causes of paleoceanographic events in the Black Sea at 8.4 and 7.15 ky BP. In V. Yanko-Hombach, A. S. Gilbert, N. Panin and P. M. Dolukhanov (Eds.), The Black Sea Flood Question: Changes in Coastline, Climate, and Human Settlement. Netherlands, Springer.

Hiscott, R. N., A. E. Aksu, P. J. Mudie, F. Marret, T. Abrajano, M. A. Kaminski, J. Evans, A. I. Çakiroğlu and D. Yaşar, 2007a. A gradual drowning of the southwestern Black Sea shelf: Evidence for a progressive rather than abrupt Holocene reconnection with the eastern Mediterranean Sea through the Marmara Sea Gateway. Quatern. Int. 167-168, 19-34.

Hiscott, R. N., A. E. Aksu, D. Yasar, M. A. Kaminski, P. J. Mudie, V. Kostylev, J. C. MacDonald and A. R. Lord, 2002. Deltas south of the Bosporus record persistent Black Sea outflow to the Marmara Sea since ~10 ka. Marine Geology 190, 95-118.

Ivanova, E. V., I. O. Murdmaa, A. L. Chepalyga, T. M. Cronin, I. V. Pasechnik, O. V. Levchenko, H. S.S, A. V. Manushkina and E.A.Platonova, 2007. Holocene sea-level oscillations and environmental changes on the Eastern Black Sea shelf. Palaeogeogr. Palaeoclimatol. Palaeoecol. 246, 228-259.

Jones, G. A. and A. R. Gagnon, 1994. Radiocarbon chronology of Black Sea sediments. Deep Sea Research 41, 531-557.

Kaplin, P. A. and A. O. Selivanov, 2004. Late glacial and Holocene sea level changes in semi-enclosed seas of North Eurasia: Examples from the contrasting Black and White seas. Palaeogeogr. Palaeoclimatol. Palaeoecol. 209, 19-36.

Kaplin, P. A. and F. A. Shcherbakov, 1986. Reconstructions of paleogeographic environments on the shelf during the late Quaternary time. Oceanology 26, 736-738.

Konikov, E., O. Likhodedova and G. Pedan, 2007. Paleogeographic reconstructions of sea-level change and coastline migration on the northwestern Black Sea shelf over the past 18kyr. Quatern. Int. 167-168, 49-60.

Kouli, K., H. Brinkhuis and B. Dale, 2001. Spiniferites cruciformis: a fresh water dinoflagellate cyst? Rev. Palaeobot. Palyno. 113, 273-286.

Krom, M. D., A. Michard, R. A. Cliff and K. Strohle, 1999. Sources of sediment to the Ionian Sea and western Levantine Basin of the Eastern Mediterranean during S-1 sapropel times. Marine Geology 160, 45-61.

Kuprin, P. N., F. A. Scherbakov and I. I. Morgunov, 1974. Correlation, age and distribution of the postglacial continental terrace sediments of the Black Sea. Baltica 5, 241-249.

Kvasov, D. D., 1968. Paleohydrology of eastern Europe in late Quaternary time. Yezhegodnkkh Chetniyakh Pamyati L.S. Berga Doklady Izd. Nauka, Leningrad, 65-81.

Kwiecien, O., W. A. Helge, L. Frank, P. Birgit, B. André and H. H. Gerald, 2009. North Atlantic control on precipitation pattern in the eastern Mediterranean/Black Sea region during the last glacial. Quaternary Research 71.

Latif, M. A., E. Ozsoy, T. Oguz and Ü. Ünlüata, 1991. Observations of the Mediterranean inflow into the Black Sea. Deep-Sea Research 38, S711-S723.

Lericolais, G., C. Bulois, H. Gillet and F. Guichard, 2009. High frequency sea level fluctuations recorded in the Black Sea since the LGM. Global Planet Change 66, 65-75.

Lericolais, G., I. Popescu and F. Guichard, 2007. A Black Sea lowstand at 8500 yr BP indicated by a relict coastal dune system at a depth of 90 m below sea level. In J. Harff, W. W. Hay and D. M. Tetzlaff (Eds.), Coastline Changes: Interrelation of Climate and Geological Processes., GSA Books; Allen Press, Inc, 426**,** 171-188.

Major, C., S. Goldstein, W. Ryan, G. Lericolais, A. M. Piotrowski and I. Hajdas, 2006. The co-evolution of Black Sea level and composition through the last deglaciation and its paleoclimatic significance. Quatern. Sci. Rev. 25, 2031-2047.

Major, C., W. Ryan, G. Lericolais and I. Hajdas, 2002. Constraints on Black Sea outflow to the Sea of Marmara during the last glacial–interglacial transition. Marine Geology.

Manheim, F. T. and K. M. Chan, 1974. Interstitial waters of Black Sea sediments: New data and review. In E. T. Degens and D. A. Ross (Eds.), The Black Sea - Geology, Chemistry and Biology. Tusla, Mem. Am. Assoc. Petrol. Geol., 20**,** 155-180.

Marret, F., S. LeRoy, F. Chalié and F. Gasse, 2004. Palaeoenvironment and dinoflagellate cyst stratigraphy of the Pliocene in northern Belgium at the southern margin of the North Sea Basin. Geol. Mag. 141, 353-378.

Marret, F., P. Mudie, A. Aksu and R. N. Hiscott, 2009. A Holocene dinocyst record of a two-step transformation of the Neoeuxinian brackish water lake into the Black Sea. Quatern. Int. 197, 72-86.

Mortlock, R., 2010. Description of stable isotope analysis at the Department of Earth and Planetary Sciences. Rutgers University.

Mudie, P., A. Aksu and D. Yaşar, 2001. Late Quaternary dino¸agellate cysts from the Black, Marmara and Aegean seas: variations in assemblages, morphology and paleosalinity. Mar. Micropaleontol. 43, 155-178.

Mudie, P. J., A. Rochon, A. E. Aksu and H. Gillespie, 2004. Late glacial, Holocene and modern dinoflagellate cyst assemblages in the Aegean-Marmara-Black Sea corridor. Rview of Palaeobotany and Palynology 256, 1-26.

Mudie, P. J., V. Yanko-Hombach and S. Kadurin, 2014. The Black Sea dating game and Holocene marine transgression. Open Journal of Marine Science 4, 1-7.

Myers, P. G., C. Wielki, S. B. Goldstein and E. J. Rohling, 2003. Hydraulic calculations of postglacial connections between the Mediterranean and the Black Sea. Mar. Geol. 201, 253-267.

Naudts, L., J. Greinert, Y. Artemov, P. Staelens, J. Poort, P. V. Rensbergen and M. De Batist, 2006. Geological and morphological setting of 2778 methane seeps in the Dnepr paleodelta, northwestern Black Sea. Marine Geology 227, 177-199.

Naukova, D., 1984. Radioulerodnoe datirovanie. In E. F. Shnyukov (Eds.), Geologii Shel'fa USSR, Limany. Kiev.

Nevesskaya, L. A., 1965. Late Quaternary bivalve mollusks of the Black Sea: Their systematics and ecology. Akad. Nauk SSSR Paleont. Inst. Trydy 105, 1-390.

Nicholas, W. A. and A. R. Chivas, 2014. Late Quaternary sea-level change on the Black Sea shelves. In F. L. Chiocci and A. R. Chivas (Eds.), Continental shelves of the world: their evolution during the last glacial-eustatic cycle. London, Geological Society, 41**,** 199-212.

Nicholas, W. A., A. R. Chivas, C. V. Murray-Wallace and D. Fink, 2011. Prompt transgression and gradual salinisation of the Black Sea during the early Holocene constrained by amino acid racemization and radiocarbon dating. Quatern. Sci. Rev. 30, 3769-3790.

Nowaczyk, N. R., H. W. Arz, U. Frank, J. Kind and B. Plessen, 2012. Dynamics of the Laschamp geomagnetic excursion from Black Sea sediments. Earth and Planetary Science Letters 351-352, 54-69.

Öszoy, E., T. Oğuz, M. A. Latif and Ü. Ünlüata, 1986. Oceanography of the Turkish Straits-First Annual Report. Physical Oceanography of the Turkish Straits, İçel 1.

Öszoy, E., T. Oğuz, M. A. Latif, Ü. Ünlüata, H. I. Sur and Ş. Beşiktepe, 1988. Oceanography of the Turkish Straits-SecondAnnual Report. Physical Oceanography of the Turkish Straits Inst. Mar.Sci., METU. Erdemlo, İçel 1.

Palmer, M. R. and J. M. Edmond, 1989. The strontium budget of the modern ocean. Earth and Planetary Science Letters 92, 11-26.

Paul, H. A., S. M. Bernasconi, D. W. Schmid and J. A. McKenzie, 2001. Oxygen isotopic composition of the Mediterranean Sea since the Last Glacial Maximum: constraints from pore water analyses. Environmental Science Letters 192, 1-14.

Pirazzoli, P. A. (1996). Sea-level changes: the last 20,000 years. New York, John Wiley and Sons.

Popescu, I., 2008. Processus sédimentaires récents dans l'éventail profond du Danube (Mer Noire). Geo-Eco-Marina Special Publication No. 2.

Popescu, I., G. Lericolais, N. Panin, Ç. N., A. Normand, C. Dinu, DC and E. Le Drezen, 2004. The Danube Submarine Canyon (Black Sea): morphology and sedimentary processes. Marine Geology 206, 249-265.

Reimer, P. J., E. Bard, A. Bayliss, P. G. Blackwell, C. B. Ramsey, C. E. Buck, H. Cheng, R. L. Edwards, M. Friedrich, P. M. Grootes, T. P. Guilderson, H. Haflidason, I. Hajdas, C. Hatté, T. J. Heaton, D. L. Hoffmann, A. G. Hogg, K. A. Hughen, K. Kaiser, F.;, B. Kromer, S. W. Manning, M. Niu, R. W. Reimer, D. A. Richards, E. M. Scott, J. R. Southon, R. A. Staff, C. S. M. Turney and J. ven der Plicht, 2013. Incal13 and Marine13 radiocarbon age calibration curves 0-50,000 years Cal B.P. Radiocarbon 55, 1869-1887.

Ross, D. and E. Degens, 1974. Recent Sediments of Black Sea: Sediments.

Ross, D. A. and E. T. Degens, 1974. Recent sediments of the Black Sea. In E. T. Degens and D. A. Ross (Eds.), The Black Sea - Geology, Chemistry and Biology. Tulsa, Amer. Assoc. Petrol. Geol. Mem., 20**,** 183-199.

Ross, D. A., E. T. Degens and J. MacIlvaine, 1970. Black Sea: recent sedimentary history. Science 170, 163-165.

Ryan, W. B. F., 2007. Status of the Black Sea flood hypothesis. In V. Yanko-Hombach, A. S. Gilbert, N. Panin and P. M. Dolukhanov (Eds.), The Black Sea Flood Question: Changes

in Coastline, Climate, and Human Settlement. Dordrecht, The Netherlands, Springer**,** 63-88.

Ryan, W. B. F., C. O. Major, G. Lericolais and S. L. Goldstein, 2003. Catastrophic flooding of the Black Sea. Annual Reviews of Earth and Planetary Sciences 31, 525-554.

Ryan, W. B. F., W. C. Pitman, III, C. O. Major, K. Shimkus, V. Moskalenko, G. Jones, P. Dimitrov, N. Gorur, M. Sakinc and H. Yuce, 1997. An abrupt drowning of the Black Sea shelf. Marine Geology 138, 119-126.

Ryan, W. B. F., W. C. Pitman, C. O. Major, K. Shimkus, V. Moscalenko, G. A. Jones, D. Dimitrov, P. Gorür, M. Sakinç and H. Y. Seyir, 1996. An abrupt drowning of the Black Sea shelf at 7.5 kyr BP. Geo-Eco-Marina, Malnas, Romania.

Ryan, W. B. F., D. Vachtman, C. McHugh, M. N. Çagatay and Y. Mart, 2013. A channeled shelf fan initiated by flooding of the Black Sea. In S. Gofredo and Z. Dubinsky (Eds.), The Mediterranean Sea: Its history and present challenges**,** 11-27.

Scherbakov, F. A. and Y. V. Babak, 1979. Stratigraphic subdivision of the Neoeuxinian deposits in the Black Sea. Oceanology 19, 298-300.

Schornikov, E. I., 2011. Ostracods of the Caspian origin in the Azov-Black Sea basin. In M. Gross (Eds.), European Ostracologists Meeting Graz, Universalmuseum, 7**,** 180-184.

Siddall, M., L. J. Pratt, K. R. Helfrich and L. Giosan, 2004. Testing the physical oceanographic implications of the suggested sudden Black Sea infill 8400 years ago. Paleoceanography 19, PA1024-PA1035.

Sorokin, V. M. and P. N. Kuprin, 2007. On the character of Black Sea level rise during the Holocene. Moscow University Geology Bulletin 62.

Soulet, G., G. Delaygue, C. Vallet-Coulomb, M. E. Böttcher, C. Sonzogni, G. Lericolais and E. Bard, 2010. Glacial hydrologic conditions in the Black Sea reconstructed using geochemical pore water profiles. Earth and Planetary Science Letters 296.

Soulet, G., G. Ménot, V. Garreta, F. Rostek, S. Zaragosi, G. Lericolais and E. Bard, 2011a. Black Sea "Lake" reservoir age evolution since the Last Glacial — Hydrologic and climatic implications. Earth Planet. Sc. Lett. 308, 245-258.

Soulet, G., G. Ménot, G. Lericolais and E. Bard, 2011b. A revised calendar age for the last reconnection of the Black Sea to the global ocean. Quaternary Science Reviews 30.

Stein, M., A. Starinsky, A. Katz, S. L. Goldstein, M. Machlus and A. Schramm, 1997. Strontium isotopic, chemical, and sedimentologi- cal evidence for the evolution of Lake Lisan and the Dead Sea. Geochim. Cosmochim. Acta 61, 3975-3992.

Strakhov, N. M., 1971. Chemical evolution of the Black basin the Holocene. Lithology and Mineral Resources 3, 263-274.

Wall, D. and B. Dale, 1974. Dinoflagellates in Late Quaternary Deep-Water Sediments of Black Sea. Tulsa, Amer. Assoc. Petrol. Geol.

Wesselingh, F., 2015. Species Identification.

Yanko-Hombach, V., A. S. Gilbert and P. Dolukhanov, 2007. Controversy over the great flood hypotheses in the Black Sea in light of geological, paleontological, and archaeological evidence. Quatern. Int. 167-168, 91-113.

Yanko-Hombach, V., P. J. Mudie, S. Kadurin and E. Larchenkov, 2014. Holocene marine transgression in the Black Sea: New evidence from the northwestern shelf. Quaternary International 345, 100-118.

Yanko-Hombach, V., E. V. Smintina, S. Kadurin, E. P. Larchenkov, I. V. Motnenko, S. V. Kakaranza and D. V. Kiosak, 2011. Kolebaniya urovnya Chernogo Moria i adaptatsionnaya strategia drevnego cheloveka za posldenie 30 tysiach let (the Black Sea level change and adaptation strategy of ancient humans for the last 30 thousand years). Geologiya i poleznie iskopamye Mirovogo Okeana (Geology and mineral resources of the World Ocean) 2, 61-94.

Figure captions

Figure 3-1: Four proposed lake /sea level curves for the Black Sea-Lake: first school of thought and Kuprin et al., (1974) (green), second school of thought and Hiscott et al., (2007a) (blue); third school of thought and Lericolais et al., (2009) (red); fourth school of thought and Nicholas and Chivas, (2014) (black).

Figure 3-2: (1) Location of the cores discussed in this study (colored circles); (2) Location of the reflection profiles WC-6_13, B008, B2ch049, B2ch007, B2ch013, and B2ch036 discussed in this paper (black dashed contours); (3) Location of the inferred paleshoreline (i.e., thick red circumventing contour at -95 mbsl) around the periphery of the Black Sea; (4) Location of the Dniprovs'ko-Buhs'kyi Liman (thick yellow contour).

Figure 3-3: The WC-6_13_0200-2040 chirp profile across the outer and middle Ukrainian margin with location of cores AK93-06, 01, 02, 03-2, 04 and 05. Insert (A) provides greater detail of the outermost shelf with location of cores AK93-07, 10, 08, 11 and 06. Inserts (B, C and D) show ancient river channels directly overlain by an erosion surface followed by a thin drape of mud, both sampled in cores AK93-01 and 05.

Figure 3-4: Passage in the seaward direction across the outer Ukraine shelf, zoom into WC-6_13_0200-2040 from 120 to 75 mbsl, from a narrow belt of dunes to steep paleo-shoreface to a terrace above truncated seaward-dipping reflectors.

Figure 3-5: The concave-upward strata belonging to the fill in buried channels on the Ukraine shelf, zoom into WC-6_13_200-2040 at 45 mbsl. The fill is truncated by an erosion surface that is itself covered everywhere by a thin uniform drape.

Figure 3-6: The BLASON1-B008 chirp profile from the outer Romanian margin with superimposition of cores BLKS98-09, 08, 07 and 06. The ^{14}C dates of mollusk shells from different levels in the cores are noted. This chirp profile covers 300 to 125 mbsl water depth. The substrate below ages 10,260 and 11,100 ^{14}C years has decreased moisture and increased bulk density.

Figure 3-7: The B2ch049 chirp profile with superimposition of cores AKAD09-19, AKAD01-AB18, AKAD01-AB20, AKAD01-AB17, AKAD09-28. The red contour traces the erosion surface α from the middle shelf to the uppermost slope

Figure 3-8: Location of cores and reflection profiles on the Bulgarian margin. The cores are grouped into five transects.

Figure 3-9: The (a) Cape Emine and (b) Varna transect bathymetry with location of cores and reflection profiles.

Figure 3-10: Reflection profile XXIV belonging to the Cape Emine transect. Here color is used to outline the dune interiors (yellow), the surficial drape (green), foreset clinoforms (blue) of presumed previous interglacial age. Cores are projected a few km at most onto this profile, with

their ^{14}C dates and lithologies, including the coquina. Pebbles are present in sediment of late glacial age.

Figure 3-11: Reflection profile XV belonging to the Varna Transect Core AKAD11-19 sampled shell debris dated as old as 35.7 kyr BP (^{14}C) from the interior of one of the dunes. Wood is present beneath the coquina on this dune.

Figure 3-12: Perspective view of the dune field, shoreface, and offshore ramp on the Emine Transect.

Figure 3-13: Location of chirp profiles (07 = B2ch007, 13 = B2ch013, 36 = B2ch036). The black dots are cores. The boxes 1-2 and 4 are areas of detailed mapping with chirp reported in (Ryan et al., 2013).

Figure 3-14: The B2ch007 chirp profile. The a erosion surface extends right out to the shelf break. It is covered first by highly reflective mounds located the interior of banks, levees and elongate transverse ridges belonging to a branching network of channels carrying saline Mediterranean water from the Bosporus Strait to the heads of submarine canyons. A wavy transparent layer (sampled in core MedEx05-10) forms a younger surficial drape that thins seaward. Two channels (noted by a symbol of concentric circles) are still active with the direction of flow into the page.

Figure 3-15: The B2ch036 chirp profile, further illustrating the shelf-wide a erosion surface that here reaches all the way to the shelf break at 120 mbsl.

Figure 3-16: B2ch013 chirp profile on the outermost Turkish shelf north of the Bosporus Strait. Here core MAR98-04 sampled a mollusk shell dated at 33.5 kyr BP (^{14}C) from a sandy coquina at the level of reflector α.

Figure 3-17: A range chart of specimens in core AK93-01 on the Ukraine shelf at 68 mbsl. L.A. Nevesskaya performed the species identification (personal communication). The ages are un-calibrated AMS ^{14}C measurements on individual shells. New Black Sea in this core ranges from 0 to 75 cm (present to 5.5 kyr BP), Old Black Sea from 75 to 110 cm (5.5 to 6.2 kyr BP), Bugaz from 110 to 135 cm (6.2 to 7.2 kyr BP). Core penetration stopped at the coquina deposit, sampled only in the core catcher as pulverized, bleached fragments of *Dreissena sp*. with rare *Cardium edule* and *Dreissena polymorpha*. The size of the symbols is qualitatively related to the abundance of each respective species the symbol represents.

Figure 3-18: Range of species and specimens in core AKAD11-19 located at 85 mbsl on a dune within the Varna transect on the Bulgarian margin. Articulated specimens are identified by filled in symbols. The two single valves of *Dreissena sp*. below 60 cm are sampled from the interior of a mud crack. The down core sequence of layers begins with 1) New Black Sea (NBS) and followed by 2) Old Black Sea (OBS), 3) Bugaz of mud with and minor sand, 4) upper coquina of sandy mud with mostly fragmented shells and separated valves, 5) lower coquina that is mostly muddy sand with articulated *Dreissena sp*., 6) a black band rich in pieces of wood and plant

remains, and 7) a mud-free sandy gravel (mostly shell debris along with quartz and other minerals) with some lithic pebbles.

Figure 3-19: (a) Split surface of core AKAD11-19 showing the contact between sediments belonging to the Bugaz stage (left) and the underlying coquina (right), (b) washed shells from the Bugaz with a mixture of fresh, brackish, and saltwater species, (c) unwashed shells from the coquina with only fresh and brackish species; the *Dreissena sp*. exist as fully-articulated specimens, single valves fragments and some with a blackened coating, (d) *Dreissena sp*. recovered in mud-crack cut into the black band of mud covering the surface of the underlying dune.

Figure 3-20: The Burgas transect across the paleo-shoreline showing the extent of the former shore zone and probable interior bays. Only core AKAD09-27, using vibra-coring methods, was able to penetrate into a sample strata below the coquina. (a) Shows locations of interior islands, barrier island and beach, and the offshore zone relative to the location of AKAD09-27. (b) Shows the location of AKAD09-27 relative to the depth profile of the Burgas transect.

Figure 3-21: Ranges of species and specimens in core AKAD09-27 located at 92.2 mbsl on a dune on the Bulgarian margin. As AKAD11-19, the down-core sequence of layers begins with 1) NBS and followed by 2) OBS, 3) Bugaz with pebbles, 4) upper coquina of sandy mud with fragmented shells and separated valves, 5) lower coquina that is mostly muddy sand with articulated *Dreissena sp*., and 6) a mud-free sandy gravel.

Figure 3-22: Water content (%), represented by black diamonds, and bulk density (g/cc), represented by red diamonds, in sediments of (a) AQ93-11 at 91 mbsl, (b) AQ93-08 at 99 mbsl, (c) AQ93-24 at 110 mbsl, (d) AQ93-09 at 123 mbsl, (e) AQ93-22 at 129 mbsl, (f) AQ93-14 at 140 mbsl, (g) AQ93-23 at 150 mbsl, (h) AQ93-15 at 165 mbsl. The yellow color represents the marine period of deposition, the green color the Bugaz, the orange color the coquina, the blue color the glacial and deglacial sediments, the purple color specifically those sediments belonging to the meltwater event, and the gray and dark blue to stiff clay, possibly identified as deltaic.

Figure 3-23: (a) $^{87}Sr/^{86}Sr$ and $\delta^{18}O$ profiles from the Bugaz, coquina, and dune (or barrier island) interior sampled by AKAD09-27; (b) $^{87}Sr/^{86}Sr$ and $\delta^{18}O$ profiles from the Bugaz, muddy coquina, and mud-free coquina of AKAD11-19.

Figure 3-24: (a) $^{87}Sr/^{86}Sr$ composition of the mollusks in the coquina deposit as a function of shelf depth; (b) ^{14}C age of the mollusks in the shell hash as a function of shelf depth; (c) $\delta^{13}C$ composition of the mollusks in the coquina deposit as a function of shelf depth; (d) $\delta^{18}O$ composition of the mollusks in the coquina deposit as a function of shelf depth. Depths at the core sites are meters below today's sea level.

Figure 3-25: From top to bottom: (a) Calculated ^{14}C reservoir change from 40,000 to present derived from calibrating measured ^{14}C ages to isotope signatures using stalagmites in from the Sofular Cave; (b) Change in $\delta^{18}O$; (c) Change in $\delta^{13}C$; (d) Change in $^{87}Sr/^{86}Sr$. The transition from fresh to saltwater following the connection of the Mediterranean with the Black Sea-Lake occurs during the time interval expressed by the green band marked with a "T". Note an absence

of samples from the Preboreal stage of the Holocene Epoch (pink band marked with "PB") for samples from cores landward of the shelf break.

Figure 3-26: Dniprovs'ko-Bush'kyi Liman adopted from Naukova, (1984). Rf: translated as watered down; Q^4_{III} ant, pt: Fluvial during regression and dated between 15 and 22.5 kyr; pr-st: Alluvial, flood and streambed deposits and dated between 12 and 14.5 kyr; nev: Neoeuxine, clay with *Monodacna caspia* and *Dreissena sp.* Dated between 9.5 and 12 kyr; Q^1_{IV}: unconformity and Bugaz dated between 9.5 and 7.5 kyr; Q^2_{IV}: Old Black Sea dated between 7.5 and 2.5 kyr; Q^3_{IV}: New Black Sea dated between 2.5 and 0 kyr.

Figure 3-27: Presents (1) the water depth at which mollusks lived with a corresponding calendar age and (2) the water depth at which peat formed with a corresponding calendar age. The presentation of the mollusks is broken up by the type of mollusk: marine (i.e., *Cardium edule*, *Mytilus galloprovincialis*, *Mytilaster lineatus*), transitional (i.e., *Dreissena polymorpha*, *Monodacna caspia*), lacustrine (i.e., *Dreissena rostriformis*), perched lake (mollusks that are found at anomalously at shallow depths and have outlier isotopic signatures), and river (those mollusks that colonized a fluvial environment). The figure also illustrates location and dates of wood and distinguishes between those mollusks that are heavily reworked and polished and those that are not. The yellow contour presents a proposed water level in the Black Sea basin from the last glacial period to the present.

Figure 3-28: The varying character and statigraphic location of the erosion surface, coquina and Bugaz deposits as a function of cores retrieved landward, in the vicinity of, and seaward of the

~95 mbsl paleoshoreline. The upper two units are New Black Sea (yellow) and Old Black Sea (orange). The transition deposits lie below these units: Bugaz (pink), muddy coquina unit (green), and the clean coquina unit (blue-green). Below the transition deposits in the vicinity of the paleoshoreline are features of coastal dunes. Below the transition deposit landward of the paleoshoreline are aeolian dunes, paleo-river beds, and truncated non-reverberant reflectors. Below the transition deposit seaward of the paleoshoreline are Younger Dryas (blue) and Glacial to Post glacial (dark blue) deposits, each separated by an unconformity (curved contour). The different deposition environments are separated to inner, middle, and outer shelf.

Figure 3-1

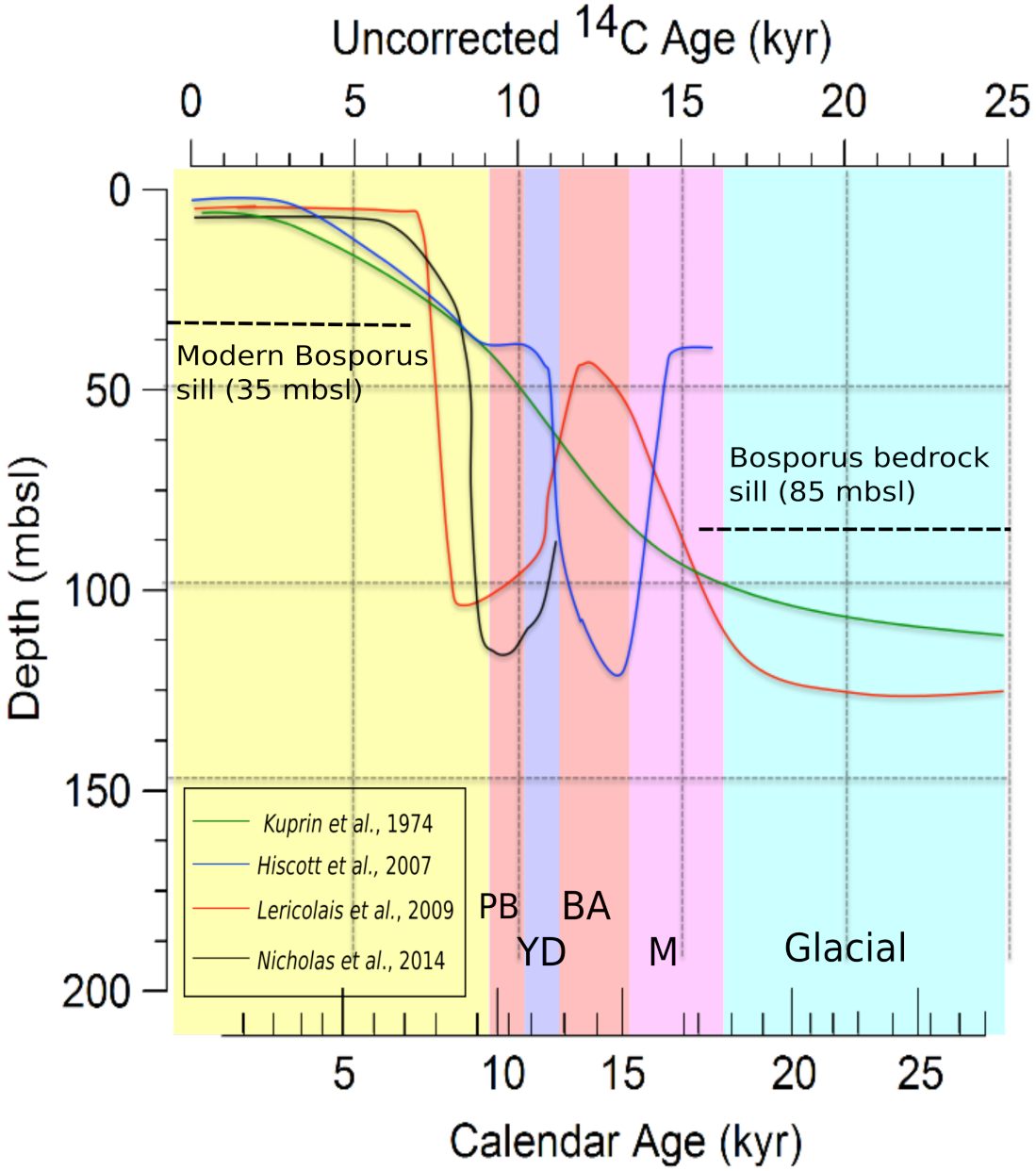
Uncorrected 14C Age (kyr)
0
5
10
15
20
25
Depth (mbsl)
0
50
100
150
200
Modern Bosporus sill (35 mbsl)
Bosporus bedrock sill (85 mbsl)
Kuprin et al., 1974
Hiscott et al., 2007
Lericolais et al., 2009
Nicholas et al., 2014
PB
BA
YD
M
Glacial
5
10
15
20
25
Calendar Age (kyr)

Figure 3-2

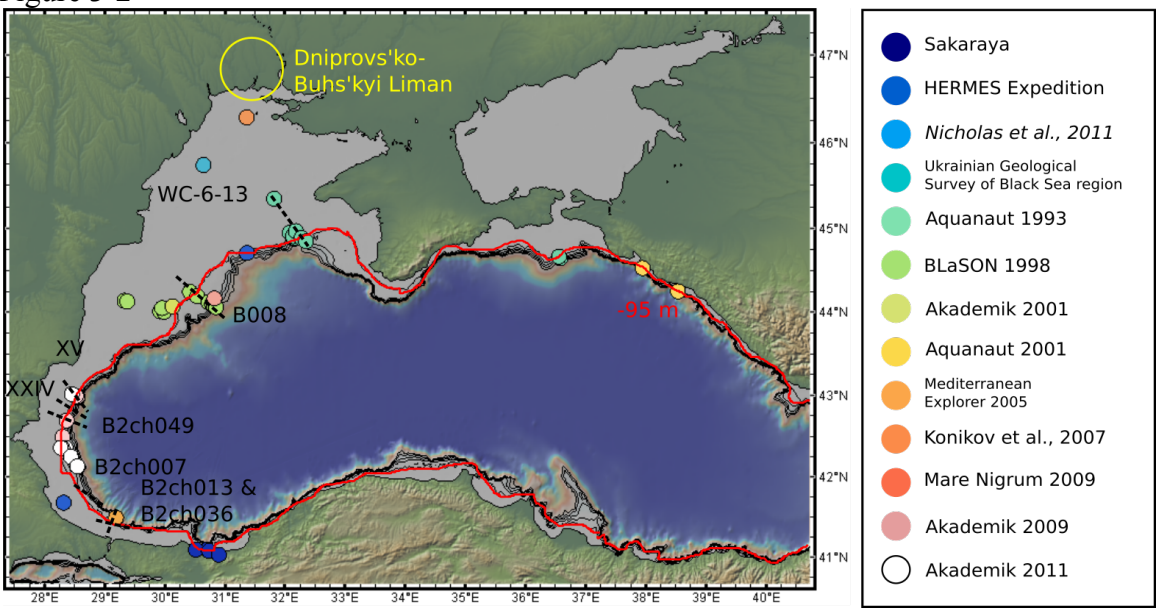
Dniprovs'ko-
Buhs'kyi Liman
WC-6-13
B008
-95 m
XV
XXIV
B2ch049
B2ch007
B2ch013 &
B2ch036
47°N
46°N
45°N
44°N
43°N
42°N
41°N
28°E
29°E
30°E
31°E
32°E
33°E
34°E
35°E
36°E
37°E
38°E
39°E
40°E
Sakaraya
HERMES Expedition
Nicholas et al., 2011
Ukrainian Geological Survey of Black Sea region
Aquanaut 1993
BLaSON 1998
Akademik 2001
Aquanaut 2001
Mediterranean Explorer 2005
Konikov et al., 2007
Mare Nigrum 2009
Akademik 2009
Akademik 2011

Figure 3-3

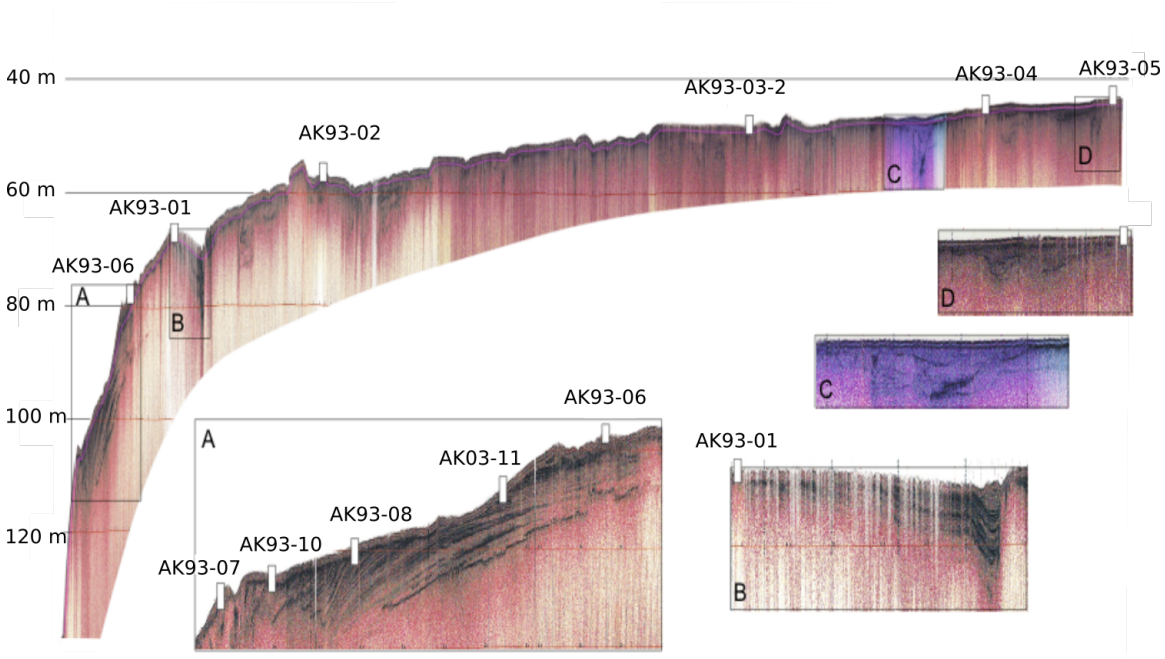
40 m
60 m
80 m
100 m
120 m
AK93-06
AK93-01
AK93-02
AK93-03-2
AK93-04
AK93-05
A
B
C
D
AK93-06
AK03-11
AK93-08
AK93-10
AK93-07
AK93-01

Figure 3-4

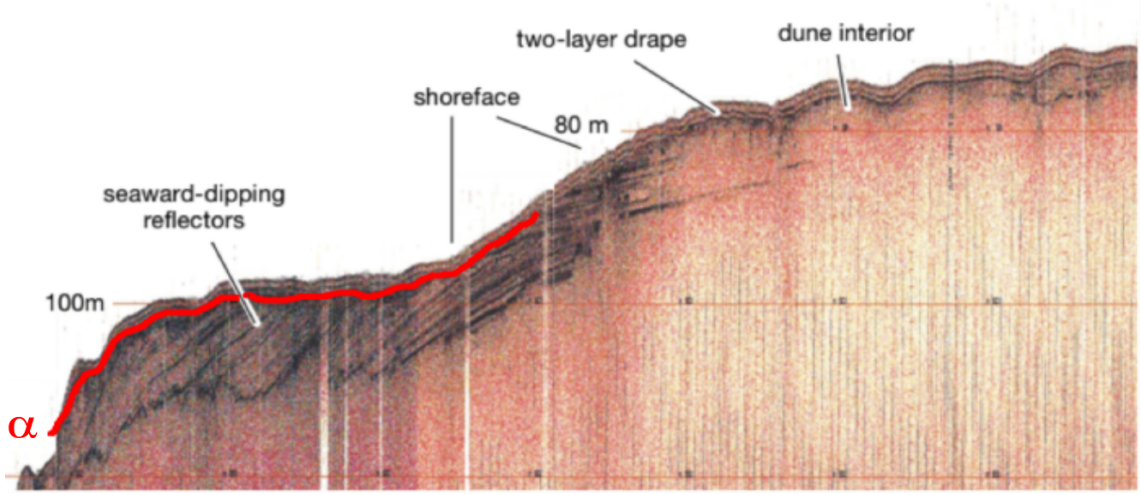
two-layer drape
dune interior
shoreface
80 m
seaward-dipping
reflectors
100m
α

Figure 3-5

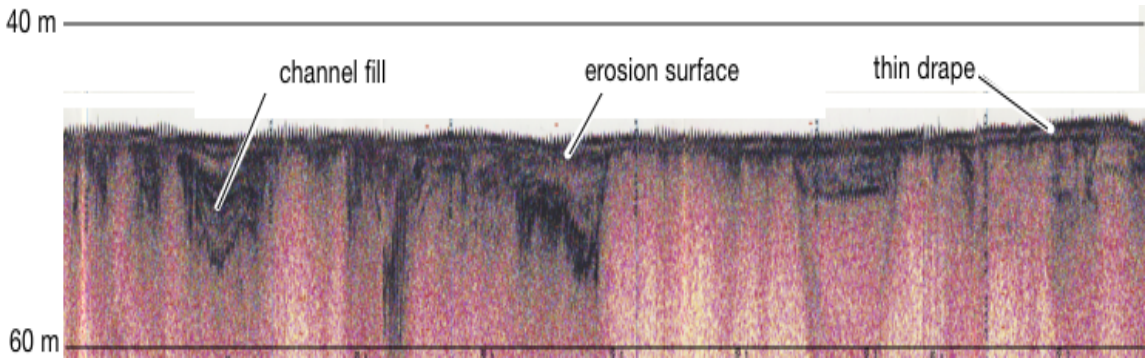

Figure 3-6

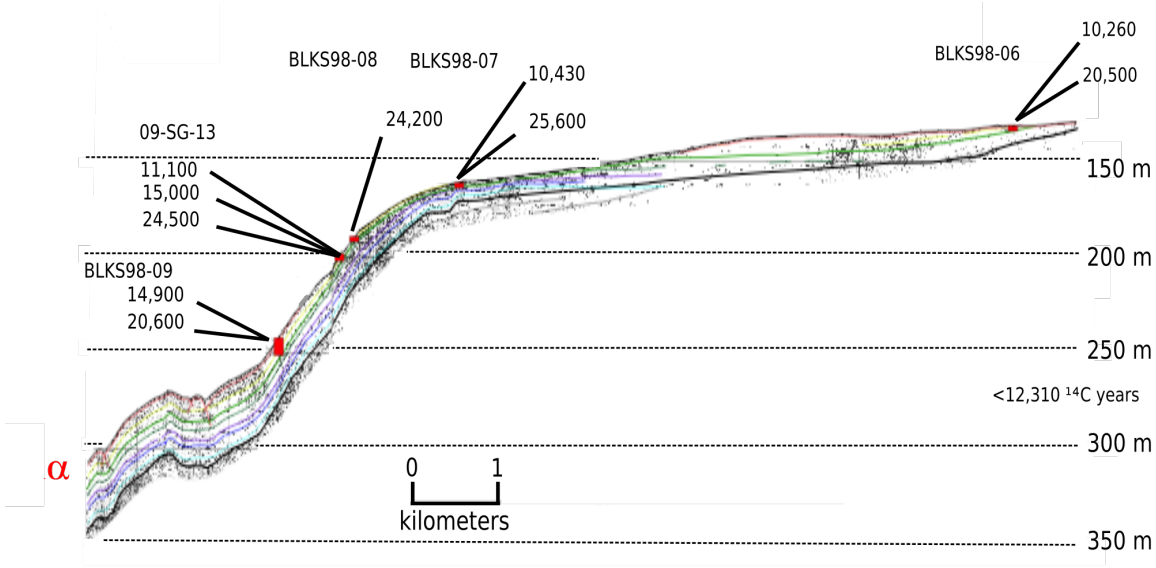
BLKS98-08
BLKS98-07
10,430
24,200
25,600
BLKS98-06
10,260
20,500
09-SG-13
11,100
15,000
24,500
BLKS98-09
14,900
20,600
150 m
200 m
250 m
<12,310 ¹⁴C years
300 m
α
0
1
kilometers
350 m

Figure 3-7

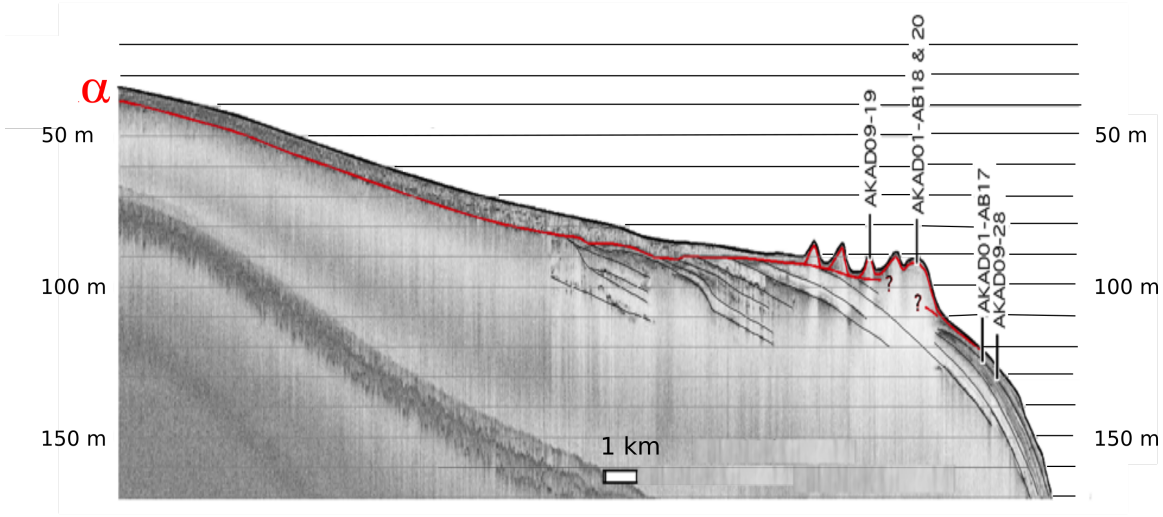
α
50 m
100 m
150 m
AKAD09-19
AKAD01-AB18 & 20
AKAD01-AB17
AKAD09-28
?
?
1 km
50 m
100 m
150 m

Figure 3-8

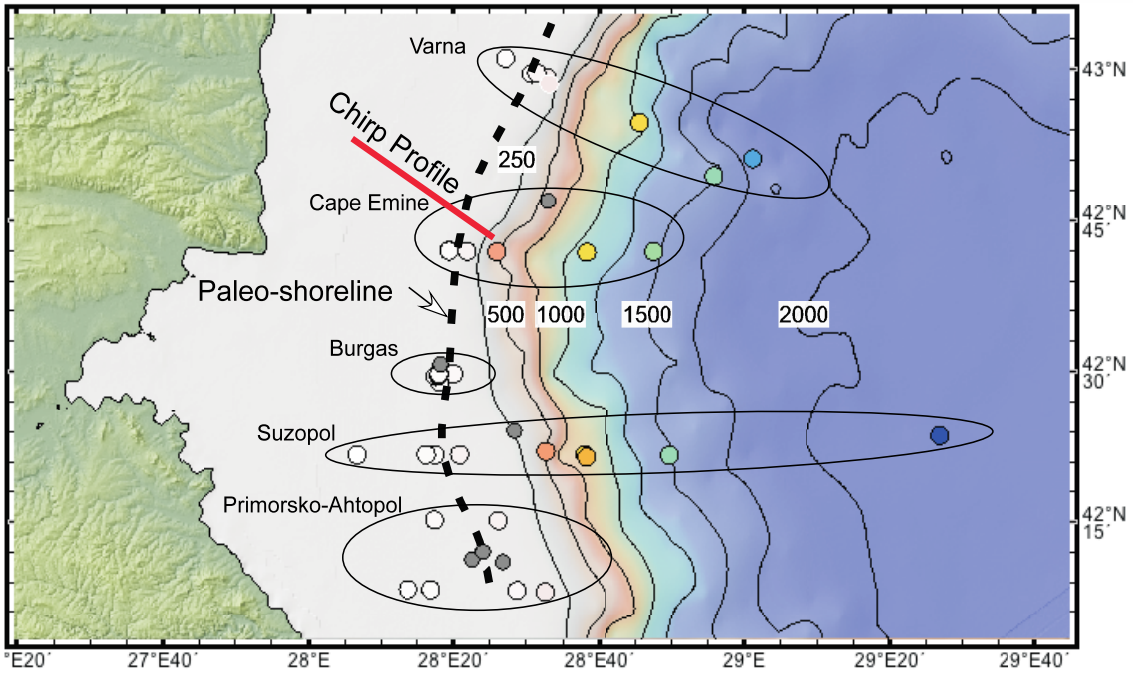
Varna
Chirp Profile
250
Cape Emine
Paleo-shoreline
500
1000
1500
2000
Burgas
Suzopol
Primorsko-Ahtopol
43°N
42°N
45´
42°N
30´
42°N
15´
°E20´
27°E40´
28°E
28°E20´
28°E40´
29°E
29°E20´
29°E40´

Figure 3-9

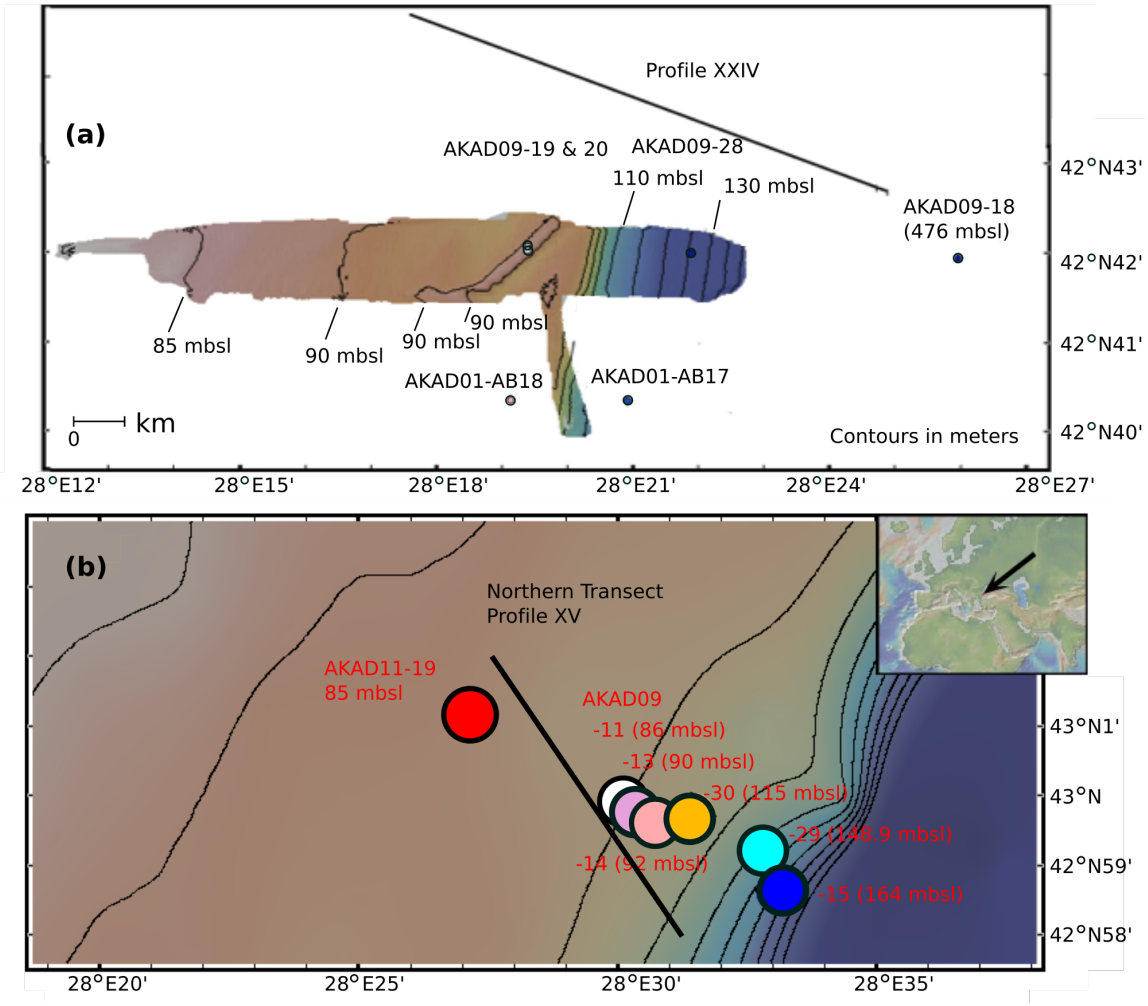
(a)
Profile XXIV
AKAD09-19 & 20
AKAD09-28
110 mbsl
130 mbsl
AKAD09-18
(476 mbsl)
85 mbsl
90 mbsl
90 mbsl
90 mbsl
AKAD01-AB18
AKAD01-AB17
0
km
Contours in meters
42°N43'
42°N42'
42°N41'
42°N40'
28°E12'
28°E15'
28°E18'
28°E21'
28°E24'
28°E27'
(b)
Northern Transect
Profile XV
AKAD11-19
85 mbsl
AKAD09
-11 (86 mbsl)
-13 (90 mbsl)
-30 (115 mbsl)
-29 (146.9 mbsl)
-14 (92 mbsl)
-15 (164 mbsl)
43°N1'
43°N
42°N59'
42°N58'
28°E20'
28°E25'
28°E30'
28°E35'

Figure 3-10

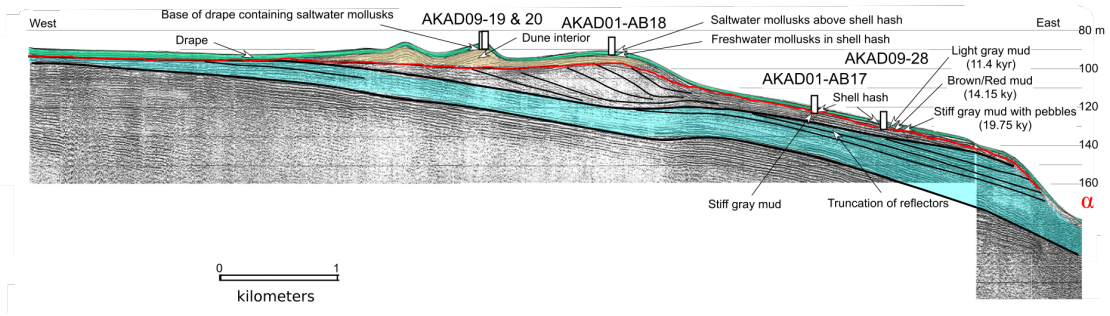
West
East
Base of drape containing saltwater mollusks
Drape
AKAD09-19 & 20
AKAD01-AB18
Dune interior
Saltwater mollusks above shell hash
Freshwater mollusks in shell hash
AKAD09-28
AKAD01-AB17
Shell hash
Light gray mud
(11.4 kyr)
Brown/Red mud
(14.15 ky)
Stiff gray mud with pebbles
(19.75 ky)
Stiff gray mud
Truncation of reflectors
80 m
100
120
140
160
α
0
1
kilometers

Figure 3-11

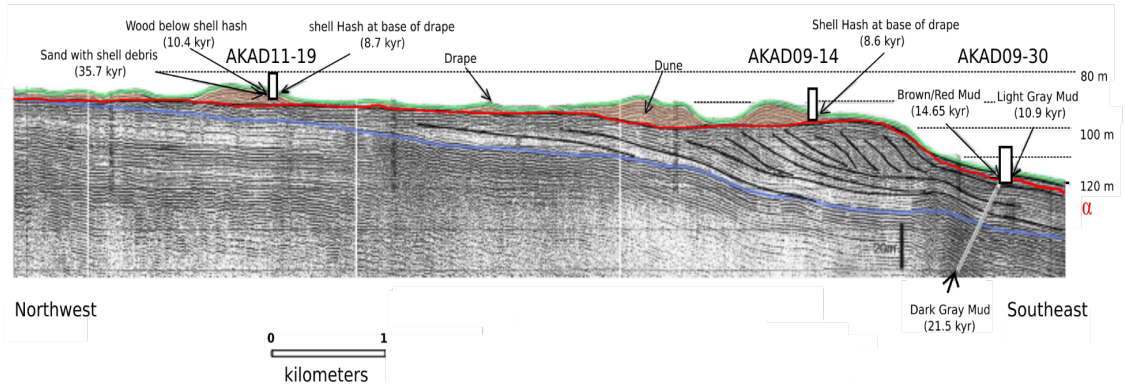
Wood below shell hash
(10.4 kyr)
shell Hash at base of drape
(8.7 kyr)
Sand with shell debris
(35.7 kyr)
AKAD11-19
Drape
Dune
Shell Hash at base of drape
(8.6 kyr)
AKAD09-14
AKAD09-30
80 m
Brown/Red Mud
(14.65 kyr)
Light Gray Mud
(10.9 kyr)
100 m
120 m
α
Northwest
Dark Gray Mud
(21.5 kyr)
Southeast
0
1
kilometers

Figure 3-12

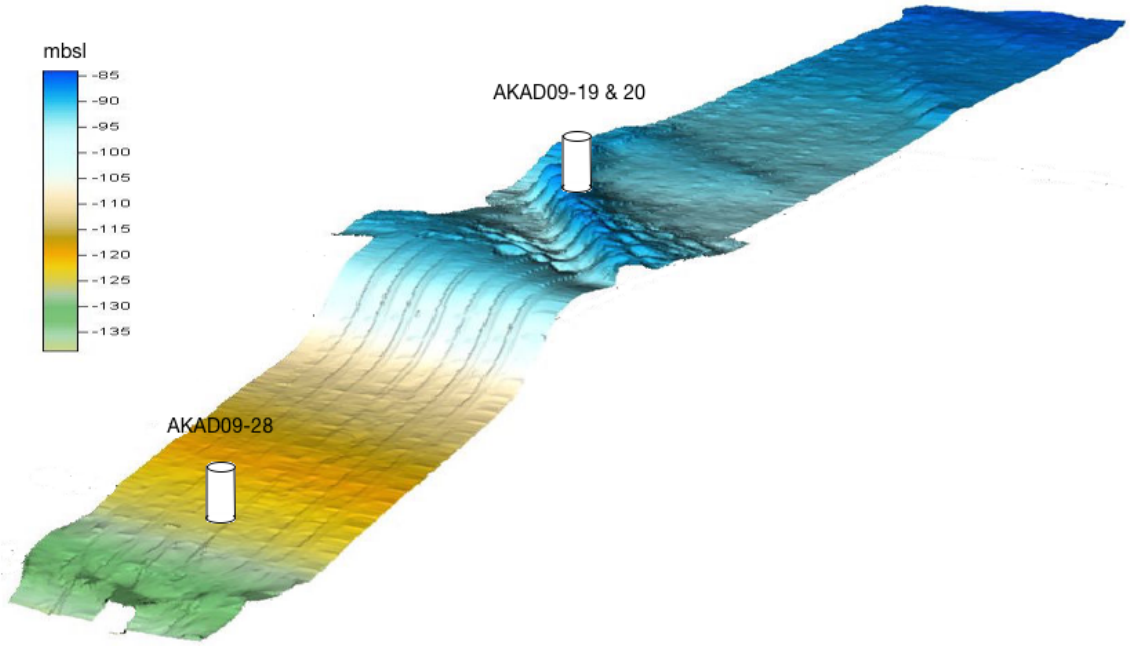
mbsl
-85
-90
-95
-100
-105
-110
-115
-120
-125
-130
-135
AKAD09-19 & 20
AKAD09-28

Figure 3-13

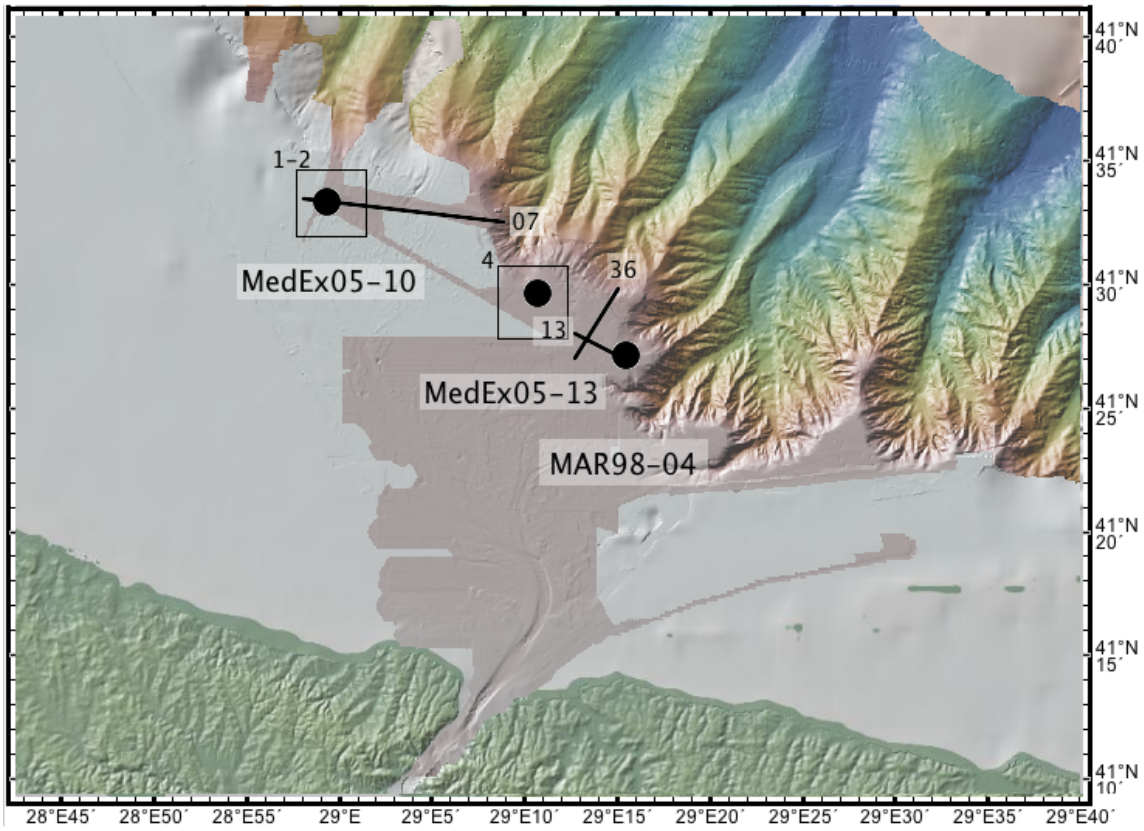
1-2
07
4
36
13
MedEx05-10
MedEx05-13
MAR98-04
41°N 40´
41°N 35´
41°N 30´
41°N 25´
41°N 20´
41°N 15´
41°N 10´
28°E45´
28°E50´
28°E55´
29°E
29°E5´
29°E10´
29°E15´
29°E20´
29°E25´
29°E30´
29°E35´
29°E40´

Figure 3-14

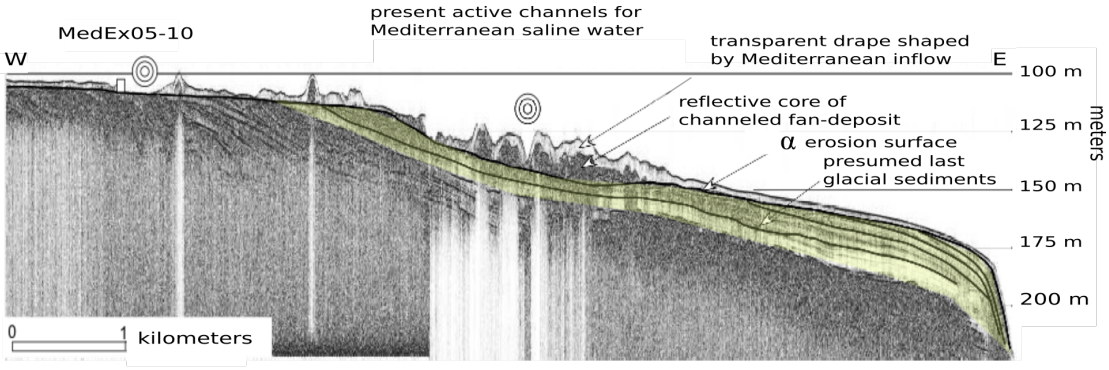
present active channels for
Mediterranean saline water
MedEx05-10
W
transparent drape shaped
by Mediterranean inflow
E
100 m
reflective core of
channeled fan-deposit
125 m
α erosion surface
presumed last
glacial sediments
150 m
175 m
200 m
meters
0
1
kilometers

Figure 3-15

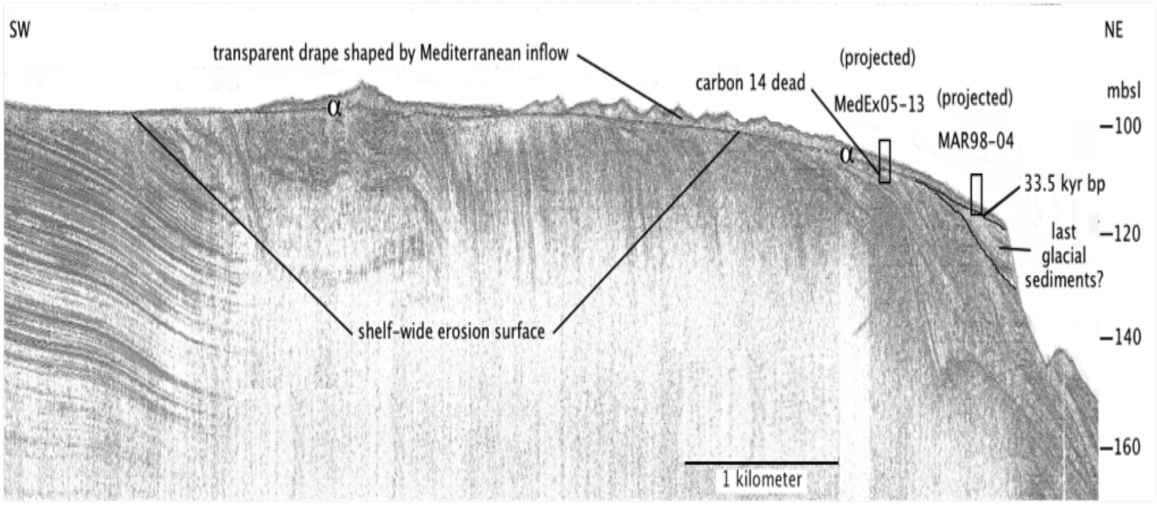
SW
NE
transparent drape shaped by Mediterranean inflow
carbon 14 dead
(projected)
MedEx05-13
(projected)
MAR98-04
mbsl
−100
−120
−140
−160
33.5 kyr bp
last glacial sediments?
shelf-wide erosion surface
1 kilometer

Figure 3-16

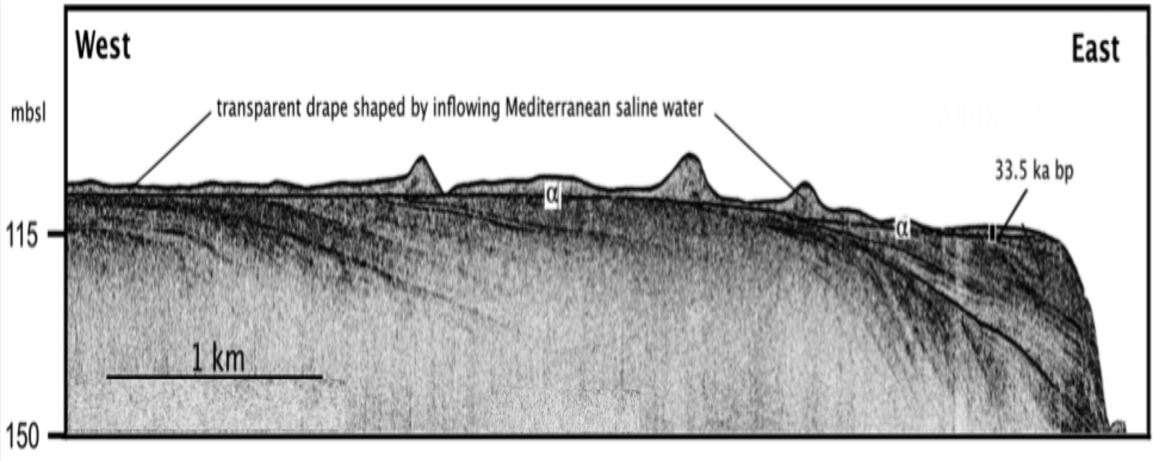
West
East
mbsl
transparent drape shaped by inflowing Mediterranean saline water
33.5 ka bp
α
α
115
1 km
150

Figure 3-17

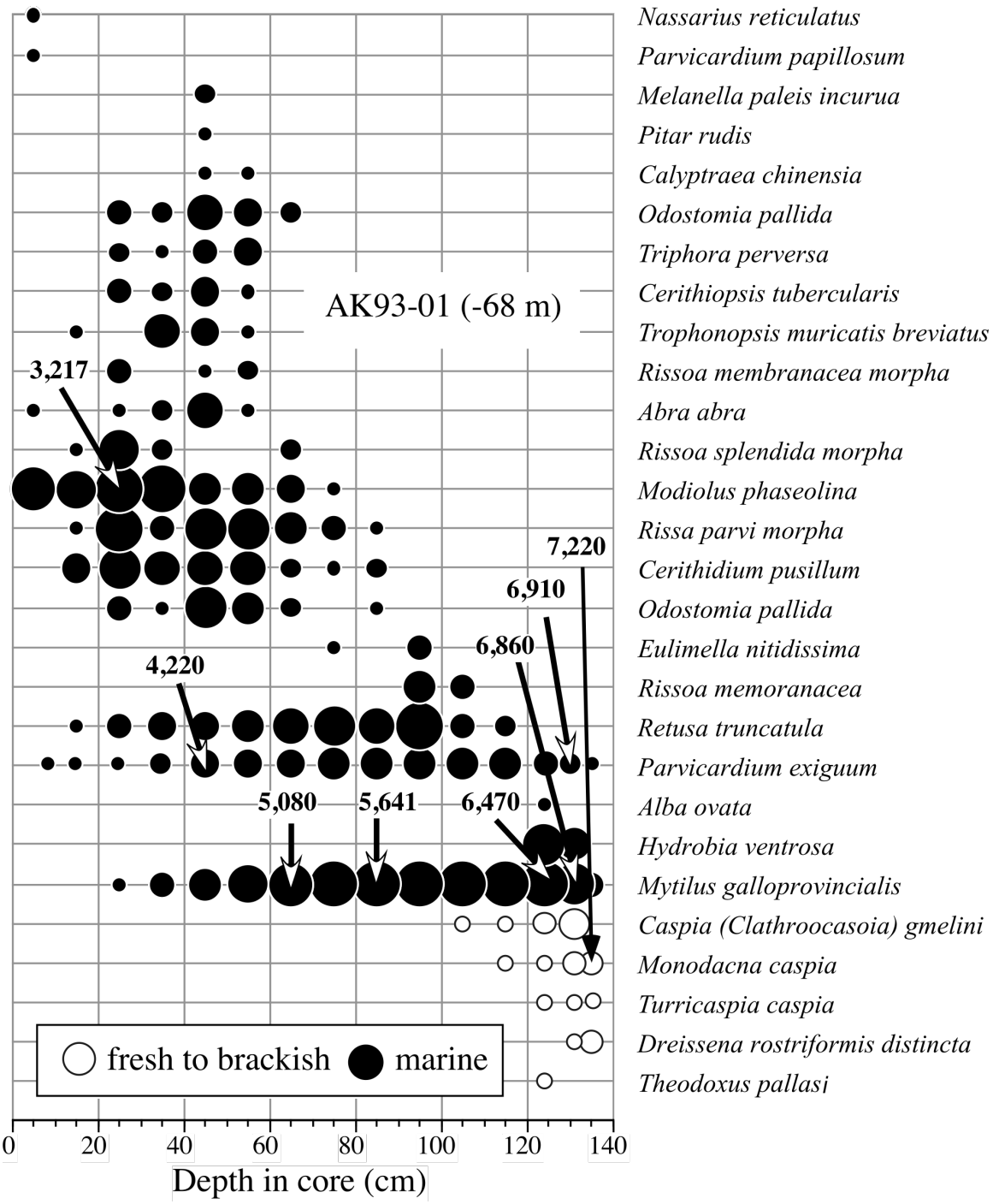
AK93-01 (-68 m)
3,217
4,220
5,080
5,641
6,470
6,860
6,910
7,220
fresh to brackish
marine
0
20
40
60
80
100
120
140
Depth in core (cm)
Nassarius reticulatus
Parvicardium papillosum
Melanella paleis incurua
Pitar rudis
Calyptraea chinensia
Odostomia pallida
Triphora perversa
Cerithiopsis tubercularis
Trophonopsis muricatis breviatus
Rissoa membranacea morpha
Abra abra
Rissoa splendida morpha
Modiolus phaseolina
Rissa parvi morpha
Cerithidium pusillum
Odostomia pallida
Eulimella nitidissima
Rissoa memoranacea
Retusa truncatula
Parvicardium exiguum
Alba ovata
Hydrobia ventrosa
Mytilus galloprovincialis
Caspia (Clathroocasoia) gmelini
Monodacna caspia
Turricaspia caspia
Dreissena rostriformis distincta
Theodoxus pallasi

Figure 3-18

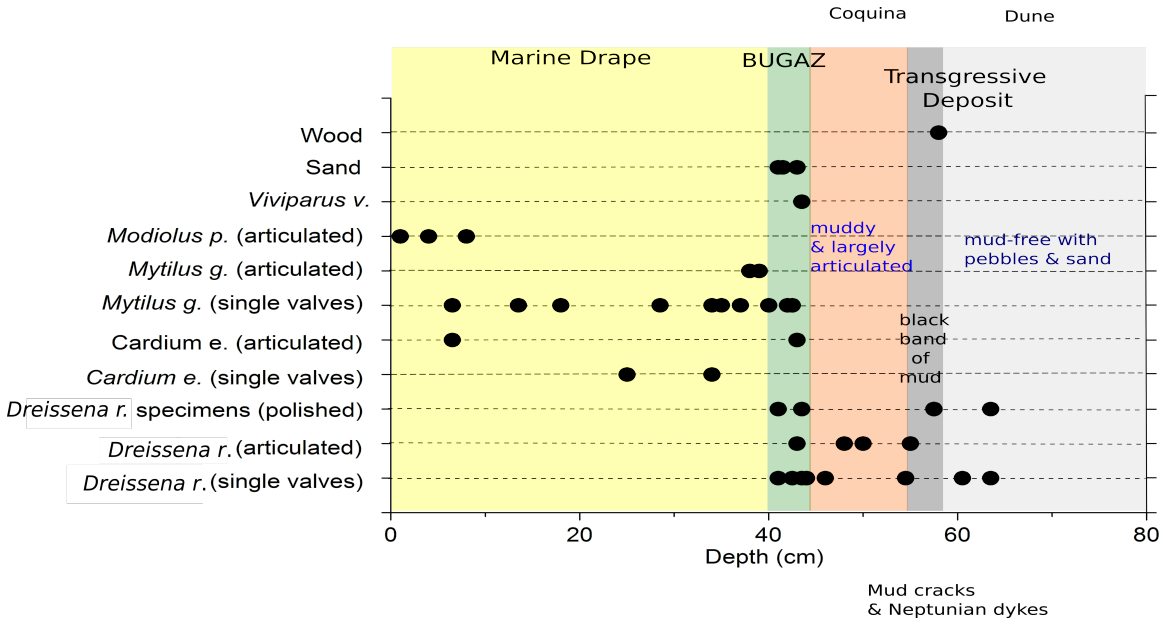
Coquina
Dune
Marine Drape
BUGAZ
Transgressive Deposit
Wood
Sand
Viviparus v.
Modiolus p. (articulated)
Mytilus g. (articulated)
Mytilus g. (single valves)
Cardium e. (articulated)
Cardium e. (single valves)
Dreissena r. specimens (polished)
Dreissena r. (articulated)
Dreissena r. (single valves)
muddy & largely articulated
mud-free with pebbles & sand
black band of mud
0
20
40
60
80
Depth (cm)
Mud cracks & Neptunian dykes

Figure 3-19

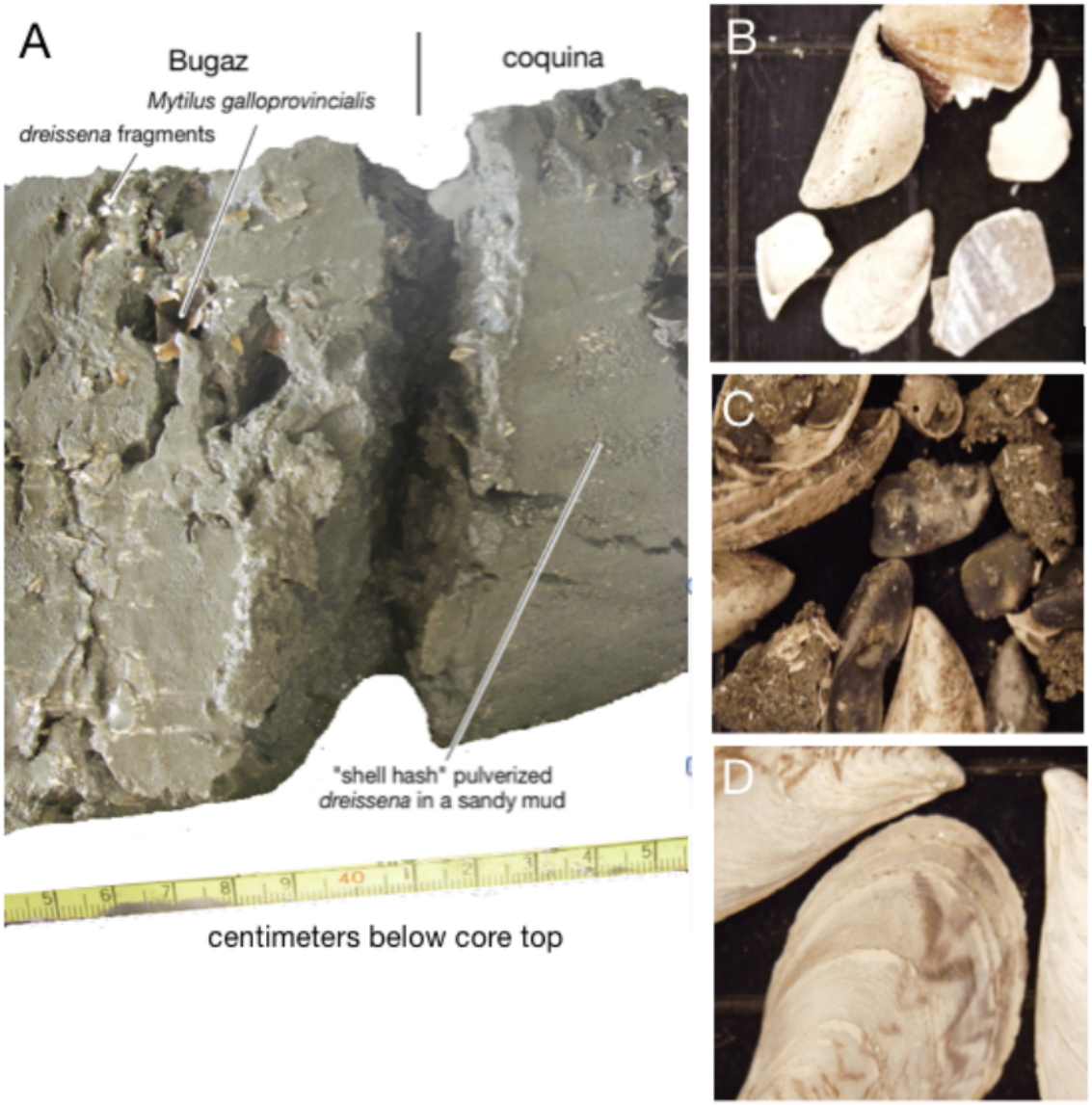
A
Bugaz
coquina
Mytilus galloprovincialis
dreissena fragments
"shell hash" pulverized
dreissena in a sandy mud
centimeters below core top
B
C
D

Figure 3-20

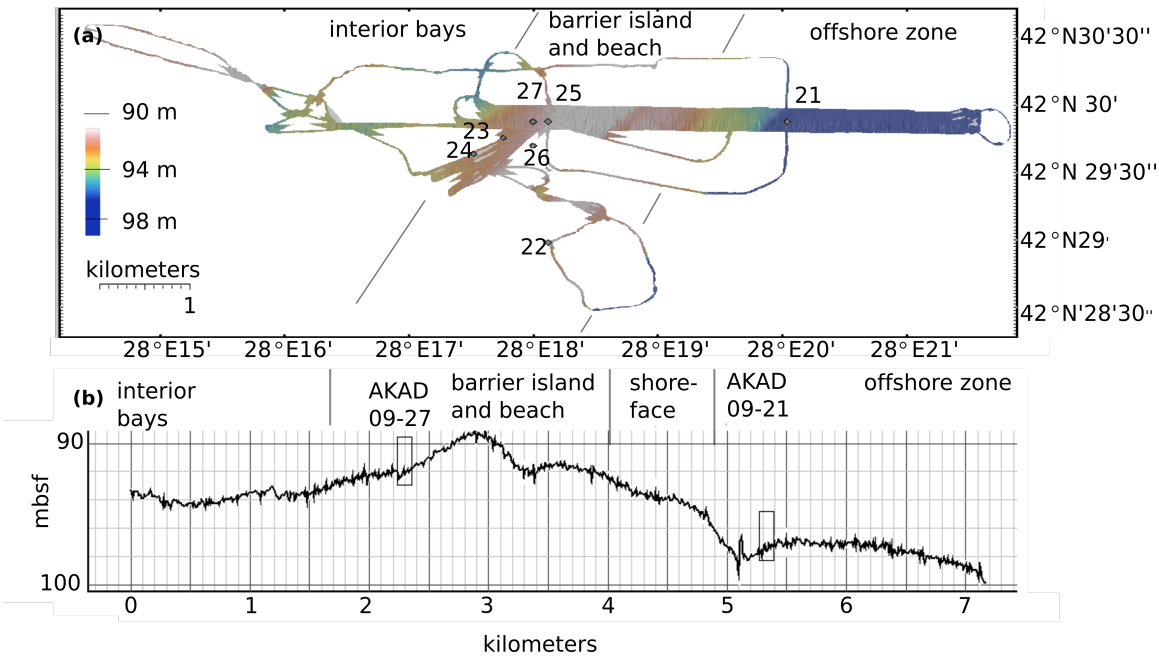
(a)
interior bays
barrier island and beach
offshore zone
90 m
94 m
98 m
kilometers
1
27
25
21
23
24
26
22
42°N30'30''
42°N 30'
42°N 29'30''
42°N29'
42°N'28'30''
28°E15'
28°E16'
28°E17'
28°E18'
28°E19'
28°E20'
28°E21'
(b)
interior bays
AKAD 09-27
barrier island and beach
shore-face
AKAD 09-21
offshore zone
mbsf
90
100
0
1
2
3
4
5
6
7
kilometers

Figure 3-21

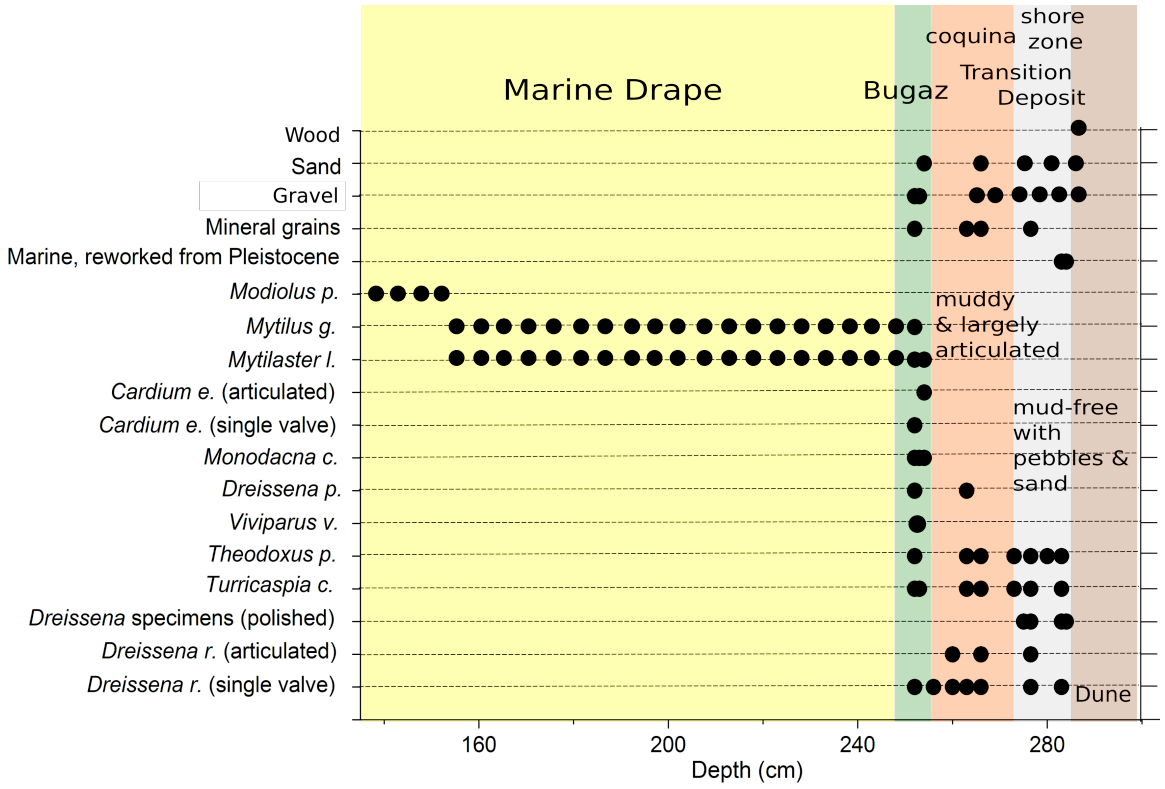
Marine Drape
Bugaz
coquina
shore zone
Transition Deposit
Wood
Sand
Gravel
Mineral grains
Marine, reworked from Pleistocene
Modiolus p.
Mytilus g.
Mytilaster l.
Cardium e. (articulated)
Cardium e. (single valve)
Monodacna c.
Dreissena p.
Viviparus v.
Theodoxus p.
Turricaspia c.
Dreissena specimens (polished)
Dreissena r. (articulated)
Dreissena r. (single valve)
muddy & largely articulated
mud-free with pebbles & sand
Dune
160
200
240
280
Depth (cm)

Figure 3-22

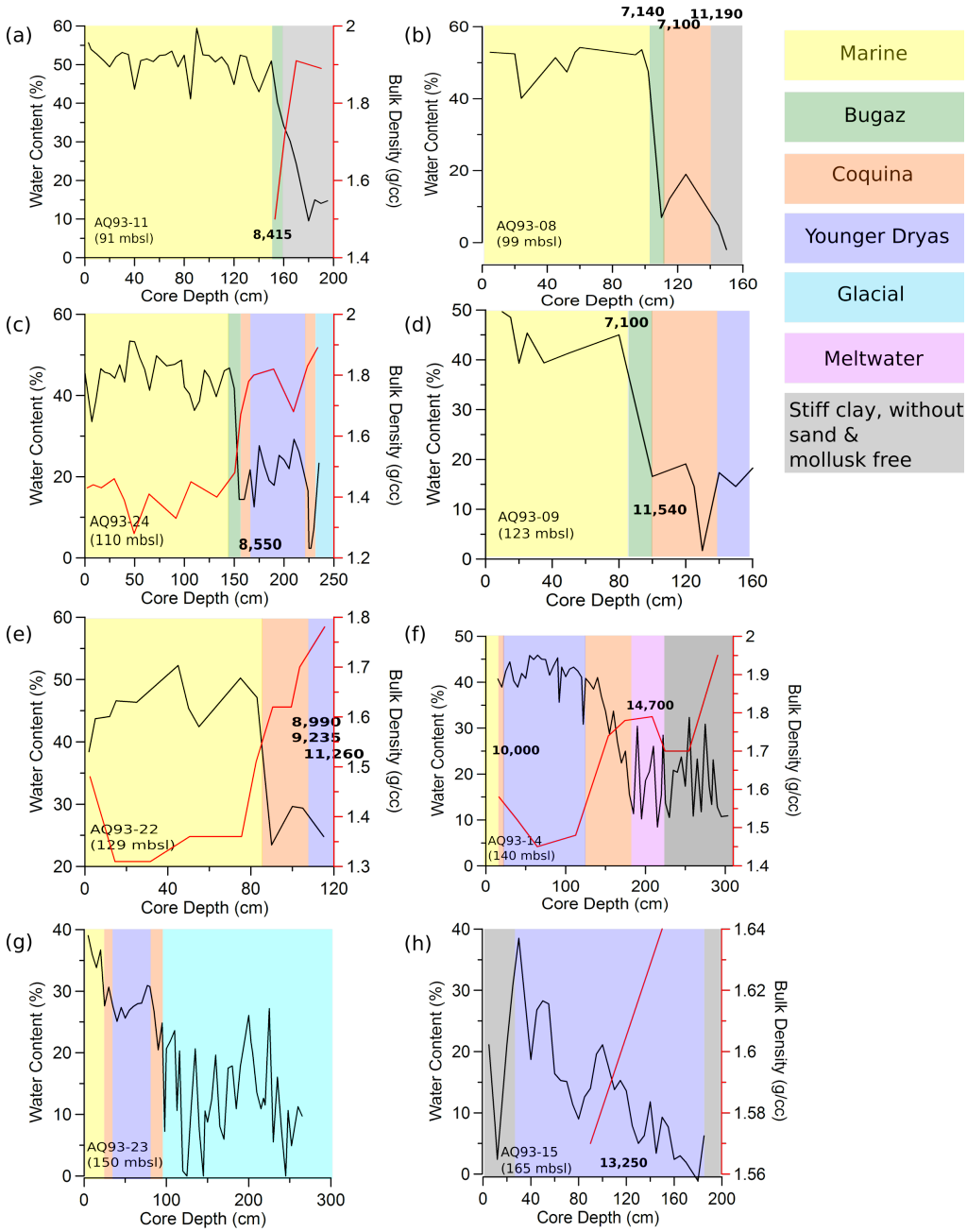
(a)
AQ93-11
(91 mbsl)
8,415
(b)
7,140
11,190
7,100
AQ93-08
(99 mbsl)
(c)
AQ93-24
(110 mbsl)
8,550
(d)
7,100
AQ93-09
(123 mbsl)
11,540
(e)
8,990
9,235
11,260
AQ93-22
(129 mbsl)
(f)
14,700
10,000
AQ93-14
(140 mbsl)
(g)
AQ93-23
(150 mbsl)
(h)
AQ93-15
(165 mbsl)
13,250
Water Content (%)
Bulk Density (g/cc)
Core Depth (cm)
Marine
Bugaz
Coquina
Younger Dryas
Glacial
Meltwater
Stiff clay, without sand & mollusk free

Figure 3-23

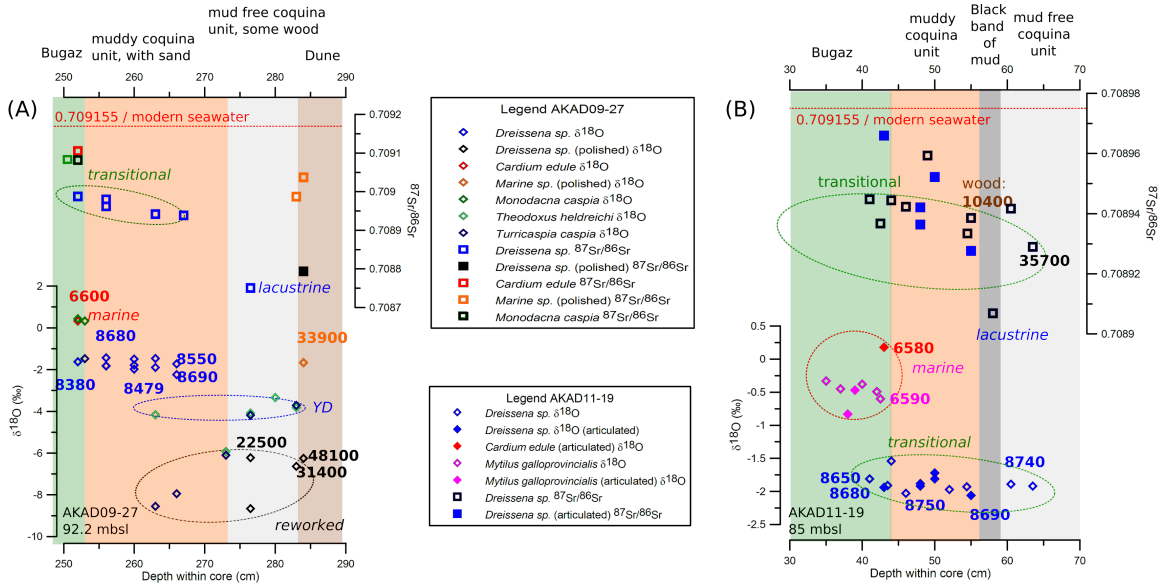
(A)
Bugaz
muddy coquina unit, with sand
mud free coquina unit, some wood
Dune
0.709155 / modern seawater
transitional
lacustrine
marine
YD
reworked
6600
8680
8550
8690
8380
8479
33900
22500
48100
31400
AKAD09-27
92.2 mbsl
Depth within core (cm)
δ18O (‰)
87Sr/86Sr
Legend AKAD09-27
Dreissena sp. δ18O
Dreissena sp. (polished) δ18O
Cardium edule δ18O
Marine sp. (polished) δ18O
Monodacna caspia δ18O
Theodoxus heldreichi δ18O
Turricaspia caspia δ18O
Dreissena sp. 87Sr/86Sr
Dreissena sp. (polished) 87Sr/86Sr
Cardium edule 87Sr/86Sr
Marine sp. (polished) 87Sr/86Sr
Monodacna caspia 87Sr/86Sr
Legend AKAD11-19
Dreissena sp. δ18O
Dreissena sp. δ18O (articulated)
Cardium edule (articulated) δ18O
Mytilus galloprovincialis δ18O
Mytilus galloprovincialis (articulated) δ18O
Dreissena sp. 87Sr/86Sr
Dreissena sp. (articulated) 87Sr/86Sr
(B)
Bugaz
muddy coquina unit
Black band of mud
mud free coquina unit
0.709155 / modern seawater
transitional
wood:
10400
35700
lacustrine
6580
marine
6590
transitional
8740
8650
8680
8750
8690
AKAD11-19
85 mbsl
Depth within core (cm)
δ18O (‰)
87Sr/86Sr

Figure 3-24

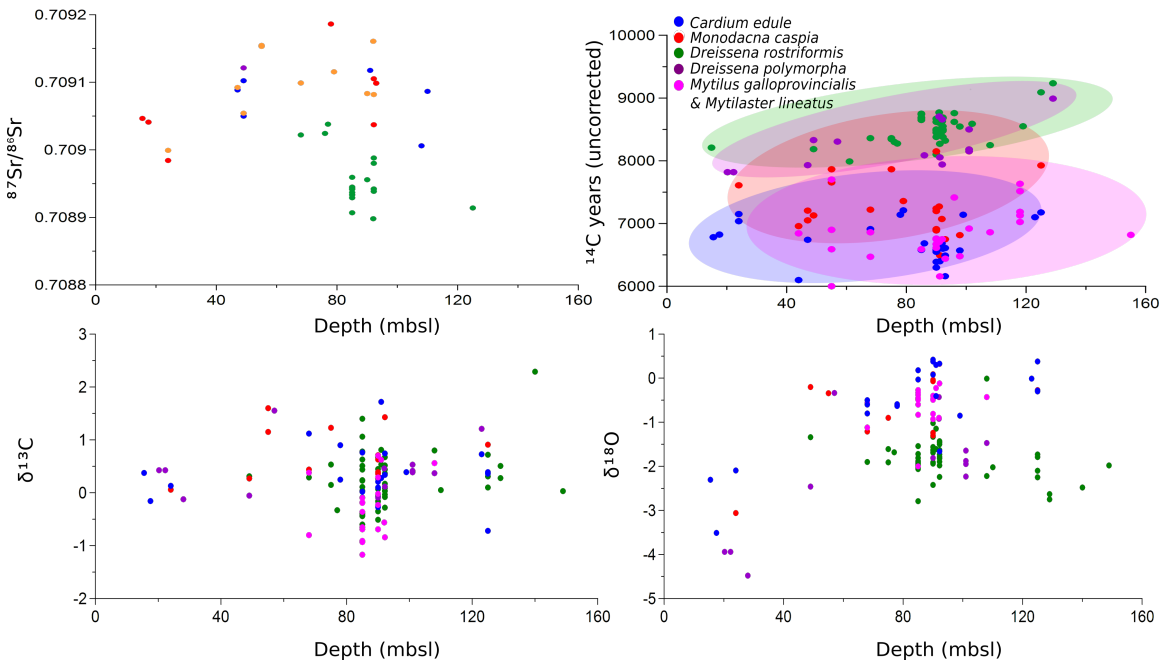
0.7092
0.7091
0.709
0.7089
0.7088
$^{87}Sr/^{86}Sr$
0
40
80
120
160
Depth (mbsl)
Cardium edule
Monodacna caspia
Dreissena rostriformis
Dreissena polymorpha
Mytilus galloprovincialis
& Mytilaster lineatus
10000
9000
8000
7000
6000
^{14}C years (uncorrected)
Depth (mbsl)
3
2
1
0
-1
-2
$\delta^{13}C$
Depth (mbsl)
1
0
-1
-2
-3
-4
-5
$\delta^{18}O$
Depth (mbsl)

Figure 3-25

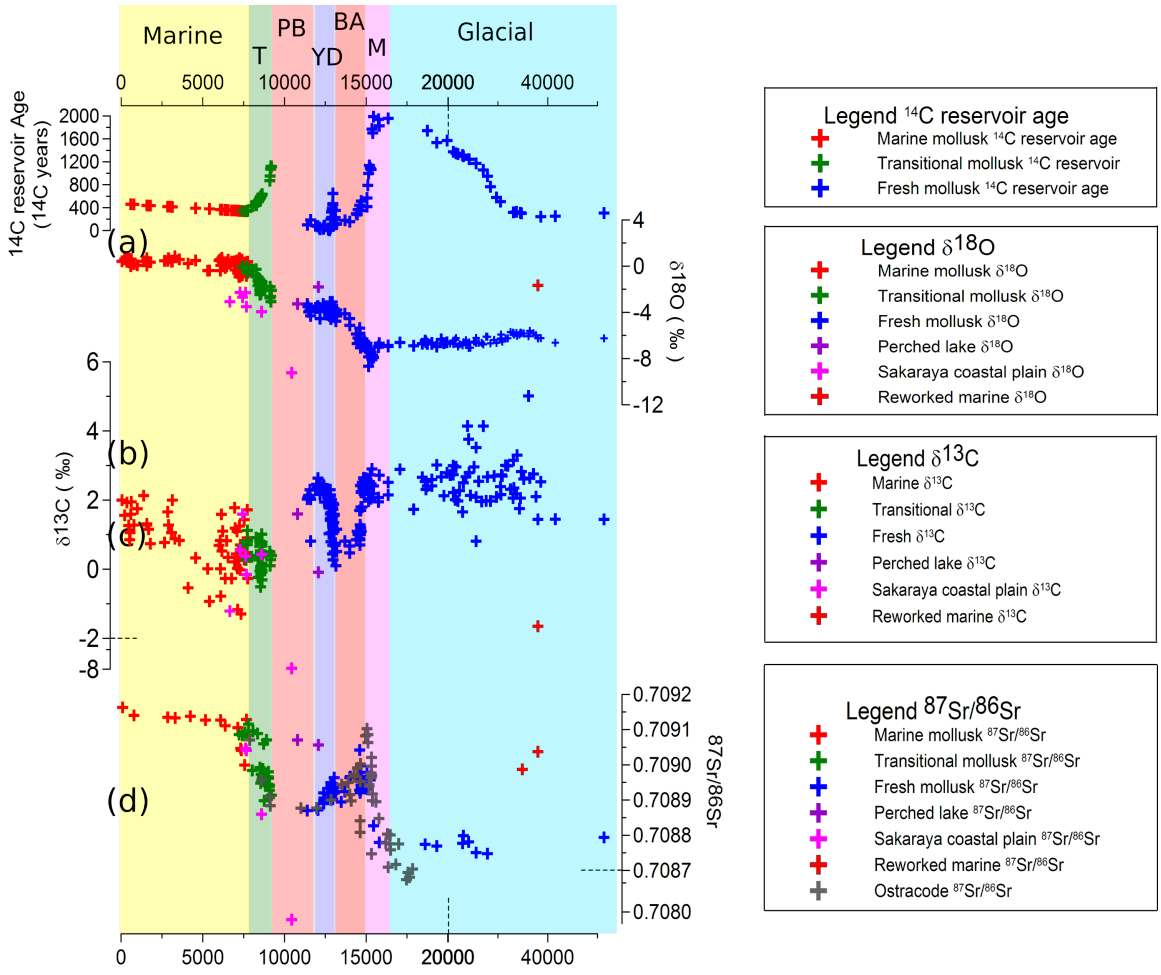
Marine
PB
BA
T
YD
M
Glacial
0
5000
10000
15000
20000
40000
14C reservoir Age
(14C years)
2000
1600
1200
800
400
0
(a)
δ18O (‰)
4
0
-4
-8
-12
6
4
2
0
-2
-8
δ13C (‰)
(b)
(c)
(d)
87Sr/86Sr
0.7092
0.7091
0.7090
0.7089
0.7088
0.7087
0.7080
Legend 14C reservoir age
Marine mollusk 14C reservoir age
Transitional mollusk 14C reservoir
Fresh mollusk 14C reservoir age
Legend δ18O
Marine mollusk δ18O
Transitional mollusk δ18O
Fresh mollusk δ18O
Perched lake δ18O
Sakaraya coastal plain δ18O
Reworked marine δ18O
Legend δ13C
Marine δ13C
Transitional δ13C
Fresh δ13C
Perched lake δ13C
Sakaraya coastal plain δ13C
Reworked marine δ13C
Legend 87Sr/86Sr
Marine mollusk 87Sr/86Sr
Transitional mollusk 87Sr/86Sr
Fresh mollusk 87Sr/86Sr
Perched lake 87Sr/86Sr
Sakaraya coastal plain 87Sr/86Sr
Reworked marine 87Sr/86Sr
Ostracode 87Sr/86Sr

Figure 3-26

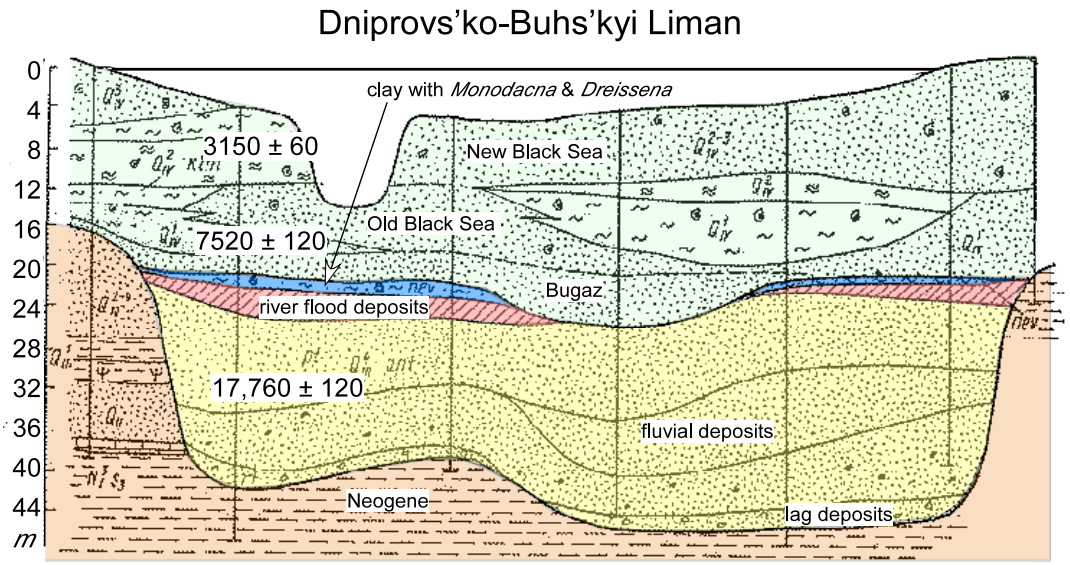
Dniprovs'ko-Buhs'kyi Liman
0
4
8
12
16
20
24
28
32
36
40
44
m
clay with *Monodacna* & *Dreissena*
3150 ± 60
New Black Sea
Old Black Sea
7520 ± 120
Bugaz
river flood deposits
17,760 ± 120
fluvial deposits
Neogene
lag deposits

Figure 3-27

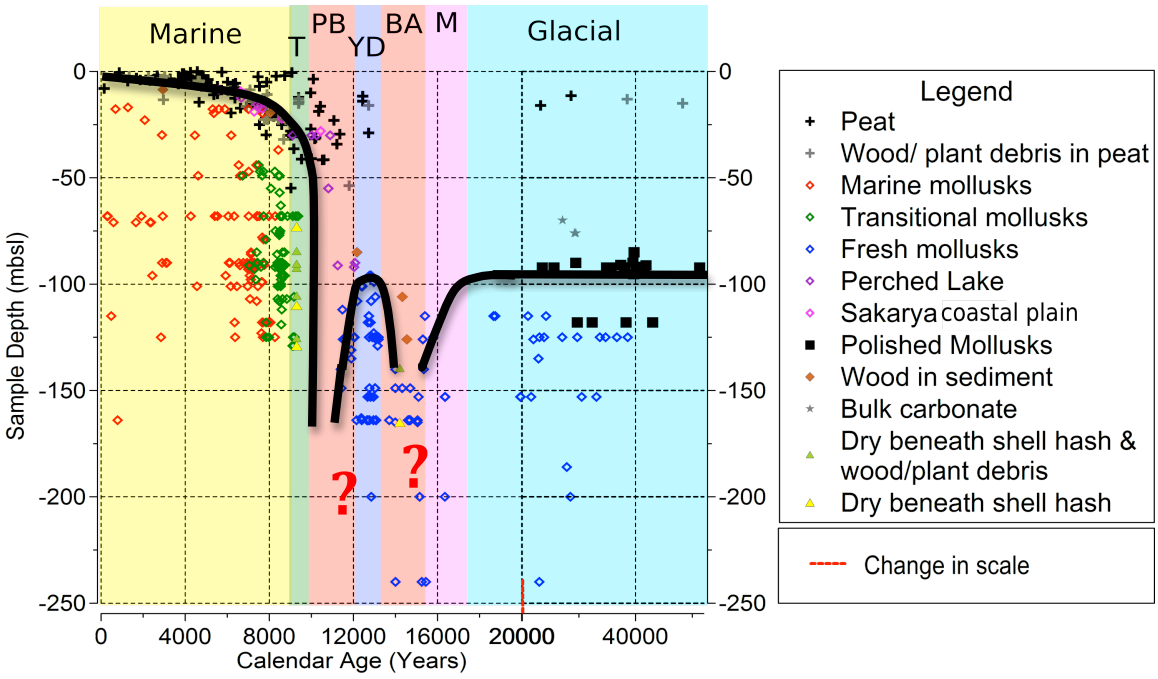
Marine
T
PB
YD
BA
M
Glacial
0
-50
-100
-150
-200
-250
Sample Depth (mbsl)
0
4000
8000
12000
16000
20000
40000
Calendar Age (Years)
?
?
Legend
Peat
Wood/ plant debris in peat
Marine mollusks
Transitional mollusks
Fresh mollusks
Perched Lake
Sakarya coastal plain
Polished Mollusks
Wood in sediment
Bulk carbonate
Dry beneath shell hash & wood/plant debris
Dry beneath shell hash
Change in scale

Figure 3-28

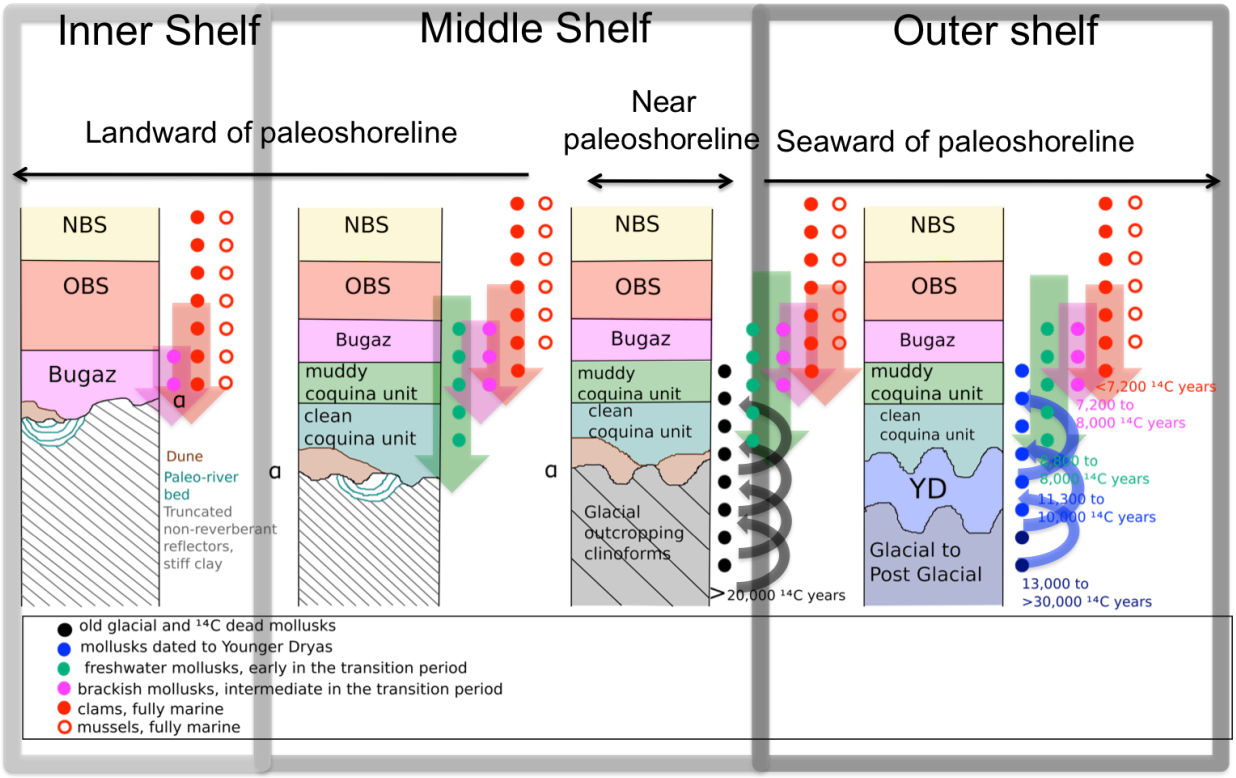
Inner Shelf
Middle Shelf
Outer shelf
Landward of paleoshoreline
Near paleoshoreline
Seaward of paleoshoreline
NBS
OBS
Bugaz
muddy coquina unit
clean coquina unit
Glacial outcropping clinoforms
YD
Glacial to Post Glacial
a
Dune
Paleo-river bed
Truncated non-reverberant reflectors, stiff clay
>20,000 ¹⁴C years
<7,200 ¹⁴C years
7,200 to 8,000 ¹⁴C years
8,000 to 11,300 ¹⁴C years
11,300 to 13,000 ¹⁴C years
13,000 to >30,000 ¹⁴C years
old glacial and ¹⁴C dead mollusks
mollusks dated to Younger Dryas
freshwater mollusks, early in the transition period
brackish mollusks, intermediate in the transition period
clams, fully marine
mussels, fully marine

Appendix 3-1

Core name	Lat (N)	Lon (E)	Core Depth (m)	Cruise and/or first reference
KSK-20	41.06	30.74	0	Turkish State Waterworks, *Görür et al.*, 2001
KSK-18	41.01	30.70	0	Turkish State Waterworks, *Görür et al.*, 2001
KSK-16	41.01	30.52	0	Turkish State Waterworks, *Görür et al.*, 2001
KSK-4	41.04	30.90	0	Turkish State Waterworks, *Görür et al.*, 2001
M02-45TWC	41.69	28.32	-69	Trigger core; *Hiscott et al.*, 2007
M02-45P	41.69	28.32	-69	Piston core; *Hiscott et al.*, 2007
45B	44.71	31.37	-107	Ukrainian HERMES Cruise; *Nicholas et al.*, 2011
721	42.99	41.04	-14.9	Apakidze and Burchuladze, 1987
342	45.74	30.64	-30	Ukrainian Geological Survey of Black Sea region Nicholas et al., 2011
AQ93-01	44.95	32.08	-68	Aquanaut 1993
AQ93-3-2	45.35	31.82	-49	Aquanaut 1993
AQ93-07	44.88	32.15	-108	Aquanaut 1993
AQ93-08	44.90	32.13	-99	Aquanaut 1993
AQ93-09	44.88	32.15	-123	Aquanaut 1993
AQ93-10	44.89	32.15	-106	Aquanaut 1993
AQ93-11	44.91	32.13	-91	Aquanaut 1993
AQ93-12	44.97	32.18	-78	Aquanaut 1993
AQ93-13	44.88	32.28	-165	Aquanaut 1993
AQ93-14	44.85	32.35	-140	Aquanaut 1993
AQ93-22	44.65	36.58	129	Aquanaut 1993
AQ93-24	44.67	36.56	-110	Aquanaut 1993
BLKS9801	44.25	30.42	-92	BlaSON, 1998
BLKS9804	44.20	30.54	-101	BlaSON, 1998
BLKS9806	44.13	30.73	-135	BlaSON, 1998
BLKS9807	44.10	30.79	-163	BlaSON, 1998
BLKS9808	44.10	30.79	-186	BlaSON, 1998
BLKS9809	44.09	30.81	-240	BlaSON, 1998
BLKS9810	44.07	30.85	-378	BlaSON, 1998
BLKS9814	44.14	29.33	-55	BlaSON, 1998
BLKS9815	44.14	29.37	-55	BlaSON, 1998
BLKS9831	44.02	29.92	-75	BlaSON, 1998
BLKS9837	44.02	29.99	-68	BlaSON, 1998
BLKS9838	44.06	29.96	-77	BlaSON, 1998

AKAD01-AB8	44.08	30.13	-90	Akademik, 2001
AK-500	44.53	37.95	-71	Aquanaut, 2001
AK-521	44.26	38.54	-101	Aquanaut, 2001
Medex05-13	41.50	29.19	-118	Mediterranean Explorer, 2005
37-82	46.29	31.36	-24	*Konikov*, 2007
09-SG-13	44.17	30.82	-200	Mare Nigrum, 2009
AKAD09-15	42.98	28.55	-164	Akademik, 2009
AKAD09-27	42.50	28.30	-92.2	Akademik, 2009
AKAD09-28	42.70	28.36	-126	Akademik, 2009
AKAD09-29	42.99	28.55	-148.9	Akademik, 2009
AKAD09-30	43.00	28.52	-115	Akademik, 2009
AKAD11-01	42.36	28.35	-125	Akademik, 2011
AKAD11-02	42.36	28.29	-90	Akademik, 2011
AKAD11-03	42.36	28.27	-90	Akademik, 2011
AKAD11-05	42.25	28.44	-125	Akademik, 2011
AKAD11-07	42.13	28.54	-153	Akademik, 2011
AKAD11-19	43.02	28.45	-85	Akademik, 2011

CHAPTER 4

The dynamic nature of the Bosporus sill and its influence on the connection between the Black Sea and the Sea of Marmara

Abstract

The delayed entry of Mediterranean water into the Black Sea in the early Holocene indicates that the threshold depth of the Bosporus sill was 35 mbsl at that time. Yet, there is evidence of a 95 mbsl paleo-shoreline on all of the Black Sea margins, coincident with persistent outflow when the Black-Sea Lake was at this level during the glacial and deglacial periods. Reflection profiles, cores, and geochemical measurements in the form of ^{14}C, $\delta^{18}O$, $\delta^{13}C$, and $^{87}Sr/^{86}Sr$ from all of the Black Sea shelves are brought together here support a proposed resolution to this apparent inconsistency in the form of a dynamic sill. Erosive outflow lowered the sill to its bedrock minimum during the glacial period. Loose sediment filled the sill to its shallower modern depth during Bølling/Allerød regression. This shallower sill prevented inflow of water from the Mediterranean until the early Holocene, well after the entry of Mediterranean water into the Sea of Marmara. It is likely that the phenomenon of a dynamic sill is not unique to the most recent deglaciation but also characterized the Marine Isotope 6 to Marine Isotope 5 transition, and may be an integral feature of the Black Sea and its variable connection to the global ocean.

1. Introduction

The Black Sea is a large and deep meromictic body of water connected to the global ocean via a system of straits and marginal basins (Ünlüata et al., 1990). In the modern

configuration, the water exchange that controls the basin's hydrological balance is estuarine across the Bosporus sill at ~35 mbsl, allowing for water exchange between the Black Sea and the Sea of Marmara, and across the Strait of Dardanelles at ~83 mbsl, allowing for water exchange between the Sea of Marmara and the Aegean Sea. During glacial periods, the inter-basin exchange is severed. The Black Sea-Lake fails to receive inflow from the Mediterranean Sea as the global sea level recedes below the threshold depth of the Bosporus and Dardanelles Straits. As the input of water into the basin changed to exclusively river inflow and precipitation, the Black Sea transitions into a freshwater lake. During interglacial periods, the global sea level rises and the water from the Mediterranean breaches the sills, creating a basin that receives water from both riverine and marine sources. The most recent occurrence of this event is in the Early Holocene.

When the Black Sea basin is cut off from the global ocean, it has two possible modes of behavior. The first involves a scenario in which the level of the lake is above that of the sill, leading to outflow from the Black Sea-Lake to the Marmara Sea-Lake. The lake level will be stabilized at the depth of the sill. This is a consequence of positive hydrological balance in the lake resulting in excess water and outflow. In this scenario, the waters of the Marmara Sea-Lake, downstream from the outflowing Black Sea, must also be fresh and will have a similar isotopic composition as the Black Sea. Due to its much smaller size relative to the Black Sea, the Marmara Sea-Lake must also be in a positive hydrologic balance with outflow to the Mediterranean Sea. The second involves a scenario in which the level of the Black Sea-Lake basin is below that of the sill. This leads to the severing of communication between the lake and the global ocean, while the lake level varies as a function of the hydrological balance between evaporation on the one hand and combined precipitation and river inflow on the other. The

Bosporus and Dardanelles sill depths are therefore crucial to understanding the evolution of water exchange between basins.

One of the remaining questions is the apparent inconsistency between the widespread observation of a lowstand paleoshoreline (Kuprin et al., 1974; Scherbakov and Babak, 1979; Kaplin and Shcherbakov, 1986) established on the Black Sea shelf during the glacial periods, and robust evidence for the delayed entry of marine water into the Black Sea-Lake during the interglacial periods (Deuser, 1972; Ross and Degens, 1974; Ryan et al., 1996; Ryan et al., 1997; Major et al., 2006; Ryan, 2007; Soulet et al., 2011a) that suggests the Bosporus sill was much shallower, as it is today. Nicholas and Chivas, (2014) suggested that this might be explained by the Bosporus sill becoming infilled with sediments sometime during the deglaciation but without strong arguments for when this phenomena would have occurred and also without strong evidence for this proposition. This paper assembles a series of data-sets that include: (1) chirp profiles from the Ukrainian, Romanian, Bulgarian, and Turkish shelves, (2) thorough radiocarbon dating of mollusks, (3) stable isotopes of mollusks, and (4) radiogenic isotopes of mollusks to propose an answer to this question in the context of a progression of the Black Sea and the Sea of Marmara water exchange from Marine Isotope Stage 6 (MIS 6) to present.

2. Materials and Methods

2.1 Reflection profiles and core collection

The cores used in this study are a compilation from multiple cruises from the Black Sea and the Sea of Marmara (**Figure 4-1**). The cores were recovered using numerous methods that include gravity, borehole, vibracoring, and piston methods. The full list is presented in Appendix A. The cores collected in the Black Sea cover a broad area of the shelf, slope, and the basin

interior whereas those collected in the Sea of Marmara are only from the basin interior. Cores retrieved from the Black Sea shelf areas (i.e., Ukrainian, Romanian, Bulgarian, and Turkish) are used to derive an age model for the cores, reservoir age, stable isotope measurements, and radiogenic isotope measurements. Cores retrieved from Black Sea the slope and basin areas are used to supplement radiogenic measurements. Cores retrieved from the Sea of Marmara slope and basin are used for radiogenic measurements and are taken from the unpublished work of (Major, 2015). The respective measurements will be further elaborated later in the methodology description.

The chirp profiles presented from the Black Sea include WC-6-12 from the Kerch Strait and WC-6-14 from the Ukrainian margin taken during the R/V Aquanaut expedition in 1993, B008 taken during the BLaSON expedition in 1998, B2ch049 and B2ch007 from the Bulgarian and Turkish margins, respectively, taken on the BLaSON2 expedition in 2002.

2.2 Geochemical measurements and age model

The age model for the cores used in this study is derived from ^{14}C measurements, stable isotope measurements, and aligning the ^{14}C dated isotope measurements to thoroughly U/Th dated nearby stalagtite records shown to sample evaporated Black Sea water (Fleitmann et al., 2009; Badertscher et al., 2011).

The material used for radiocarbon dating includes mollusks, ostracodes, and occasional pieces of wood. The carbonate material analyzed in this study was subject to a treatment procedure. This procedure involved sonification of the carbonate for 30s in Quartz Distilled water and methanol to remove any contaminating detrital matter. Samples were sent to Woods Hole Oceanographic Institution and ETH-Zurich for ^{14}C dating where they were run using CO_2-

reduction and carbonate hydrolysis methods. Supplemental dates were used from prior publications (Apakidze and Burchuladze, 1987; Major et al., 2002; Major et al., 2006; Ivanova et al., 2007; Konikov et al., 2007; Lericolais et al., 2007; Nicholas et al., 2011; Soulet et al., 2011a).

^{14}C dated mollusks were also measured for their $\delta^{13}C$ and $\delta^{18}O$ composition by gas-sourced mass spectrometry at the Department of Earth and Planetary Sciences at Rutgers University (Mortlock, 2010) and at Rensselaer Polytechnic Institute (RPI) (Cohen and Ryan, 2011). A subsample of each shell was taken in the weight range of 700 to 1200 μg. Crushed samples were loaded onto a Multi-prep device attached to a Micromass Optima Stable Isotope Mass Spectrometer and reacted in 100 % phosphoric acid at 90°C for 800 seconds. The measurements were corrected relative to an NBS-19 value from the analysis of an internal laboratory standard as a function of V-PBD. The errors for each measurement were calculated to be 0.04 ‰ for $\delta^{13}C$ and 0.06 ‰ for $\delta^{18}O$. Additional results are taken from Cohen and Ryan, (2011), Major et al., (2002), and Major et al., (2006).

The age model for the cores used in this manuscript and for the respective stable isotope measurements of the surface Black Sea water was composed by aligning the ^{14}C dated mollusk stable isotope measurements to the U/Th dated stalagtite stable isotope measurements of Sofular Cave. It was noted that the cave $\delta^{18}O$ record is identical to the Black Sea mollusk $\delta^{18}O$ record and pointed out that the cave must sample evaporated Black Sea water. The cave $\delta^{13}C$ record also is remarkably similar to the Black Sea mollusk $\delta^{13}C$ record. It is possible that the Sofular Cave and the surface Black Sea would sample the same source of dissolved inorganic carbonate (DIC) as this source is terrestrially derived. The ^{14}C reservoir ages were derived from calculating the corresponding atmospheric ^{14}C age from the calibrated calendar age using the conversions from Reimer et al., (2013) and subtracting it from the measured ^{14}C age.

Mollusks were also measured for their $^{87}Sr/^{86}Sr$ composition. The ostracodes collected from some of the deeper cores were used for supplemental $^{87}Sr/^{86}Sr$ measurements as the $^{87}Sr/^{86}Sr$ composition of water is independent of depth, contrary to the $\delta^{18}O$ and $\delta^{13}C$ which change as a function of water density and biological productivity. The carbonate was leached following a procedure modified from (Bailey et al., 2000). The first leach consisted of a one-minute sonification of the sample in 0.1 N hydrochloric acid. The isotope ratios were measured by a dynamic multi-collector on a VG Sector 54 thermal ionization mass spectrometer (TIMS) at Lamont-Doherty Earth Observatory. The $^{87}Sr/^{86}Sr$ ratios were corrected for mass fractionation by normalizing to $^{86}Sr/^{88}Sr=0.1194$. Beam size was maintained at close to 4.5 x 10-11 A for ^{88}Sr. The measurements were further corrected for instrumental drift by analysis of NBS987 which gave $^{87}Sr/^{86}Sr=0.710255 \pm 2.31143^{-05}$, 2σ error of the mean. Prior $^{87}Sr/^{86}Sr$ measurements supplement those made in this study (Major et al., 2006; Cohen and Ryan, 2011).

The age model for the $^{87}Sr/^{86}Sr$ measurements from cores from the Sea of Marmara is constructed by aligning those $^{87}Sr/^{86}Sr$ measurements in the deglacial period prior to the connection of the Marmara Sea-Lake to the Mediterranean with those calendar ages calculated for the Black Sea-Lake as they are nearly identical. Those $^{87}Sr/^{86}Sr$ measurements taken in the period once the Sea of Marmara is connected with the Mediterranean are converted to a calendar age with a ^{14}C reservoir correction of 400 years, the modern ^{14}C reservoir of the surface global ocean, using the conversion of (Reimer et al., 2013).

3. Results

3.1 Reflection profiles

The reflection chirp profiles presented include those from the Kerch, Ukrainian, Romanian, Bulgarian, and Turkish shelves. The chirp profile from the Kerch shelf (**Figure 4-2**), 6-12-304, spreads 140 to 60 mbsl. In the isobath 100 to 120 mbsl, below a uniform drape and erosion surface α is a set of seaward dipping clinoforms. The very bottom of core AK93-24, retrieved from 110 mbsl, samples sediments that contain some plant material but not mollusk shells for identification. The top section of the core samples the uniform drape that is composed of two layers: the upper layer with mollusks identified as the *Modiolus phaseolina* and the lower layer with mollusks identified as the Mytilus galloprovincialis. The lower layer is also black in color and high in organic content. The uniform drape is separated from the mollusk-free bottom of the core by a coquina layer, a mollusk identified as a *Dreissena rostriformis* was ^{14}C dated to 8.550 ± 50 kyr ^{14}C.

The profile from the Ukrainian shelf (**Figure 4-3**), WC-6-15, spreads 110 to 75 mbsl. A uniform drape is the top most layer of the profile. Above 80 mbsl, the uniform drape sits upon features such as dunes whereas below 100 mbsl, the uniform drape sits upon an erosion surface and seaward dipping clinoforms, respectively. A shoreface separates the isobath between 80 and 100 mbsl.

The profile from the Romanian margin (**Figure 4-4**), B008, spreads 350 to 150 mbsl. A uniform drape sits upon the entire chirp profile but thins significantly in the depth range 150 to 200 mbsl. Below 200 mbsl is a uniform set of reflectors with alternating reflectivity, more and less reflective. The topmost reflectors are sampled by a set of cores along this profile, BLKS98-06 at 135 mbsl, BLKS98-07 at 163 mbsl, BLKS98-08 at 186 mbsl, 09-SG-13 at, and BLKS98-09 at 240 mbsl. The topmost uniform drape, specifically sampled by 09-SG-13, is characterized as a sapropel and is very dark in color. The material below that is predominantly gray clay.

These reflectors identify a series of periods of sediment deposition that date to ~10.20 kyr ^{14}C, 15 kyr ^{14}C, and 20 to 25 kyr ^{14}C years. They do not sample material below those clinoforms that are ^{14}C dated. BLKS98-06 has two erosion surfaces, α1 and α. A coquina sits upon both of these surfaces. The bottom most coquina separates material that dates to 10.20 and >20 kyr ^{14}C. Those clinoforms below material dated between 20 and 25 kyr ^{14}C years are similar to those clinoforms dated in the top most clinoforms that are composed of uniform drape and gray clay.

The chirp profile from the Bulgarian shelf (**Figure 4-5**), B2ch049, spreads 170 to 20 mbsl. In the isobath below 100 mbsl below the uniform drape and α erosion surface, is a set of seaward dipping clinoforms. Cores AKAD01-AB17 at 120 mbsl and AKAD09-28 at 126 mbsl sample these clinoforms. Above 100 mbsl, cores AKAD09-19 and AKAD01-AB18 and -20 at 90 mbsl sample sediment belonging to shore dune formations. A uniform drape forms the top most layer in the chirp profile. AKAD09-28 samples material that belongs to the uniform drape, composed of two layers as previously identified in the Romanian chirp profile. The core also samples material belonging to sediments older than 14 kyr ^{14}C and those in the range of 10,00 to 11,500 ^{14}C years. Each unit of deposition is separated by an erosion surface followed by a coquina and an abrupt change in ^{14}C age.

Another chirp profile from the Bulgarian shelf (**Figure 4-6**) illustrates the erosion surface, the outcropping clinoforms seaward of ~95 mbsl, the uniform drape that covers the Bulgarian shelf everywhere, and the coastal dunes and barrier bars at 80 mbsl. The outcropping clinoforms are truncated such that their topsets are cut off by the erosion surface.

The chirp profile from the Turkish shelf (**Figure 4-7**), B2ch007, spreads 200 to 100 mbsl. The topmost unit is identified as a uniform drape, akin to that one that also covers the shelves of the Kerch, Ukrainian, Romanian, and Bulgarian shelves. Below the α erosion surface and a shelf

channeled-fan deposit, previously described and interpreted in (Ryan et al., 2013), is a set of seaward dipping clinoforms. These reflectors, as are those found on other shelves, have alternating reflectivity.

Chirp profile from the northern shelf of the Sea of Marmara (**Figure 4-8**), adopted from Fig. 7 of (Karakilcik et al., 2014), shows the location of lacustrine shelf-edge deposits in the depth range of 100 to 90 mbsl relative to the location of the erosion surface and marine drape. The wave cut terrace is located at 80 mbsl. The erosion surface truncates the clinoforms beneath it, similar to the scenario that occurs on the Black Sea shelf areas. The marine drape is of uniform thickness, with the exception of the outcropping of Neogene bedrock at 70 mbsl, and covers the entire shelf area in this particular chirp profile. Cores MedEx05-1, retrieved from a depth of 103 mbsl, and MedEx05-2, retrieved from a depth of 93.95 mbsl, are projected onto the profile. Both of the cores have sediments that belong to lacustrine conditions (McHugh et al., 2004).

3.2 Reservoir ages

The ^{14}C reservoir ages progressively rose from approximately 0 to >2,000 ^{14}C years from MIS 4 to MIS 2. The ^{14}C reservoir ages calculated from the data of Nowaczyk et al., (2012) is higher than those presented in Soulet et al., (2011a). At 21.70 kyr BP, Kwiecien et al., (2009) present a ^{14}C reservoir age of 1,450 ^{14}C years in a water depth of 1220 mbsl. Ryan, (2007) also ascribe a high ^{14}C reservoir age of 1,600 ^{14}C years during the glacial period, that is comparable to those of Nowaczyk et al., (2012), Soulet et al., (2011a), and Kwiecien et al., (2009).

At the onset of the meltwater pulse that is responsible for the deposition of the red layers in the Black Sea, the ^{14}C reservoir drops to 0 in essentially all of the calculations presented. This

is very clear from the record derived from the mollusk-cave $\delta^{18}O$ alignment. The drop occurs slightly later than that calculated from Soulet et al., (2011a) and much more rapid than that calculated from the data of Nowaczyk et al., (2012). During both the Bølling/Allerød and Preboreal periods, the ^{14}C reservoir rises. During the Bølling Allerød, it is as high as 800 ^{14}C years and during the Preboreal, it is as high as 1,100 ^{14}C years. During the Younger Dryas, the ^{14}C reservoir age is low. It drops abruptly from 800 ^{14}C years to 200 ^{14}C years. The ^{14}C reservoir drops again at the onset of the entrance of the Mediterranean water in the transition period to 400 ^{14}C years and remains low until today.

3.3 Stable isotopes

The $\delta^{18}O$ and $\delta^{13}C$ measurements from the Black Sea mollusk record and the Sofular cave are aligned next to each other (**Figure 4-9**). In the Glacial period, the mollusk stable isotope record is limited, largely as a consequence of limited sampling. In the Sofular cave $\delta^{18}O$ record, small increases of 0.5 to 1 ‰ are interpreted as Dansgaard / Oeschger (D/O) cycles whereas small decreases of 0.5 to 1 ‰ are interpreted as Heinrich Events (Fleitmann et al., 2009; Badertscher et al., 2011). In the Sofular cave $\delta^{13}C$ record, decreases up to 2 to 3 ‰ are interpreted as D/O cycles and increases of 1 to 2 ‰ are interpreted as Heinrich events. There is no cave deposition in the period of 24 21.50 kyr BP. This is near the timing of the Heinrich Event 2 at 24 kyr BP (Bond et al., 1992; Bond et al., 1993; Hemming, 2004).

At the onset of the meltwater at 16.35 kyr BP, near but not entirely coincidental with the timing of Heinrich Event 1 at 16.80 kyr BP (Bond et al., 1992; Bond et al., 1993; Hemming, 2004), the $\delta^{18}O$ drops 1.2 ‰ and remains low until 15 kyr BP in both the mollusk and Sofular cave $\delta^{18}O$ records. The $\delta^{13}C$ composition of the Sofular Cave drops rises by about 1 ‰. This

change is not very clear in the mollusk $\delta^{13}C$ record. After the end of the meltwater event in the Black Sea, the $\delta^{18}O$ rises by 0.5 ‰ in both the mollusk and Sofular Cave $\delta^{18}O$ records in the period referred to as the Older Dryas, 15 to 14.70 kyr BP. The $\delta^{13}C$ composition in the mollusk record and Sofular Cave records remains unchanged.

Large changes occur at the onset of the Bølling/Allerød period in both the $\delta^{18}O$ and $\delta^{13}C$ records. The $\delta^{18}O$ increases by 2 ‰ and the $\delta^{13}C$ decreases by 2 ‰. There is limited mollusk stable isotope data after the onset of the Bølling/Allerød as the records are absent because of a regression of the lake and exposure of the shelf to the atmosphere, arresting the accumulation of lake sediments. The $\delta^{18}O$ and $\delta^{13}C$ composition of the Sofular Cave both stabilizes by the end of the Bølling/Allerød.

At the onset of the Younger Dryas, the trends in the $\delta^{18}O$ and $\delta^{13}C$ composition of the mollusk and Sofular cave reverse. The $\delta^{18}O$ stabilizes in the mollusk record at 4 ‰ and in the Sofular cave record at – 12 ‰. The $\delta^{13}C$ rises by 2.5 ‰ in the mollusk and Sofular cave records. At the onset of the Preboreal period, the trends in the $\delta^{18}O$ and $\delta^{13}C$ composition reverse again. The mollusk stable isotope record is largely absent, once again because records are not available as a consequence of regression. In the Sofular Cave, the $\delta^{18}O$ rises by about 2 ‰ and the $\delta^{13}C$ drops by 3 ‰, a larger change than that which occurs during the Bølling/Allerød warming earlier.

The Preboreal period in the Black Sea ends upon the connection of the Black Sea with the Mediterranean at 9.30 kyr BP. The $\delta^{18}O$ rises by 2 ‰ in the mollusk record and by about 1 ‰ in the Sofular cave record; the change is more abrupt in the mollusk records. The $\delta^{13}C$ rises by about 1 ‰ in both the mollusk and the Sofular cave records. For the duration of the Holocene, the $\delta^{18}O$ of both the mollusk record and the Sofular cave record is stable at 0.5 ‰ and

-8 ‰, respectively. The $\delta^{13}C$ of the mollusk and Sofular cave records oscillates by about 1 ‰. In the Sofular cave record, there are two large changes that occur at 6 and 3.90 kyr BP.

3.4 Radiogenic isotopes

During the glacial period, the $^{87}Sr/^{86}Sr$ composition of both the Black Sea-Lake and Marmara Sea-Lake is in the range of 0.7086 to 0.7088. There is a decrease in the $^{87}Sr/^{86}Sr$ of Marmara Sea-Lake water at 20 kyr BP and a subsequent rise to 0.7088 500 years later. It is not clear if the $^{87}Sr/^{86}Sr$ of the Black Sea-Lake is identical to that of the Marmara Sea-Lake near this time as the record is not thorough. Immediately prior to the onset of the meltwater event into the Black Sea-Lake and Marmara Sea-Lake, the $^{87}Sr/^{86}Sr$ of both lakes is 0.7087. At the onset of the meltwater, the $^{87}Sr/^{86}Sr$ abruptly rises to 0.7091. The magnitude of the shift is identical in both lakes. At the onset of the Older Dryas, the $^{87}Sr/^{86}Sr$ in the Black Sea-Lake drops to below 0.7088 whereas in the Marmara Sea-Lake drops to 0.7085. The $^{87}Sr/^{86}Sr$ composition is identical immediately after that at 14.80 kyr BP.

At 14.70 kyr BP, the $^{87}Sr/^{86}Sr$ composition of the two lakes bifurcates. The $^{87}Sr/^{86}Sr$ composition of Marmara Sea-Lake rises to 0.70915 and the $^{87}Sr/^{86}Sr$ composition of the Black Sea-Lake remains at 0.70885. The $^{87}Sr/^{86}Sr$ composition of the Sea of Marmara remains at 0.70915 for the duration of the record (i.e., Bølling/Allerød to present). The $^{87}Sr/^{86}Sr$ composition of the Black Sea during the Younger Dryas drops slightly to 0.70884. The $^{87}Sr/^{86}Sr$ composition of the Black Sea during the Preboreal is not recorded due to absence of mollusks during this period and not supplemented by the $^{87}Sr/^{86}Sr$ composition of the ostracodes. At 9,300 calendar years, the $^{87}Sr/^{86}Sr$ composition rises to 0.70913. The Black Sea water $^{87}Sr/^{86}Sr$ composition remains at this value for the duration of the record.

4. Discussion

4.1 Marine Isotope Stage 6

During Marine Isotope Stage 6 (MIS 6), a period spreading from 185 to 130 kyr (Emiliani, 1955; Lisiecki and Raymo, 2004), it is inferred from the chirp profiles (**Figures 4-2 through 4-8**) and from dinoflagellate cyst assemblages (Shumilovskikh et al., 2013) that the Black Sea-Lake was fresh and outflowing to the Sea of Marmara and consequently, to the Mediterranean Sea (**Figure 4-12**). The Mediterranean Sea, connected to the global ocean, was depressed relative to the Dardanelles and Bosporus inlets, and reconstructed to a depth of 100 to 130 mbsl (Lambeck et al., 2002; Siddall et al., 2003; Rohling et al., 2010). Ross, (1978), Svitoch, (2009), Fleitmann et al., (2009), and Badertscher et al., (2011) all show the Black Sea-Lake was fresh during glacial periods/stadials and marine during warmer periods/interstadials. This is particularly clear in the $\delta^{18}O$ and $\delta^{13}C$ reconstructions from a thoroughly dated speleothem deposit from Sofular Cave on the northern Turkish coast (Fleitmann et al., 2009; Badertscher et al., 2011). The speleothem $\delta^{18}O$ reflects evaporated Black Sea water (Fleitmann et al., 2009; Badertscher et al., 2011) and $\delta^{13}C$ reflects a common source of DIC (Yanchilina et al., submitted). The chirp profiles on all of the Black Sea-Lake shelves (**Figures 4-2 to 4-7**) and on the Marmara Sea-Lake (**Figure 4-8**) shelf show continuous build up of sediment and river deltas seaward of the inferred 95 mbsl paleoshoreline. It is inferred that the Bosporus sill was at its bedrock depth and therefore much deeper than today (Fig. 11).

4.2 Marine Isotope Stage 5

During Marine Isotope Stage 5 (MIS 5), a period spreading from to 130 to 80 kyr (Emiliani, 1955; Lisiecki and Raymo, 2004), the Black Sea and the Sea of Marmara were connected to the Mediterranean Sea and the global ocean (**Figure 4-13**). This was a warm interglacial stage with a global sea level up to 5 m above modern global sea level (Lambeck et al., 2002; Siddall et al., 2003; Rohling et al., 2010). The Black Sea and the Sea of Marmara were fully marine during this period (Ross, 1978; Fleitmann et al., 2009; Svitoch, 2009; Badertscher et al., 2011). It is likely that the fresher water outflowed at the surface and the marine water entered as an undercurrent across the Dardanelles and Bosporus inlets as it does today (Ünlüata et al., 1990). Dating the change in the dinoflagellate cyst assemblage Shumilovskikh et al., (2013) suggests that the depths of the Bosporus and Dardanelles inlets were at 15 mbsl (**Figure 4-13**) and much shallower relative to what their depths were during the preceding glacial period. This is a similar phenomenon that occurred during the deglaciation from Marine Isotope Stage 2 to the Holocene, when the Bosporus sill was likely infilled at a time when it was subaerial. Shumilovskikh et al., (2013) also shows that the connection between the global ocean and the Black Sea-Lake occurred at 128 kyr, a transition that was delayed relative to a situation in which the Bosporus sill would be much deeper and at its bedrock.

4.3 Marine Isotope Stage 3

During Marine Isotope Stage 3 (MIS 3), a period spreading from 57 to 30 kyr (Emiliani, 1955; Lisiecki and Raymo, 2004), the Black Sea-Lake was fresh, its lake level at the bedrock sill, and outflowing to the Sea of Marmara and consequently to the Mediterranean Sea (**Figure 4-14**). It is certain the Black Sea-Lake was fresh during this period from the porewater $\delta^{18}O$ reconstruction (Manheim and Chan, 1974; Soulet et al., 2010), fauna, and $\delta^{18}O$ isotopes. It is

also certain the Black Sea-Lake was outflowing to the Sea of Marmara as the two basins shared $CaCO_3$ concentration in sediments (Çağatay et al., 2015). The lake level of both the Black Sea-Lake and the Sea of Marmara was at approximately 80 mbsl as there is no sediments deposited dated to this period landward of the inferred paleoshoreline for both basins. This inference suggests that the global sea level had to be below 80 mbsl during MIS 3, an interpretation that is in conflict with the global sea level curve constructed for this period (Lambeck et al., 2002; Siddall et al., 2003; Rohling et al., 2010).

This inference also suggests that more water from the global ocean was locked up in ice sheets, necessary to depress the global sea level relative to what it is now interpreted to be at MIS 3. Hence, the global ocean $\delta^{18}O$ would imply it was much warmer during MIS 3 from the $\delta^{18}O$-temperature relationship (Erez and Luz, 1983) than the $\delta^{18}O$ and paleotemperature reconstructions show for that time period. Alternatively, it may be argued that the outflow from the Black Sea-Lake and the Marmara Sea-Lake was so strong that it would prevent any inflow from the Mediterranean Sea. This possibility cannot be ruled out as Lane-Serff et al., (1997) previously showed that for an outflow rate equal to that of today across the Bosporus strait, the global sea level would have to be 5 m higher relative to sill for this scenario to occur. However, even if this was true, the global sea level would still have to be at the very most 75 mbsl, a depth that is still lower than many of the modern global sea level reconstructions for MIS 3.

4.4 Marine Isotope Stage 2

During the beginning of the Marine Isotope Stage 2, a period spreading 29 to 11.7 kyr (Emiliani, 1955; Lisiecki and Raymo, 2004), but here focused on the early part of MIS 2, 29 to 24 kyr, the Black Sea-Lake continued to be fresh and outflowing through a deep sill to the

Marmara Sea-Lake and the Mediterranean Sea (**Figure 4-15**). During MIS 2, the global sea level was at 120 mbsl (Lambeck et al., 2002; Siddall et al., 2003; Rohling et al., 2010). It is certain that the Black Sea-Lake was outflowing to the Marmara Sea-Lake as the $^{87}Sr/^{86}Sr$ composition of the water of both basins at this period is identical (**Figure 4-11**). The $\delta^{18}O$ of the Black Sea surface water is uniform, suggesting it was continuously fed by water of uniform $\delta^{18}O$ composition (**Figure 4-10**) and did not experience any regressions. Such a scenario would otherwise have a much more dramatic effect on the $d^{18}O$, as processes such as evaporation and negative water balance would increase $\delta^{18}O$.

It is likely that the Black Sea responded to a colder climate relative to MIS 3 by growing perennial ice cover. This is interpreted from an increased ^{14}C reservoir of the surface Black Sea water (**Figure 4-9**). Currently, there are many observations of methane seeps on the Black Sea basin floor (Peckmann et al., 2001; Reitner et al., 2005; Schmale et al., 2005; Naudts et al., 2006) and a surface ^{14}C reservoir age of 470 ^{14}C years (Siani et al., 2000). In its modern configuration, the Black Sea surface water is in contact with the atmosphere and allows for ^{14}C equilibration. In a scenario where such an exchange would be prevented to take place, such as perennial ice cover, the ^{14}C reservoir of the surface water would rise.

4.5 Heinrich Event 2

Heinrich Event 2 (HE 2) occurred from 24.5 to 21 kyr (Hemming, 2004). This event coincides with a period of non-deposition in the Sofular Cave (Fleitmann et al., 2009; Badertscher et al., 2011). This observation suggests that the Black Sea-Lake may have completely frozen over and ceased outflow (**Figure 4-16**). It may have gotten so cold in northern Turkey as a result of colder conditions and increased ice cover that all of the water that

previously percolated through soil to build the carbonate deposited in the Sofular Cave became frozen and became permafrost. An ice-covered lake surface covering ~400,000 km^2 would reinforce the colder regional temperatures through an albedo effect. This interpretation is supported by $^{87}Sr/^{86}Sr$ composition of Black Sea-Lake and Marmara Sea-Lake as there is a slight bifurcation between the two $^{87}Sr/^{86}Sr$ respective records during this period (**Figure 4-11**). The $^{87}Sr/^{86}Sr$ of the Marmara Sea-Lake decreases to a less radiogenic composition, suggesting a larger fraction of Turkish water relative to the average inflow from the Black Sea-Lake (0.7088) (Major et al., 2006). The $\delta^{18}O$ composition of Black Sea-Lake (**Figure 4-10**) and Marmara Sea-Lake (Vidal et al., 2010) are very similar and do not show this potential arrest of Black Sea-Lake outflow to the Marmara Sea-Lake at this period. The ^{14}C age of the surface water continues to rise extensively during this period, also suggesting at colder conditions, given that its rise is caused by increase in perennial ice cover. A more thorough $^{87}Sr/^{86}Sr$ and/or ε_{Nd} reconstructions would be able to more clearly show whether or not this phenomena occurred as these proxies are not effected by vital effects or changes in the hydrological balance such as evaporation.

4.6 LGM

After the end of the HE 2 event and with the beginning of the Last Glacial Maximum (LGM) at 21 kyr (Yokoyama et al., 2000), the Black Sea-Lake resumed outflow to the Marmara Sea-Lake which outflowed to the global ocean at a global sea level of 120 mbsl (**Figure 4-17**). This is interpreted from observations of common $^{87}Sr/^{86}Sr$ (**Figure 4-11**) and $\delta^{18}O$ composition of water (i.e., (**Figure 4-10** and (Vidal et al., 2010)) in both the Black Sea-Lake and Marmara Sea-Lake. The Bosporus sill continued to be at 80 mbsl as observed from accumulation of sediments of this age only seaward of the inferred paleoshoreline of 95 mbsl. The Black Sea-

Lake continued to be fresh as observed from the faunal composition dominated by a freshwater mollusk *Dreissena rostriformis*. The ^{14}C reservoir age reaches its highest value at this time, as large as 2000 ^{14}C years (**Figure 4-9**). This observation is interpreted by proposing a scenario in which the temperatures increased such that outflow from the Black Sea-Lake to the Marmara Sea-Lake resumed but did not increase so much as to melt enough ice to allow the surface Black Sea-Lake water to exchange with the atmosphere to bring the ^{14}C reservoir age down.

4.7 Meltwater

Conditions that persisted in the Black Sea-Lake and Marmara Sea-Lake during the glacial period came to end upon the onset of a gigantic meltwater event of deglacial water that entered the Black Sea-Lake and also, the Marmara Sea-Lake, outflowing to the Mediterranean Sea (**Figure 4-18**). The global sea level continued to be low during this period at 120 mbsl (Lambeck et al., 2007). The amount of meltwater that entered the Black Sea-Lake and then, the Marmara Sea-Lake, was so large such as to change both the $^{87}Sr/^{86}Sr$ and $\delta^{18}O$ composition of the entire water column of both the Black Sea-Lake and the Marmara Sea-Lake (**Figure 4-11**, **Figure 4-10**) and (Vidal et al., 2010). The sediments that belong to this event are identified by a unique red/brown chocolate color (Chepalyga, 1984; Major et al., 2002; Major et al., 2006; Chepalyga, 2007; Soulet et al., 2013) and are found everywhere on the northwestern Black Sea shelf seaward of the 95 mbsl paleoshoreline, slope and basin (**Figures 4-2 to 4-8**). The water that enters the Black Sea-Lake drops the accumulated ^{14}C reservoir age of the water to essentially zero (**Figure 4-9**). The meltwater that enters the Black Sea-Lake is completely equilibrated with the atmosphere and comes in such vast volumes, such as potentially displace all of the water in the Black Sea-Lake. The meltwater decreases is able the Black Sea-Lake's ^{14}C

reservoir age and ventilates the entire Black Sea water column as this change in the ^{14}C reservoir is independent of depth.

4.8 Older Dryas

During the period referred to as the Older Dryas that occurred from 15 kyr to 14.8 kyr in the Black Sea-Lake (Yanchilina et al., submitted), the Black Sea-Lake continued to outflow to the Marmara Sea-Lake, which continued to outflow to the Mediterranean Sea (**Figure 4-19**). This event is ascribed to take time from 15 kyr to 14.8 kyr from an alignment of the $\delta^{18}O$ and $\delta^{13}C$ isotopes in the Black Sea mollusk and Sofular cave records. The global sea level reached 90 mbsl by 14.8 kyr (Lambeck et al., 2007). The Bosporus sill remained deep and at its bedrock as no sediments are found landward of the inferred 95 mbsl paleoshoreline that date to this time period (**Figure 4-7**). Major et al., (2006) was the first to recognize the Older Dryas in the context of the Black Sea paleoceanography. It is contested that the Black Sea-Lake continued to outflow to the Marmara Sea-Lake from the identical $^{87}Sr/^{86}Sr$ and $\delta^{18}O$ composition of water in both basins ((**Figure 4-10**, **Figure 4-11**) and (Vidal et al., 2010)), as was the case for the MIS 2, LGM, and ME. The $^{87}Sr/^{86}Sr$ composition of water became less radiogenic in both basins, indicative of an arrest of meltwater from the north and resumption of pre-meltwater river activity. The ^{14}C reservoir age of the water column in the Black Sea-Lake continued to be low, essentially zero, suggesting water continued to equilibrate with the atmosphere very efficiently.

4.9 Bølling/Allerød

In the Bølling/Allerød stage of the Black Se paleoceanographic history, a period that occurred between 14.8 to 12.9 kyr BP, the global sea level rose to 60 mbsl (Lambeck et al.,

2007). Three very large changes occurred. Foremost, the Black Sea-Lake no longer outflowed to the Sea of Marmara (**Figure 4-20**). The warmer temperatures (Soulet et al., 2011a) during the Bølling/Allerød changed the hydrologic balance of the Black Sea-Lake such that evaporation exceeded river inflow and precipitation, leading to a severe regression of at least 165 mbsl, maybe lower. This regression is interpreted from a lack of sediments that date to this period from depths of 95 mbsl to 165 mbsl everywhere on the Black Sea-Lake Ukrainian, Romanian, Bulgarian, and Turkish shelves. The $\delta^{18}O$ composition of the water increased. This is partially explained by the increase of $\delta^{18}O$ of northern precipitation but also is likely to be characteristic of evaporation, a process that would lead to preferential evaporation of the lighter of the oxygen isotopes and leading an enrichment in the heavier isotope of oxygen, ^{18}O. The $^{87}Sr/^{86}Sr$ composition of the water remains unchanged during this period, indicating that the $^{87}Sr/^{86}Sr$ of inflowing river remains unchanged. This is also a period when the ^{14}C reservoir of the surface water rises and likely expresses thermobaric stratification, limiting the ^{14}C equilibration of all but the very surface water of the Black Sea. The mollusks which were used to measure the $\delta^{18}O$ and $\delta^{13}C$ composition likely inhabited water that was 50 mbsl deep and hence do not necessarily represent the surface water $\delta^{18}O$ and $\delta^{13}C$ composition and acquired a ^{14}C reservoir age.

The bifurcation of the $^{87}Sr/^{86}Sr$ water composition of the Black Sea-Lake and the Sea of Marmara at the onset of the Bølling/Allerød suggests that the Black Sea-Lake remained fresh at this period while the Sea of Marmara became connected with the global ocean. The $\delta^{18}O$ water composition of the Sea of Marmara also rises to that of the global ocean (Vidal et al., 2010). Nicholas and Chivas, (2014) was first to propose that the Bosporus sill likely changed its depth sometime in the deglacial period. The close examination of the $^{87}Sr/^{86}Sr$ isotopes and global sea

level reconstructions (Lambeck et al., 2007) allow to suggest that the Bosporus sill likely filled up with sediments at the very beginning of the Bølling/Allerød.

4.10 Younger Dryas

The Younger Dryas period in the Black Sea occurred between 12.9 and 11.9 kyr BP. The global sea level rose to 52 mbsl by the end of the stadial (Lambeck et al., 2007). With the onset of Younger Dryas and the change of surface lake temperature to colder (Soulet et al., 2011a), the level of the Black Sea-Lake regressed to at least 95 mbsl (**Figures 4-2 to 4-8**). The regression is inferred from the deposition of sediments that date to this time period from shelf depths of 95 mbsl and below. These sediments on the shelf also accumulate on a coquina, interpreted as a ravinement surface, that was progressively colonized by mollusks as it formed. The lake continued to be fresh from the observation of the trends in $\delta^{18}O$ (Fig. 9), $^{87}Sr/^{86}Sr$ (**Figure 4-11**), and porewater chlorinity (Soulet et al., 2010). The mollusk assemblage continued to be dominated by *Dreissena rostriformis*. The $\delta^{18}O$ composition of the surface water remained stable at 4 ‰, likely indicating decreased evaporation and a uniform river source. The ^{14}C reservoir age of the surface water decreased, likely explained by increased ventilation of the water column.

It is not clear what was the actual rise in lake level during Younger Dryas (**Figure 4-21**). The accumulation of sediments on the shelf clearly shows that the lake level rose to at least 95 mbsl. It is not clear whether the lake may have risen higher than that, as the depth of the Bosporus sill, would have to be at 35 mbsl during this period to prevent inflow from the Sea of Marmara. It may be a mere coincidence that the lake level rose to 95 mbsl, the inferred glacial

paleoshoreline that formed as a consequence of a deep Bosporus sill, but is an inconsistency between observations and interpretations that needs to be explored and discussed further.

4.11 Preboreal

The Preboreal period in the Black Sea occurred from 11.9 to 9.3 kyr BP. The surface water temperature rose at this time (Soulet et al., 2011a). The global sea level rose to 35 mbsl during this period (Lambeck et al., 2007). The Black Sea-Lake level regressed again, identical to the scenario that occurred during the Bølling/Allerød warming, also at least to a depth of 165 mbsl (**Figure 4-22**). The $\delta^{18}O$ continued to rise as indicated from the increase in the $\delta^{18}O$ composition of Sofular cave (**Figure 4-10**). This trend is not observed in the mollusk $\delta^{18}O$ composition as mollusks are absent from shelf sediment during this period, ascribed to the regression of the lake. The ^{14}C reservoir age of the water increased again to a value higher than that ascribed to the Bølling/Allerød warming. This observation is also explained by the thermobaric stratification of the water column as a consequence of warmer temperatures and increased evaporation rates. The Black Sea-Lake remained fresh during this interval as observed from the $\delta^{18}O$ composition of bulk carbonate (Major et al., 2006), $\delta^{18}O$ of deep water, porewater chloride (Soulet et al., 2010), and dinoflagellate assemblage (Filipova-Marinova et al., 2013). $^{87}Sr/^{86}Sr$ measurements from mollusks on the shelf are absent for this period as the water level regressed and sediments on the shelf did not accumulate and $^{87}Sr/^{86}Sr$ measurements from ostracodes are not available but will be the focus of future work.

4.12 Transgression

At 9.3 kyr BP, the global sea level reached 35 mbsl (Lambeck et al., 2007) and breached the Bosporus sill at its modern depth of 35 mbsl and marine water from the Sea of Marmara entered the Black Sea-Lake (**Figure 4-23**). This phenomena is observed in the increase of $^{87}Sr/^{86}Sr$ to that of the global ocean (**Figure 4-11**), the increase of Sr/Ca to higher values (Bahr et al., 2008), increase of $\delta^{18}O$ of surface water to that of the global ocean (**Figure 4-10**), and a decrease of the ^{14}C reservoir of the water to 330 ^{14}C years. It is likely that the much denser marine water from the Sea of Marmara descended into the interior of the Black Sea and lifted the surface water, fresh and light, progressively mixing in. The surface water changed salinity much slower than the interior water due to initial strong stratification between the two layers. The marine mollusks colonized the regression surface after the initial salinification and those mollusks that are found in situ with the freshwater mollusks (Yanchilina et al., submitted) bioturbated into the sediment below, a phenomena that is prevalent everywhere in the upper 10 cm of sediment with a sufficient oxygen content. This initial transgression and salinification occurred at most in a couple decades and was a rapid event.

4.13 Post connection

After the Black Sea-Lake connected to the Sea of Marmara and the global ocean at 9.3 kyr BP, the Black Sea rose in tandem with global sea level to its modern depth (**Figure 4-24**). The complete salinification of the Black Sea took 1,500 calendar years (**Figure 4-10** and **Figure 4-11**) as observed from the time it takes the marine mollusks to achieve the modern $^{87}Sr/^{86}Sr$ and $\delta^{18}O$ water composition. The rising level of the global sea level relative to the Bosporus sill also eventually allowed for the modern flow across the Bosporus to be developed, similar to that which developed in the Sea of Marmara at 14.7 kyr BP. The ^{14}C reservoir age remained low and

similar to that of the global ocean at 415 ^{14}C years (Siani et al., 2000). The Sofular cave shows several oscillations in its $\delta^{18}O$ and $\delta^{13}C$ composition of the carbonate but these changes are not seen in the Black Sea mollusk record. This observation is ascribed to a poor age model for the post-connection Holocene and a necessity for more detailed $\delta^{18}O$ and $\delta^{13}C$ measurements.

5. Conclusions

Synthesis of chirp profiles, cores, radiocarbon dating, stable and radiogenic isotopes allows the development of an alternative view to the paradigms of water exchange over a fixed-depth sill linking the Black Sea, Sea of Marmara, and the Mediterranean Sea from MIS 6 to present. The major changes that have occurred are separated into thirteen time periods:

- MIS 6: During MIS 6, the Black Sea Lake was in a positive hydrological balance and outflowing to the Sea of Marmara, which was consequently also outflowing to the Mediterranean Sea/global ocean.
- MIS 5: During MIS 5, the Black Sea and the Sea of Marmara were connected to the Mediterranean Sea/global ocean and were both marginal saline seas. The configuration of water circulation was similar to the present.
- MIS 3: During MIS 3, the Black Sea was a freshwater lake outflowing to the Sea of Marmara (also a lake), which was consequently outflowing to the global ocean.
- MIS 2: During MIS 2, the configuration of water exchange between the Black Sea-Lake and the Marmara Sea-Lake was similar to that of MIS 3 except when temperatures became sufficiently cold such that perennial ice cover started to grow.

- Heinrich Event 2: During extreme regional climate conditions of Heinrich Event 2, the Black Sea-Lake may have completely frozen over, and possibly causing a marked decrease or even cessation of outflow to the Marmara Sea-Lake.
- Last Glacial Maximum: During the Last Glacial Maximum, the Black Sea-Lake resumed outflow to the Marmara Sea-Lake although perennial ice cover continued.
- Meltwater Event: As the Earth started to come out of the glacial period at the time of HE 1, the first major deglaciation event involved large amounts of meltwater entering the Black Sea-Lake and Marmara Sea-Lake, leading in turn to substantial outflow to the Mediterranean Sea/global ocean.
- Older Dryas: Upon the end of the meltwater delivery from the melting ice sheets, prior river activity resumed. The Black Sea-Lake continued to be in a positive hydrologic balance and continued to outflow to the Marmara Sea-Lake which outflowed to the Mediterranean Sea/global ocean.
- Bølling/Allerød: Upon the onset of a regional warming interval, the hydrologic budge in the Black Sea-Lake changed and the lake largely regressed so that the outflow to the Marmara Sea-Lake was disrupted. At this time, the global sea level reached the threshold depth of the Dardanelles sill and marine water entered the Sea of Marmara. The Bosporus sill depth became infilled with sediments over tens of meters and evolved from deep to shallow.
- Younger Dryas: In response to a change to regionally colder conditions during Younger Dryas, the hydrological balance in the Black Sea-Lake became positive and the lake transgressed but did not reach the threshold depth of the Bosporus sill and did not outflow to the Sea of Marmara.

- Preboreal: The end of the Younger Dryas interval brought a return change in the regional deglacial climate towards warmer temperatures. This shifted the hydrological balance in the Black Sea towards negative and the lake regressed again.
- Early Holocene Transgression: Once the global sea level reached the threshold depth of the shallow Bosporus sill, marine water breached the sill and led to a rapid transgression across the Black Sea shelf such.
- Holocene marine stage: After the end of the initial transgression, the Black Sea level rose in tandem with the global sea level.

The delayed entry of marine water into the Black Sea-Lake during the Eemian and early Holocene intervals both require a shallow sill whereas it is clear that in the preceding glacial periods, the sill was deeper. Careful examination of the data presented in this manuscript for the most recent scenario allows to infer that the Bosporus sill must have filled up with sediments early in the Bølling/Allerød warming. This is likely the case for the MIS 6 to Eemian deglacial transition as well. Knowledge regarding the level of the sill that allows exchange of water between basins serves as a potentially powerful tool for estimating prior global sea level. The inferred sill depth of 80 mbsl during MIS 3, combined with the absence of any evidence for a marine incursion into the Black Sea, strongly suggests that the global sea level must have remained below that level throughout the interval, and implies that global temperatures at that time based on foraminifera $\delta^{18}O$ may be underestimated.

References

Apakidze, A. M. and A. A. Burchuladze, 1987. Radiouglerodnoe datirovanie arkheologicheskikh i paleobotanicheskikh abraztzov Gruzii (Radiocarbon dating of archaeological and paleobotanical samples in georgia). Tbilisi, Georgia, Metsniereba.

Badertscher, S., D. Fleitmann, H. Cheng, R. L. Edwards, O. M. Göktürk, A. Zumbühl, M. Leuenberger and O. Tüysüz, 2011. Pleistocene water intrusions from the Mediterranean and Caspian seas into the Black Sea. Nat. Geosci. 4, 236-239.

Bahr, A., F. Lamy, H. W. Arz, C. Major, O. Kwiecien and G. Wefer, 2008. Abrupt changes of temperature and water chemistry in the late Pleistocene and early Holocene Black Sea. Geochem. Geophy. Geosy. 9.

Bailey, T. R., J. M. McArthur, H. Prince and M. F. Thirwall, 2000. Dissolution methods for strontium isotope stratigraphy: Whole rock analysis. Chemical Geology 167, 313-319.

Bond, G., W. Broecker, S. Johnsen, J. McManus, L. Labeyrie, J. Jouzel and G. Bonani, 1993. Correlations between climate records from North Atlantic sediments and Greenland ice. Nature 365, 143-147.

Bond, G., H. Heinrich, ;, W. Broecker, L. Labeyrie, J. McManus, J. Andrews, S. Huon, R. Jantschik, S. Clasen, C. Simet, K. Tedesco, M. Klas, G. Bonani and S. Ivy, 1992. Evidece for massive discharges of icebergs into the North Atlantic ocean during the last glacial period. Nature 360, 245-249.

Çağatay, M. N., S. Wulf, Ü. Sancar, A. Özmaral, L. Vidal, P. Henry, O. Appelt and L. Gasperini, 2015. The tephra record from the Sea of Marmara for the last ca. 70 ka and its paleoceanographic implications. Marine Geology 361, 96-100.

Chepalyga, A., 2007. The late glacial great flood in the ponto-caspian basin. In: V. Yanko-Hombach, A. Gilbert, N. Panin and P. Dolukhanov (Eds.), The Black Sea flood Question: Changes in Coastline, Climate, and Human Settlement. Dordrecht, The Netherlands, Springer**:** 119-148.

Chepalyga, A. L., 1984. Inland sea basins. In: A. A. Velichko, H. E. J. Wright and W. Barnosky-Cathy (Eds.), Late Quaternary environments of the Soviet Union. Mineapolis, MN, United States, Univ. Minn. Press.**:** 229-247.

Cohen, D. and W. B. F. Ryan, 2011. Black Sea low stands during the Holocene and Pleistocene and reconnection with the global ocean.

Deuser, W. G., 1972. Late-Pleistocene and Holocene history of the Black Sea as indicated by stable isotope studies. Jour. Geophys. Res. 77, 1071-1077.

Emiliani, C., 1955. Pleistocene Temperatures. The Journal of Geology 63, 538-578.

Erez, J. and B. Luz, 1983. Experimental paleotemperature equation for planktonic formainifera. Geochimica et Cosmochimica Acta 47, 1025-1031.

Filipova-Marinova, M., D. Pavlov, M. Coolen and L. Giosan, 2013. First high-resolution marinopalynological stratigraphy of Late Quaternary sediments from the central part of the Bulgarian Black Sea area. Quatern. Int. 293, 170-183.

Fleitmann, D., H. Cheng, S. Badertscher, R. L. Edwards, M. Mudelsee, O. M. Göktürk, A. Fankhauser, R. Pickering, C. C. Raible, A. Matter, J. Kramers and O. Tüysüz, 2009. Timing and climatic impact of Greenland interstadials recorded in stalagmites from northern Turkey. Geophysical Research Letters 36.

Hemming, S. R., 2004. Heinrich events: massive late Pleistocene detritus layers of the north Atlantic and their global climate imprint. Reviews of Geophysics 42, RG1005.

Ivanova, E. V., I. O. Murdmaa, A. L. Chepalyga, T. M. Cronin, I. V. Pasechnik, O. V. Levchenko, H. S.S, A. V. Manushkina and E.A.Platonova, 2007. Holocene sea-level oscillations and environmental changes on the Eastern Black Sea shelf. Palaeogeogr. Palaeoclimatol. Palaeoecol. 246, 228-259.

Kaplin, P. A. and F. A. Shcherbakov, 1986. Reconstructions of paleogeographic environments on the shelf during the late Quaternary time. Oceanology 26, 736-738.

Karakilcik, H., U. Can Unlugenc and M. Okyar, 2014. Late glacial-Holocene shelf evolution of the Sea of Marmara west of Istanbil. Journal of African Sciences 100, 365-378.

Konikov, E., O. Likhodedova and G. Pedan, 2007. Paleogeographic reconstructions of sea-level change and coastline migration on the northwestern Black Sea shelf over the past 18kyr. Quatern. Int. 167-168, 49-60.

Kuprin, P. N., F. A. Scherbakov and I. I. Morgunov, 1974. Correlation, age and distribution of the postglacial continental terrace sediments of the Black Sea. Baltica 5, 241-249.

Kwiecien, O., W. A. Helge, L. Frank, P. Birgit, B. André and H. H. Gerald, 2009. North Atlantic control on precipitation pattern in the eastern Mediterranean/Black Sea region during the last glacial. Quaternary Research 71.

Lambeck, K., T. M. Esat and E.-K. Potter, 2002. Links between climate and sea levels for the past three million years. Nature 419, 199-206.

Lambeck, K., D. Sivan and A. Purcell, 2007. Timing of the last Mediterranean Sea: Black Sea connection from isostatic models and regional sea-level data. In: V. Yanko-Hombach and A. S. Gilbert (Eds.), The Black Sea Flood Question: Changes in Coastline, Climate and Human Settlement. Heidelberg, Germany., Springer**:** 797-808.

Lane-Serff, G. F., E. J. Rohling, H. L. Bryden and H. Charnock, 1997. Post-glacial connection of the Black Sea to the Mediterranean and its relation to the timing of sapropel formation. Paleoceanography 12, 169-174.

Lericolais, G., I. Popescu and F. Guichard, 2007. A Black Sea lowstand at 8500 yr BP indicated by a relict coastal dune system at a depth of 90 m below sea level. In: J. Harff, W. W. Hay and D. M. Tetzlaff (Eds.), Coastline Changes: Interrelation of Climate and Geological Processes., GSA Books; Allen Press, Inc. 426**:** 171-188.

Lisiecki, L. E. and M. E. Raymo, 2004. A Pliocene-Pleistocene stack of 57 globally distributed benthic d18O records Paleoceanography 20.

Major, C., S. Goldstein, W. Ryan, G. Lericolais, A. M. Piotrowski and I. Hajdas, 2006. The co-evolution of Black Sea level and composition through the last deglaciation and its paleoclimatic significance. Quatern. Sci. Rev. 25, 2031-2047.

Major, C., W. Ryan, G. Lericolais and I. Hajdas, 2002. Constraints on Black Sea outflow to the Sea of Marmara during the last glacial–interglacial transition. Marine Geology.

Major, C. O., 2015. Unpublished $^{87}/^{86}$Sr records for Sea of Marmara: 25 kyr to present.

Manheim, F. T. and K. M. Chan, 1974. Interstitial waters of Black Sea sediments: New data and review. In: E. T. Degens and D. A. Ross (Eds.), The Black Sea - Geology, Chemistry and Biology. Tusla, Mem. Am. Assoc. Petrol. Geol. 20**:** 155-180.

McHugh, C. M. G., D. Gurung, W. B. F. Ryan, U. Sancar, L. Burckle, M. N. Çagatay, L. Capotondi and e. al., 2004. Late Pleistocene to Holocene Lacustrine to Marine Transition in the Marmara Sea: Implications for Climate and Water Mass Exchange. Geophysical Research Abstracts 6, 05897.

Mortlock, R., 2010. Description of stable isotope analysis at the Department of Earth and Planetary Sciences. Rutgers University.

Naudts, L., J. Greinert, Y. Artemov, P. Staelens, J. Poort, P. V. Rensbergen and M. De Batist, 2006. Geological and morphological setting of 2778 methane seeps in the Dnepr paleodelta, northwestern Black Sea. Marine Geology 227, 177-199.

Nicholas, W. A. and A. R. Chivas, 2014. Late Quaternary sea-level change on the Black Sea shelves. In: F. L. Chiocci and A. R. Chivas (Eds.), Continental shelves of the world: their evolution during the last glacial-eustatic cycle. London, Geological Society. 41**:** 199-212.

Nicholas, W. A., A. R. Chivas, C. V. Murray-Wallace and D. Fink, 2011. Prompt transgression and gradual salinisation of the Black Sea during the early Holocene constrained by amino acid racemization and radiocarbon dating. Quatern. Sci. Rev. 30, 3769-3790.

Nowaczyk, N. R., H. W. Arz, U. Frank, J. Kind and B. Plessen, 2012. Dynamics of the Laschamp geomagnetic excursion from Black Sea sediments. Earth and Planetary Science Letters 351-352, 54-69.

Peckmann, J., A. Reimer, U. Luth, C. Luth, B. T. Hansen, C. Heinicke, J. Hoefs and J. Reitner, 2001. Methane-derived carbonates and authigenic pyrite from the northwestern Black Sea. Marine Geology 177, 129-150.

Reimer, P. J., E. Bard, A. Bayliss, P. G. Blackwell, C. B. Ramsey, C. E. Buck, H. Cheng, R. L. Edwards, M. Friedrich, P. M. Grootes, T. P. Guilderson, H. Haflidason, I. Hajdas, C. Hatté, T. J. Heaton, D. L. Hoffmann, A. G. Hogg, K. A. Hughen, K. Kaiser, F.;, B. Kromer, S. W. Manning, M. Niu, R. W. Reimer, D. A. Richards, E. M. Scott, J. R. Southon, R. A. Staff, C. S. M. Turney and J. ven der Plicht, 2013. Incal13 and Marine13 radiocarbon age calibration curves 0-50,000 years Cal B.P. Radiocarbon 55, 1869-1887.

Reitner, J., J. Peckmann, M. Blumenberg, W. Michaelis, A. Reimer and V. Thiel, 2005. Concretionary methane-seep carbonates and associated microbial communities in Black Sea sediments. 227, 18-30.

Rohling, E. J., K. Braun, K. Grant, M. Kucera, A. P. Roberts, M. Siddall and G. Trommer, 2010. Comparison between Holocene and Marine Isotope Stage-11 sea-level histories. Earth and Planetary Science Letters 291, 97-105.

Ross, D. A., 1978. Black Sea stratigraphy. In: D. A. Ross and Y. P. Neprochnov (Eds.), Initial Reports of the Deep Sea Drilling Project. Washington DC, US Government Printing Office. 42, Part 2**:** 17-26.

Ross, D. A., 1978. Summary of results of Black Sea drilling. In: D. A. Ross, Y. P. Neprochnov and . (Eds.), Initial Reports of the Deep Sea Drilling Project. Washington, DC, US Government Printing Office. 42 Part 2**:** 1149 -1178.

Ross, D. A. and E. T. Degens, 1974. Recent sediments of the Black Sea. In: E. T. Degens and D. A. Ross (Eds.), The Black Sea - Geology, Chemistry and Biology. Tulsa, Amer. Assoc. Petrol. Geol. Mem. 20**:** 183-199.

Ryan, W. B. F., 2007. Status of the Black Sea flood hypothesis. In: V. Yanko-Hombach, A. S. Gilbert, N. Panin and P. M. Dolukhanov (Eds.), The Black Sea Flood Question: Changes in Coastline, Climate, and Human Settlement. Dordrecht, The Netherlands, Springer**:** 63-88.

Ryan, W. B. F., W. C. Pitman, III, C. O. Major, K. Shimkus, V. Moskalenko, G. Jones, P. Dimitrov, N. Gorur, M. Sakinc and H. Yuce, 1997. An abrupt drowning of the Black Sea shelf. Marine Geology 138, 119-126.

Ryan, W. B. F., W. C. Pitman, C. O. Major, K. Shimkus, V. Moscalenko, G. A. Jones, D. Dimitrov, P. Gorür, M. Sakinç and H. Y. Seyir, 1996. An abrupt drowning of the Black Sea shelf at 7.5 kyr BP. Geo-Eco-Marina, Malnas, Romania.

Ryan, W. B. F., D. Vachtman, C. McHugh, M. N. Çagatay and Y. Mart, 2013. A channeled shelf fan initiated by flooding of the Black Sea. In: S. Gofredo and Z. Dubinsky (Eds.), The Mediterranean Sea: Its history and present challenges**:** 11-27.

Scherbakov, F. A. and Y. V. Babak, 1979. Stratigraphic subdivision of the Neoeuxinian deposits in the Black Sea. Oceanology 19, 298-300.

Schmale, O., J. Greinert and G. Rehder, 2005. Methane emission from high-intensity marine gas seeps in the Black Sea into the atmosphere. Geophysical Research Letters 32.

Shumilovskikh, L. S., F. Marret, D. Fleitmann, H. W. Arz, N. R. Nowaczyk and H. Behling, 2013. Eemian and Holocene sea-surface conditions in the southern Black Sea: Organic-walled dinoflagellate cyst record from core 22-GC3. Marine Micropaleontology 101, 146-160.

Siani, G., M. Paterne, M. Arnold, E. Bard, B. Métivier, N. Tisnerat and F. Bassinot, 2000. Radiocarbon reservoir ages in the Mediterranean Sea and Black Sea. Radiocarbon 42, 271-280.

Siddall, M., E. J. Rohling, A. Almogi-Labin, C. Hemleben, D. Meischner, I. Schmelzer and D. A. Smeed, 2003. Sea-level fluctuations during the last glacial cycle. Nature 423, 853-858.

Soulet, G., G. Delaygue, C. Vallet-Coulomb, M. E. Böttcher, C. Sonzogni, G. Lericolais and E. Bard, 2010. Glacial hydrologic conditions in the Black Sea reconstructed using geochemical pore water profiles. Earth and Planetary Science Letters 296.

Soulet, G., G. Menot, G. Bavon, F. Rostek, E. Ponsevera, S. Toucanne, G. Lericolais and E. Bard, 2013. Abrupt drainage cycles of the Fennoscandian Ice Sheet Proceedings of the National Academy of Sciences 110, 6682-6687.

Soulet, G., G. Ménot, V. Garreta, F. Rostek, S. Zaragosi, G. Lericolais and E. Bard, 2011a. Black Sea "Lake" reservoir age evolution since the Last Glacial — Hydrologic and climatic implications. Earth Planet. Sc. Lett. 308, 245-258.

Svitoch, A. A., 2009. Khvalynian transgression of the Caspian Sea was not a result of water overflow from the Siberian Proglacial lakes, nor a prototype of the Noachian flood. Quatern. Int. 197, 115-125.

Ünlüata, Ü., T. Oguz, M. A. Latif and E. Özsoy, 1990. On the physical oceanography of the Turkish Straits. In: L. J. Pratt (Eds.), The Physical Oceanography of Sea Straits. Deventer, The Netherlands, Kluwer**:** 25-60.

Vidal, L., G. Ménot, C. Joly, H. Bruneton, F. Rostek, M. N. Çağatay, C. Major and E. Bard, 2010. Hydrology in the Sea of Marmara during the last 23 ka: Implications for timing of Black Sea connections and sapropel deposition. Paleoceanography 25.

Yanchilina, A. G., W. B. F. Ryan, J. F. McManus, P. Dimitrov, D. Dimitrov, K. Slavova and M. Filipova-Marinova, submitted. Rapid transgression and gradual salinification of the Black Sea from inflow of Mediterranean water in the Holocene. Marine Geology.

Yokoyama, Y., K. Lambeck, P. De Deckker, P. Johnston and K. Fifield, 2000. Timing of the Last Glacial Maximum from observed sea-level minima. Nature 406, 713-716.

Figures

Figure 4-1: (1) Location of the cores discussed in this study (colored circles); (2) Location of the inferred paleshoreline (i.e., thick red circumventing contour at -95 mbsl) around the periphery of the Black Sea; (3) Location of sills connecting Black Sea, Sea of Marmara, and Aegean Sea (aka global ocean basins) (yellow) and names of basins (black).

Figure 4-2: Chirp profile 6-12-304 from the Kerch area of the Black Sea. The clinoforms interpreted as those dating to MIS 3, 4, 6, etc are located between 100 and 120 mbsl.

Figure 4-3: Chirp profile WC-6-15-0005 from the Ukraine margin of the Black Sea. The clinoforms interpreted as those dating to MIS 3, 4, 6, etc are located below 100 mbsl.

Figure 4-4: Chirp profile BLaSON1-B008 from the Romanian margin of the Black Sea. The clinoforms interpreted as those dating to MIS 3, 4, 6, etc are located below 150 mbsl.

Figure 4-5: Chirp profile B2ch049 from the Bulgarian margin of the Black Sea. The clinoforms interpreted as those dating to MIS 3, 4, 6, etc are located below 100 mbsl.

Figure 4-6: Chirp profile composed by Dimitar Dimitrov (personal communication) for the Bulgarian shelf.

Figure 4-7: Chirp profile B2ch007 from the Turkish margin of the Black Sea. The clinoforms interpreted as those dating to MIS 3, 4, 6, etc are located below 100 mbsl.

Figure 4-8: Chirp profile adopted from Figure 7 of *Karakilcik et al*., [2014]. This is a line collected south of Yeşilköy, a neighborhood of Istanbul on the northern shelf (Çekmece), by the Department of Navigation, Hydrography, and Oceanography of the Turkish Navy in 1998. The profile shows the projection of two cores, MedEx05-2 and MedEx05-01 and the location of features that include: Neogene bedrock, erosion surface, lacustrine shelf-edge deposits, erosion surface, wave-cut cliff at the paleoshoreline and the marine drape.

Figure 4-9: The ^{14}C age of the surface water as a function of calendar age from multiple records: Derivation from work of *Nowaczyk et al*., [2013] (light blue dashed line); ash from deep cores published in *Kwiecen et al*., [2008] (navy blue diamonds); Comparison between ^{14}C dated wood and *Dreissena rostriformis* in AKAD09-28 (brown diamond); Published ^{14}C age from *Ryan et al*., [2007] (gray dashed line); published ^{14}C age from *Soulet et al*., [2011] (purple dashed line); ^{14}C age calculated from alignment of stable isotope records from surface mollusk record to that of Sofular Cave (solid red line); Adopted ^{14}C age of the water in the manuscript (dashed red line).

Figure 4-10: Top: $\delta^{18}O$ as a function of calendar age for Black Sea surface water (red diamonds) and Sofular Cave (gray contour); Bottom: same as (Top) but for $\delta^{13}C$. The different periods of deposition are indicated at the top; the numerous mollusk records are indicated in the legend.

Figure 4-11: $^{87}Sr/^{86}Sr$ for Black Sea and Sea of Marmara. The record used for each sea is indicated in the legend. The calendar age at which the two records diverge is indicated by a yellow contour oval.

Figure 4-12: Black Sea-Lake was outflowing to the Marmara Sea-Lake and the Mediterranean Sea, a basin connected to the global ocean and reconstructed to 100 to 130 mbsl (blue dashed line) during Marine Isotope Stage 6 (MIS 6). The diagram is reconstructed for a time period centered at the end of MIS6 at 145 kyr. The Bosporus sill and the Dardanelles sill are inferred to be at 80 mbsl and 83 mbsl, respectively. The Black Sea-Lake was fresh.

Figure 4-13: The Black Sea was connected to the Sea of Marmara and the Mediterranean Sea during Marine Isotope Stage 5 (MIS5). This figure is for the period at 120 kyr. The sea level was identical to that of the global ocean, reconstructed to 5 m above modern global sea level. A similar flow of water across the Bosporus and Dardanelles sills existed relative to today (black arrows). The sills are inferred to be infilled and shallower (15 mbsl).

Figure 4-14: Black Sea-Lake and Marmara Sea-Lake were fresh, at the bedrock sill of Bosporus and Dardanelles sills, and outflowing to the global ocean during Marine Isotope Stage 3 (MIS 3). The representative time for this period is taken at 40 kyr. The global sea level had to be deeper (below at least 75 mbsl) than previously reconstructed global sea level at the time (45-60 mbsl).

Figure 4-15: Black Sea-Lake is outflowing to the Marmara Sea-Lake and global ocean during the earlier period of Marine Isotope Stage 2 (MIS 2). Here, the beginning of MIS 2 is taken at 27 kyr. The arrows indicate outflow. The Bosporus and Dardanelles sills are deep at 80 mbsl and 83 mbsl, respectively. The global ocean is taken to be at 120 mbsl.

Figure 4-16: Black Sea-Lake became completely frozen over during Heinrich Event 2 (HE 2) and the outflow to the Marmara Sea-Lake and the global ocean may have ceased.

Figure 4-17: Black Sea-Lake is outflowing to the Marmara Sea-Lake which is outflowing to the Mediterranean Sea/global ocean during the Last Glacial Maximum (LGM). The global sea level is at 120 mbsl and the lake levels of Black Sea-Lake and Marmara Sea-Lake are at the level of their sills, 80 mbsl and 83 mbsl, respectively.

Figure 4-18: During the Meltwater Event (ME), a phenomenon that occurs from 16.35 kyr to 15 kyr, a gigantic amount of meltwater enters the Black Sea-Lake and the Marmara Sea-Lake from the north and west, likely sourced from melting Eurasian and Alpine ice sheets, respectively. The meltwater outflows from the Black Sea-Lake and Marmara Sea-Lake to the Mediterranean Sea/global ocean. The global sea level is at 120 mbsl at this time.

Figure 4-19: The Black Sea-Lake outflowed to the Marmara Sea-Lake, which outflowed to the Mediterranean Sea/global ocean during Older Dryas, a period that occurred from 15 to 14.8 kyr in the Black Sea. The global sea level rose to 90 mbsl from 95 mbsl. This rise is illustrated by an arrow directed up and by a lighter blue relative to that of the prior global ocean.

Figure 4-20: During the Bølling/Allerød period, in the Black Sea occurred between 14.8 kyr to 12.9 kyr, the Black Sea stopped its outflow to the Sea of Marmara. The lake level in the Black

Sea regressed to a level of at least 165 mbsl. The Sea of Marmara connected to the Mediterranean Sea at the very beginning of the Bølling/Allerød and rose together with the global sea level from a depth of 95 mbsl to 60 mbsl. The Dardanelles sill remained at a depth of 83 mbsl while the Bosporus sill depth became infilled to a level higher than 60 mbsl, and likely 35 mbsl, the modern Bosporus sill depth.

Figure 4-21: During the Younger Dryas period, a climate event that occurred from 12.9 kyr to 11.9 kyr in the Black Sea-Lake, the global sea level increased from 60 to 52 mbsl (indicated by the arrow directed up) and the modern flow through the Dardanelles sill was established. The lake level in the Black Sea transgressed to at least a depth of 95 mbsl (dashed line) but the exact increase in lake level is not certain.

Figure 4-22: During the Preboreal period, a period that occurred from 11.9 to 9.3 kyr, the global sea level rose to 35 mbsl. The Black Sea-Lake was isolated and its level decreased to at least 165 mbsl. The Bosporus sill remained at 35 mbsl.

Figure 4-23: At 9.3 kyr, the global sea level reached 35 mbsl and the water from the Mediterranean breached the Bosporus sill and inflowed into the regressed Black Sea-Lake to a depth of 35 mbsl. The water from the Mediterranean likely first descended to the bottom of the Black Sea and then lifted the Black Sea surface water, fresh, to the top. The arrows indicate the direction of water ventilation and flow.

Figure 4-24: From 9.3 kyr to present, the Black Sea-Lake rose in tandem with global sea level. This allowed for the modern flow to develop through the Bosporus sill such that fresh water was expelled at the surface and saline water entered as an undercurrent from the Mediterranean and Sea of Marmara.

Figure 4-1

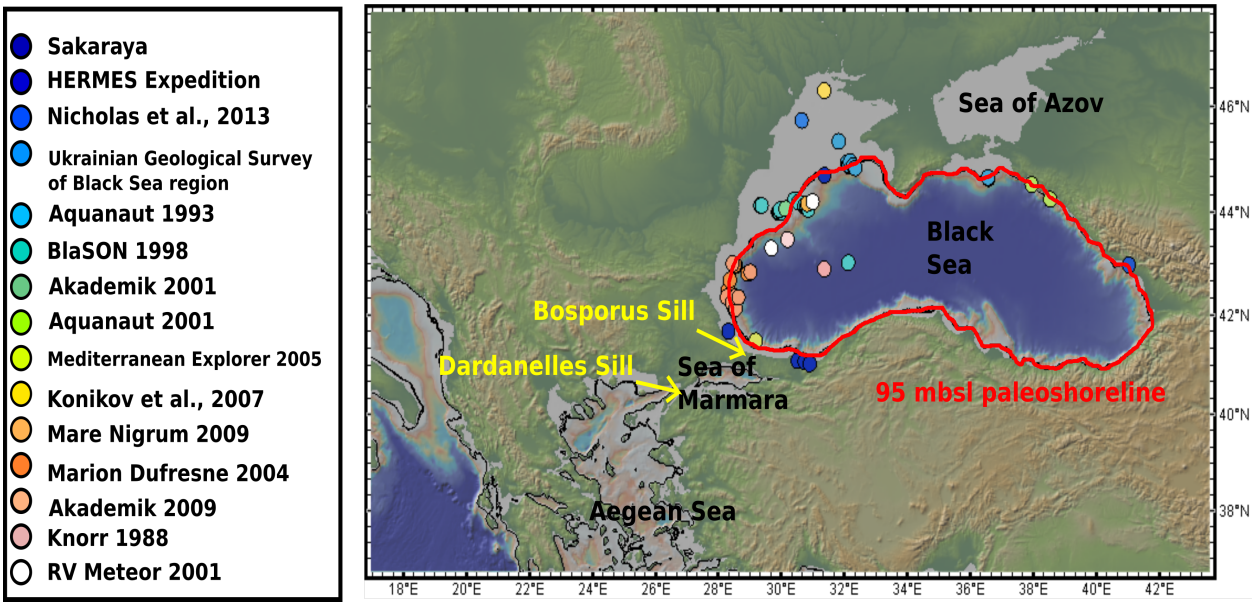
Sakaraya
HERMES Expedition
Nicholas et al., 2013
Ukrainian Geological Survey of Black Sea region
Aquanaut 1993
BlaSON 1998
Akademik 2001
Aquanaut 2001
Mediterranean Explorer 2005
Konikov et al., 2007
Mare Nigrum 2009
Marion Dufresne 2004
Akademik 2009
Knorr 1988
RV Meteor 2001
Sea of Azov
Black Sea
Bosporus Sill
Dardanelles Sill
Sea of Marmara
95 mbsl paleoshoreline
Aegean Sea
46°N
44°N
42°N
40°N
38°N
18°E
20°E
22°E
24°E
26°E
28°E
30°E
32°E
34°E
36°E
38°E
40°E
42°E

Figure 4-2

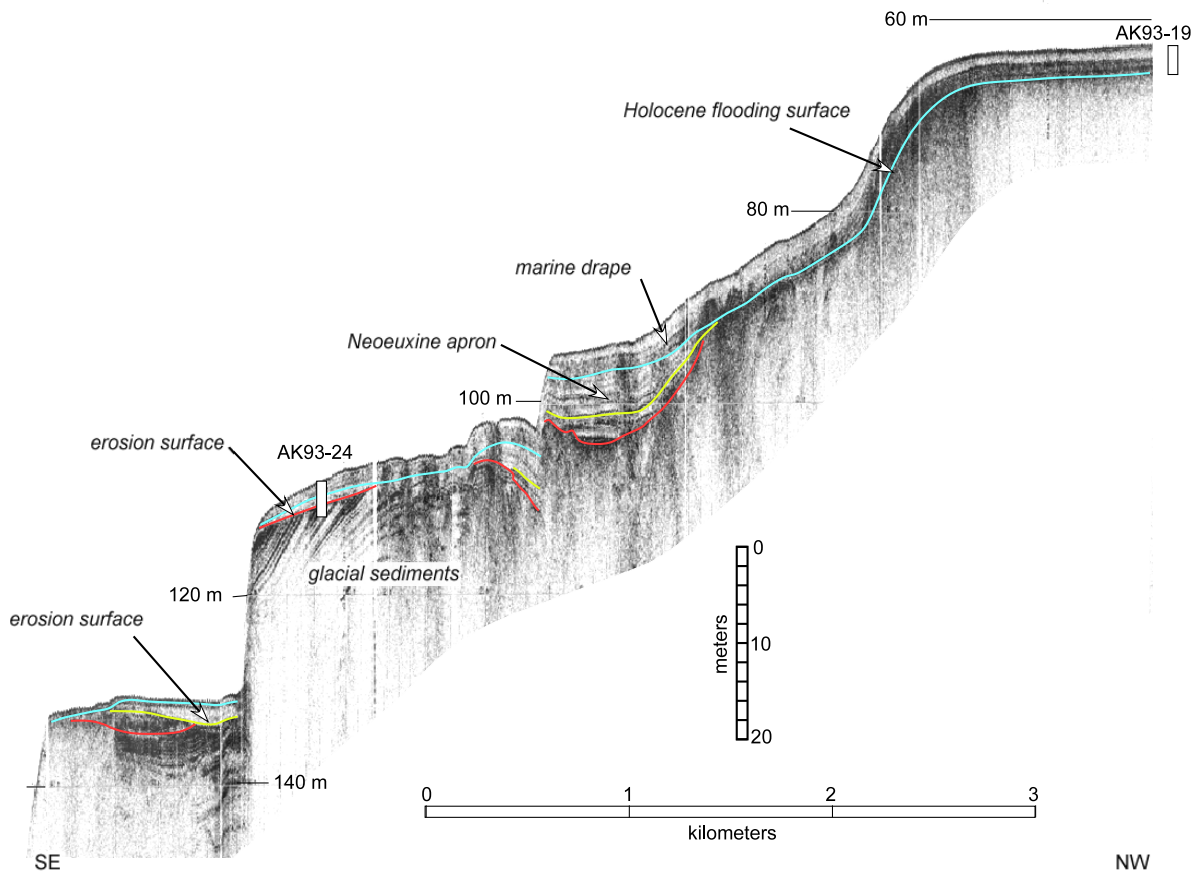
60 m
AK93-19
Holocene flooding surface
80 m
marine drape
Neoeuxine apron
100 m
erosion surface
AK93-24
glacial sediments
120 m
erosion surface
140 m
0
10
20
meters
0
1
2
3
kilometers
SE
NW

Figure 4-3

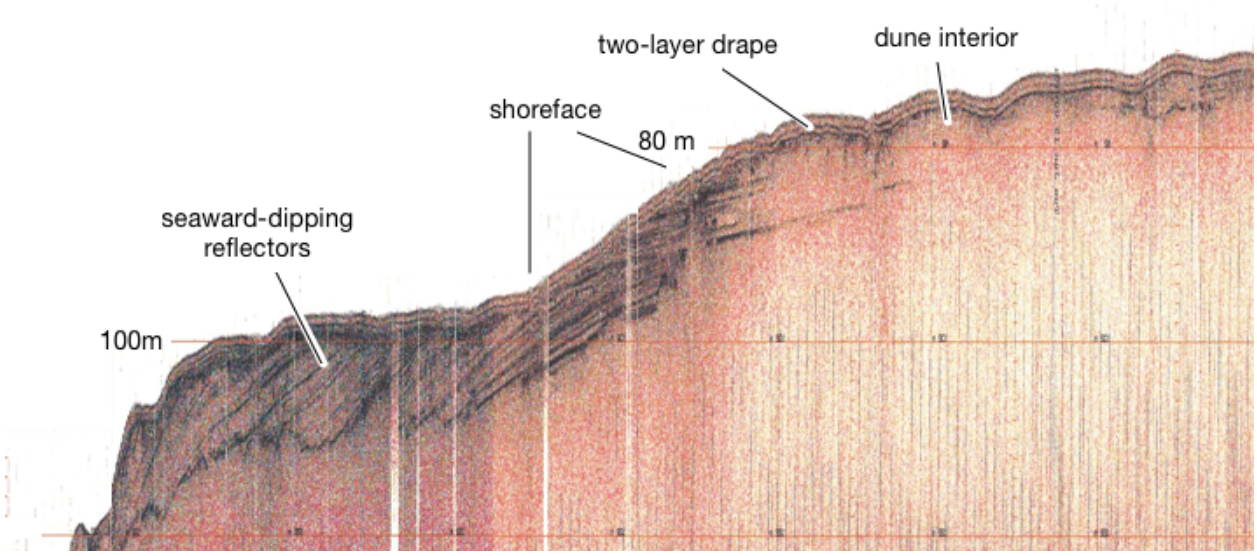
two-layer drape
dune interior
shoreface
80 m
seaward-dipping
reflectors
100m

Figure 4-4

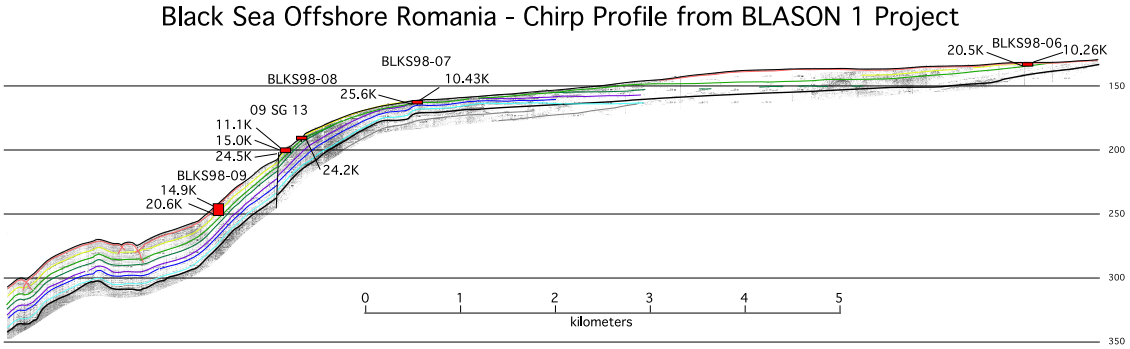
Black Sea Offshore Romania - Chirp Profile from BLASON 1 Project
20.5K
BLKS98-06
10.26K
BLKS98-07
BLKS98-08
10.43K
25.6K
09 SG 13
11.1K
15.0K
24.5K
24.2K
BLKS98-09
14.9K
20.6K
150
200
250
300
350
0
1
2
3
4
5
kilometers

Figure 4-5

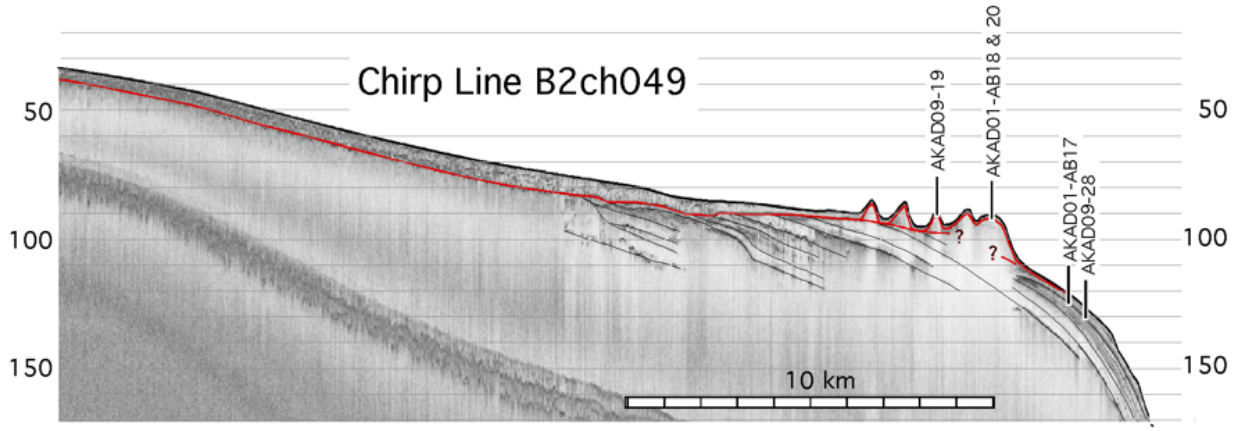
Chirp Line B2ch049
50
100
150
AKAD09-19
AKAD01-AB18 & 20
AKAD01-AB17
AKAD09-28
?
?
10 km

Figure 4-6

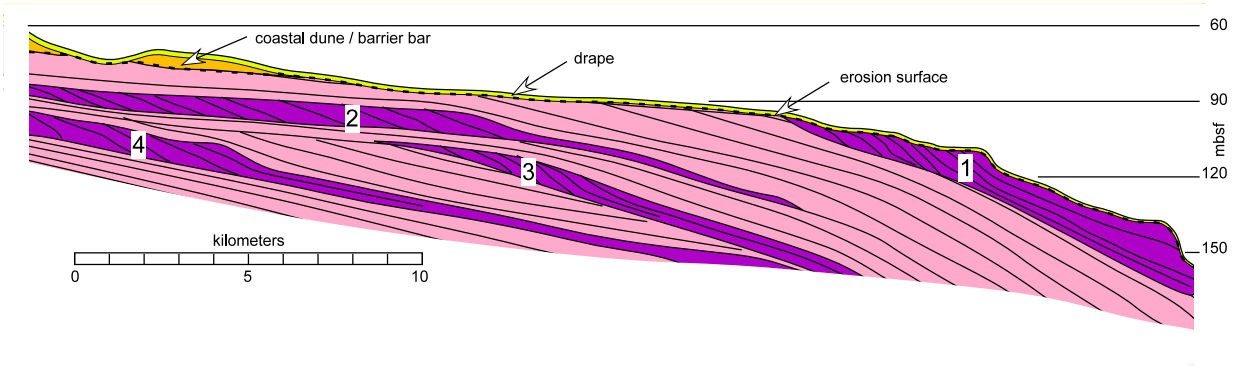
coastal dune / barrier bar
drape
erosion surface
60
90
120
150
mbsf
1
2
3
4
kilometers
0
5
10

Figure 4-7

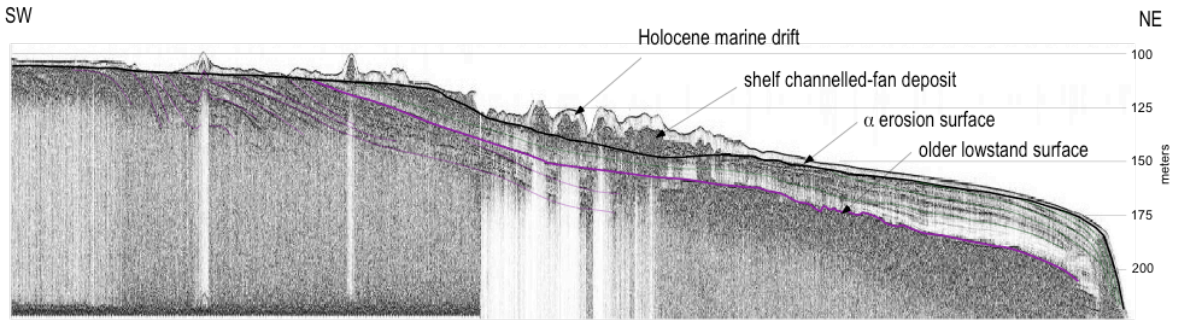
SW
NE
Holocene marine drift
shelf channelled-fan deposit
α erosion surface
older lowstand surface
100
125
150
175
200
meters

Figure 4-8

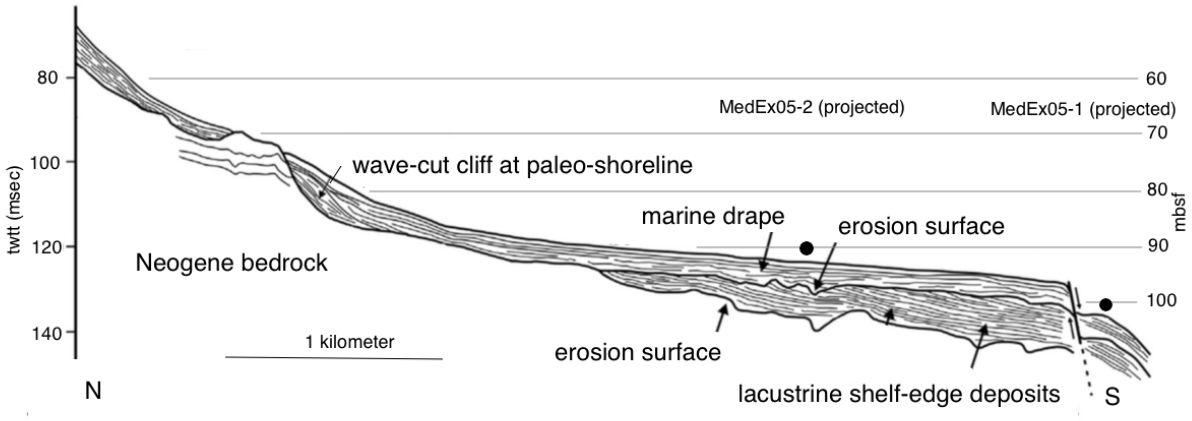
80
100
120
140
twt (msec)
60
70
80
90
100
mbsf
MedEx05-2 (projected)
MedEx05-1 (projected)
wave-cut cliff at paleo-shoreline
marine drape
erosion surface
Neogene bedrock
1 kilometer
erosion surface
lacustrine shelf-edge deposits
N
S

Figure 4-9

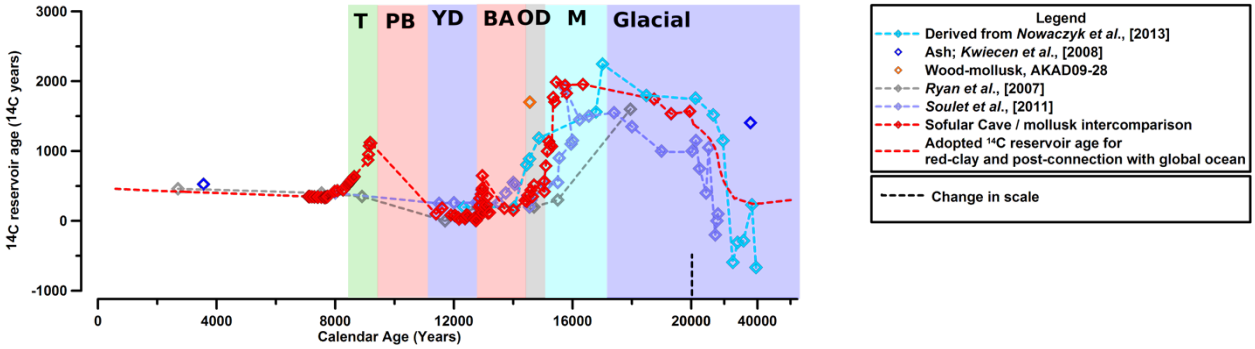
T
PB
YD
BA
OD
M
Glacial
14C reservoir age (14C years)
3000
2000
1000
0
-1000
0
4000
8000
12000
16000
20000
40000
Calendar Age (Years)
Legend
Derived from Nowaczyk et al., [2013]
Ash; Kwiecen et al., [2008]
Wood-mollusk, AKAD09-28
Ryan et al., [2007]
Soulet et al., [2011]
Sofular Cave / mollusk intercomparison
Adopted 14C reservoir age for red-clay and post-connection with global ocean
Change in scale

Figure 4-10

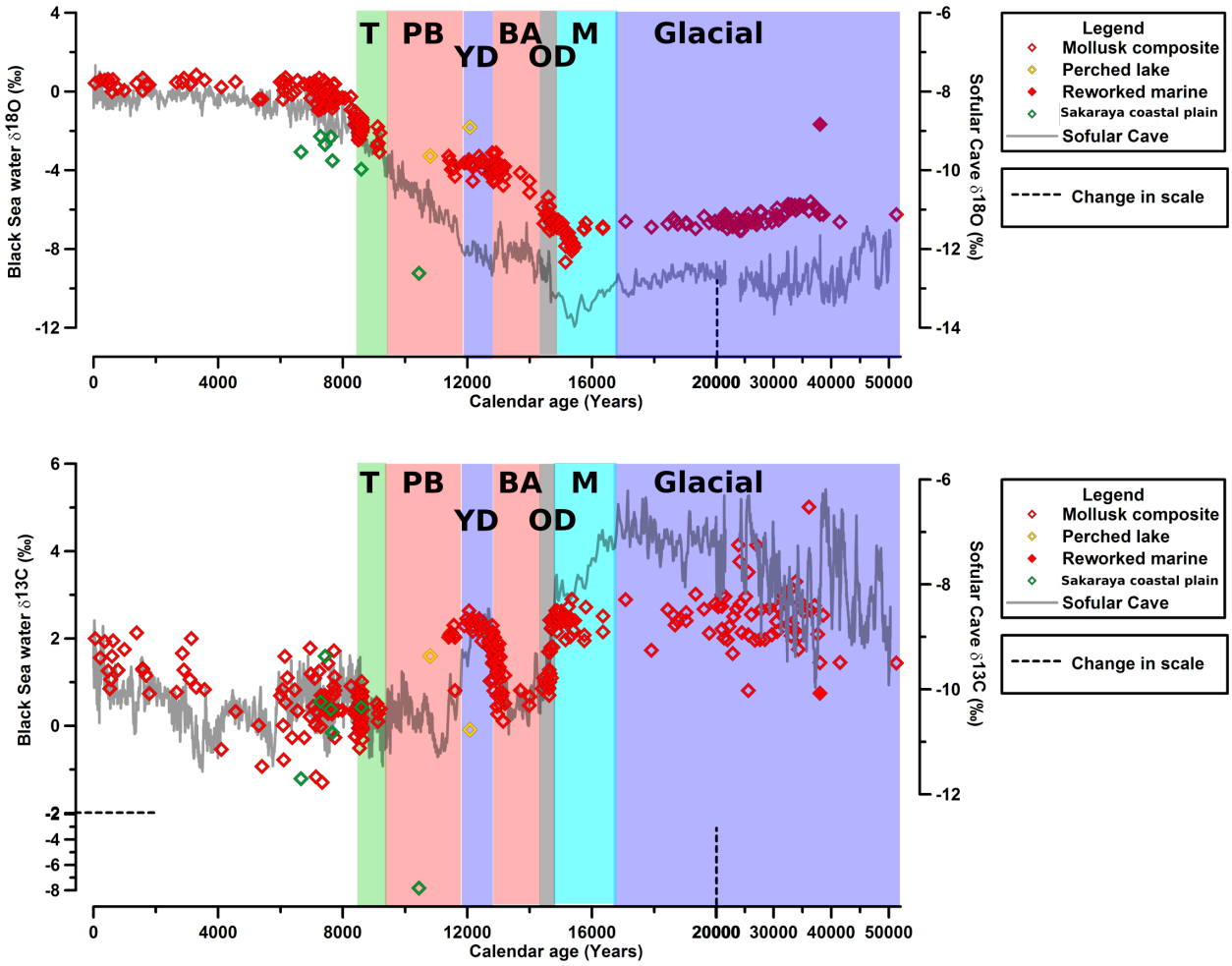
T
PB
YD
BA
OD
M
Glacial
Black Sea water δ18O (‰)
Sofular Cave δ18O (‰)
Calendar age (Years)
Legend
Mollusk composite
Perched lake
Reworked marine
Sakaraya coastal plain
Sofular Cave
Change in scale
Black Sea water δ13C (‰)
Sofular Cave δ13C (‰)
Calendar age (Years)

Figure 4-11

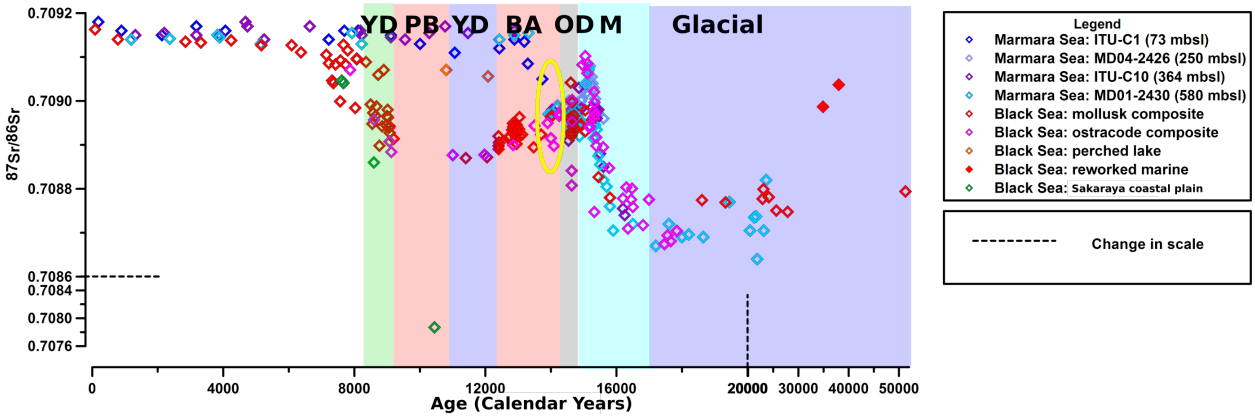
YD
PB
YD
BA
OD
M
Glacial
87Sr/86Sr
0.7092
0.7090
0.7088
0.7086
0.7084
0.7080
0.7076
0
4000
8000
12000
16000
20000
30000
40000
50000
Age (Calendar Years)
Legend
Marmara Sea: ITU-C1 (73 mbsl)
Marmara Sea: MD04-2426 (250 mbsl)
Marmara Sea: ITU-C10 (364 mbsl)
Marmara Sea: MD01-2430 (580 mbsl)
Black Sea: mollusk composite
Black Sea: ostracode composite
Black Sea: perched lake
Black Sea: reworked marine
Black Sea: Sakaraya coastal plain
Change in scale

Figure 4-12

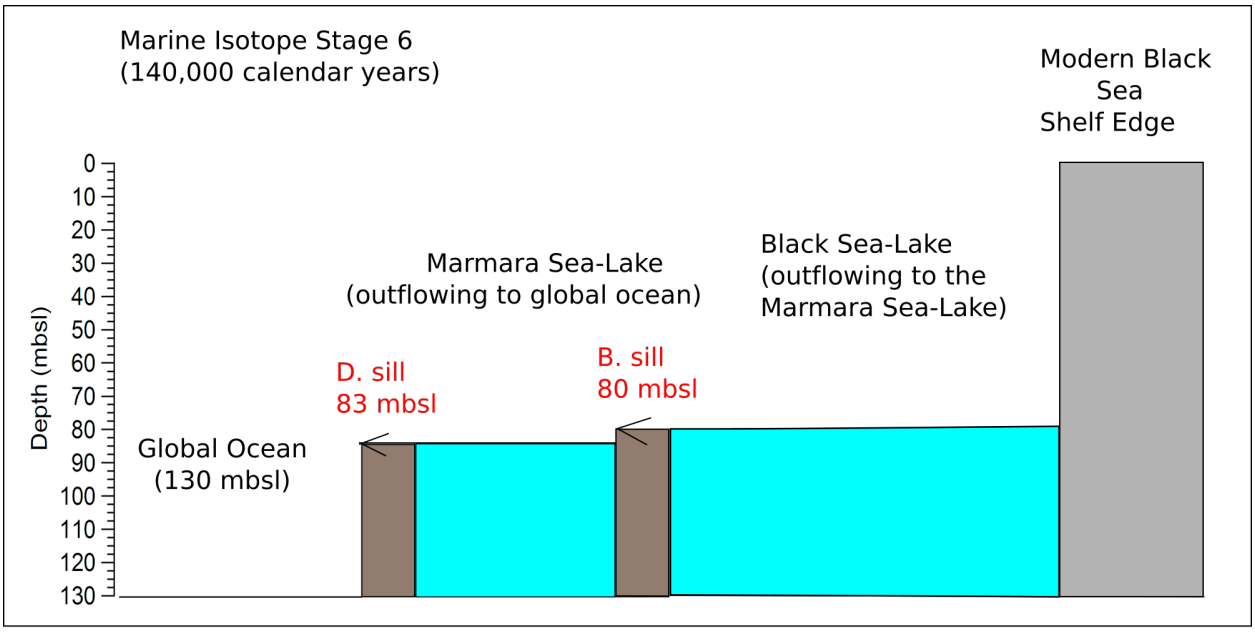
Marine Isotope Stage 6
(140,000 calendar years)
Modern Black
Sea
Shelf Edge
Depth (mbsl)
0
10
20
30
40
50
60
70
80
90
100
110
120
130
Marmara Sea-Lake
(outflowing to global ocean)
Black Sea-Lake
(outflowing to the
Marmara Sea-Lake)
D. sill
83 mbsl
B. sill
80 mbsl
Global Ocean
(130 mbsl)

Figure 4-13

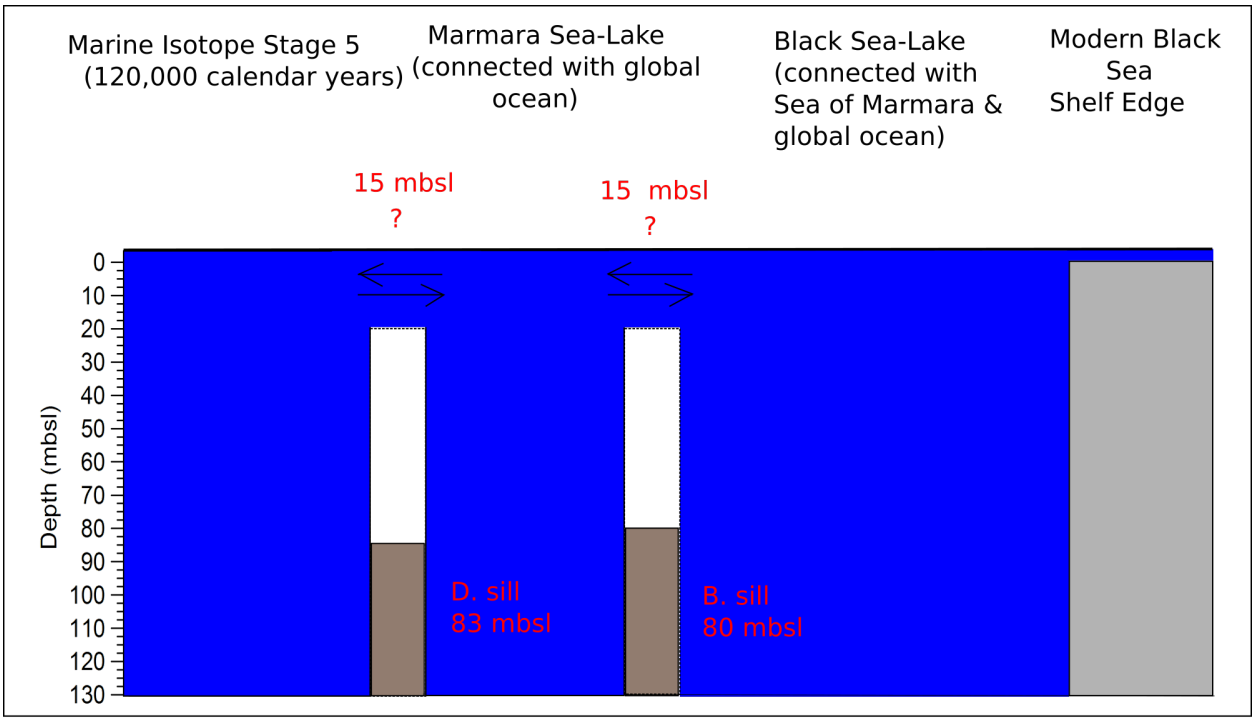
Marine Isotope Stage 5
(120,000 calendar years)
Marmara Sea-Lake
(connected with global ocean)
Black Sea-Lake
(connected with Sea of Marmara & global ocean)
Modern Black Sea
Shelf Edge
15 mbsl
?
15 mbsl
?
Depth (mbsl)
0
10
20
30
40
50
60
70
80
90
100
110
120
130
D. sill
83 mbsl
B. sill
80 mbsl

Figure 4-14

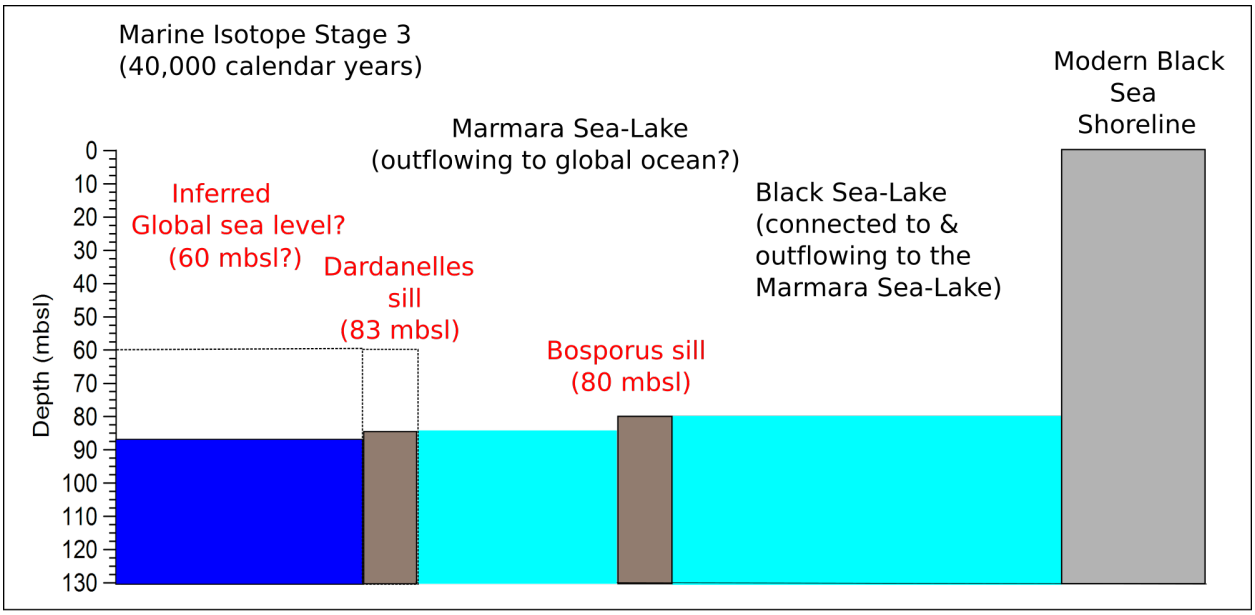
Marine Isotope Stage 3
(40,000 calendar years)
Modern Black Sea Shoreline
Marmara Sea-Lake
(outflowing to global ocean?)
Inferred
Global sea level?
(60 mbsl?)
Dardanelles sill
(83 mbsl)
Black Sea-Lake
(connected to &
outflowing to the
Marmara Sea-Lake)
Bosporus sill
(80 mbsl)
Depth (mbsl)
0
10
20
30
40
50
60
70
80
90
100
110
120
130

Figure 4-15

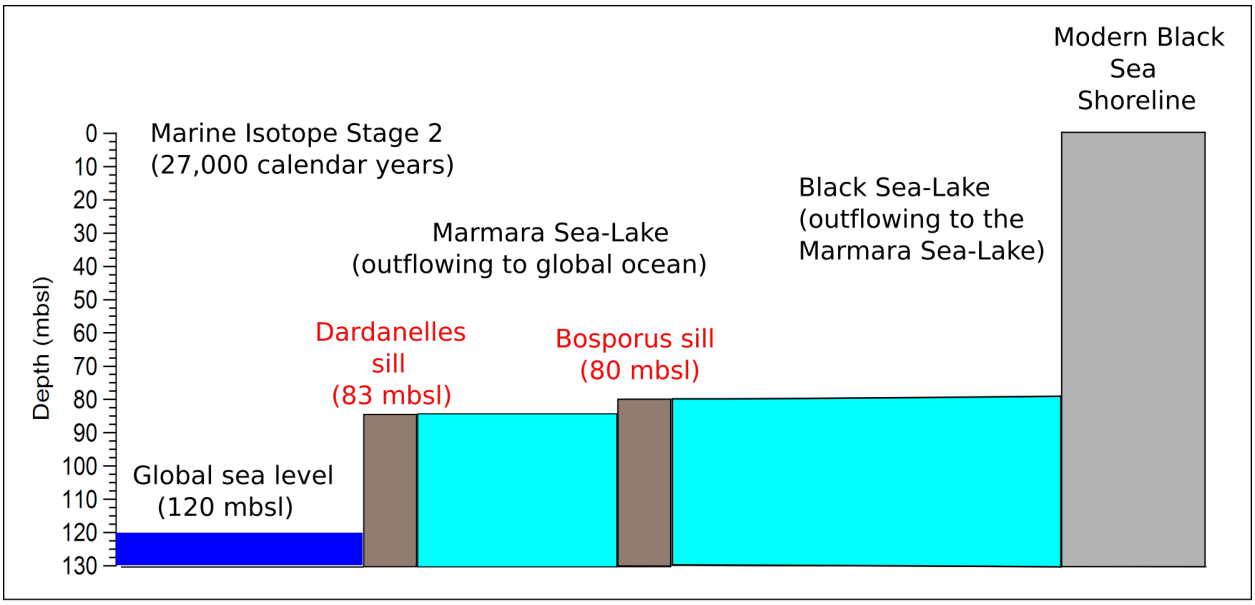
Modern Black Sea Shoreline
Marine Isotope Stage 2
(27,000 calendar years)
Black Sea-Lake
(outflowing to the
Marmara Sea-Lake)
Marmara Sea-Lake
(outflowing to global ocean)
Dardanelles
sill
(83 mbsl)
Bosporus sill
(80 mbsl)
Global sea level
(120 mbsl)
Depth (mbsl)
0
10
20
30
40
50
60
70
80
90
100
110
120
130

Figure 4-16

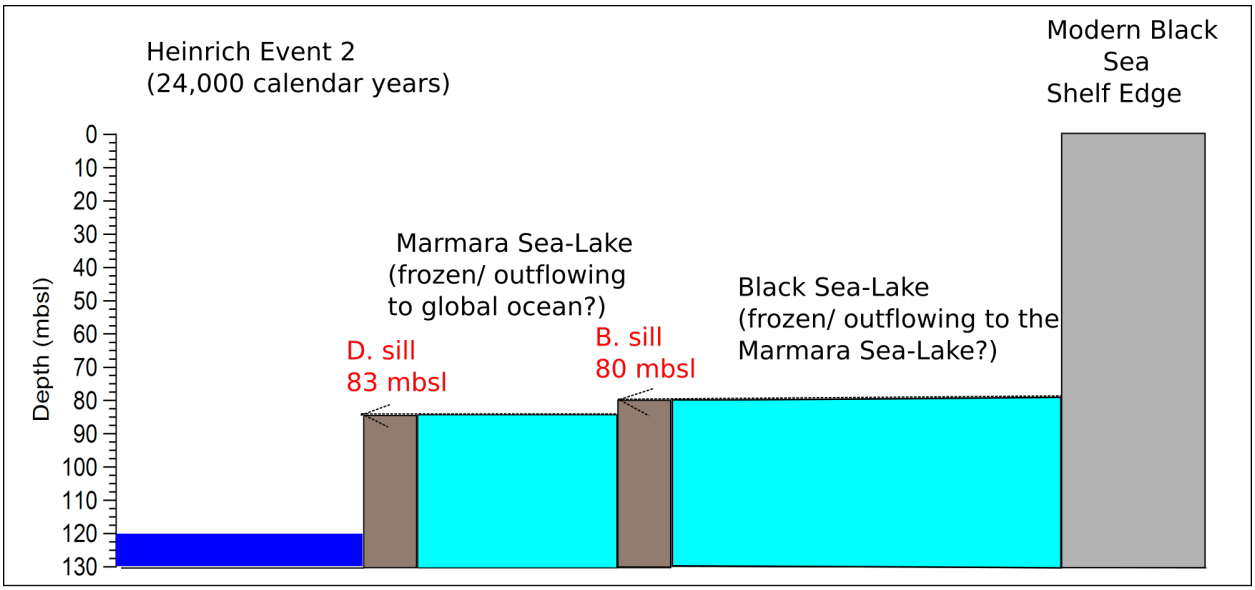
Heinrich Event 2
(24,000 calendar years)
Modern Black Sea
Shelf Edge
Depth (mbsl)
0
10
20
30
40
50
60
70
80
90
100
110
120
130
Marmara Sea-Lake
(frozen/ outflowing
to global ocean?)
D. sill
83 mbsl
B. sill
80 mbsl
Black Sea-Lake
(frozen/ outflowing to the
Marmara Sea-Lake?)

Figure 4-17

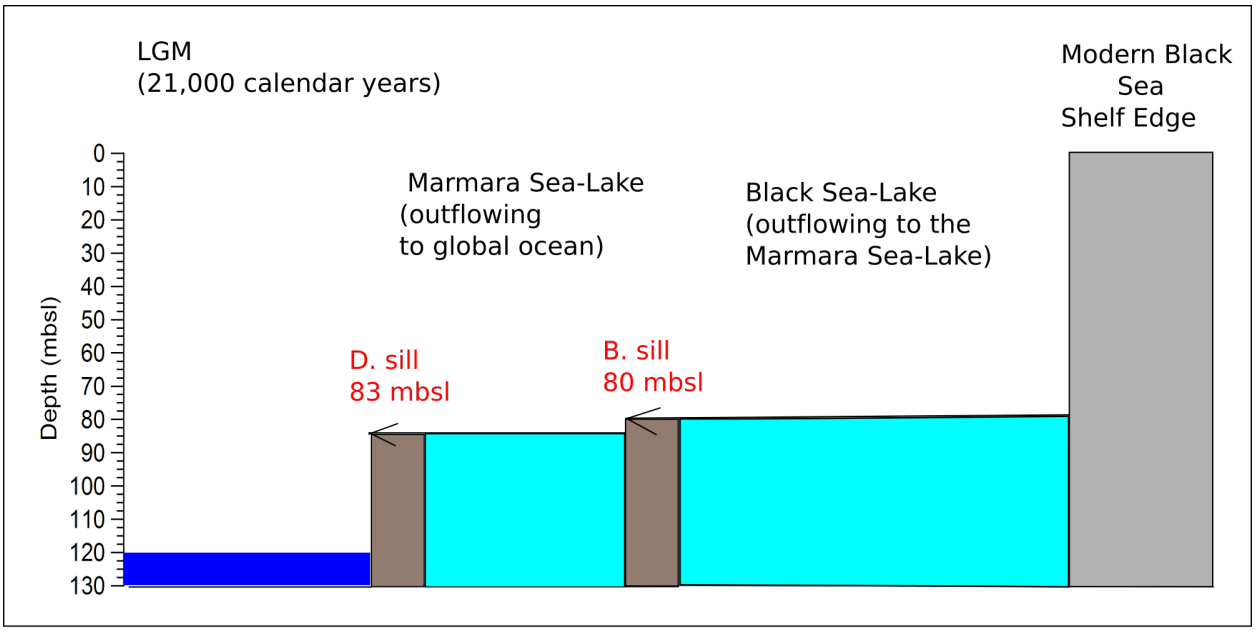
LGM
(21,000 calendar years)
Modern Black Sea Shelf Edge
Depth (mbsl)
0
10
20
30
40
50
60
70
80
90
100
110
120
130
Marmara Sea-Lake
(outflowing
to global ocean)
Black Sea-Lake
(outflowing to the
Marmara Sea-Lake)
D. sill
83 mbsl
B. sill
80 mbsl

Figure 4-18

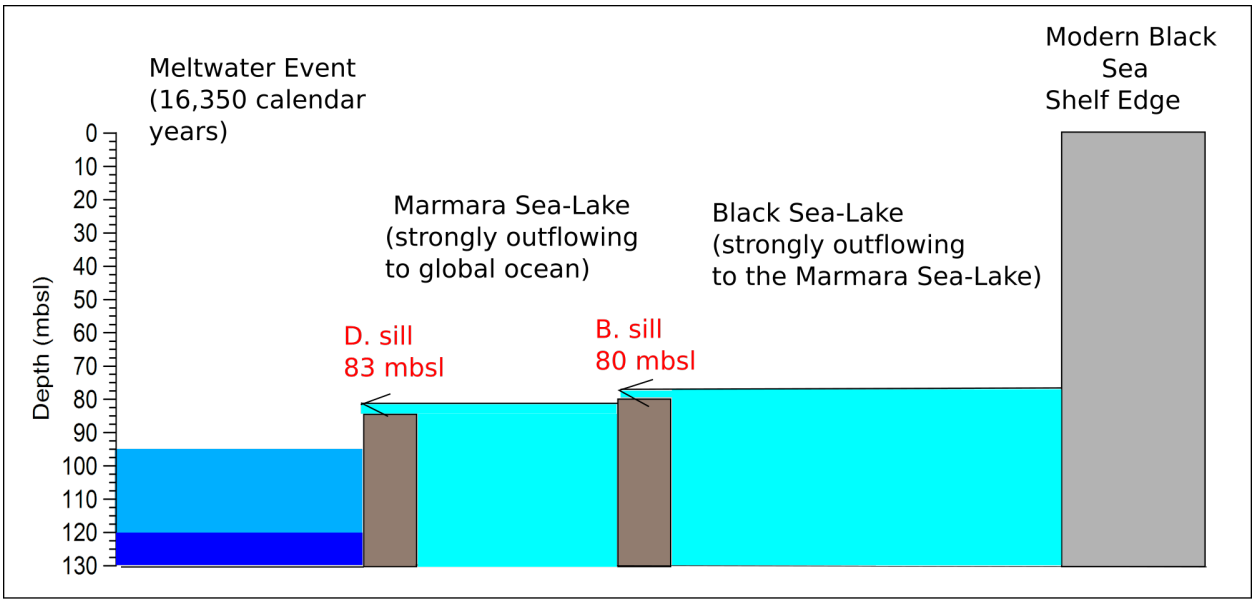
Meltwater Event
(16,350 calendar
years)
Modern Black
Sea
Shelf Edge
Marmara Sea-Lake
(strongly outflowing
to global ocean)
Black Sea-Lake
(strongly outflowing
to the Marmara Sea-Lake)
D. sill
83 mbsl
B. sill
80 mbsl
Depth (mbsl)
0
10
20
30
40
50
60
70
80
90
100
110
120
130

Figure 4-19

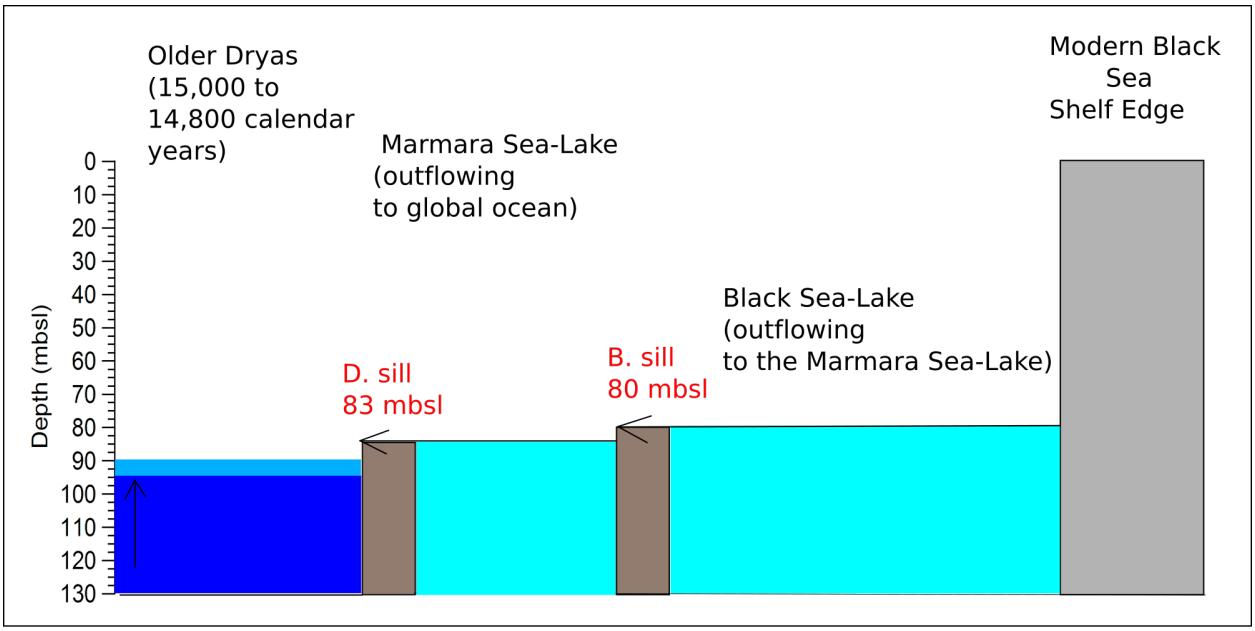
Older Dryas
(15,000 to
14,800 calendar
years)
Marmara Sea-Lake
(outflowing
to global ocean)
Modern Black
Sea
Shelf Edge
Depth (mbsl)
0
10
20
30
40
50
60
70
80
90
100
110
120
130
D. sill
83 mbsl
B. sill
80 mbsl
Black Sea-Lake
(outflowing
to the Marmara Sea-Lake)

Figure 4-20

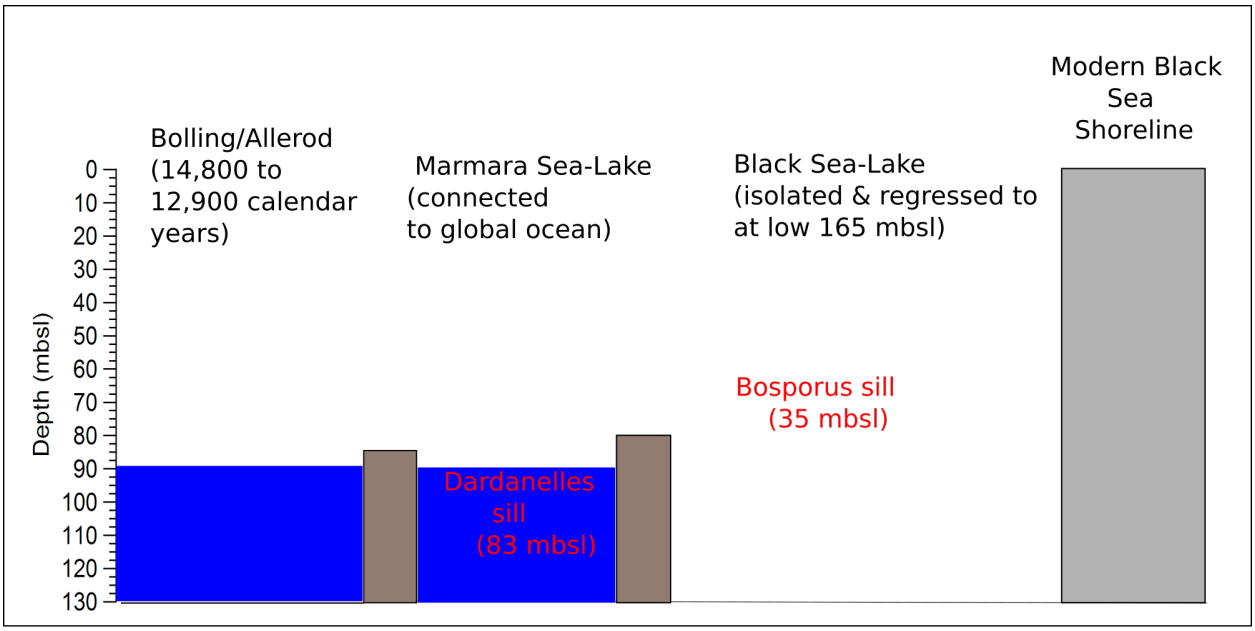
Modern Black Sea Shoreline
Bolling/Allerod (14,800 to 12,900 calendar years)
Marmara Sea-Lake (connected to global ocean)
Black Sea-Lake (isolated & regressed to at low 165 mbsl)
Depth (mbsl)
0
10
20
30
40
50
60
70
80
90
100
110
120
130
Bosporus sill (35 mbsl)
Dardanelles sill (83 mbsl)

Figure 4-21

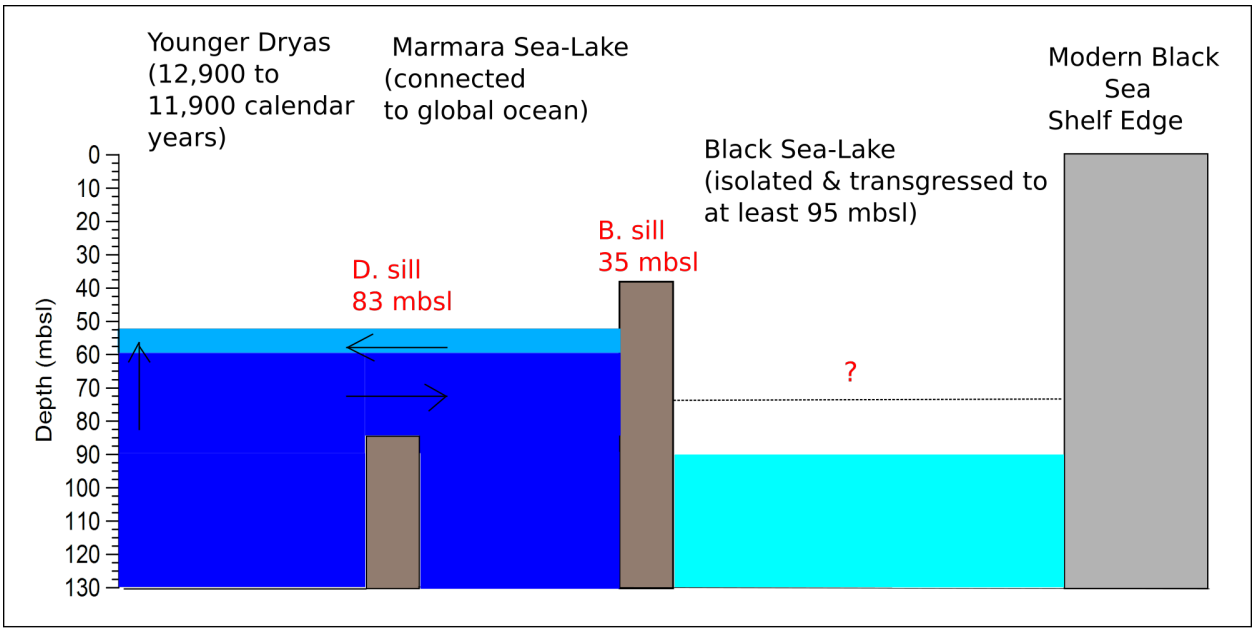
Younger Dryas
(12,900 to
11,900 calendar
years)
Marmara Sea-Lake
(connected
to global ocean)
Modern Black
Sea
Shelf Edge
Black Sea-Lake
(isolated & transgressed to
at least 95 mbsl)
B. sill
35 mbsl
D. sill
83 mbsl
?
Depth (mbsl)
0
10
20
30
40
50
60
70
80
90
100
110
120
130

Figure 4-22

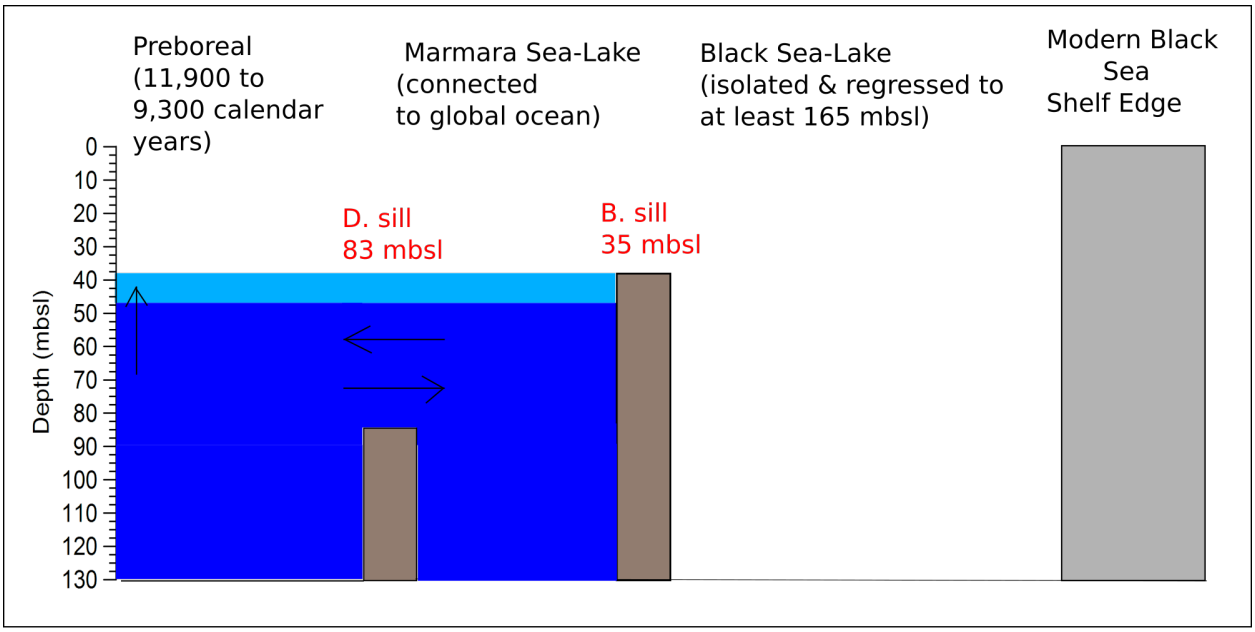
Preboreal
(11,900 to
9,300 calendar
years)
Marmara Sea-Lake
(connected
to global ocean)
Black Sea-Lake
(isolated & regressed to
at least 165 mbsl)
Modern Black
Sea
Shelf Edge
D. sill
83 mbsl
B. sill
35 mbsl
Depth (mbsl)
0
10
20
30
40
50
60
70
80
90
100
110
120
130

Figure 4-23

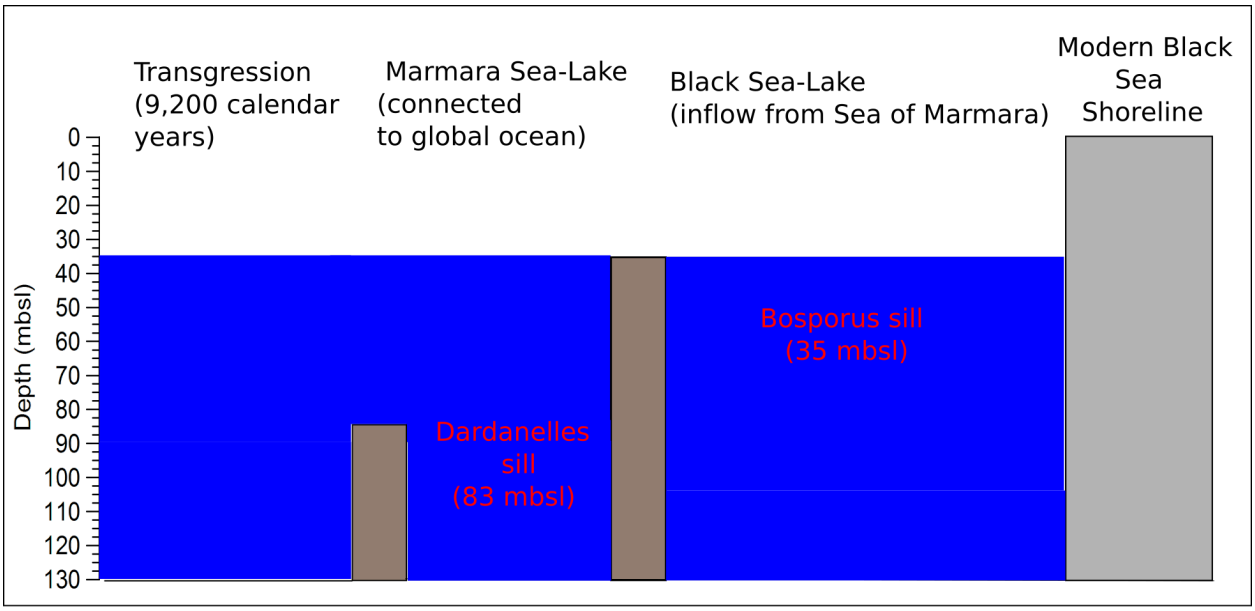
Transgression
(9,200 calendar
years)
Marmara Sea-Lake
(connected
to global ocean)
Black Sea-Lake
(inflow from Sea of Marmara)
Modern Black
Sea
Shoreline
Depth (mbsl)
0
10
20
30
40
50
60
70
80
90
100
110
120
130
Dardanelles
sill
(83 mbsl)
Bosporus sill
(35 mbsl)

Figure 4-24

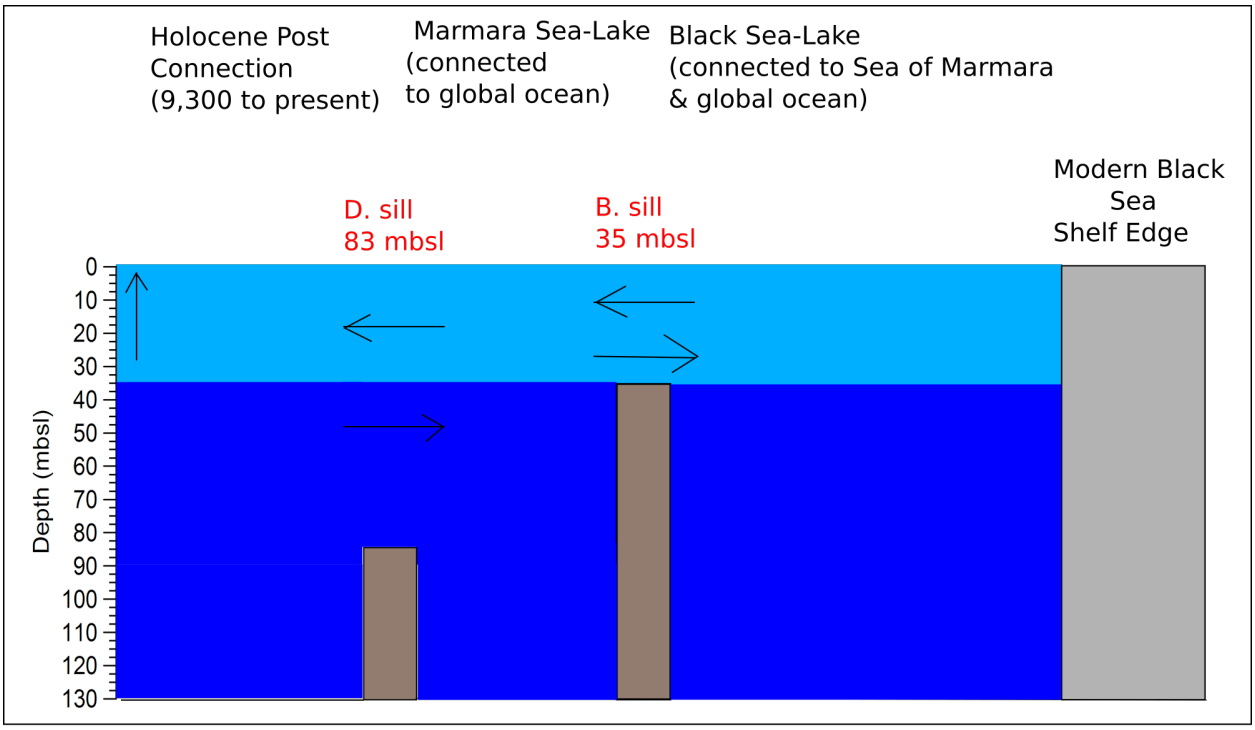
Holocene Post
Connection
(9,300 to present)
Marmara Sea-Lake
(connected
to global ocean)
Black Sea-Lake
(connected to Sea of Marmara
& global ocean)
Modern Black
Sea
Shelf Edge
D. sill
83 mbsl
B. sill
35 mbsl
Depth (mbsl)
0
10
20
30
40
50
60
70
80
90
100
110
120
130

Appendix 4-1

Table 1

Core name	Lat (N)	Lon (E)	Core Depth (m)	Cruise and/or first reference
KSK-20	41.06	30.74	0	Turkish State Waterworks, *Görür et al*., 2001
KSK-18	41.01	30.70	0	Turkish State Waterworks, *Görür et al*., 2001
KSK-16	41.01	30.52	0	Turkish State Waterworks, *Görür et al*., 2001
KSK-4	41.04	30.90	0	Turkish State Waterworks, *Görür et al*., 2001
M02-45TWC	41.69	28.32	-69	Trigger core; *Hiscott et al*., 2007
M02-45P	41.69	28.32	-69	Piston core; *Hiscott et al*., 2007
45B	44.71	31.37	-107	Ukrainian HERMES Cruise; *Nicholas et al*., 2011
721	42.99	41.04	-14.9	Apakidze and Burchuladze, 1987
342	45.74	30.64	-30	Ukrainian Geological Survey of Black Sea region Nicholas et al., 2011
AQ93-01	44.95	32.08	-68	Aquanaut 1993
AQ93-3-2	45.35	31.82	-49	Aquanaut 1993
AQ93-07	44.88	32.15	-108	Aquanaut 1993
AQ93-08	44.90	32.13	-99	Aquanaut 1993
AQ93-09	44.88	32.15	-123	Aquanaut 1993
AQ93-10	44.89	32.15	-106	Aquanaut 1993
AQ93-11	44.91	32.13	-91	Aquanaut 1993
AQ93-12	44.97	32.18	-78	Aquanaut 1993
AQ93-13	44.88	32.28	-165	Aquanaut 1993
AQ93-14	44.85	32.35	-140	Aquanaut 1993
AQ93-22	44.65	36.58	129	Aquanaut 1993
AQ93-24	44.67	36.56	-110	Aquanaut 1993
BLKS9801	44.25	30.42	-92	BlaSON, 1998
BLKS9804	44.20	30.54	-101	BlaSON, 1998
BLKS9806	44.13	30.73	-135	BlaSON, 1998
BLKS9807	44.10	30.79	-163	BlaSON, 1998
BLKS9808	44.10	30.79	-186	BlaSON, 1998
BLKS9809	44.09	30.81	-240	BlaSON, 1998
BLKS9810	44.07	30.85	-378	BlaSON, 1998
BLKS9814	44.14	29.33	-55	BlaSON, 1998
BLKS9815	44.14	29.37	-55	BlaSON, 1998
BLKS9822	43.04	32.13	-2100	BlaSON, 1998

BLKS9830	44.01	29.90	-57	BlaSON, 1998
BLKS9831	44.02	29.92	-75	BlaSON, 1998
BLKS9834	44.04	29.95	-67	BlaSON, 1998
BLKS9837	44.02	29.99	-68	BlaSON, 1998
BLKS9838	44.06	29.96	-77	BlaSON, 1998
AKAD01-AB8	44.08	30.13	-90	Akademik, 2001
AK-500	44.53	37.95	-71	Aquanaut, 2001
AK-521	44.26	38.54	-101	Aquanaut, 2001
Medex05-13	41.50	29.19	-118	Mediterranean Explorer, 2005
37-82	46.29	31.36	-24	*Konikov*, 2007
09-SG-13	44.17	30.82	-200	Mare Nigrum, 2009
MD04-2770	44.21	30.99	-358	Marion Dufresne, 2004
MD04-2788	43.32	29.68	-1224	Marion Dufresne, 2004
AKAD09-09	42.83	28.93	-1500	Akademik, 2009
AKAD09-15	42.98	28.55	-164	Akademik, 2009
AKAD09-16	42.98	28.55	-1445	Akademik, 2009
AKAD09-27	42.50	28.30	-92.2	Akademik, 2009
AKAD09-28	42.70	28.36	-126	Akademik, 2009
AKAD09-29	42.99	28.55	-148.9	Akademik, 2009
AKAD09-30	43.00	28.52	-115	Akademik, 2009
AKAD11-01	42.36	28.35	-125	Akademik, 2011
AKAD11-02	42.36	28.29	-90	Akademik, 2001
AKAD11-03	42.36	28.27	-90	Akademik, 2001
AKAD11-05	42.25	28.44	-125	Akademik, 2001
AKAD11-07	42.13	28.54	-153	Akademik, 2001
AKAD11-11	42.37	28.54	-510	Akademik, 2001
AKAD11-13	42.36	28.64	-860	Akademik, 2001
AKAD11-17	42.85	29.02	-1805	Akademik, 2001
AKAD11-19	43.02	28.45	-85	Akademik, 2001
KN134-GC01	42.91	31.36	-2210	Knorr, 1988
GeoB7608-1	43.49	30.20	-1202	Meteor, 2001 and *Bahr et al*., 2005